

**AD-A243 599****DOCUMENTATION PAGE**Form Approved  
OMB No. 0704-0188

ation is estimated to average 1 hour per response, including the time for reviewing instructions, searching existing data sources, completing and reviewing the collection of information. Send comments regarding this burden estimate or any other aspect of this reducing this burden, to Washington Headquarters Services, Directorate for Information Operations and Reports, 1215 Jefferson, and to the Office of Management and Budget, Paperwork Reduction Project (0704-0188), Washington, DC 20503.

2. REPORT DATE

3. REPORT TYPE AND DATES COVERED

THESIS/DISSERTATION

## 4. TITLE AND SUBTITLE

Evaluation of Lowtran and Modtran for Use Over High  
Zenith Angle/Long Path Length Viewing

## 5. FUNDING NUMBERS

## 6. AUTHOR(S)

Jonathan C. Wright, Captain

## 7. PERFORMING ORGANIZATION NAME(S) AND ADDRESS(ES)

AFIT Student Attending: Rochester Institute of Technology

8. PERFORMING ORGANIZATION  
REPORT NUMBER

AFIT/CI/CIA- 91-075

## 9. SPONSORING/MONITORING AGENCY NAME(S) AND ADDRESS(ES)

AFIT/CI  
Wright-Patterson AFB OH 45433-658310. SPONSORING/MONITORING  
AGENCY REPORT NUMBER

## 11. SUPPLEMENTARY NOTES

## 12a. DISTRIBUTION/AVAILABILITY STATEMENT

Approved for Public Release IAW 190-1  
Distributed Unlimited  
ERNEST A. HAYGOOD, 1st Lt, USAF  
Executive Officer

## 12b. DISTRIBUTION CODE

## 13. ABSTRACT (Maximum 200 words)

## 14. SUBJECT TERMS

15. NUMBER OF PAGES  
91

16. PRICE CODE

17. SECURITY CLASSIFICATION  
OF REPORT18. SECURITY CLASSIFICATION  
OF THIS PAGE19. SECURITY CLASSIFICATION  
OF ABSTRACT

20. LIMITATION OF ABSTRACT

EVALUATION OF LOWTRAN AND MODTRAN  
FOR USE OVER HIGH ZENITH ANGLE/  
LONG PATH LENGTH VIEWING

by

Jonathan C. Wright

A thesis submitted in partial fulfillment  
of the requirements for the degree of  
Master of Science in the Center for  
Imaging Science in the College of  
Graphic Arts and Photography of the  
Rochester Institute of Technology

May 1991

Signature of the Author

*Jonathan C. Wright*

Accepted by

*Robert A. P. RAVAN*

Coordinator, M. S. Degree Program

DEFENSE TECHNICAL INFORMATION CENTER



9117945



Accession For	
NTIS GRA&I	<input checked="" type="checkbox"/>
DTIC Tab	<input type="checkbox"/>
Unannounced	<input type="checkbox"/>
Justification	
By	
Distribution/	
Availability Codes	
Dist	Avail and/or Special
A-1	

COLLEGE OF GRAPHIC ARTS AND PHOTOGRAPHY  
ROCHESTER INSTITUTE OF PHOTOGRAPHY  
ROCHESTER, NEW YORK

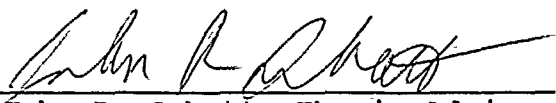
CERTIFICATE OF APPROVAL

---

M. S. DEGREE THESIS

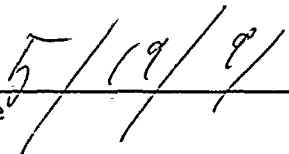
---

The M.S. Degree Thesis of Jonathan C. Wright  
has been examined and approved  
by the thesis committee as satisfactory  
for the thesis requirement for the  
Master of Science degree

  
Dr. John R. Schott, Thesis Advisor

  
Mr. Carl Salvaggio

  
Dr. E. Stokes Fishburne

  
Date

THESIS RELEASE PERMISSION FORM

ROCHESTER INSTITUTE OF TECHNOLOGY  
COLLEGE OF GRAPHIC ARTS AND PHOTOGRAPHY

Title of Thesis: Evaluation of LOWTRAN and MODTRAN for use  
Over High Zenith Angle/Long Path Viewing

I, Jonathan C. Wright, hereby grant permission to the Wallace  
Memorial Library of R.I.T. to reproduce my thesis in whole or  
in part. Any reproduction will not be for commercial use of  
profit.

Signature: Jonathan C. Wright

Date: 14 MAY 1991


EVALUATION OF LOWTRAN AND MODTRAN  
FOR USE OVER HIGH ZENITH ANGLE/  
LONG PATH LENGTH VIEWING


by

Jonathan C. Wright

Submitted to the  
Center for Imaging Science  
in partial fulfillment of the requirements  
for the Master of Science Degree  
at the Rochester Institute of Technology

ABSTRACT

— — — — —  LOWTRAN and MODTRAN were evaluated in the 2.0-5.5 micron region against field collection data at high zenith angle/long path lengths to determine the degree of uncertainty associated with these models under these conditions. Matching data sets were developed using data from the Air Force Geophysics Laboratory Flying Infrared Signatures Technology Aircraft (FISTA) as the field reference. The Kolmogorov-Smirnov test was applied to determine the degree to which the outputs of LOWTRAN and MODTRAN follow the same distribution as the field data. The percent difference between the model and field data was also studied.

Agreement between the model and field data was found to be better than 97% for most cases. Median percent difference was within 10% for zenith angles less than 90 degrees. 

### Acknowledgements

It is said that no man is an island. This thesis is certainly a reflection of that concept. While it is only fair and fitting that any inaccuracies of fact, failing of intellect and insight, or butchery of standard written diction be laid at the feet of the author, the accomplishment of this thesis was by no means a solo feat. Thus, a few words of thanks to some of those who made this thesis possible.

Each of my advisors contributed in a unique way. Discussions with Stokes Fishburne were responsible for the concept. John Schott kept my feet to the fire and is in many ways responsible for the necessary rigor of the discussions and results. Carl Salvaggio provided invaluable assistance in keeping the focus on results rather than computer gymnastics.

Brian Sandford of the Air Force Geophysics Laboratory provided the data set, as well as advance copies of work in progress within the Laboratory updating the description of the sensor platform. His prompt response to a call out of the blue requesting data generated years earlier as well as detailed sensor information was and is extraordinary. I only hope I have the opportunity of fulfilling such an obviously irrational request in the future to somehow return the favor.

Jim Lisowski of Scitec provided sanity whenever it was needed. He, along with Stu Augustin, helped decipher the final calibration issues for which I am eternally grateful. They also kept my feet to the fire and corrected me when I strayed from the straight and narrow, something only friends would do. But that's another story.

## Dedication

To my wife Kathy and my daughter Caitlin.

They graciously allowed me to satisfy my academic curiosity.

Why, I'll never know. Something about love I guess.

## Table of Contents

	Page
1. Introduction	1
2. Background	4
2.1 Atmospheric Transmission	4
2.2 LOWTRAN	17
2.3 MODTRAN	25
2.4 Field Data	28
2.5 Statistical Tools	32
2.6 Previous Efforts	34
3. Approach	36
3.1 Field Data Generation	37
3.2 Computer Model Data Generation	47
3.3 Data Set Equivalence	51
4. Results	53
4.1 Kolmogorov-Smirnov Analysis	60
4.2 Percent Difference Analysis	63
5. Conclusions and Recommendations	88
6. References	91

### Appendices

- Appendix 1 - Cundiff and Lisowski Report Extracts
- Appendix 2 - AFGL File Format and VAX Backup Notes
- Appendix 3 - Run 01 Numeric File
- Appendix 4 - Run 01 Data File
- Appendix 5 - Run 01 Calibrated Comparison File
- Appendix 6 - Run 01 Interpolated Data File (cm<sup>-1</sup> units)
- Appendix 7 - Run 01 Interpolated Data File (micron units)
- Appendix 8 - Figures 30 - 65



Tables	Page
Table 1 - Mission 8202 Flight Parameters	39
Table 2 - Sample AFGL Mission 8202 File Header	41
Table 3 - Effect of Aerosol Model on Radiance Values	49
Table 4 - Comparison of LOWTRAN PC vs Mainframe Data	50
Table 5 - Results of the Kolmogorov-Smirnov Test	61
Table 6 - Summary Results From "limited" Percent Difference Comparisons	65
Table 7 - Statistics of "limited" Percent Difference Comparisons	67

## Figures

	Page
Figure 1 - Solar Irradiance	7
Figure 2 - Total Transmittance	8
Figure 3 - Water Vapor Transmittance	9
Figure 4 - CO <sub>2</sub> Transmittance	10
Figure 5 - N <sub>2</sub> O Transmittance	11
Figure 6 - CH <sub>4</sub> Transmittance	12
Figure 7 - Hemispheric Viewing Angles for Equation 2	15
Figure 8 - Geometry for Path Viewing	24
Figure 9 - Geometry for Optical Correction Factor	33
Figure 10 - Mission Geometry	38
Figure 11 - Smoothed Correction Curve	44
Figure 12 - Corrected Response Curve (With Neutral Density Filter)	45
Figure 13 - Corrected Response Curve (Without Neutral Density Filter)	46
Figure 14 - AFGL & MODTRAN(270K BB, .1 Emitter) Run 02	54
Figure 15 - AFGL & MODTRAN(285K BB, .1 Emitter) Run 02	55
Figure 16 - AFGL & MODTRAN(285K BB, .2 Emitter) Run 02	56
Figure 17 - AFGL & MODTRAN(285K BB, .15 Emitter) Run 02	57
Figure 18 - MODTRAN and AFGL Data, Run 01	58
Figure 19 - LOWTRAN and AFGL Data, Run 01	59
Figure 20 - Number of MODTRAN "limited" Points	69
Figure 21 - Number of LOWTRAN "limited" Points	70
Figure 22 - Percent of MODTRAN "limited" Points	71
Figure 23 - Percent of LOWTRAN "limited" Points	72
Figure 24 - MODTRAN Mean % Difference	73
Figure 25 - LOWTRAN Mean % Difference	74
Figure 26 - MODTRAN Median % Difference	75
Figure 27 - LOWTRAN Median % Difference	76
Figure 28 - MODTRAN Standard Deviation	77
Figure 29 - LOWTRAN Standard Deviation	78
Figure 30-38 - MODTRAN % Difference Plots (Odd Runs)	*
Figure 39-47 - MODTRAN % Difference Plots (Even Runs)	*
Figure 48-56 - LOWTRAN % Difference Plots (Odd Runs)	*
Figure 57-65 - LOWTRAN % Difference Plots (Even Runs)	*
Figure 66 - MODTRAN Median % Difference (Odd Runs vs Zenith Angle)	81
Figure 67 - MODTRAN Median % Difference (Even Runs vs Zenith Angle)	82
Figure 68 - LOWTRAN Median % Difference (Odd Runs vs Zenith Angle)	83
Figure 69 - LOWTRAN Median % Difference (Even Runs vs Zenith Angle)	84

\* = Appendix 8

## 1. INTRODUCTION

Proper interpretation of events viewed through the earth's atmosphere requires that the effects of atmospheric transmission and radiance be quantified when analysis of the remotely sensed data is performed. Computer models of the atmosphere have been developed to allow system designers and data analysts to perform this quantification. Two of the more commonly used models are LOWTRAN and MODTRAN, developed by the USAF Geophysics Laboratory. These models are computer codes which calculate atmospheric transmission and background radiance in the ultraviolet (UV) through infrared (IR) regions of the electromagnetic spectrum.

Traditionally, remote sensing has been performed within a viewing cone  $\pm 45^\circ$  from earth normal, either uplooking or downlooking. This self-imposed limitation by remote sensing system designers and data analysts was due to concerns over optical system quality and atmospheric effects. The increased call for remote sensing to fill needs in both commercial (industrial and environmental) and military areas is resulting in systems which are required to make use of wider viewing. Examples of this are the desire to use data from

meteorological satellites for use in nonmeteorological applications (eg like LANDSAT images) and broader area coverage from environmental missions of high altitude aircraft such as the NASA U-2.

This thesis reviews the modeling by the LOWTRAN and MODTRAN codes and compares them statistically against actual field measurements in high zenith angle viewing (60-90 degrees) with long path distances (>50 km). By testing the codes along these extreme viewing conditions it is hoped that the effectiveness of the modeling can be ascertained. Key to this focus on modeling errors is the use of high altitude measurements. By using high altitude measurements atmospheric variability is significantly reduced (the atmosphere is relatively stable and predictable at tropospheric and stratospheric altitudes). In a statistical sense this allows the effects of atmospheric uncertainty in any given measurement to be blocked out and only modeling errors should remain.

Determining the modeling errors is important for two general classes of problems. In many remote sensing applications either LOWTRAN or MODTRAN are used to determine the effect of the atmosphere on data collected in a measurement program. This effect is then used to back out the

losses to arrive at the original radiance of the object of interest. Modeling errors would thus lead directly to measurement errors in the processed data. These errors could lead to incorrect results in the analysis of that data.

The codes are also useful in this problem's inverse. Sensors are usually designed against a minimum signal of interest. This signal is often defined as the signal of the target less the attenuation of the atmosphere. The attenuation is determined using codes such as either LOWTRAN or MODTRAN. Errors in the codes can thus lead to incorrect system design. Incorrect designs are either lacking in sensitivity or have excess sensitivity resulting from overdesign. Either is an inefficient use of resources. The intent of this thesis is to determine the level of error in these codes due to modeling. This characterization can be used to isolate errors in both sensor design and data analysis to allow for more efficient utilization of scarce remote sensing resources.

## 2. BACKGROUND

Performance of this thesis required an understanding of three major areas, (A) atmospheric transmission and radiance modeling programs or codes, (B) data used as reference against which the codes will be compared, and (C) the statistical tools and terminology used in comparing the code output with these reference data. This discussion outlines these three major areas, their underlying theory, and the procedures used in performing the work associated with each area.

### 2.1. Atmospheric Transmission

The propagation of energy is central to remote sensing. Remote sensing can be taken to imply any sensing and analysis of events while not in direct proximity to them. This thesis shall employ a convention that defines remote sensing in a macroscopic sense; viewing of large scale events over relatively large distances. This is best defined by using the common examples of airborne or satellite sensing, although ground based systems can also be included. In addition, this thesis focuses on remote sensing performed in the part of the electromagnetic spectrum that can be optically imaged. This spans the region from 0.2 to 25 microns (ultraviolet through

deep infrared). Energy sensed in this region is dominated by two sources, propagation of the energy from the sun into the earth's atmosphere (primarily in the visible region) and thermal emissions from either the target or the earth background (dominant in the long wave infrared region).

Energy passing through the atmosphere is affected primarily by atmospheric scattering and absorption (Lillesand and Kiefer, 1987)<sup>1</sup>. Scattering is largely dependent on the size of the atmospheric constituents (molecules, particles, and aerosols) compared to the wavelength of the energy. Particles with a much smaller diameter than the wavelength of the energy cause Rayleigh scatter. Rayleigh scatter is inversely proportional to the fourth power of the wavelength, so shorter wavelengths are scattered much more than longer wavelengths. This form of scattering manifests itself in the blue color of the sky. Particles with diameters approximately the same diameter as the wavelength result in Mie scattering. Mie scattering, primarily caused by dust and water vapor, effects longer wavelengths than Rayleigh scatter. While both Rayleigh and Mie scatter have fairly well defined scattering patterns, not all scattering is so well behaved. Nonselective scatter, which results when the particle diameter is larger than the wavelength of the energy, scatters all wavelengths in random

patterns.

Absorption is the other primary source of loss in energy transfer through the atmosphere. Absorption is caused by the interaction of energy with the constituent gases of the atmosphere; including water vapor, ozone, and carbon dioxide. The characteristic energy absorption pattern of each of these gases results in blocking bands (where energy is absorbed) and window bands (where energy passes through with minimal absorption effects). Absorption is an inherently wavelength-dependent phenomenon.

The effects of atmospheric transmission losses may be seen by examining Figure 1. The exoatmospheric source function, solar radiation reaching the earth's outer atmosphere, is the dotted line. The irradiance reaching the sensor is shown as the solid line. The difference between the two lines is caused by the transmission losses described in Figure 2. Major contributors to this transmission curve are shown in Figures 3-6.

Since the object of this thesis is to examine solely the effects of the atmosphere on energy propagation, care must be taken to ensure that other errors are not induced. Remote sensing often looks at the reflectance or emission of a target. This thesis avoids the uncertainties of that problem



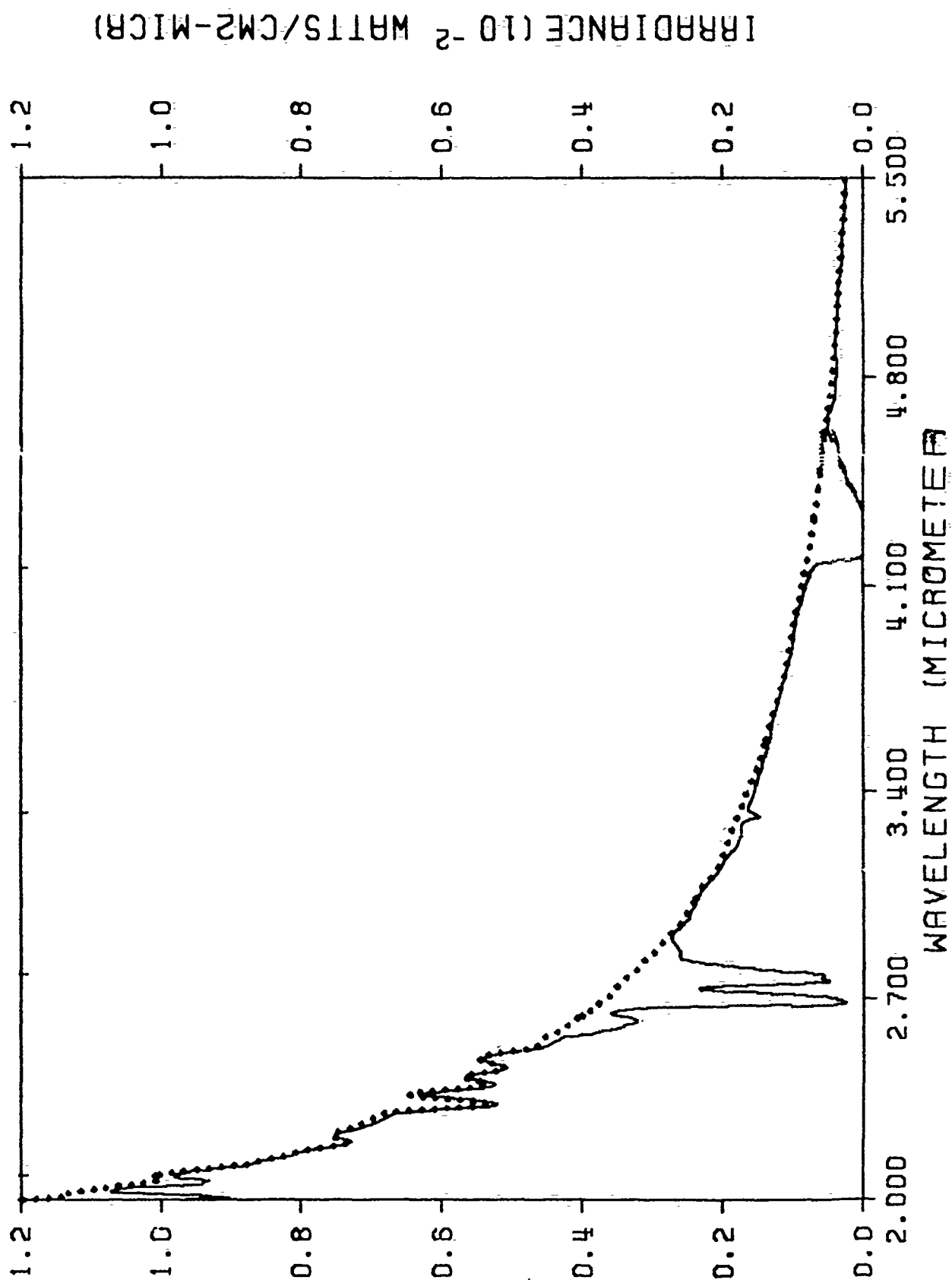
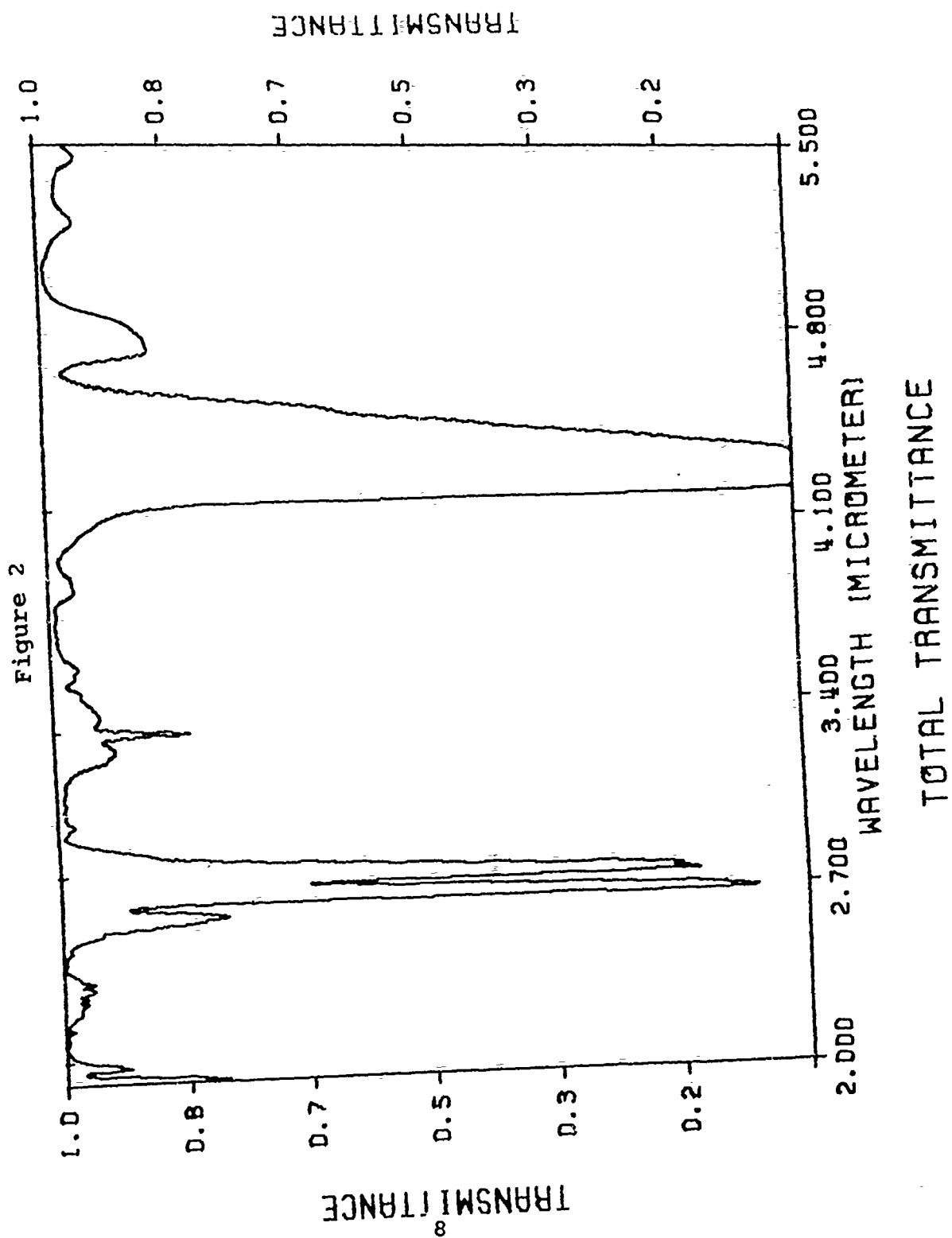


Figure 1  
IRRADIANCE (10<sup>-2</sup> WATTS/CM<sup>2</sup>-MICR)



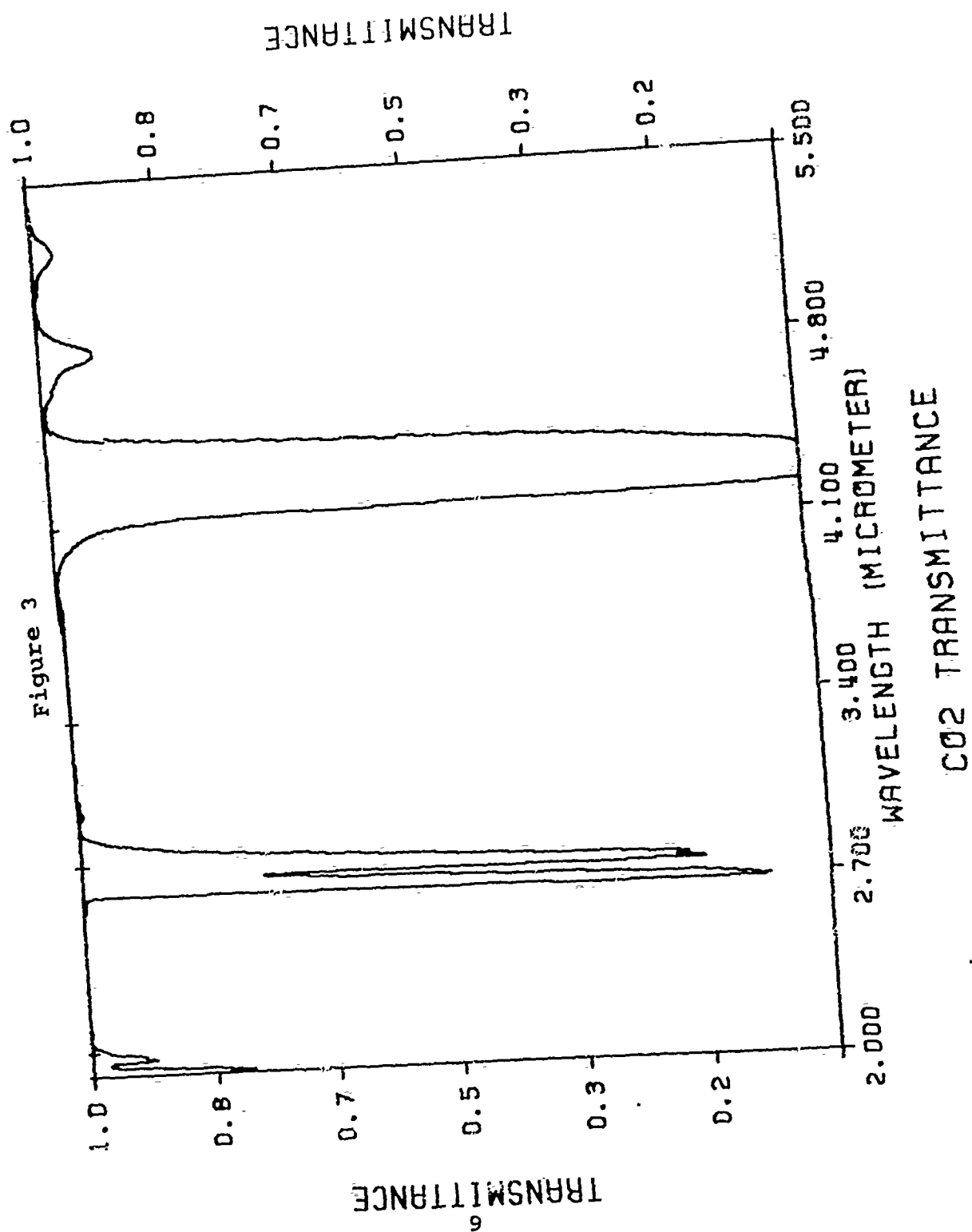
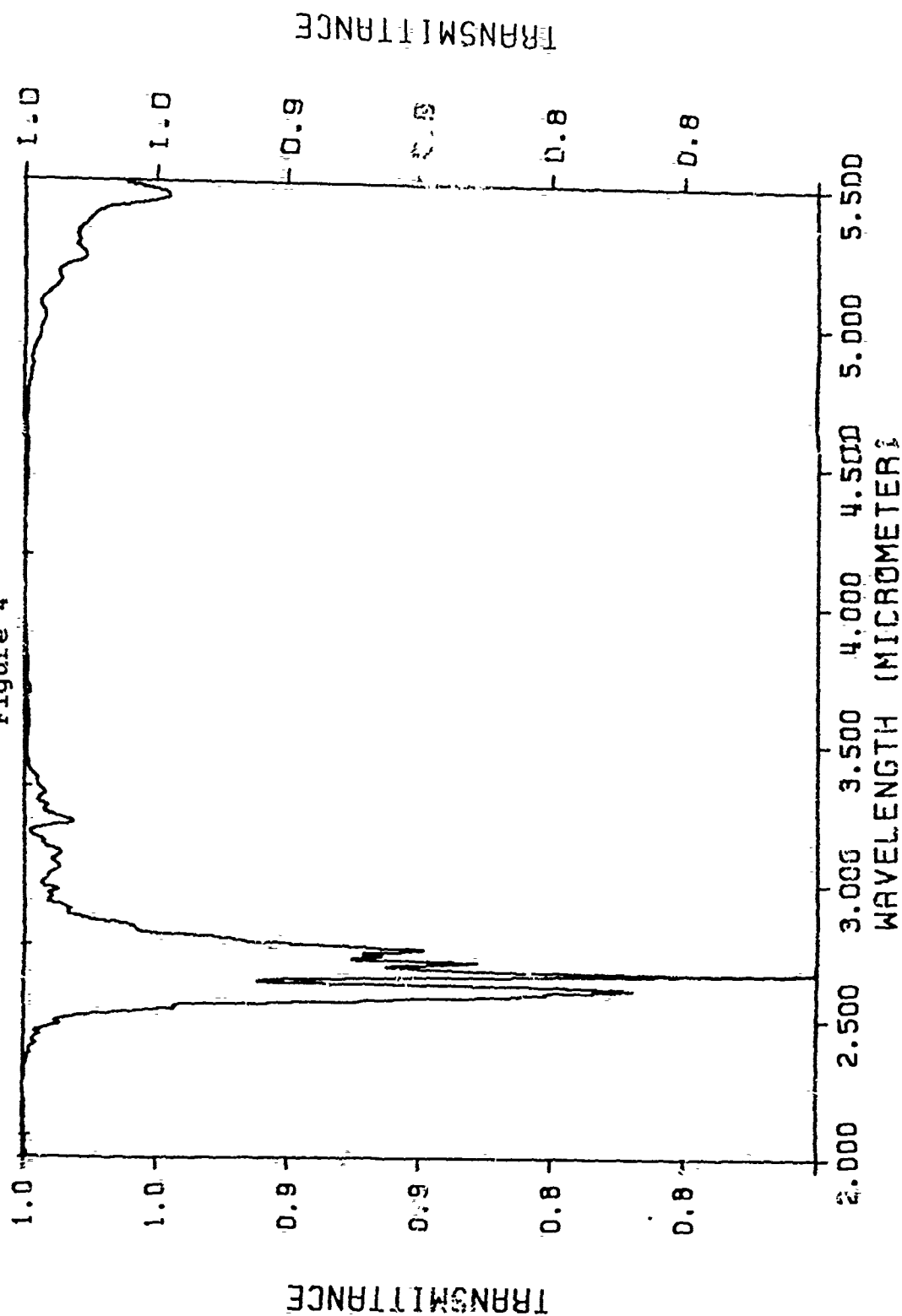
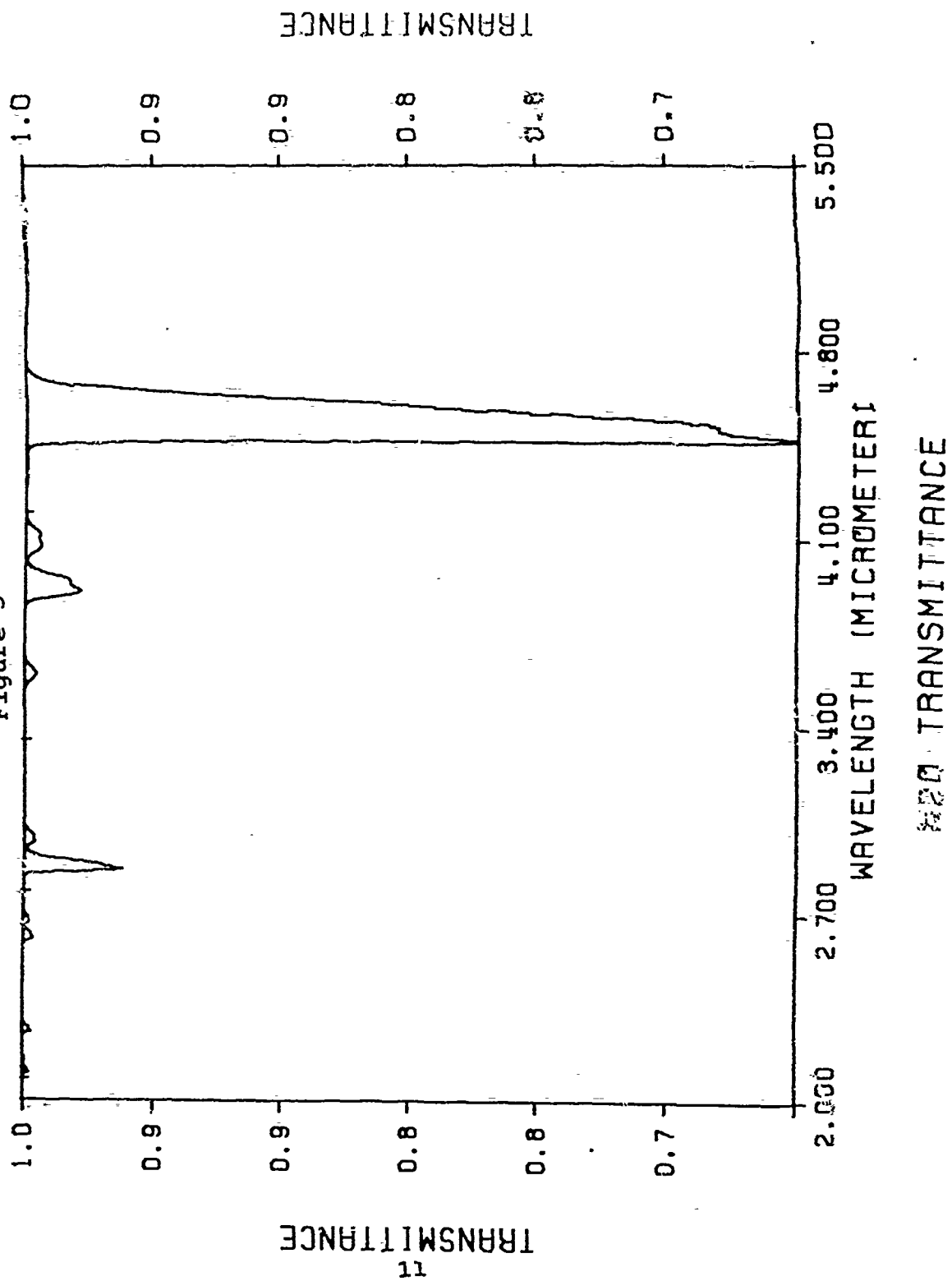


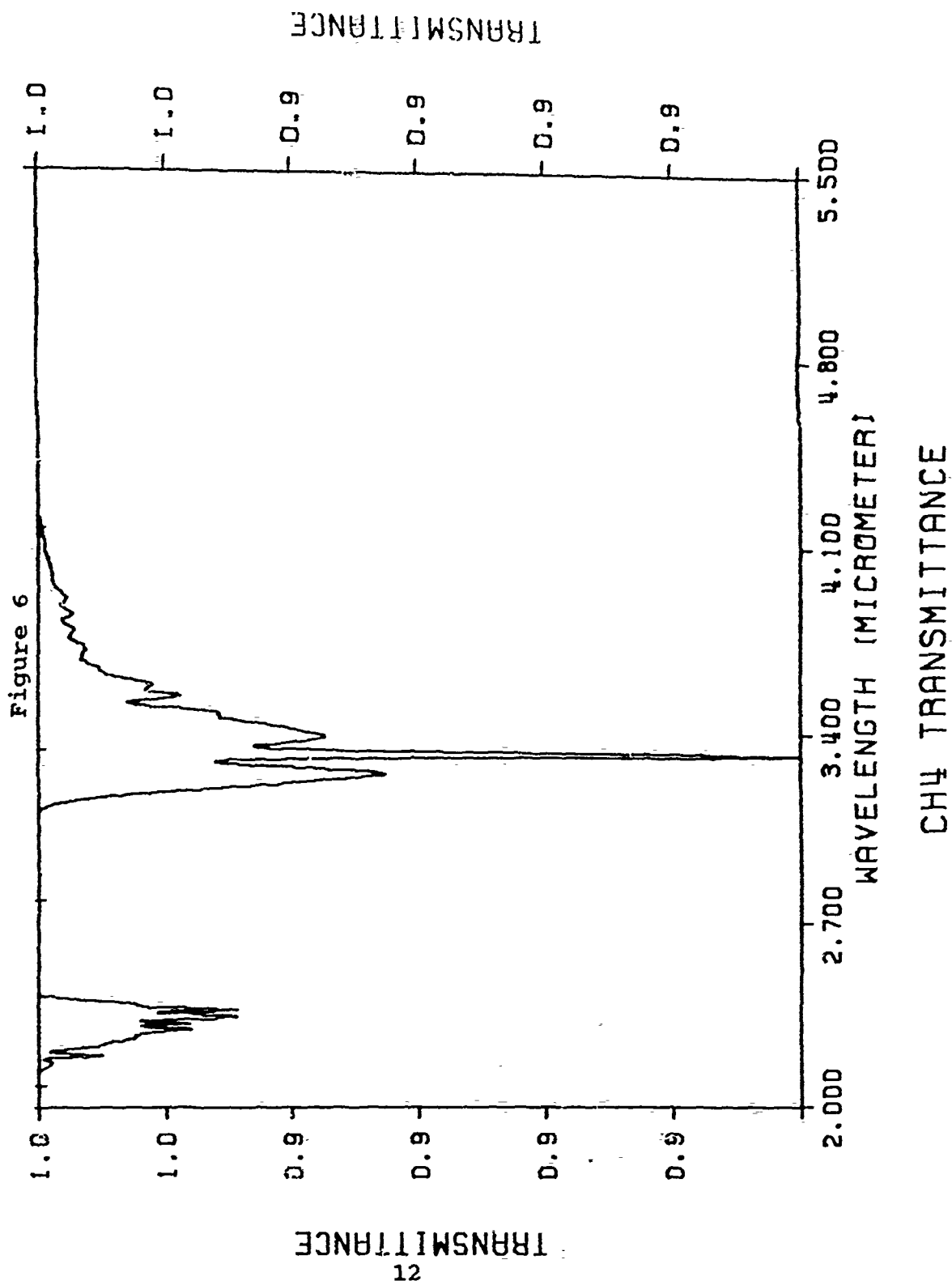
Figure 4



WATER VAPOR TRANSMITTANCE

Figure 5





(eg. specular vs lambertian reflection, wavelength dependent emission, effects of background) by looking directly at the sun. The sun may be approximated as an exoatmospheric blackbody with a temperature of  $\sim 6000^{\circ}\text{K}$ . Both LOWTRAN and MODTRAN have detailed solar source models which will make this assumption unnecessary. If this is taken as direct illumination of the focal plane, the only other sources of energy are path radiance due to the atmosphere having a finite thermal temperature and forward scatter of solar radiance.

The transmission through the atmosphere may be written using Beer's Law:

$$\tau_p = e^{-\beta z} \quad (1)$$

where  $\tau_s$  is the transmission through the path length  $z$  and  $\beta$  is the loss coefficient representing losses due to both scattering and absorption. This equation is solved for each homogeneous path of length  $z$ , and for each wavelength of interest, to find a point to point transmission for a given wavelength. A homogeneous path is defined as a path distance where the atmosphere has a constant temperature, pressure, and constituents.

Radiance at a sensor then may be approximately written including losses as (Schott, 1989)<sup>2</sup>:

$$L = (E'_s \cos \sigma e^{-\tau' \sec \sigma}) / \pi + \sum L_T (1 - \tau) \tau'' + \sum E'_s \tau_1 \beta(\theta) \tau'' \quad (2)$$

where  $L$  is the radiance received at the sensor (assuming a standard flat focal plane). Angles are defined for a hemisphere (Figure 7).

This term may be more easily understood by viewing it as three input terms. The first term is direct solar radiance:

$$L_{\text{solar rad}} = (E'_s \cos \sigma e^{-\tau' \sec \sigma}) / \pi \quad (3)$$

where  $E'_s$  is the exoatmospheric solar irradiance outside the atmosphere on a plane perpendicular to the axis of propagation,  $\sigma$  is the angle between the normal to the surface and the sun, and  $\tau'$  is the optical depth through the atmosphere normal to the earth at the target.

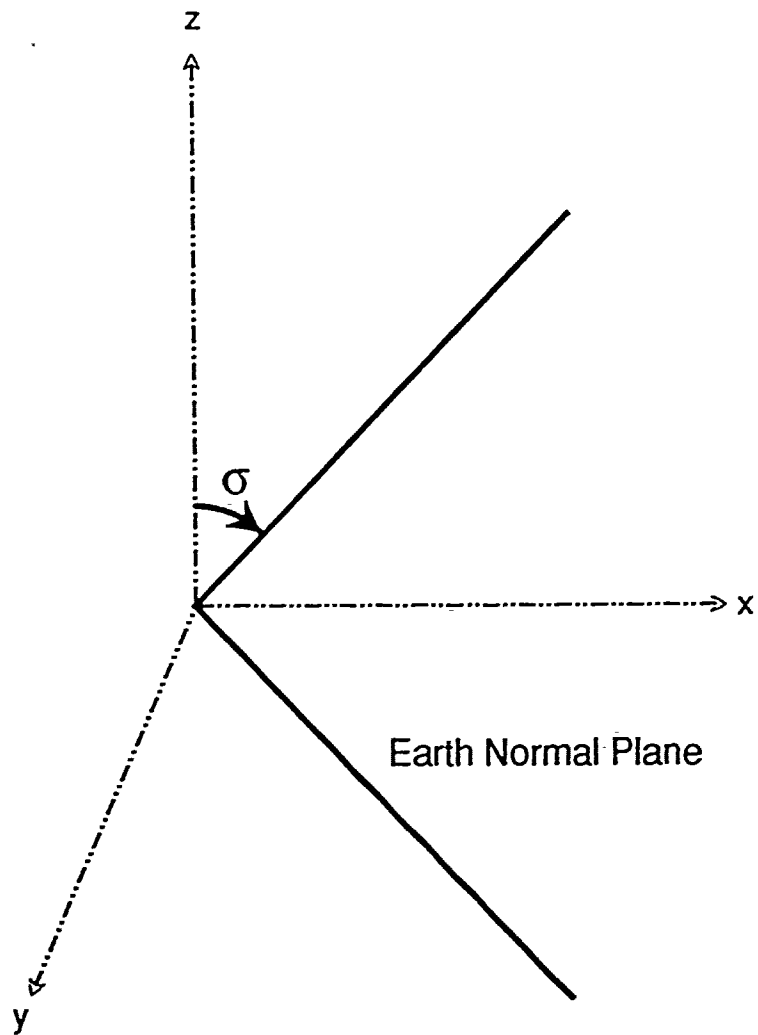
The second term is the path thermal radiance:

$$L_{\text{path thermal rad}} = \sum L_T (1 - \tau) \tau'' \quad (4)$$

where  $L_T$  is the radiance associated with a blackbody at the temperature ( $T$ ) of the atmospheric layer and  $(1 - \tau)$  is the emissivity of the layer, and  $\tau''$  is the transmissivity of the path from the layer to the sun. This term is summed over the homogeneous layers from the point of emission to the sensor.



Figure 7



Hemispheric Viewing Angle  
for Equation 2

The third term is the forward scattered radiance:

$$L_{forward\ scatt\ rad} = \sum E_s' \tau_1 B(\theta) \tau'' \quad (5)$$

$B(\theta)$  is the angle dependent loss coefficient for the scattered emission, and  $\tau_1$  and  $\tau''$  are the transmissivity of the portions of the path viewed prior to and after forward scatter. This term is summed over the homogeneous path distances traveled by the scattered radiation.

Thus, the energy received at the sensor is the energy emitted by the sun corrected for the angle by a cosine term, multiplied by the transmissivity of the atmosphere (corrected for the angle), and the thermal path radiance summed for each layer along the path (corrected for the emissivity of the path, its angle, and atmospheric transmission), and forward scattered energy of each layer along the path.

This equation, like equation 1, must be solved over homogeneous paths,  $z$ , and for each wavelength of interest. This gives rise to two effects that must be corrected for in the codes. The first is that the atmosphere is not composed of homogeneous paths. An approximation must be made to generate an estimate of atmospheric transmission, either through forced establishment of homogeneous layers (LOWTRAN), development of an approximation of an equivalent homogeneous layer path (LOWTRAN 5B and MODTRAN), or provision to allow for

solution of equations where local thermodynamic equilibrium does not exist (Fascode, a line by line transmission code also developed by the Air Force Geophysics Laboratory, (Smith, 1978)<sup>3</sup>). The second effect is known as curve of growth, an effect arising from the pressure broadening of absorption lines as a function of optical depth. This effect is not addressed in LOWTRAN (since it is a  $20 \text{ cm}^{-1}$  band model this effect is outside its effective resolution limits), but is addressed in LOWTRAN5B, MODTRAN and Fascode.

Neither LOWTRAN nor MODTRAN directly solve this radiative transfer equation. Instead, approximations are made to allow modeling to exist within the framework of available information and analytic tools.

## 2.2. LOWTRAN Model

The LOWTRAN model is a low resolution ( $20 \text{ cm}^{-1}$ ) model originally developed by the Air Force Cambridge Research Laboratory (now the Air Force Geophysics Laboratory) in 1972 (Selby et al, 1972)<sup>4</sup>. Since then, considerable improvements have been made, expanding the code to include radiance in addition to transmission. It is useful to review the form and improvements to the code beginning with version 5. LOWTRAN 5 (Kneizys et al, 1980)<sup>5</sup>, published in 1980, was a major software revision to the code and will be used as the baseline

reference for the rest of this discussion, as the extensions and improvements (Kneizys et al, 1983) (Kneizys et al, 1988)<sup>6,7</sup> incorporated since then were built onto version 5's basic structure.

LOWTRAN 5 calculates atmospheric transmission based upon molecular band absorption and scattering (the  $\beta$  term of Equation 1), aerosol extinction, and molecular continuum absorption. Absorption and scattering are not solved directly for the Beer's law formulation of equation 1. Instead, a single parameter (absorption coefficient,  $S/d$ ) look-up table is employed for each of four components. These components are water vapor, ozone, nitric acid, and the uniformly mixed gasses ( $\text{CO}_2$ ,  $\text{N}_2\text{O}$ ,  $\text{CH}_4$ ,  $\text{CO}$ ,  $\text{O}_2$ ,  $\text{N}_2$ ). Each band is represented by a single parameter generation function using a look-up parameter based upon the atmospheric conditions given in the inputs.

Improvement of these parameters is one of the major changes incorporated in the most recent version, LOWTRAN 7. The need to upgrade the accuracy in the parameters chosen for the band model approach was outlined in Zachor (1981)<sup>8</sup>. This article examined the accuracy of a band model approach to modeling the atmosphere. Zachor's primary conclusion was that the single parameter solution did not, and could not, contain

enough information to adequately describe the atmosphere. This was particularly true where multiple gasses were to be modeled in one curve. The move to independent curves for all of the major constituent gasses in LOWTRAN 7 addresses these concerns.

Using a method described by Pierluissi and Tsai (1987)<sup>9</sup> the uniformly mixed gases are now treated individually rather than as a group. The overall formulation is similar to that of the earlier LOWTRAN versions in using a look-up table rather than a direct solution to Equation 1. The effect of incorporating this change to the LOWTRAN 6 model was suggested and reviewed by Cutten (1986, 1988)<sup>10,11</sup>. Similarly, the band models for H<sub>2</sub>O have also been upgraded (Pierluissi et al, 1989)<sup>12</sup>.

The continuum model for water vapor was upgraded in LOWTRAN 6<sup>5</sup> to the form used in FASCODE 1B (Clough et al, 1981)<sup>13</sup>. This provided a major improvement in the 4.5-5.0  $\mu\text{m}$  region. These authors note that there are still great uncertainties in the modeling at the atmospheric transmission windows in the 10  $\mu\text{m}$  and 4  $\mu\text{m}$  regions. Improved results were achieved in the 4.5-5.0  $\mu\text{m}$  region.

The last major revision to the physics of the code has been in the treatment of scattering. In Version 5 all energy

scattered along the path was lost and no energy was scattered back in. As early as 1980 Ben-Shalom and others identified the effects that this would have over long path distances<sup>14</sup>. The lack of conservative scattering is estimated to cause errors as large as a factor of two under some viewing scenarios. LOWTRAN 6 introduced a single scattering model that allowed particles to scatter once before being lost. This still provided results significantly different from those shown using fully conservative scattering as suggested by Ben-Shalom. This error was because single scattering treated scattering as a source of extinction but still not as a source of radiance. Fully conservative scattering had been implemented in Fascode 2<sup>15</sup>, but this proved to be inaccurate as well since now all energy was conserved, leading to an overestimate of radiance.

All of these shortcomings were well described in an article by Isaacs, et al (1987)<sup>16</sup> in which they describe a multiple scattering modification to both LOWTRAN and FASCODE which greatly reduces errors (claimed to be less than 20% in all viewing geometries). Their approach is to model scattering using a finite stream approach. It is implemented in LOWTRAN 7. The actual results depend on the physical parameters of the single scattering albedo and the viewing

geometry (representing the scattering phase function).

Another modification that was performed to the LOWTRAN model was the inclusion of band models which gave true 5 cm<sup>-1</sup> accuracy. (Standard LOWTRAN output may be obtained at this resolution but it is interpolated from the 20 cm<sup>-1</sup> calculations.) This version, known as LOWTRAN 5B, developed by Robertson et al (1980)<sup>17</sup>, was more numerically accurate than the interpolation from the 20 cm<sup>-1</sup> output of LOWTRAN since it calculated these points. It also predated LOWTRAN 7's treatment of the uniformly mixed gases as separate parameters. However, it still lacked individual band models for all of the gasses described in LOWTRAN 7 and lack of multiple scattering. Due to the significant differences in the development of the band model parameters it will be discussed in detail at the beginning of the MODTRAN section.

Both LOWTRAN and MODTRAN treat the atmosphere as layers above the earth surface, not unlike layers of an onion around its core. This modeling form defines both how energy is propagated through the atmosphere (path length) and how the different atmospheric models are developed with their characteristic components.

The LOWTRAN 5 manual states that in general earth curvature has a greater effect on path length than refraction,

except at angles approaching 90°. With zenith angles close to 90° the increase in path length may be up to 30%. The effect of increasing path distances is to increase optical depth. Optical depth refers to the "thickness" of the viewing atmosphere. If the observer is looking straight up the depth is one atmosphere as each layer is traversed once by the energy beam along the shortest (normal) path. As the viewing angle is changed to more oblique zenith angles each layer of the atmosphere has a longer effective depth and the atmosphere appears denser. At the 90 degrees zenith viewing optical depth is approximately 39.65 atmospheres (Bemporad 1907)<sup>18</sup>.

Refraction within the atmosphere is governed by standard optical principles, principally Snell's law for the transition of energy between layers. The angle of refraction from one layer to another is defined as:

$$\sin\theta = n_0(R_0 + H_1) \sin\theta_0 / n(R_0 + z) \quad (6)$$

Where  $\theta$  is the zenith angle,  $n$  is the index of refraction between layers,  $R_0$  is the earth radius,  $H_1$  is the height of the lower layer, and  $z$  is the layer depth. The subscript 0 on the sine term indicates arrival. The term for effective path length between layers  $z_i$  and  $z_{i+1}$  is derived (Figure 8) where  $\beta$  is the angle subtended at the center of the earth as:

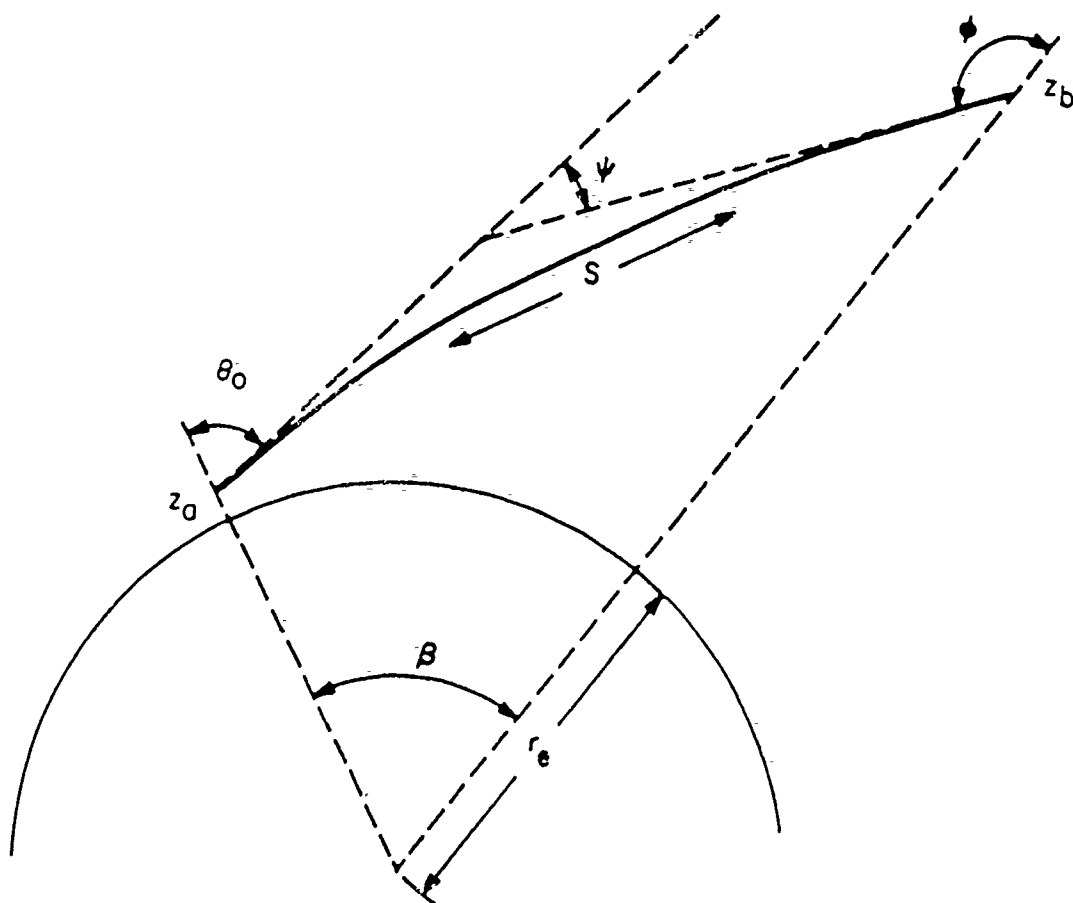


$$DS_i = (R_0 + z_{i+1}) \sin \beta_i / \sin \theta_i \quad (7)$$

Version 7 was modified to account for surface heights of other than sea level. (Previous versions enforced a uniform earth radius with all surface points at sea level.) LOWTRAN now generates a modified version of the Beer's law formula; most significant at altitudes up to six kilometers. This modification was suggested by Novoseller (1987)<sup>19</sup> and fully outlined by Shettle (1989)<sup>20</sup>. The effect of this modification is to compress the atmospheric layers so that areas where ground level is above sea level no longer suffer what amounted to truncation of the lower atmospheric layers. It should be noted that this does not change the molecular content at the upper altitudes, rather it effectively compresses the effects of lower altitudes into a single term so that the extinction is properly calculated.

Molecular content at an altitude is defined within the scope of the layer concept. Molecular quantities for important species are defined within the layers at predefined levels for the different aerosol models available in LOWTRAN and MODTRAN. The different models attempt to provide a reasonable approximation to conditions within a specified geographic area or type when measurements of atmospheric conditions are not available. Most changes in these

Figure 8



## Geometry for Path Viewing

conditions are seen in the lower atmosphere. Above these lower levels (altitudes  $> \sim 10$  km) the atmosphere is fairly uniform globally and seasonally, in the absence of volcanic activity.

In summary, the improvements to LOWTRAN focus on the addition of multiple scattering and separate band models for the most important atmospheric gasses. This is not to discount other major improvements such as the revised and highly upgraded extraterrestrial source function, aerosol models, and cirrus cloud models; it simply points out the major changes that justify a review of LOWTRAN capabilities now that more accurate results can be expected.

### 2.3. MODTRAN

MODTRAN can be viewed as an extension of the band model approach used in LOWTRAN 5B with the updated aerosol and scattering functions of LOWTRAN 7. Because of its close similarities to MODTRAN, LOWTRAN 5B is included in this section and will be discussed first.

LOWTRAN 5B was the first of the moderate resolution codes. It retained the same aerosol models as LOWTRAN 5, but utilized a significantly different method of developing the band model parameters.

It included, besides the increased spectral resolution

discussed earlier, addition of temperature dependence of the molecular absorption coefficients, and use of a multi parameter, Doppler-Lorentz band model.

The basic forms of LOWTRAN have their band model coefficients defined for an absorption coefficient,  $S/d$ , defined for standard temperature and pressure (STP; 1 atm, 273K). LOWTRAN 5B calculations for the coefficients are based on multiple temperatures (200, 225, 250, 275, and 300K) and line density,  $1/d$ , as well as the absorption coefficient  $S/d$ . Curve of growth effects are included through the combined Doppler-Lorentz band model. The Curtis-Godson approximation is used for multilayer transmittance calculations, replacing an inhomogeneous path with a homogeneous one by using average values for the various band model parameters.<sup>21</sup>

"MODTRAN<sup>22</sup> is a moderate resolution model and computer code used to predict atmospheric transmittance and background radiance in the microwave, infrared, visible, and near ultraviolet spectral regions (0 to 50,000  $\text{cm}^{-1}$  or 0.2 micron to infinity). The code maintains complete compatibility with LOWTRAN 7, specifically, MODTRAN retains all of the capabilities of the LOWTRAN 7 model. Both codes contain the same six built-in model atmospheres; spherical refractive geometry, aerosol models, clouds (water and ice), rain

attenuation and options to calculate single scattered solar/lunar radiance, solar/lunar irradiance and multiply scattered thermal and solar radiance.

"The MODTRAN code improves LOWTRAN's spectral resolution from 20 to 2  $\text{cm}^{-1}$  full width/half maximum (fwhm) with an option to vary the resolution between 2 and 50  $\text{cm}^{-1}$  (fwhm). The band model parameters were formulated from the HITRAN line atlas for twelve atmospheric gasses:  $\text{H}_2\text{O}$ ,  $\text{CO}_2$ ,  $\text{O}_3$ ,  $\text{N}_2\text{O}$ ,  $\text{CO}$ ,  $\text{CH}_4$ ,  $\text{O}_2$ ,  $\text{NO}$ ,  $\text{SO}_2$ ,  $\text{NO}_2$ ,  $\text{NH}_3$ , and  $\text{HNO}_3$ . These parameters were calculated for 1  $\text{cm}^{-1}$  bins from 0-17900  $\text{cm}^{-1}$  at five temperatures from 200 to 300K, all stored on an external data file which is accessed by the program (for the region from 17,900 to 50,000  $\text{cm}^{-1}$  the program defaults to the LOWTRAN 7 band parameters.)

"The transmittance is calculated with an equivalent-width formulation which accounts for the finite spectral width of each interval and the number of lines contained within the one  $\text{cm}^{-1}$  bin. LOWTRAN 7 uses a one-parameter band model (absorption coefficient,  $S/d$ ) plus molecular density scaling functions, while MODTRAN relies on three temperature dependent parameters, an absorption coefficient ( $S/d$ ), a line density parameter ( $l/d$ ), and an average line width. The absorption due to line centers, within the one  $\text{cm}^{-1}$  bin, is modeled separately from the absorption due to line tails (from regions

whose line centers are outside the specified fwhm interval). The absorption due to lines within each bin is calculated by integrating over a Voigt line shape. The line tail parameters consist of line contributions within  $\pm 25 \text{ cm}^{-1}$  (of the center of the fwhm region). The line tail absorption coefficient band model parameters are determined by integrating the Lorentz line shape over this interval of  $\pm 25 \text{ cm}^{-1}$ .<sup>23</sup>

The improvements to the band model parameters and supporting data structures (eg solar model, scattering model, and aerosol models) as well as the introduction of the true  $2 \text{ cm}^{-1}$  MODTRAN model suggests that computer models may now be expected to accurately model field data.

#### 2.4 Field Data

Determining the transmission and radiance accuracy of the two codes requires some form of standard against which the output is judged. In this research the object is to isolate out most possible sources of error. The simplest means of doing this would be to obtain the reference measurements in a laboratory. However, laboratory measurements cannot fully duplicate the effects on transmission and radiance in the atmosphere over long path lengths.

However, field measurements are not without their own shortfalls. The accuracy of the reference measurements can be

thought of as a function of the accuracy of the meteorological assumptions of the code inputs, the accuracy of the reference source, and the accuracy of the instrument taking the measurement. Chief among these difficulties is obtaining meteorological data to fully describe the atmospheric path through which the measurement is taken.

Ideally, meteorological data would be available over the whole path of interest. This is unrealistic for long paths. In the absence of meteorological data throughout the path model inputs will be used instead.

An additional difficulty is obtaining a good reference signal. In this thesis the sun will be used as the reference signal. The exoatmospheric source function of LOWTRAN and MODTRAN has recently been upgraded in all wavebands using data from numerous sources<sup>24</sup>; it will be assumed to be accurate (maximum discontinuity error is reported as three percent in the midwave infrared), ignoring the day to day variations induced by sun flares and other disturbances.

The accuracy of the field measurements is defined by the accuracy of the instrument. The measurements used as reference in this thesis were taken by the Air Force Geophysics Laboratory Flying Infrared Signatures Technology Aircraft (FISTA). The particular mission reference is Mission

8202 flown on 18 November 1981. The FISTA program is a suite of instruments flown on a NKC-135 aircraft. The particular instrument used for this experiment was interferometer 105. Measurements were taken of the setting sun over the Pacific Ocean from altitudes of 39,000 ft (11.89 km) and 29,000 ft (8.84 km); the majority of the measurements were obtained at the lower altitude. These heights are sufficient to allow use of the atmosphere models as inputs since most meteorological effects occur at lower altitudes. Additionally, the sky was observed to be cloud free, indicating a stable tropospheric viewing path.

Interferometer 105 is a Michelson type interferometer. Its output is a Fourier transform of the actual spectrum, which is inverse transformed to arrive at the spectral data. The theory of Fourier transform spectroscopy is covered in numerous articles and books (Huppi, et al, 1981 and Walker, 1979)<sup>2526</sup> and will not be discussed in this thesis. The FISTA instrument follows conventional design and analysis practices for this type instrument (Draft AFGL document, 1990)<sup>27</sup>.

Of greater interest is the sensitivity and resolution of the instrument and the method of background calibration and removal. The parameters of concern for this instrument (are



stated below (Mills, 1989)<sup>28</sup>:

Wavelength:	2.0 - 5.4 $\mu\text{m}$
Field of View:	1.0 degree circular
Spectral Resolution:	0.95 $\text{cm}^{-1}$
Detector:	InSb (77K)
Scan Time:	1 second
Sensitivity:	5E-10 W/cm <sup>2</sup> $\mu\text{m}$ .

Solar signatures will be significantly ( $\sim$  factor of  $10^4$ - $10^8$ ) above the instrument sensitivity for the solar viewing cases, errors should be confined to removal of background effects. This sensitivity margin will not exist for the background signatures; this level of sensitivity may not be sufficient for viewing background radiation.

Target irradiance is provided as the calibrated data product from FISTA missions. The calibration involves correction for off-axis optics effects. This calibration is performed prior to release of the data. Each annular region is described by a weighing factor. The annular zones are then used to weight the contribution to target radiance using the form of the following equation:

$$T = (T_o - gB_o) / (1 - g) \quad (8)$$

$T$  = target signal

$T_0$  = center radiance

$B_0$  = outer radiance

$g$  = fractional value assigned to outer component (Figure 9).

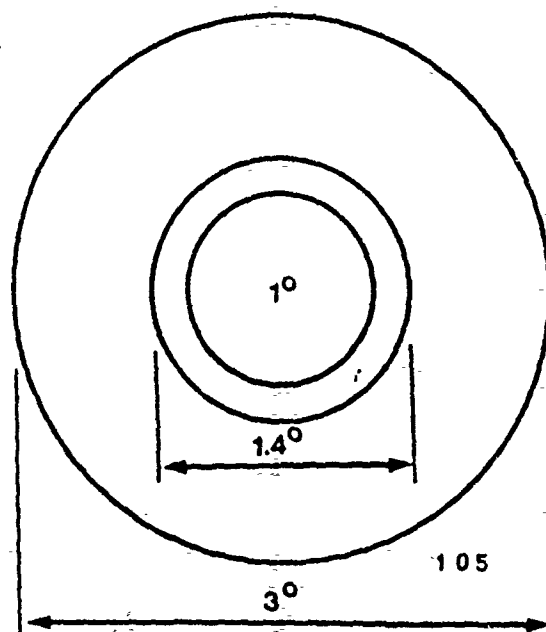
Since FISTA data has been extensively used and no problems have been noted with its calibration, it will be assumed that the FISTA data can be safely used as a standard against which to evaluate the codes.

## 2.5. Statistical Tools

Traditionally, differences between the codes and a standard have been defined as percent error over the waveband of interest. An excellent example of this type of review is available in a report by Cundiff (1986)<sup>29</sup>. In many aspects this report is a direct precursor to my thesis, examining the earlier versions of these codes. The percent difference measure is adequate only over discrete wavebands or for broadband integrated radiance.

A more statistically rigorous method for determining accuracy of the code generated estimates is obtained by comparing the code output directly with the field data, point for point. This comparison allows use of both the chi-squared and Kolmogorov-Smirnov tests. The Kolmogorov-Smirnov test is more appropriate for testing two data sets and is conservative

Figure 9



Off-axis Integrated Total Response Zones for  
Interferometers 105

for count data (as opposed to cumulative percent data). It is a nonparametric test designed specifically to test if two independent samples come from identically distributed populations (Daniel, 1990)<sup>30</sup>. By using this test, as well as focusing on percent differences in specific wavebands, the results of this thesis give a statistically sound determination of the errors associated with the two codes.

The Kolmogorov-Smirnov test is particularly applicable since the statistical tools typically used (such as analysis of variance) require an assumption of normal distributions, an assumption which cannot be made in these data. General linear model techniques are inappropriate for the determination of significant error in the match between the codes and data since the object is to determine the degree of error between points, not the ability of a polynomial model (equation) to fit the data.

## 2.6. Previous Efforts

Characterization of the errors associated with atmospheric codes is not a new or unique topic. Examples include many of the references already provided as well as others of a more general nature (Royer, 1988)<sup>31</sup>. Interest in the midwave IR bands over long path lengths limits the number of published reports considerably. Examples of these are

Cutten's publications<sup>9,10</sup>.

Rather more indicative of the efforts performed in this area are internal memos and reports like Cundiff<sup>28</sup>. This report used the same FISTA data as this thesis but earlier versions of the codes. Overall accuracy as well as band accuracy were examined as percent error figures. Extracts from this report are provided as Appendix 1. The percent differences showed maximum error in the bands where the models were the weakest, as well as when the zenith angle was increased. The charts representing these errors are presented in pages 15 and 17 of that report.

Summary results as presented from page 37 of that report are:

1. Errors increased as zenith angle increased,
2. Errors were largest in bands where the least modeling had been performed, eg the 2.1-2.4 micron CH<sub>4</sub> band,
3. Percent error measures provide adequate diagnostics only for identifying gross trends,
4. Percent error is inadequate to determining overall quality of the codes. An example of this is shown in the 2.1-2.4  $\mu\text{m}$  band at 91.7° zenith. In this graph there are clearly large errors on the order of 100 percent, but the average error is shown as near 50 percent.

Note that both FASCODE and LOWTRAN show extreme errors at near 90° zenith.

The errors near 90° zenith may not be a failure in the physical modeling but rather in the implementation. Richter (1985)<sup>32</sup> demonstrates that the dip in radiance near this angle is an artifact of the single scattering model. It is thus reasonable to expect significantly improved performance from LOWTRAN 7 and MODTRAN near 90°. This is due to the change in modeling from single scatter to multiple scattering effects in LOWTRAN 7 and MODTRAN.

Examination of individual bands is shown in Cutten's work as well as in a follow on (Lisowski, 1988)<sup>33</sup> to Cundiff's work also provided in Appendix 1. This work examined the CO<sub>2</sub> band in an attempt to chose a band model for use in a data reduction process.

The discussion shows how the computer models have evolved and describes the field data and statistical tools chosen for evaluation of the computer models. The next section will describe the approach used for this evaluation.

### 3. APPROACH

The goal of this thesis, a statistical estimate of error

between a computer model (LOWTRAN or MODTRAN) and a baseline measurement (the AFGL data set), required generation of both a calibrated field data set and a model data set. It was then necessary to make any corrections necessary to ensure that the two data sets were equivalent before making the error analysis. This section is logically divided into a discussion of these three activities.

### 3.1. Field Data Generation

The data utilized in this thesis was obtained on 18 November 1982 by the FISTA platform. The aircraft flew an orbit off of the Pacific Coast; with March AFB, CA the takeoff and landing point. During the orbit the setting sun was observed. Matching observations of the background sky were obtained on each orbit. The data are thus in pairs with the background observations oriented 180 degrees from the sun (Figure 10). The physical parameters for each observation pair are provided in Table 1.

The AFGL data set arrived as a VAX backup tape. Unfortunately, the files on the tape were in a format unique to the AFGL file storage system. The most efficient means of reading the files was to dump the files in both word and decimal format. These files were then edited using a text

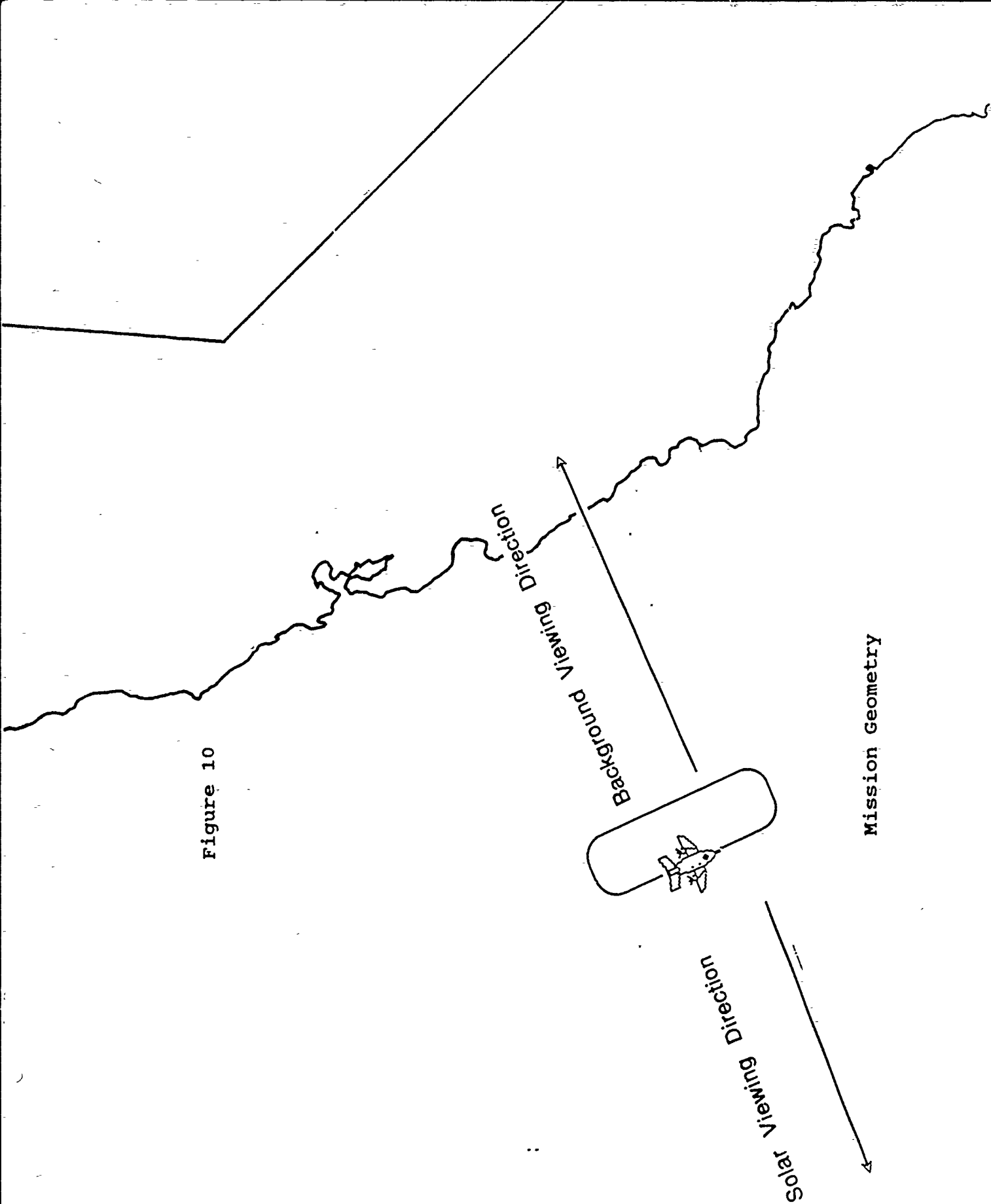


Figure 10



TABLE 1  
 Air Force Geophysics Laboratory (AFGL)  
 Flying Infrared Signatures Technology Aircraft (FISTA)  
 Mission 8202 18 November 1982  
 Interferometer 105 ( 1799.26-5199.15 wavenumbers)

Run Pair	GMT	North Lat.	West Long.	Alt (km)	Solar Elevation (Declination)	Solar Azimuth (° East of North)
1/2	21.980	34.67	121.63	11.887	61.96	214.29
3/4	22.195	34.96	121.86	11.887	63.63	216.94
5/6	22.428	35.21	121.96	8.839	65.55	219.85
7/8	22.620	34.96	121.80	8.839	67.00	222.49
9/10	22.859	34.80	121.60	8.839	69.05	225.61
11/12	23.100	34.83	121.84	8.839	71.08	228.21
13/14	23.286	35.00	121.95	8.839	72.86	230.17
17/18	23.736	34.68	121.59	8.839	77.31	235.25
19/20	23.921	34.86	121.78	8.839	79.18	236.94
21/22	0.069	34.84	121.63	8.839	80.81	238.48
23/24	0.338	35.00	121.57	8.839	83.78	241.03
25/26	0.530	34.65	121.81	8.839	85.53	242.66
27/28	0.687	34.88	121.84	8.839	87.34	244.03
29/30	0.824	34.82	121.74	8.839	88.92	245.29
31/32	0.976	34.66	121.84	8.839	90.48	246.54
33/34	1.096	34.68	121.67	8.839	91.98	247.65
35/36	1.205	34.82	121.68	8.839	93.26	248.55
37/36	1.296	34.76	121.67	8.839	94.30	249.31

Table 1 Notes:

1. 60 dB Neutral Density Filter used in all runs except 37.
2. Position Locations are for the midpoint of each data run.
3. Odd numbered runs are solar observations, even numbered runs are background observations.
4. Even numbered runs use position information generated during matching odd run.

editor to confirm the text information in the file header (already available in text format in the information provided by AFGL with the VAX backup tape, Appendix 2), and edit the data into a numeric format suitable for efficient processing on the computer. A sample text output is shown below.

Table 2

Sample Output of AFGL Mission 8202 File Header Run 01

Scale Factor:	0.95367E-06
Frequency Spacing:	1.92847
Beginning Frequency:	1799.26
Data values in the array:	1765
AFGL Mission Designator:	MISSION 8202
Archival Tape Designator:	FILE e:n00010 101.MIS202. NUU
	FROM R395-398/R491
Notes:	SUN ND IN

The numeric files were processed using the Minitab statistical spread sheet program. The routine written using this software read in the decimal numeric file, corrected the order of the data (the files should read left to right but the numeric file was inverse order, right to left), stacked the data into a single file (the AFGL tape contained numeric data in two records which together formed a composite numeric data set), and then ordered the data in column format. The output

of this process was a file with the raw calibrated counts, irradiance in watts/cm<sup>2</sup>-cm, the wavenumber for the particular irradiance data point in inverse centimeters and the equivalent wavelength in microns.

Files from the first run are provided as an example. The decimal numeric file is Appendix 3. The resulting data file is Appendix 4. Due to its length (1768 data points, over 30 pages of output) only the first and last pages of the file are provided in Appendix 4.

The relative calibrated irradiance is found by multiplying the raw count number (eg. 2026 for the first point) by the scale factor (.95367E-06 for this file). The effects of the neutral density filter utilized in this mission for solar viewing are included in this scale factor. The wavenumber is obtained by finding the offset from the initial wavenumber. The initial wavenumber is defined as 1799.26 and the step interval between each data point is 1.92847 wavenumbers. The wavenumber for the second data point is thus  $1799.26 + 1.92847 = 1801.19$  wavenumbers.

The next manipulation was to derive fully calibrated data. The irradiance values generated so far did not include any correction for sensor effects. This correction was applied by multiplying the data files point-by-point with

values from the smoothed correction curve (Figure 11). The smoothed response curve is derived from laboratory measurements taken in a Nitrogen atmosphere. The effect of this curve is shown in the plot of the corrected response curves with and without the neutral density filter (Figures 12 and 13). Only one correction curve was required. (The neutral density filter is a combination of a metal oxide filter and an adjustment to the instrument electronics and has a uniform linear effect across the spectrum of interest.<sup>34</sup>) This plot closely matches other laboratory reference curves for this and other AFGL interferometers.<sup>35</sup> The notch visible in both response curves is a result of adding a correction factor to compensate for CO<sub>2</sub> gas that will be present in the aircraft environment.

It was necessary to determine the irradiance in units of watts/cm<sup>2</sup> - micron. A simple linear interpolation was used to convert data from a reference to inverse centimeters to a reference of microns:  $x * \Delta \text{wavelength} / \Delta \text{wavenumber} / \text{a unit correction factor} = y$ , where  $x$  is irradiance (wavenumbers) and  $y$  is irradiance (microns). As example, for the second point,  $1.06\text{E-}06 * (.0154/5) / 1\text{E-}04 = 3.44\text{E-}04$ .

One final manipulation was required to place the data in the format desired for analysis. The AFGL data had a higher

Figure 11  
Smoothed Correction Curve

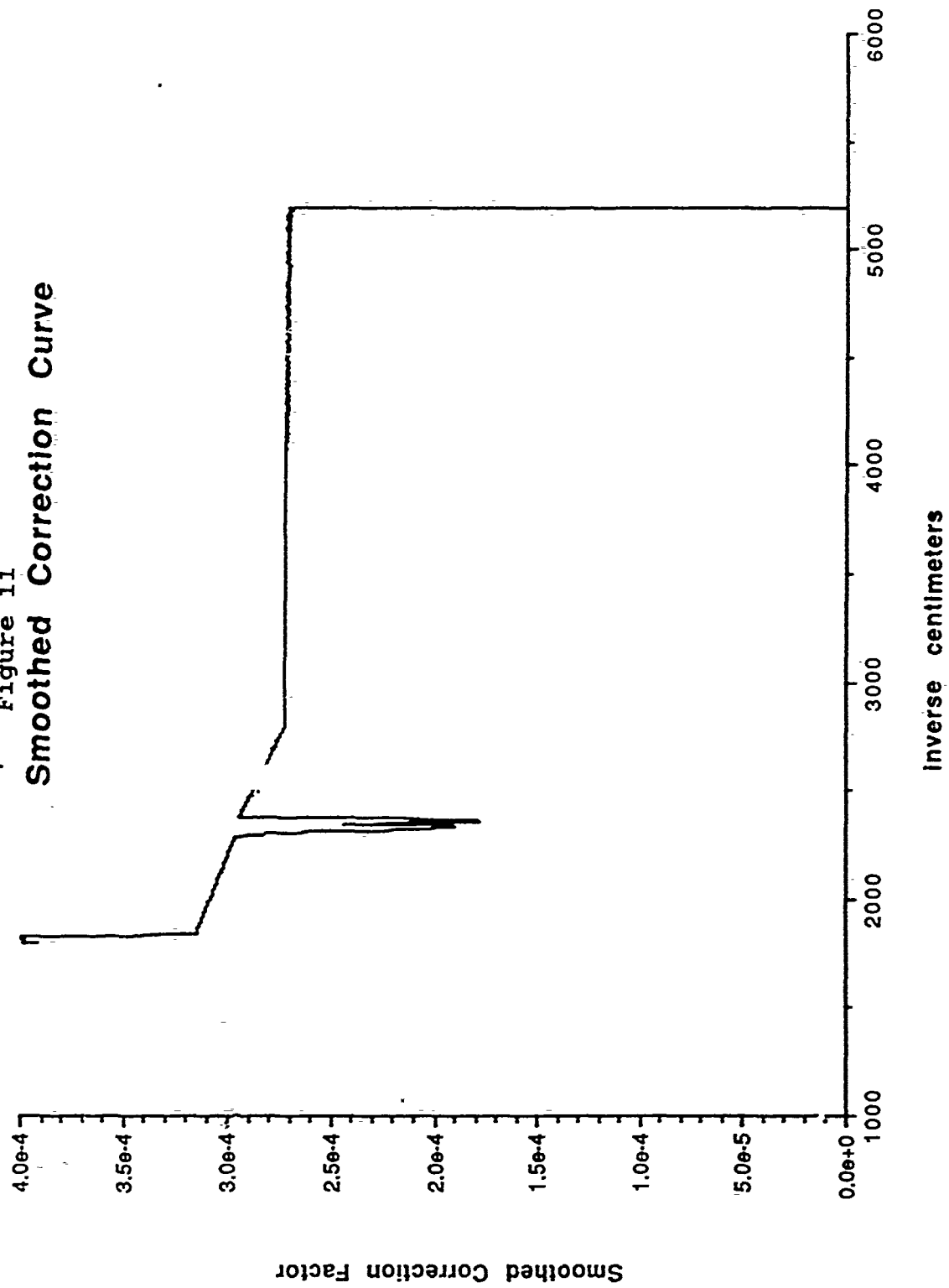


Figure 12  
Corrected Response Curve  
With Neutral Density Filter

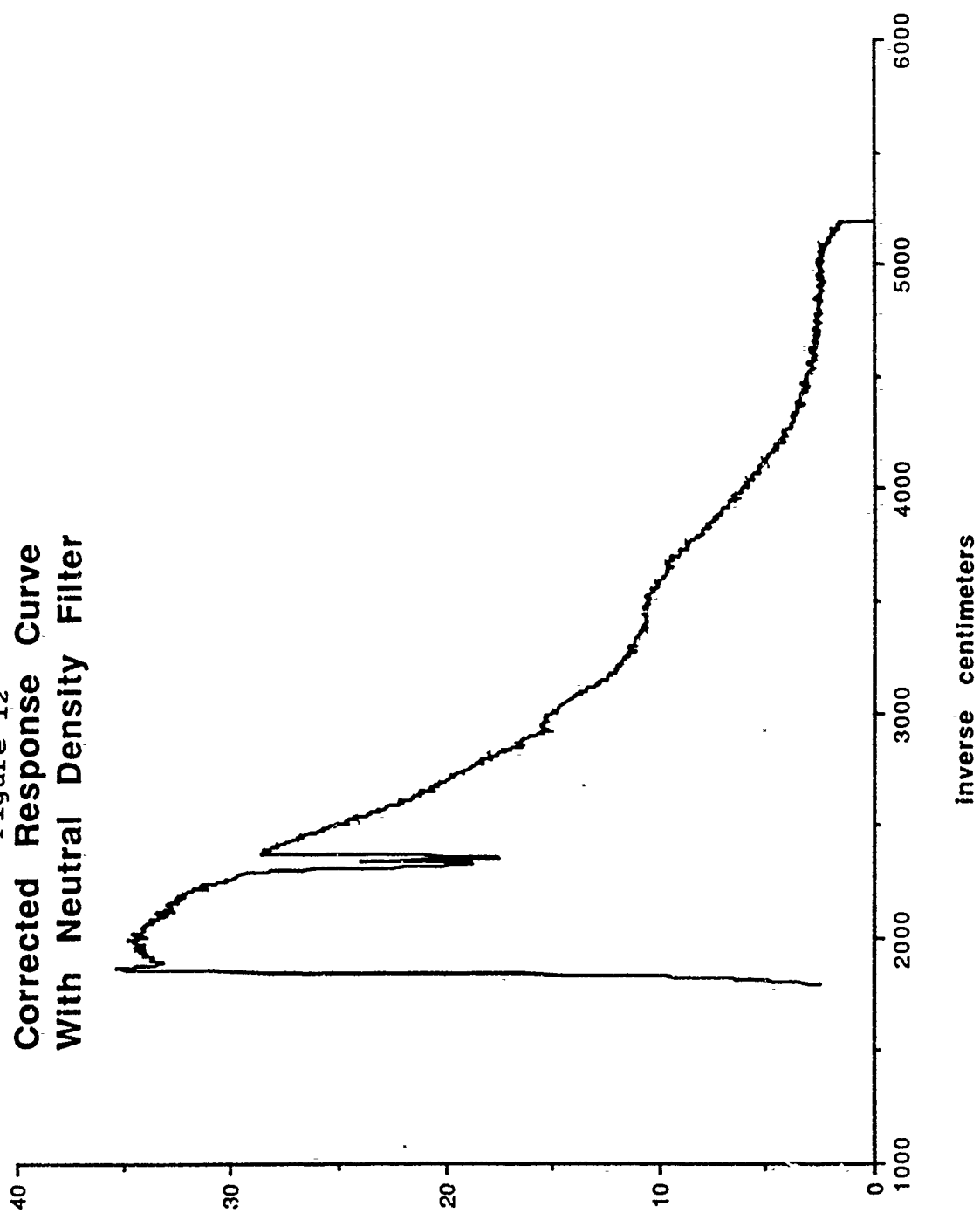
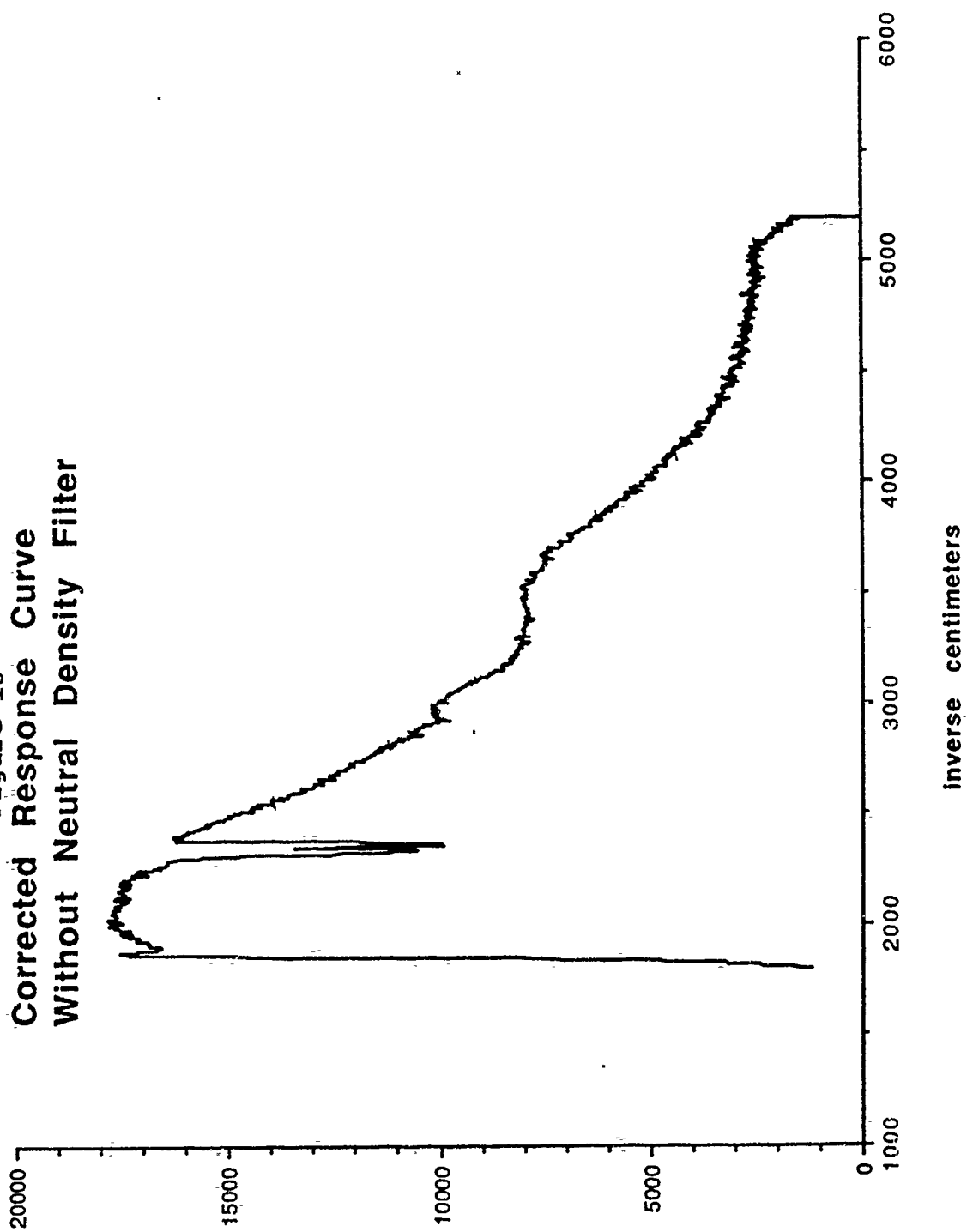


Figure 13  
Corrected Response Curve  
Without Neutral Density Filter





spectral resolution than LOWTRAN could output. Data to correspond to the five inverse centimeter LOWTRAN output was generated by interpolating the AFGL data to that resolution. This was accomplished using a shape conserving cubic spline interpolation routine available in the IMSL<sup>36</sup> software package. The resulting data file for use in the statistical comparisons is shown in Appendix 5. (All comparisons were referenced to wavelength values in microns.)

### 3.2. Computer Model Data Generation

Files were generated using both LOWTRAN 7 and MODTRAN for direct solar illumination and radiance with multiple scattering viewing conditions. The physical parameters used were those recorded by AFGL during the field data collection (Table 1). The mission data sheet did not provide a separate set of conditions for background viewing. Thus, the same physical conditions were used as inputs to generate both direct solar irradiation files and the paired radiance with multiple scattering files.

An annotation on the flight record stated that no clouds were visible in the viewing path. Due to the extremely long path lengths (ex. 183 km for Run 01 and 982 km for Run 29) it was necessary to utilize the standard atmospheres and aerosol models built into the codes. The most applicable standard

atmosphere was the tropical atmosphere. All of the other LOWTRAN 7 and MODTRAN model atmospheres were tailored to conditions of more northerly latitudes. Table 2 shows that similar results were obtained using midlatitude summer conditions (the next closest match to tropical viewing conditions) as the atmospheric model.

Several different aerosol models were examined as inputs. The most logical choice was the Maritime 23 km visibility. The Navy Maritime model was not used since it required knowledge of surface conditions in the viewing area during the preceding 24 hours. This data was not available. Analysis of Table 3 indicates that the most critical factor regarding aerosols in the computer models is simply their inclusion in the model inputs. The particular choice of aerosol model is of lesser importance.

The data for the LOWTRAN files were generated using the IBM Personal Computer (PC) based version of LOWTRAN. Table 4 shows that similar results were obtained for both the PC and mainframe versions. The PC data was used for comparison as it provided the most rigorous test and had been subject to the least review at the time of my thesis.

All of the AFGL data was in units of irradiance at the sensor. The output from the direct solar illumination models

Table 3  
Effects of Aerosol Models Choice on Radiance Values  
(Radiance values in Watts/cm<sup>2</sup>-ster-cm)

	Tropical Atmosphere				Midlatitude Summer
wave-number	No Aerosols	23 km Rural	5 km Rural	23 km Maritime	23 km Maritime
1800	3.67E-09	3.75E-09	3.75E-09	3.64E-09	3.75E-09
2050	7.77E-10	8.46E-10	8.46E-10	1.02E-09	8.46E-10
2300	4.78E-09	4.78E-09	4.78E-09	4.46E-09	4.78E-09
2550	2.80E-11	1.53E-10	1.53E-09	1.57E-09	1.53E-09
2800	1.51E-11	1.77E-10	1.77E-10	1.79E-10	1.77E-10
3050	1.33E-11	2.14E-10	2.14E-10	2.14E-10	2.14E-10
3300	1.24E-11	2.70E-10	2.70E-10	2.70E-10	2.70E-10
3550	1.39E-11	2.57E-10	2.57E-10	2.57E-10	2.57E-10
3800	2.34E-11	4.37E-10	4.37E-10	4.37E-10	4.37E-10
4050	4.06E-11	7.11E-10	7.11E-10	7.11E-10	7.11E-10
4300	4.48E-11	7.49E-10	7.49E-10	7.49E-10	7.49E-10
4550	7.03E-11	1.12E-09	1.13E-09	1.13E-09	1.13E-09
4800	1.05E-10	1.61E-09	1.61E-09	1.61E-09	1.61E-09
5050	1.49E-10	2.17E-09	2.18E-09	2.18E-09	2.18E-09

Table 4  
Comparison of LOWTRAN PC and Mainframe Results

wavenumber	Irradiance (Watts/cm <sup>2</sup> -cm)		% Difference
	PC	Mainframe	
1800	7.34E-07	7.14E-07	2.88
2050	9.64E-07	9.37E-07	2.88
2300	5.33E-09	5.18E-09	2.89
2550	1.55E-06	1.51E-06	2.65
2800	1.74E-06	1.69E-06	2.96
3050	1.91E-06	1.85E-06	3.24
3300	2.23E-06	2.17E-06	2.76
3550	1.74E-06	1.69E-06	2.96
3800	2.44E-06	2.38E-06	2.52
4050	3.22E-06	3.22E-06	0.00
4300	2.88E-06	2.79E-06	3.23
4550	3.60E-06	3.50E-06	2.86
4800	4.36E-06	4.24E-06	2.83
5050	5.01E-06	4.87E-06	2.87

Mean Percent Difference = 2.68

was in irradiance units but the output of the radiance with multiple scattering model is in radiance units. Since all of the AFGL data is in irradiance units it was necessary to convert the output of the radiance models to irradiance units. Using the formula outlined in Slater(1980)<sup>37</sup> the conversion from radiance to irradiance is defined by knowing the field of view of the sensor. The sensor has a nominal one degree field of view. The radiance values may be converted to irradiance values for this sensor by multiplying by  $2.39\text{E-}04$  steradians. (It was learned after completion of the thesis that AFGL uses an empirically derived value of  $2.5\text{E-}04$  value for converting values from this particular instrument.)

### 3.3. Data Set Equivalence

Even though both sets of data (field and computer generated) had now been established as calibrated sets with equivalent viewing conditions and units a final correction was found necessary. While attempting to compare the background files it was found that two sensor effects still existed that required correction.

The first effect was that the computer models were predicting results below the noise floor of the instrument. While not strictly a calibration issue, the effect was the same. Predictions below the noise floor have no meaning since

they cannot be obtained by the sensor. The correction for this issue was to set a noise floor for the computer values equal to the stated noise floor of the instrument. Any predicted values below this level were adjusted up by the value of the noise floor.

This adjustment allowed inclusion of points that otherwise would have had to have been discarded from the analysis. While it does not allow for full evaluation of the radiance portion of the models it does allow their evaluation within the bounds imposed by the instrument.

The second effect was apparent blackbody radiation affecting data in the longer (5.5 micron) end of the spectrum. This radiation is a result of any small temperature shift in the interferometer sensor system between the times of the cold calibration and the field collection. This effect is also believed to include emission from the telescope barrel and the instrument optics. This effect that is not removed using the smoothed correction curve<sup>38</sup>. (The smoothed correction curve is developed from the cold calibration data.) The effect was on the order of  $7\text{E-}09$  Watts/cm<sup>2</sup>-micron at its maximum (near the 5.5 micron region).

The correction was to add greybody radiation as if the optics had been a blackbody source. A series of curves was

plotted against the data. These curves utilized blackbody temperatures from 270 to 285K and emissivities from .1 to .2.

A curve from a blackbody with emissivity of 15% and temperature of 285 degrees Kelvin was found to provide a good fit to the data (Figures 14-17). These values were felt to be reasonable since the optics material,  $\text{CaF}_2$ , has a stated emissivity of 10% for pure material<sup>39</sup> and the temperature is also a reasonable approximation for a transition between the outside and inside of the aircraft platform. Figures 18 and 19 provide a graphic reference for the similarities between the calibrated MODTRAN and LOWTRAN and the AFGL data.

#### 4. RESULTS

Two sets of tests were made on the data sets. The results of the Kolmogorov-Smirnov test determine if the field data and computer data follow the same distribution. The results of the percent difference test provide details at specific wavelengths and insight into error trends.

Equivalent inputs were used in both sets of tests. For background viewing conditions (even numbered AFGL runs) the comparison took the form:

Figure 14  
 AFGL and MODTRAN  
 with 270K BB and .1 Emitter  
 Run 02

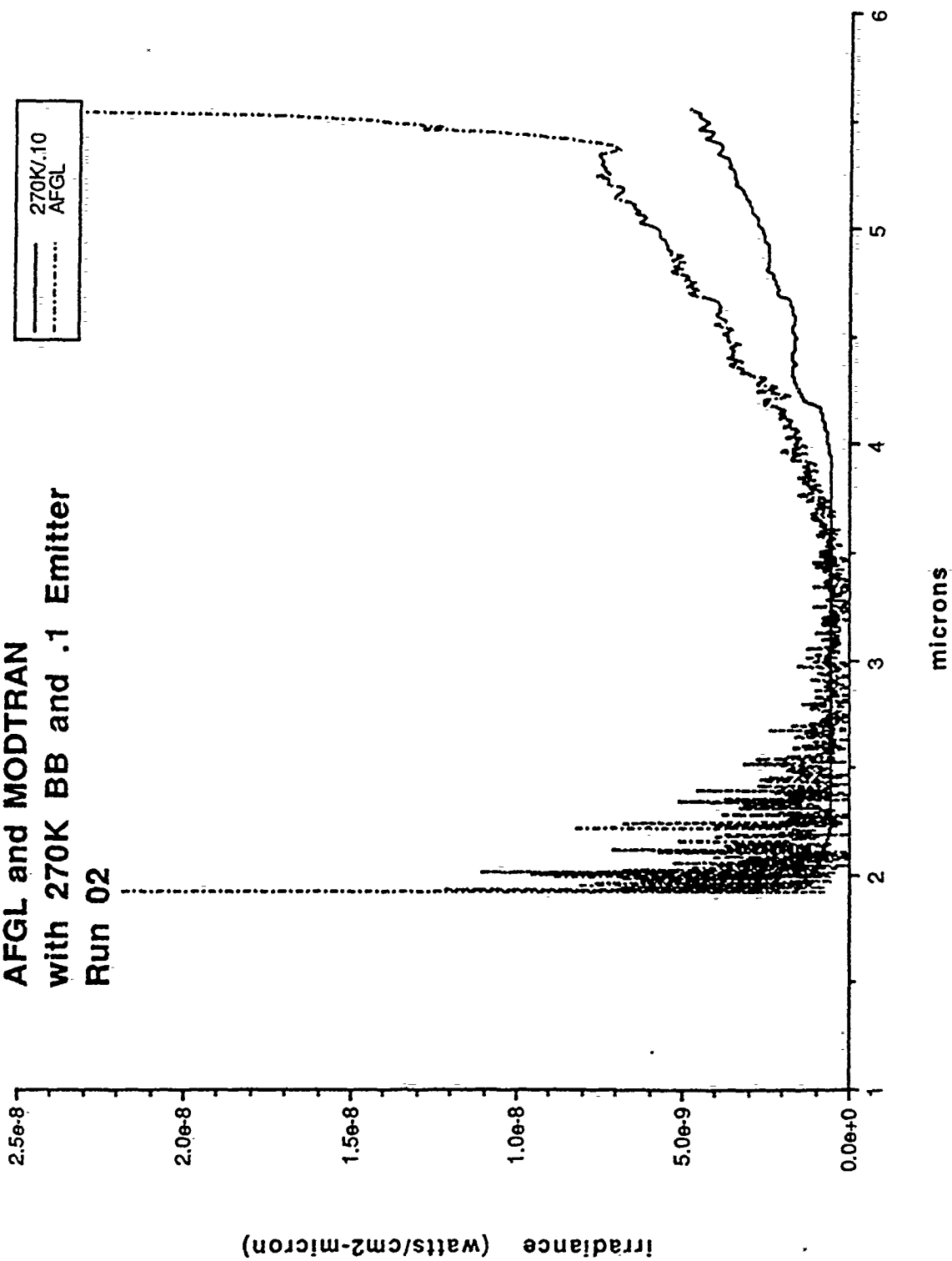




Figure 15  
AFGL and MODTRAN  
with 285K BB and .1 Emitter  
Run 02

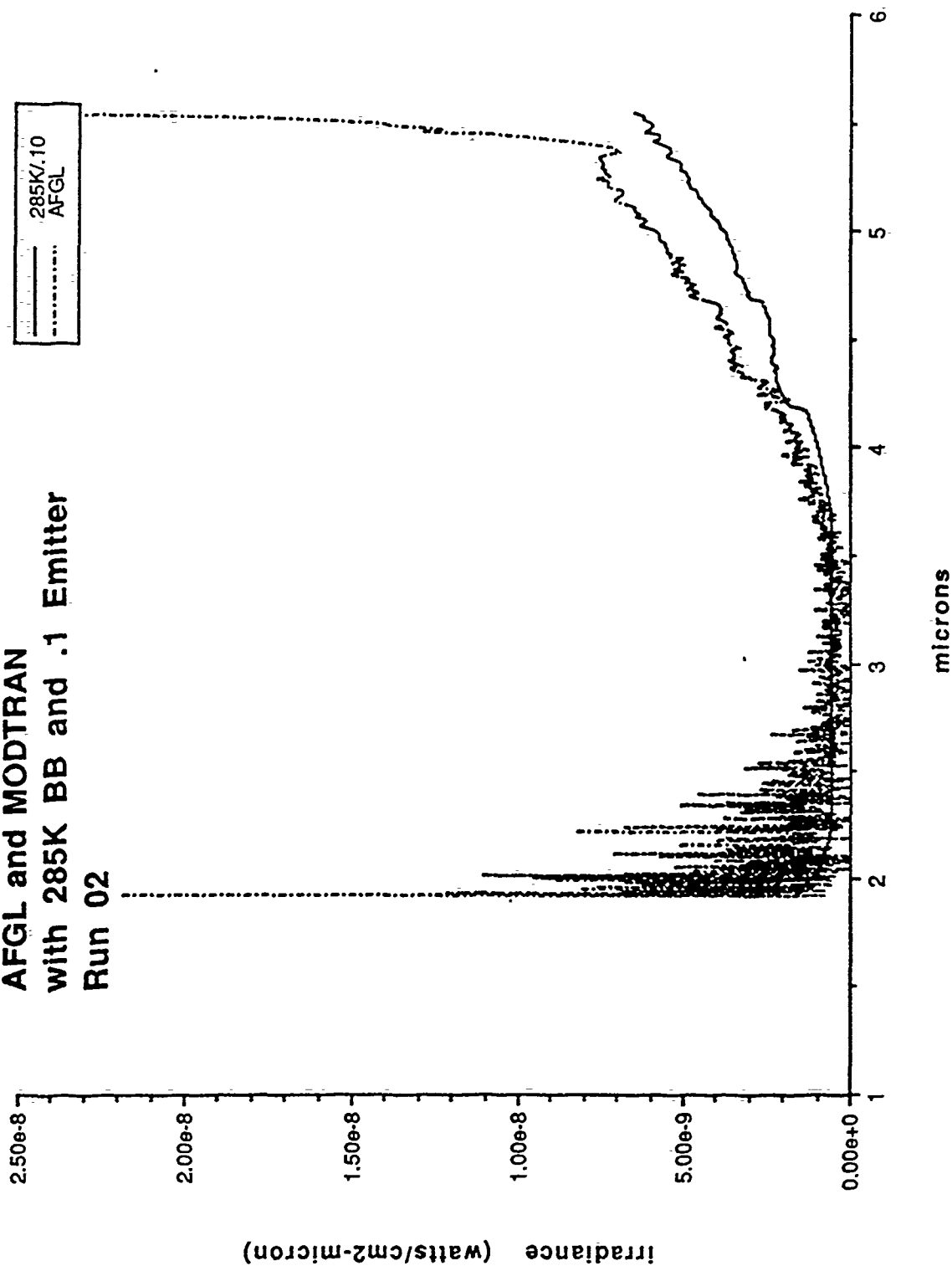


Figure 16  
AFGL and MODTRAN  
with 285K BB and .2 Emitter  
Run 02

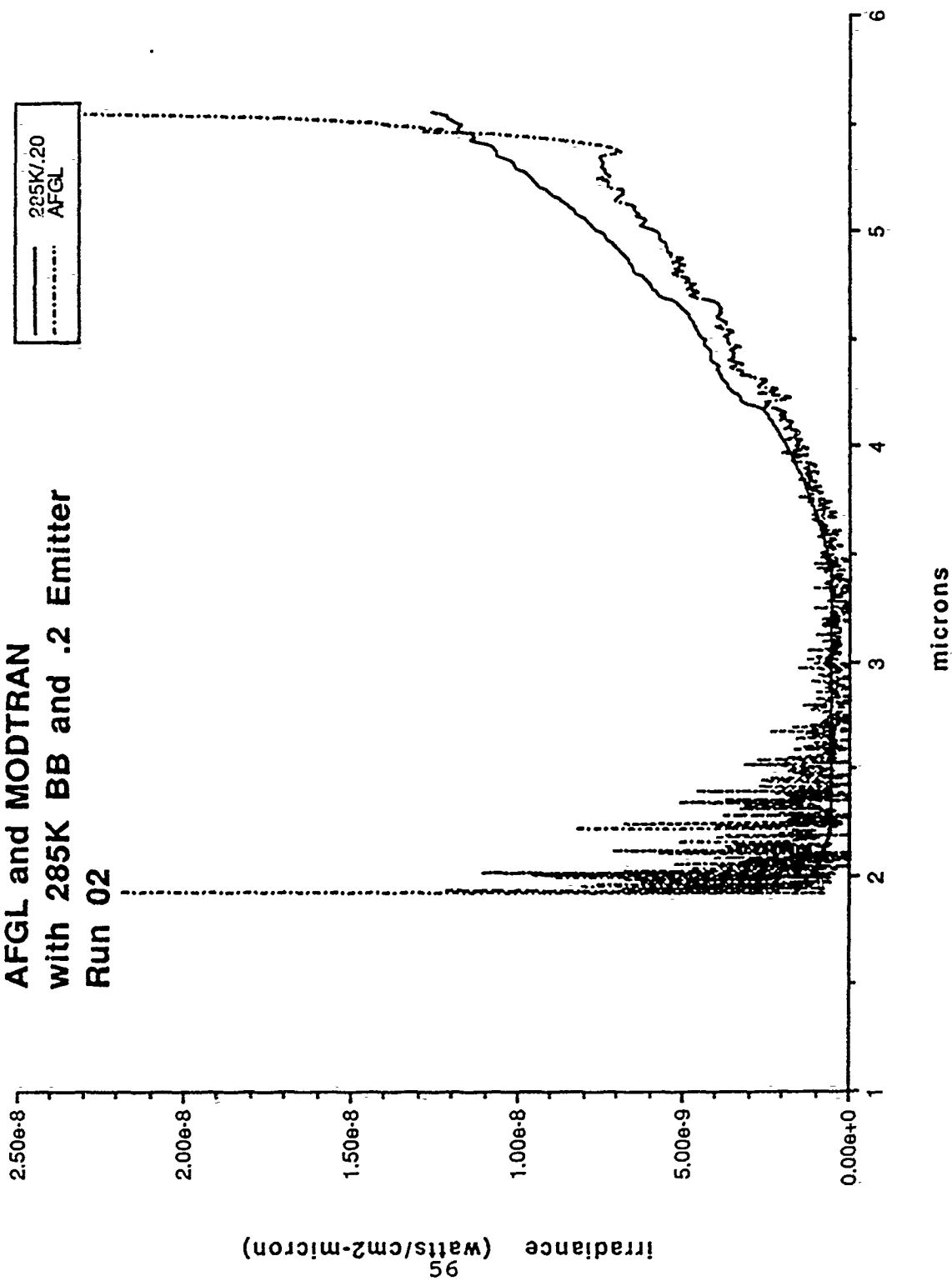


Figure 17  
 AFGL and MODTRAN  
 with 285K BB and .15 Emitter  
 Run 02

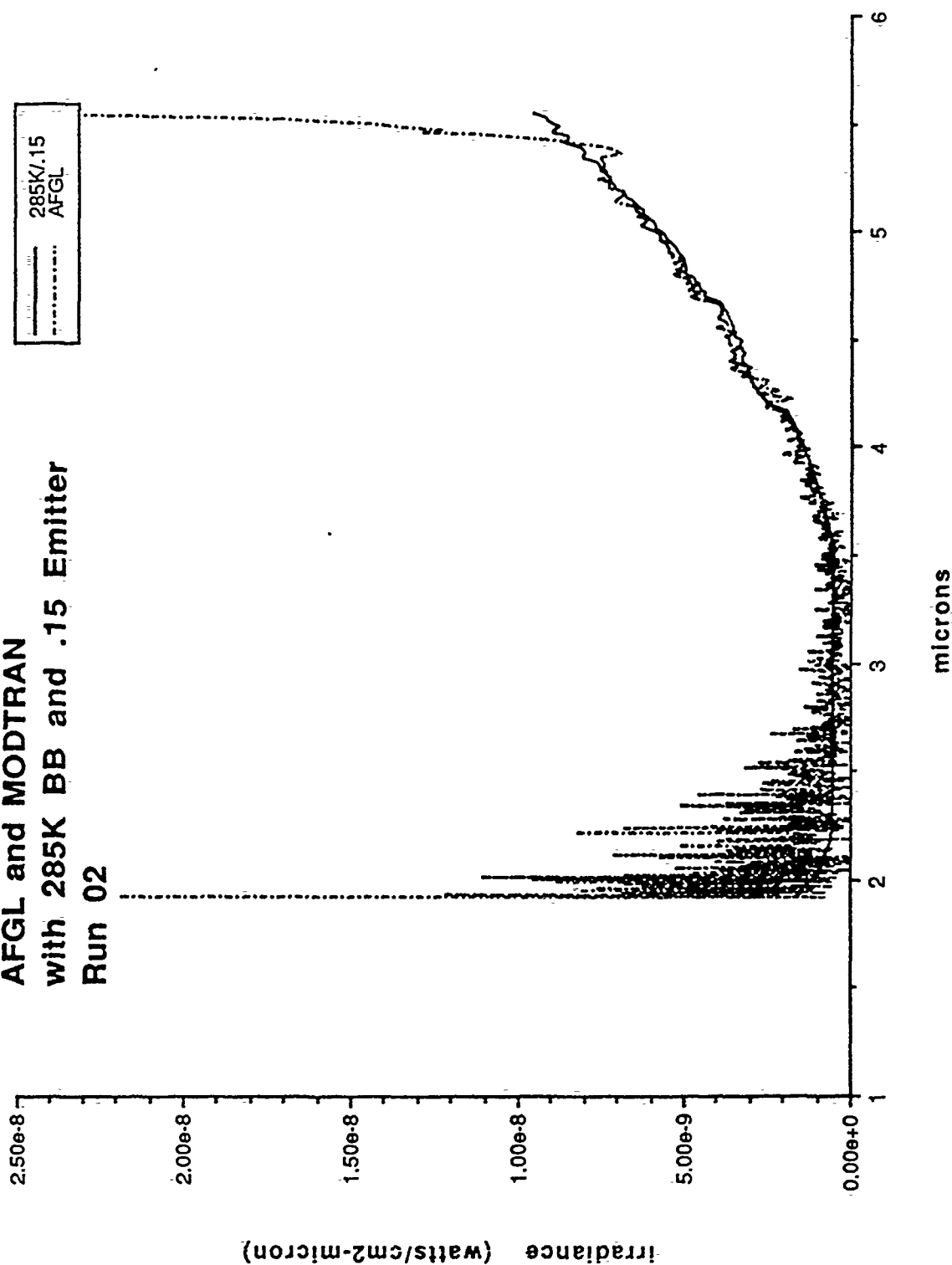
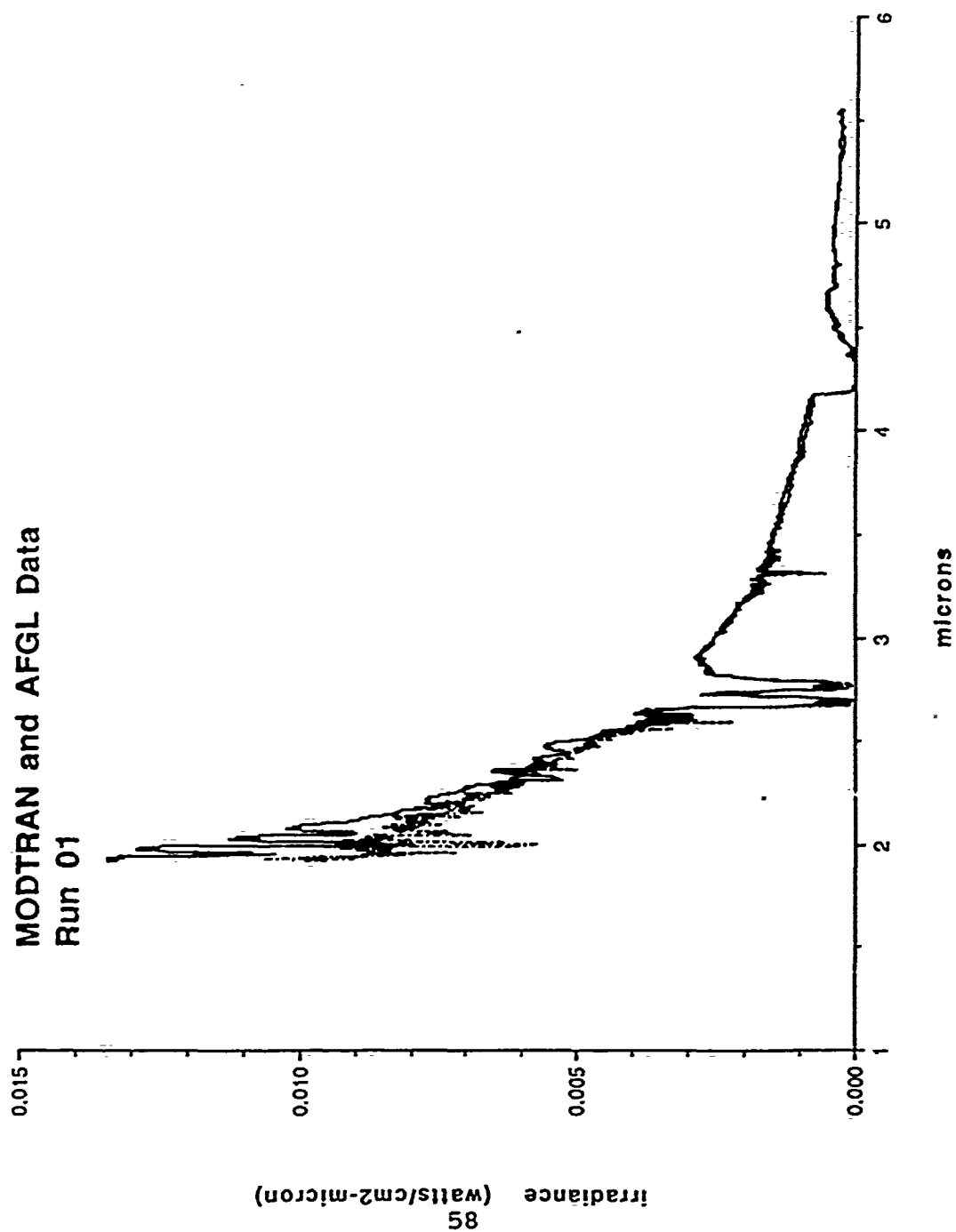


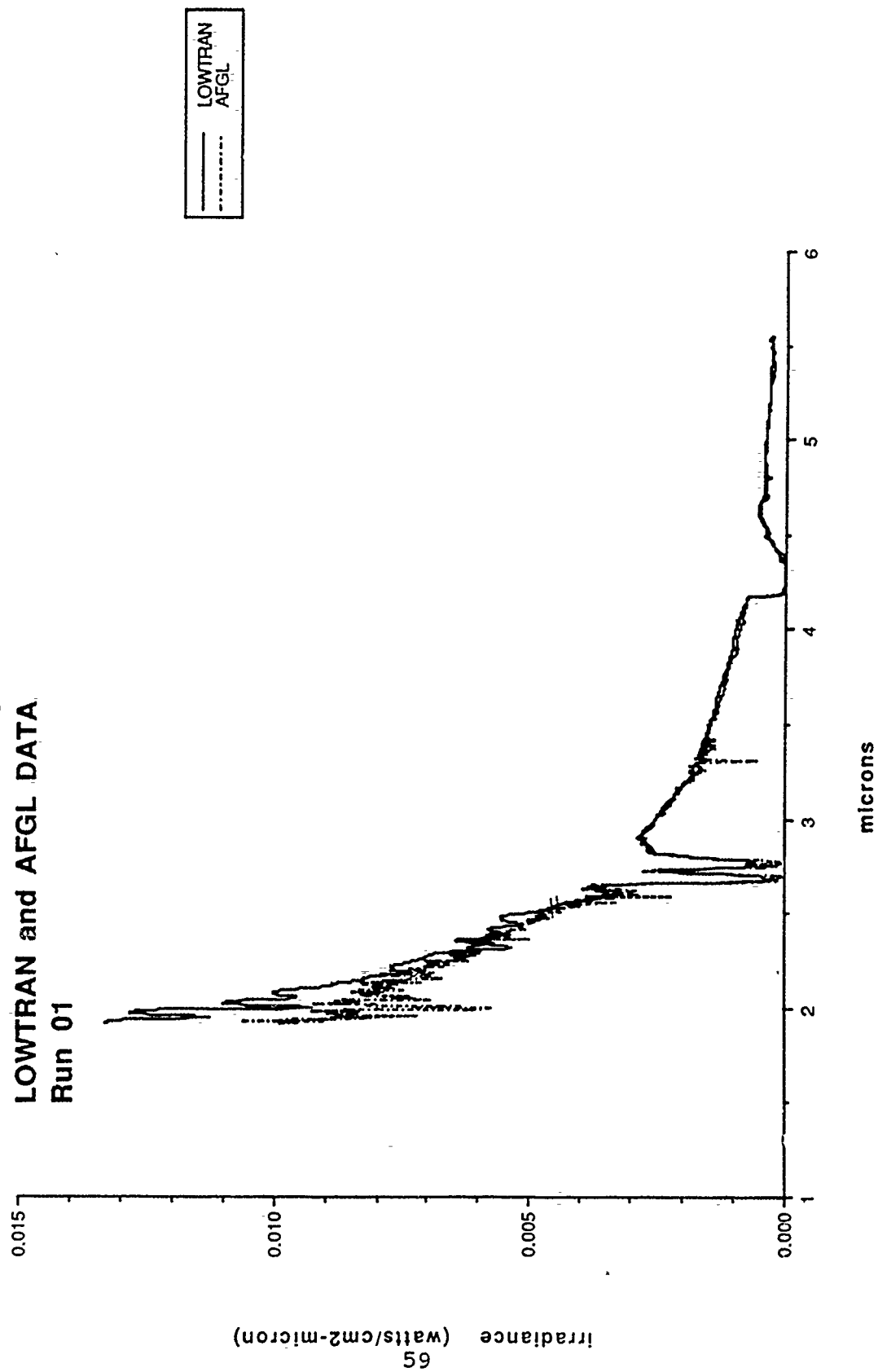
Figure 18

MODTRAN and AFGL Data  
Run 01



MODTRAN  
AFGL

Figure 19  
LOWTRAN and AFGL DATA  
Run 01



$$E_M = E_{AFGL} \text{ VS } E_{\text{Radiance with Multiple Scattering}} = E_C \quad (9)$$

For solar viewing conditions (odd numbered AFGL runs) the comparison took the form:

$$E_M = E_{AFGL} \text{ VS } E_{Dir \text{ Solar Irr}} + E_{Rad \text{ with Mult Scat}} = E_C \quad (10)$$

(AFGL solar viewing captures at the instrument both direct solar irradiance and irradiance from the sky background with multiple scattering of both sky and solar radiance). Thus, for all comparisons,  $E_M$  is the measured irradiance (field data) and  $E_C$  is the equivalent calculated irradiance (computer data) at the instrument.

#### 4.1. Kolmogorov-Smirnov Analysis

The Kolmogorov-Smirnov test is a hypothesis test that two sets of data have the same probability density function. The form of the hypothesis is as follows for the two sided case:

$$H_0(x) : F_1(x) = F_2(x) \text{ for all } x \quad (11)$$

$$H_1 : F_1(x) \neq F_2(x) \text{ for at least one } x \quad (12)$$

The test results (Table 5) are generated in terms of the two sided test statistic,  $D$ , and are shown in terms of the

Table 5  
Results of Kolmogorov-Smirnov Test

AFGL Run Number (Solar Elevation)	Probability of Greater D, Two-Sided Test	
	LOWTRAN Comparison	MODTRAN Comparison
1 (61.96°)	0.0001	0.0003
2 (61.96°)	0.0000	0.0000
3 (63.63°)	0.0003	0.0010
4 (63.63°)	0.0000	0.0000
5 (65.55°)	0.0073	0.0206
6 (65.55°)	0.0000	0.0000
7 (67.00°)	0.0005	0.0034
8 (67.00°)	0.0000	0.0000
9 (69.05°)	0.0007	0.0042
10 (69.05°)	0.0000	0.0000
11 (71.08°)	0.0004	0.0034
12 (71.08°)	0.0000	0.0000
13 (72.86°)	0.0000	0.0000
14 (72.86°)	0.0000	0.0000
17 (77.31°)	0.1735	0.1195
18 (77.31°)	0.0000	0.0000
19 (79.18°)	0.0388	0.0284
20 (79.18°)	0.0000	0.0000
21 (80.81°)	0.3368	0.1537
22 (80.81°)	0.0000	0.0000
23 (83.78°)	0.0332	0.0332
24 (83.78°)	0.0000	0.0000
25 (85.53°)	0.0801	0.0451

26 (85.53°)	0.0000	0.0000
27 (87.34°)	0.0206	0.0061
28 (87.34°)	0.0000	0.0000
29 (88.92°)	0.0000	0.0000
30 (88.92°)	0.0000	0.0000
31 (90.48°)	0.0000	0.0000
32 (90.48°)	0.0000	0.0000
33 (91.98°)	0.0000	0.0000
34 (91.98°)	0.0000	0.0000
35 (93.26°)	0.0000	0.0000
36 (93.26°)	0.0000	0.0000
37 (94.30°)	0.0000	0.0000

Table 4 Notes:

1. Odd Runs are Solar Viewing, Even Runs Background Viewing.
2. Runs 1-4 are at 11.887km, all others are at 8.839km.



resulting probability. Probability is defined as  $1-\alpha$  where  $\alpha$  is the risk of rejecting the null hypothesis when it is true. Table 4 shows that for most of the runs  $H_0$  is true with a probability greater than 97%. It is thus concluded that the two sets of data, field and computer, have the same probability distribution function. From this it can be inferred that they have statistically the same shape and that the computer models provide a good representation of the observed irradiances.

#### 4.2. Percent Difference Analysis

The percent difference was defined as:

$$\Delta\%(\lambda) = \frac{E_c(\lambda) - E_m(\lambda)}{E_m(\lambda)} \quad (13)$$

where  $E_c(\lambda)$  is the calculated value at a given wavelength and  $E_m(\lambda)$  is the measured value at a given wavelength. A positive percent difference represents an under estimate of the irradiance by the models.

Singularly large differences at a given wavelength can be generated using equation 13, especially in the blocking bands of  $H_2O$  at 2.7 microns and  $CO_2$  at 4.3 microns. These large differences arise from small differences between the actual concentrations of these atmospheric gasses and the

concentrations predicted by the computer codes. In the blocking bands small; changes in concentration result in relatively large changes in transmissivity. These large changes in transmissivity of the atmosphere have large effects on the irradiance at the sensor. Thus, it is possible to arrive at large percent changes in irradiance from errors in the calculated data that result not from errors in the model itself, but from the atmospheric parameters input to the model.

Therefore, a limit was applied to the results of the percent difference calculations. This limit sets results from equation 13 that exceed a percent difference of  $\pm 200\%$  to  $\pm 200\%$ . This was done so that singularly large differences at a given wavelength would not impede generation of useful plots or analysis at other wavelengths. The number of "limited" points can also be used as a diagnostic tool to evaluate the level of error in a given comparison; runs with larger numbers of "limited" points have greater overall error (Table 6). A tabular summary of the statistics is provided (Table 7). Plots of these values are provided as Figures 20-29.

The choice to "limit" the data was made over the alternative of declaring data in these regions invalid, as in Cundiff. Either approach has merit. Since the intent of this

Table 6  
Summary Results from "limiting"  
Percent Difference Calculations

AFGL Run #	# of LOWTRAN points "limited"	% of LOWTRAN points "limited"	# of MODTRAN points "limited"	% of MODTRAN points "limited"
1	16	2.35	14	2.06
2	106	15.63	105	15.49
3	17	2.51	16	2.35
4	116	17.11	116	17.11
5	22	3.24	30	4.43
6	78	11.50	80	11.80
7	22	3.24	27	3.98
8	74	10.91	73	10.76
9	23	3.39	32	4.72
10	76	11.21	74	10.91
11	27	3.98	37	5.46
12	57	8.41	59	8.70
13	27	3.98	36	5.31
14	51	7.52	53	7.82
17	41	6.05	43	6.34
18	174	25.66	172	25.37
19	39	5.75	44	6.49
20	31	4.57	30	4.42
21	42	6.19	55	8.11
22	27	3.98	30	4.42
23	54	7.96	62	9.14
24	12	1.77	134	19.76

25	70	10.32	57	11.06
26	12	1.77	127	18.73
27	87	12.83	92	13.57
28	6	0.09	123	18.14
29	112	16.52	116	17.11
30	9	1.33	59	8.7
31	162	23.89	185	27.29
32	7	1.03	57	8.41
33	472	69.62	509	75.07
34	13	1.92	49	7.22
35	676	99.71	676	99.71
36	25	3.69	71	10.47
37	4	0.59	26	3.83

Table 7  
Statistics for "limited" Percent Difference Comparisons

	Statistics of "limited" LOWTRAN Comparisons			Statistics of "limited" MODTRAN Comparisons		
AFGL Run #	Mean	Median	Std Dev	Mean	Median	Std Dev
1	4.10	5.90	35.78	3.87	5.79	33.35
2	-43.45	-12.08	91.13	-43.66	-11.66	91.25
3	2.49	4.86	36.58	1.67	4.78	34.96
4	-35.14	6.88	96.93	-35.24	7.17	97.02
5	-2.07	3.03	44.14	-5.43	3.34	47.61
6	-29.98	-1.65	86.28	-30.27	-2.01	86.30
7	-3.10	3.22	45.11	39.71	51.52	52.95
8	-31.96	-4.21	84.95	-31.66	-4.69	84.97
9	-2.72	3.27	45.46	-6.72	3.06	50.04
10	-31.87	-3.77	88.53	-32.25	-4.40	88.67
11	-3.97	3.17	46.72	-7.96	3.70	51.64
12	-20.46	4.48	82.40	-20.86	4.49	82.67
13	0.12	9.00	49.15	-2.25	9.07	52.95
14	-18.88	-1.96	81.79	-19.34	-2.41	81.94
17	-18.21	-7.49	52.49	-20.38	-7.88	53.11
18	-54.40	-29.78	107.96	-55.05	-30.87	108.09
19	-22.65	-11.79	52.19	-25.38	-11.74	53.39
20	-13.22	-1.73	73.84	-13.94	-2.04	74.21
21	-15.24	-3.58	55.58	-22.45	-5.13	58.42
22	-2.20	16.74	12.46	-2.97	15.55	73.18
23	-12.83	3.05	62.14	-15.53	2.30	63.38
24	5.44	9.82	63.81	-41.35	-6.26	96.17

25	-23.65	-4.21	67.43	-27.44	-5.70	69.11
26	5.44	6.19	62.76	-50.03	-17.01	94.06
27	-25.51	0.38	73.58	-28.11	-1.20	73.43
28	1.96	0.03	58.41	-62.24	-39.11	88.38
29	-27.10	5.22	82.59	-31.61	2.52	81.97
30	27.81	30.43	55.75	-22.78	5.18	82.63
31	-52.44	-8.09	91.59	-65.19	-18.61	91.27
32	25.02	31.67	58.29	-38.58	74.54	84.97
33	-167.25	-200.00	57.77	-169.68	-200.00	58.02
34	40.50	54.28	65.43	2.47	26.17	82.43
35	-199.12	-200.00	16.28	-199.12	-200.00	16.28
36	41.22	70.84	75.10	3.10	30.72	90.13
37	66.82	97.22	50.25	46.35	71.09	73.17

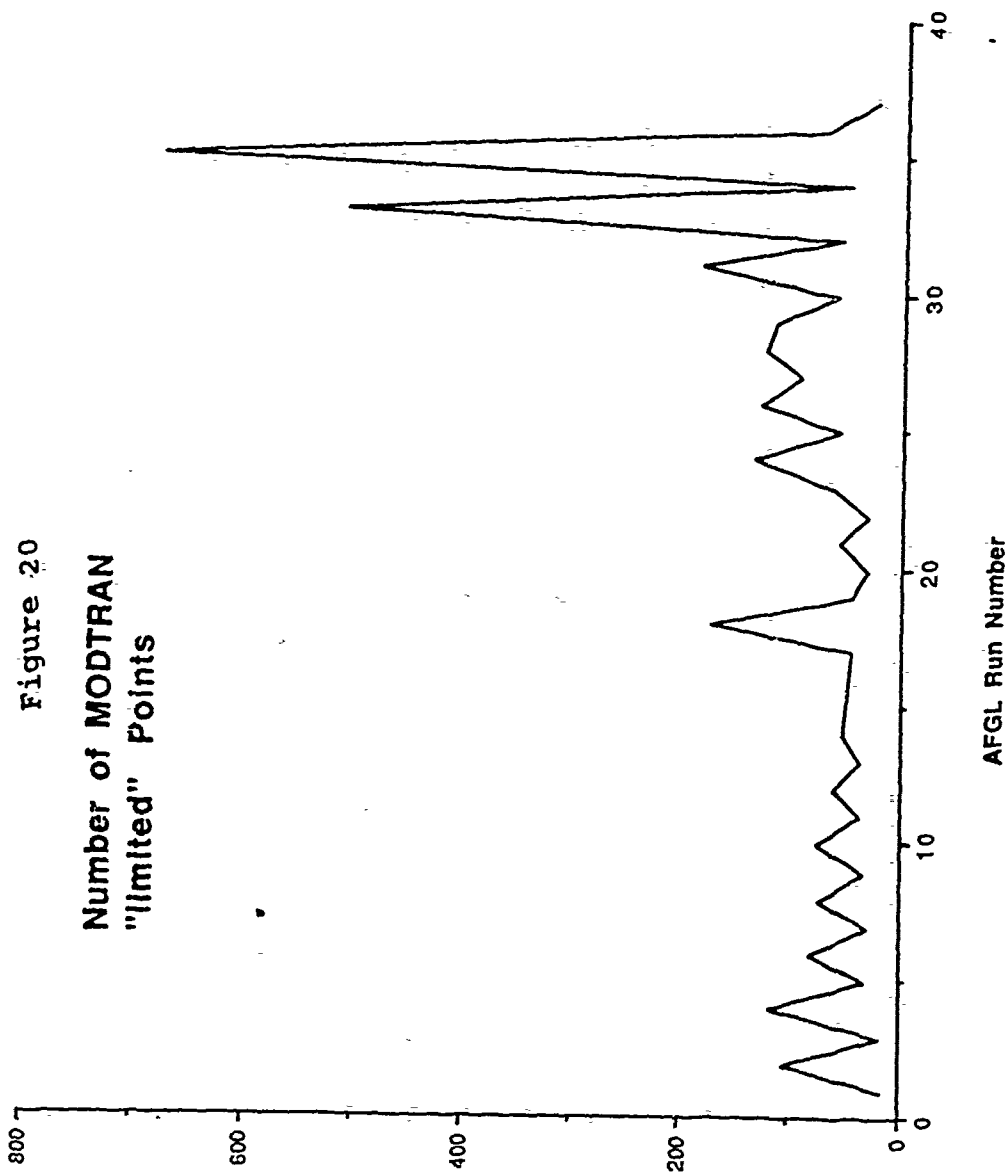
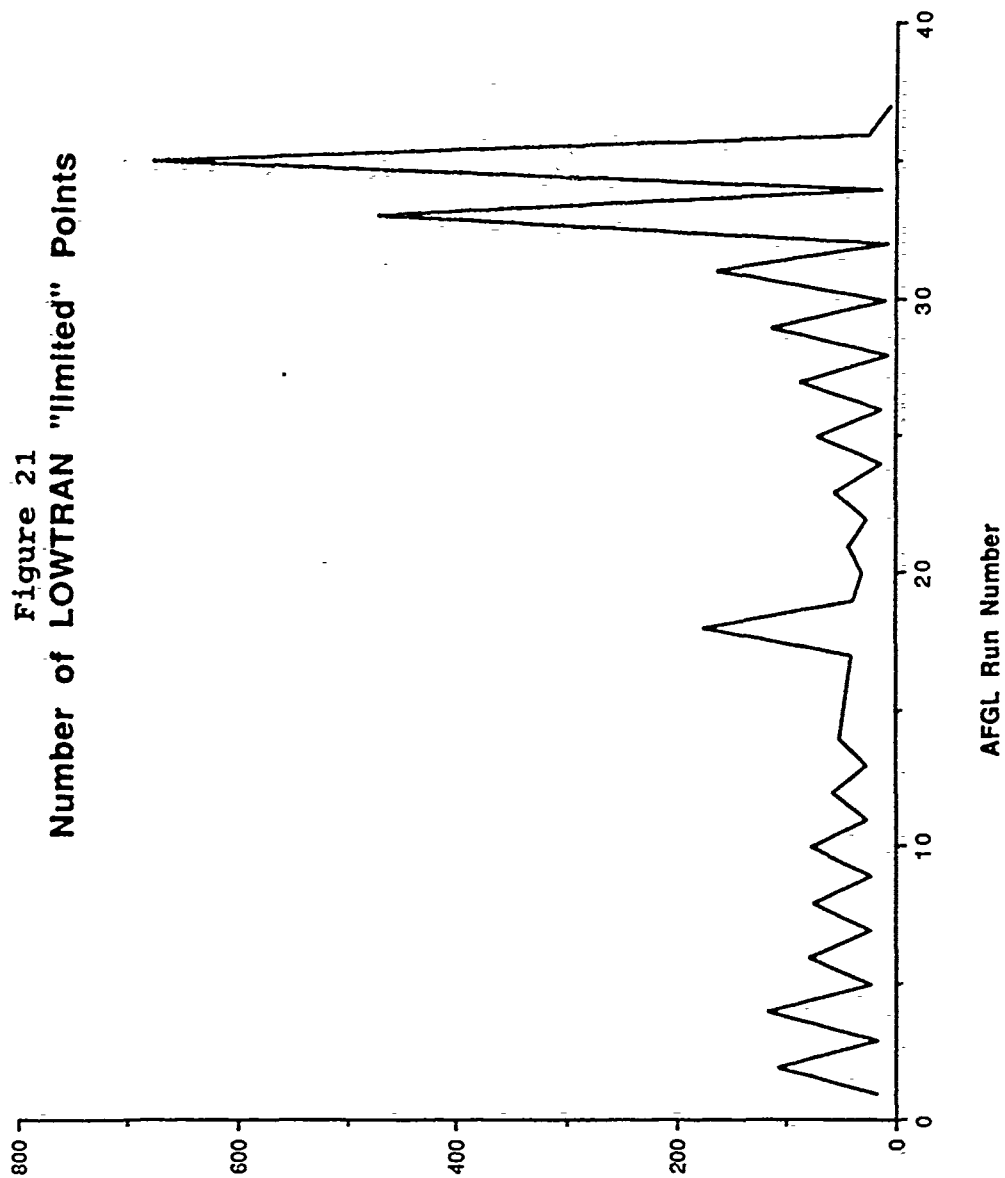


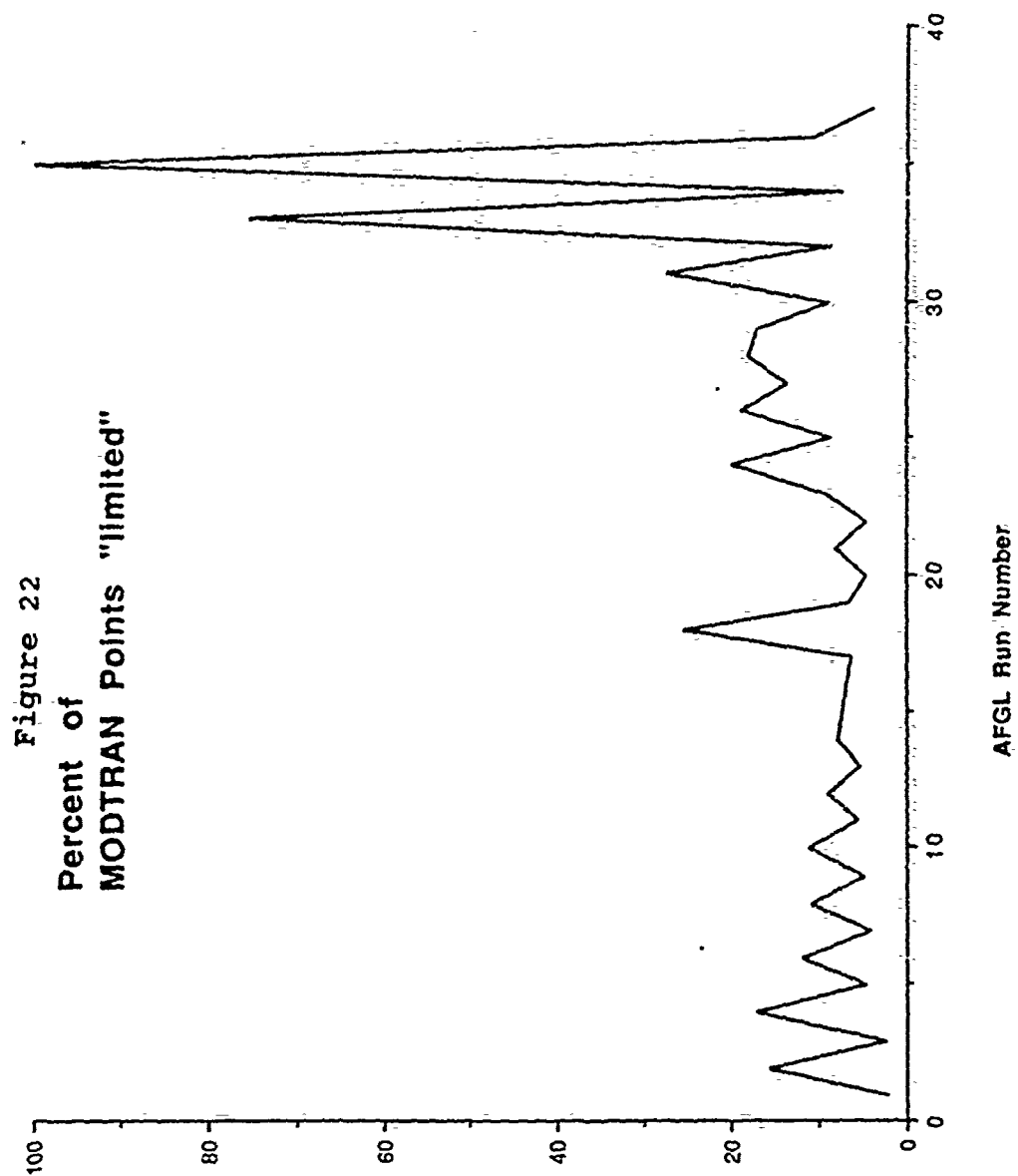
Figure 20  
Number of MODTRAN  
"limited" Points

Number of "limited" Points



Number of "Ilimited" Points





Percent of Points "limited"

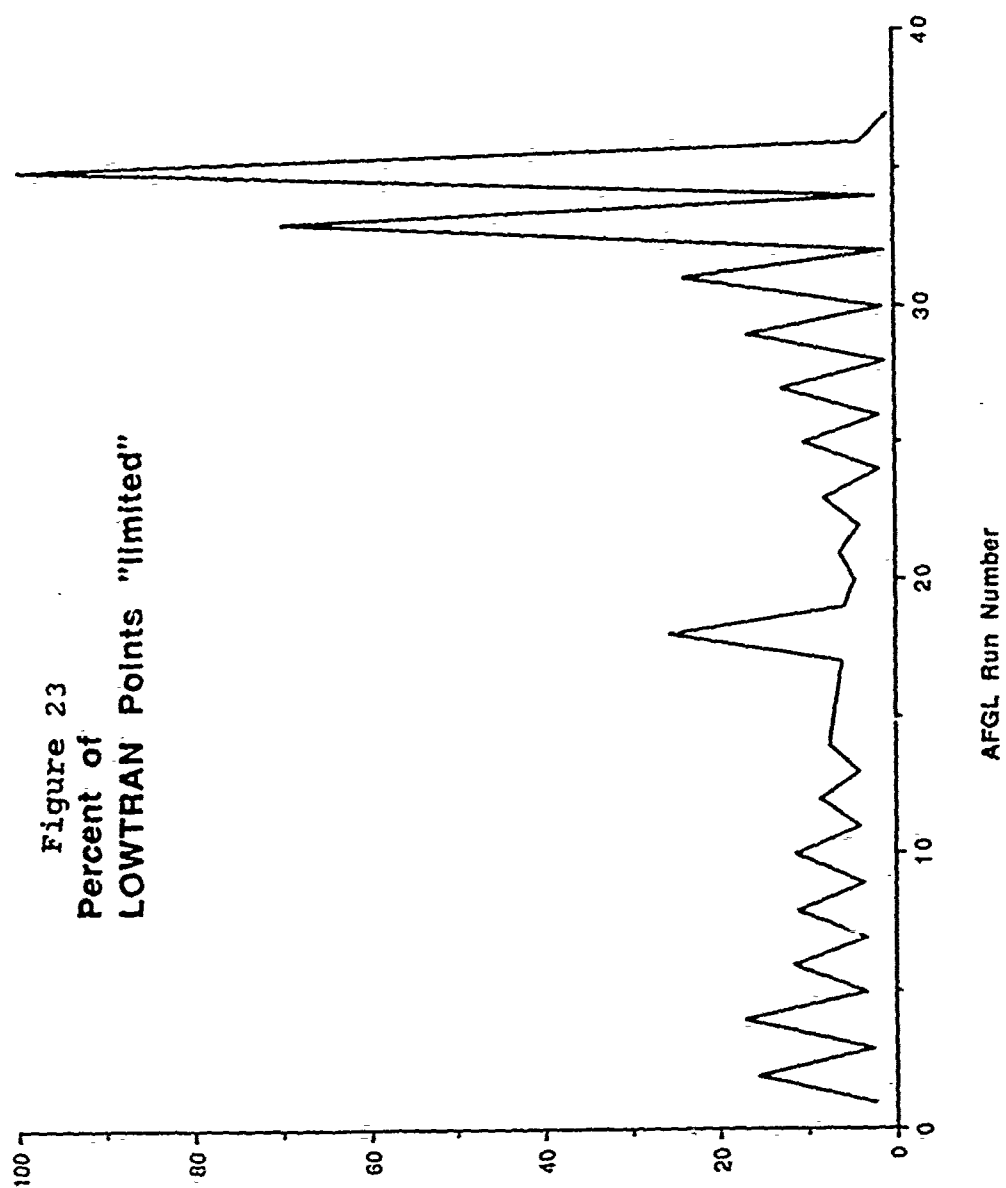
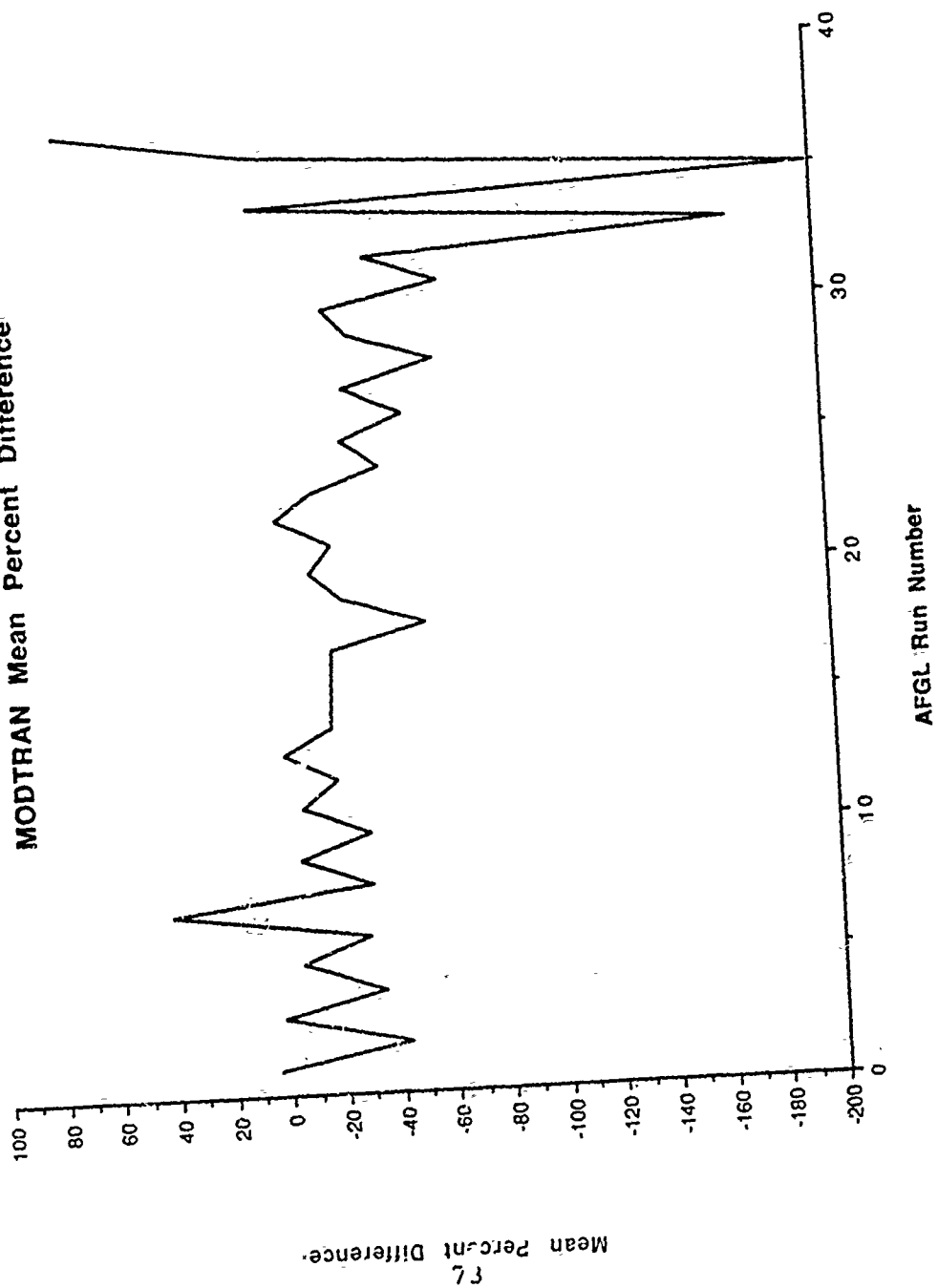
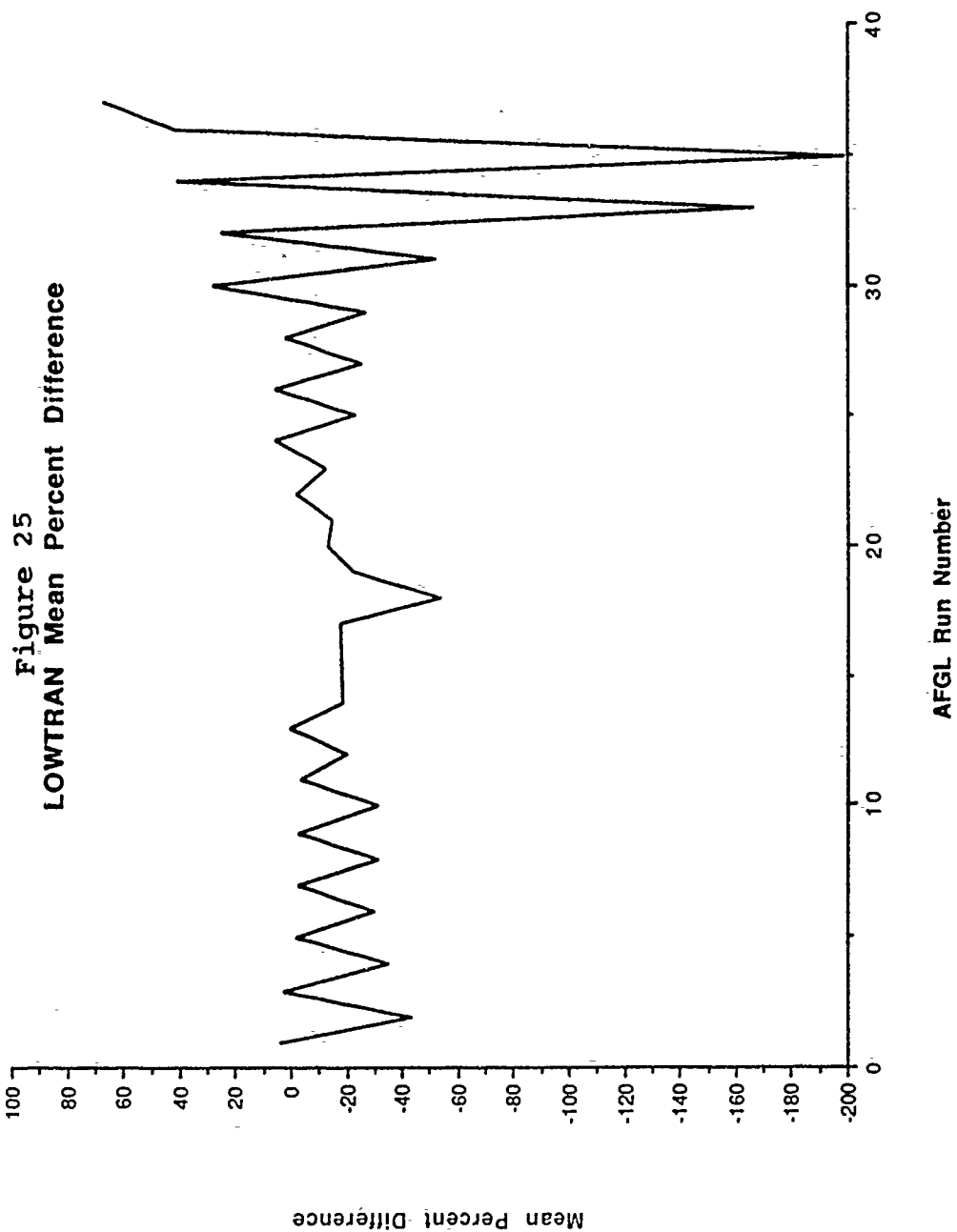
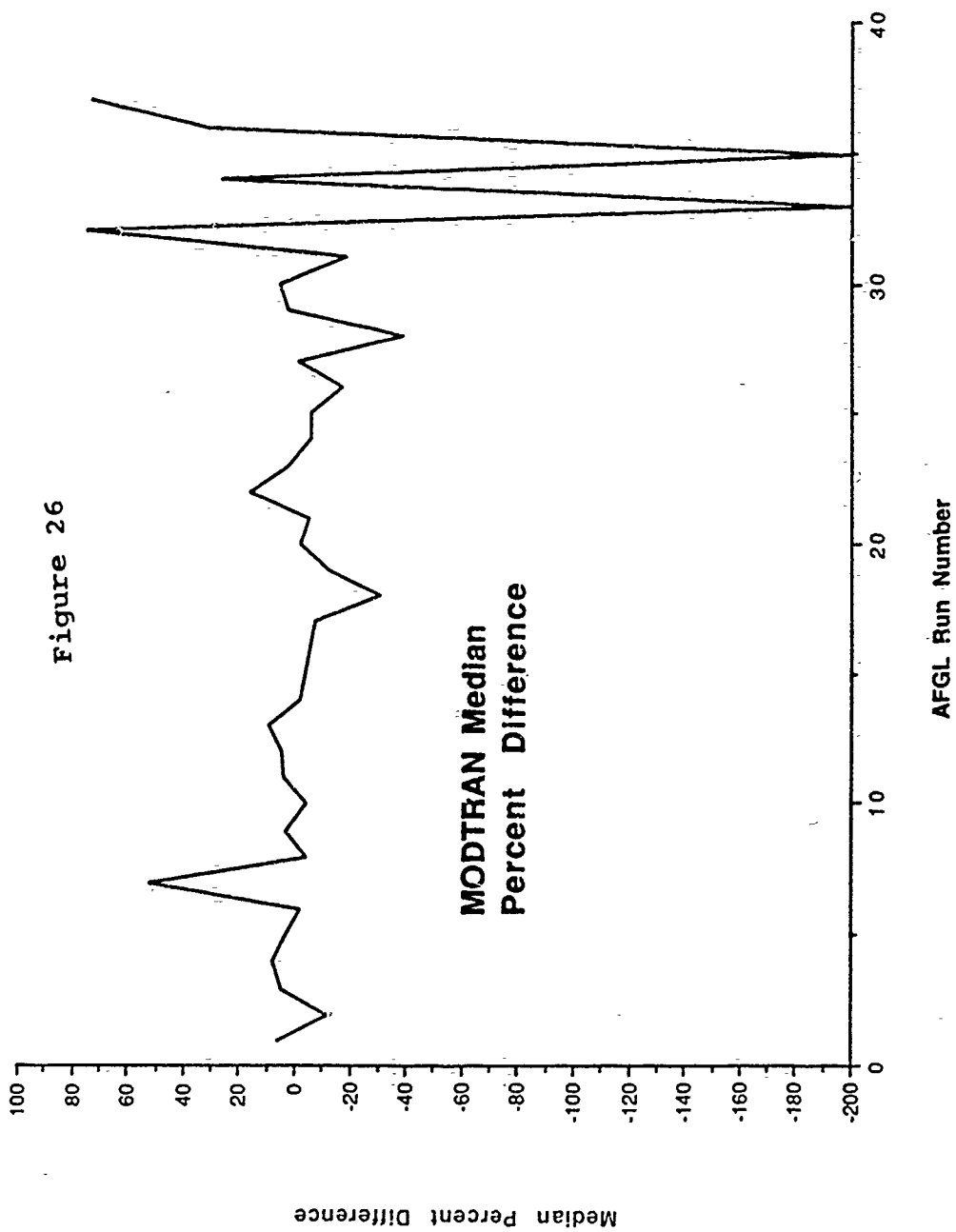


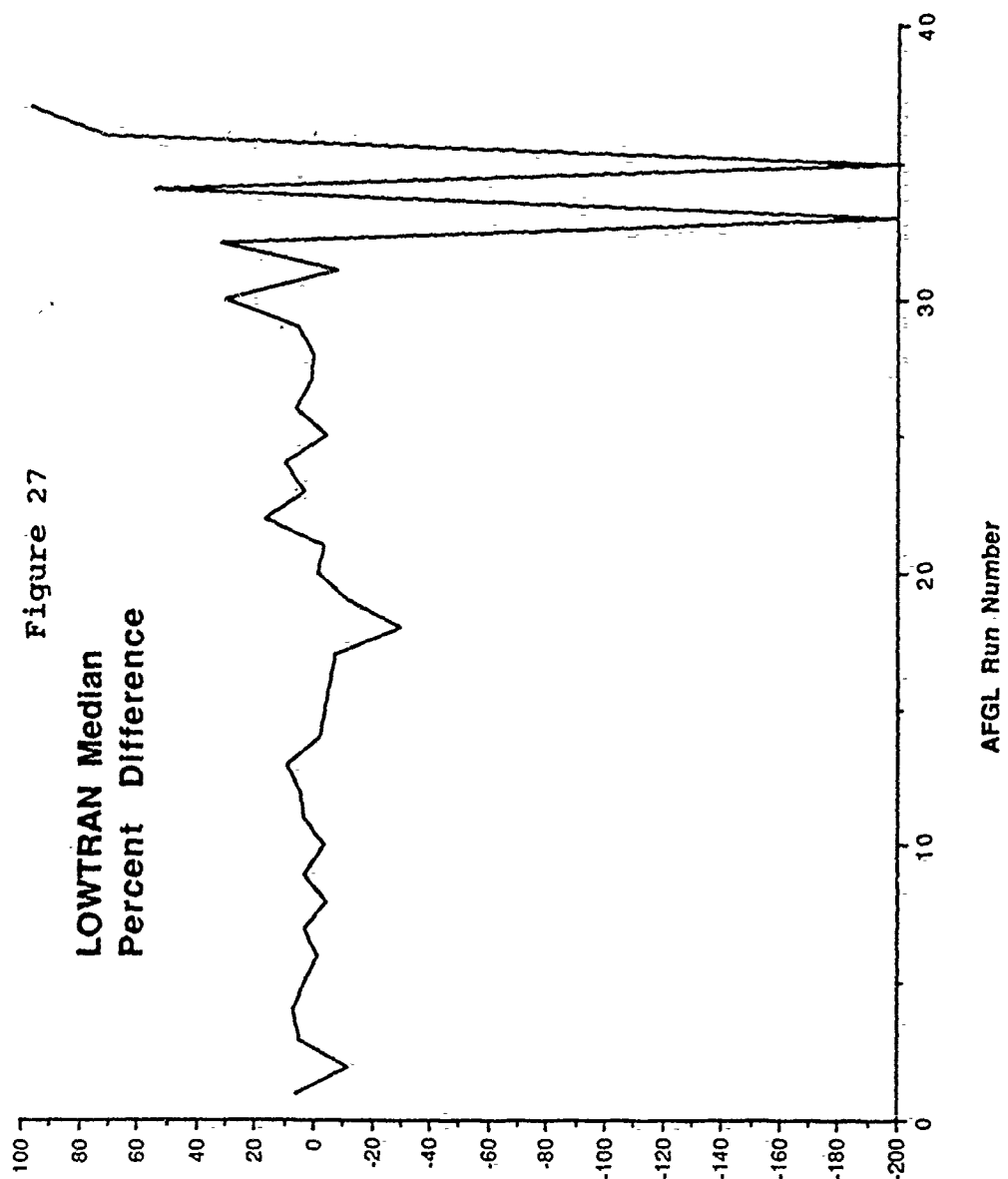
Figure 23  
Percent of  
LOWTRAN Points "limited"

Figure 24  
MODTRAN Mean Percent Difference

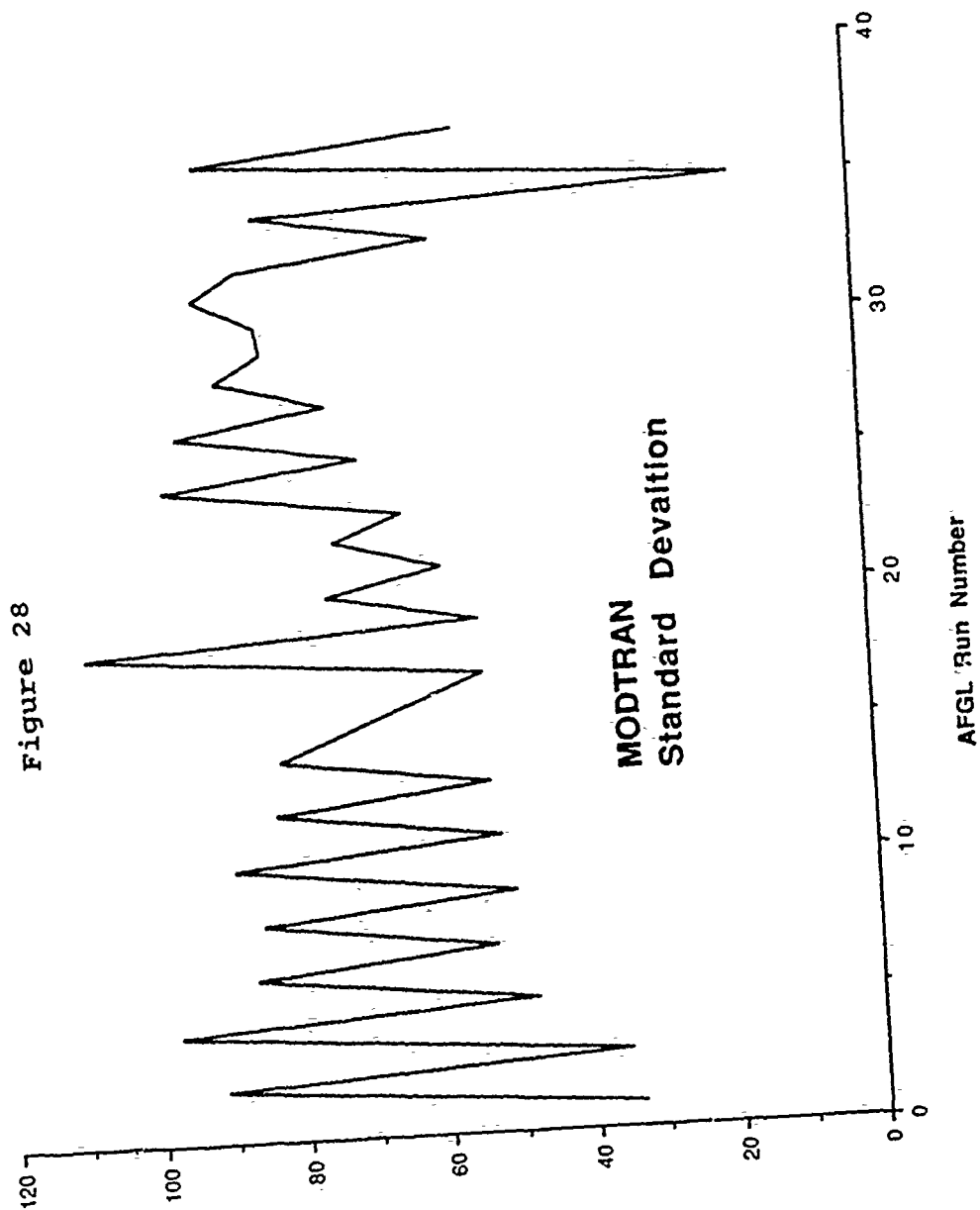


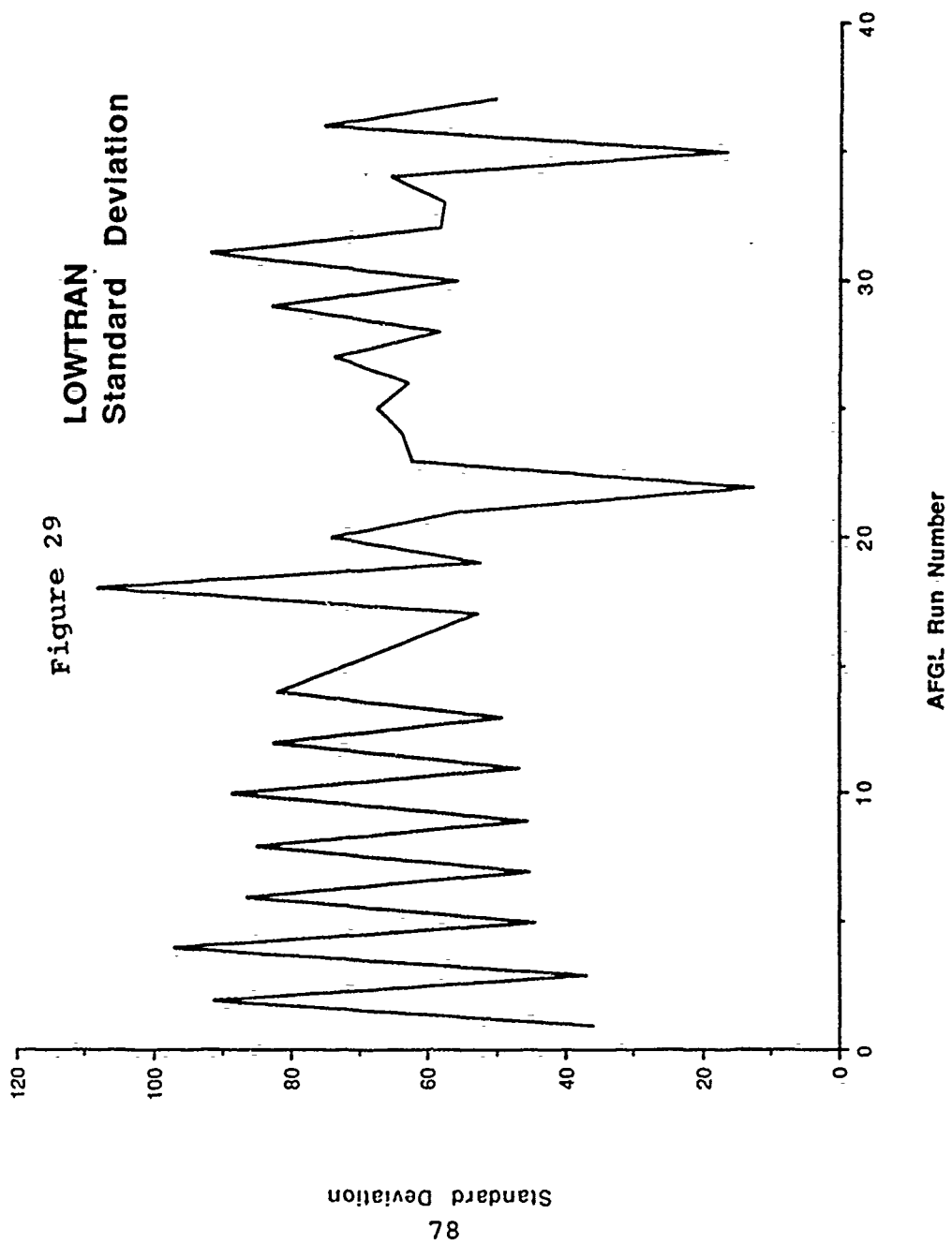






Median Percent Difference







thesis was to evaluate performance over the full 2.0-5.5 micron region, "limiting" the data provided better insight into the errors of the codes. In addition, it is difficult to decide on a single set of intervals that should be excluded as invalid due to curve of growth effects.

The optimum approach, which would have avoided the uncertainty in band exclusion intervals would have been to perform a signal to noise analysis. Data with a signal to noise ratio of less than three could be regarded as having insufficient strength to justify analysis. Since the AFGL data was provided as a processed signal this analysis could not be performed using this data set.

Plots for every fourth run are provided as Figures 30-65 in Appendix 8. Analysis of these plots and Table 7 provided the following observations:

4.2.1. Median errors are relatively small in the lower zenith angles. Errors tend to stay below an average of 10% at zenith angles less than 90 degrees (Runs 1-30), as example Figure 30. Errors are well above 10% at zenith angles equal to or larger than 90 degrees (Runs 31-37) (Figure 37). The results from the direct solar viewing cases indicate that the models for transmission and solar irradiance are essentially correct (Figures 66 and 68), except for the regions noted in

paragraphs 4.2.5 and 4.2.6. The plots of median error for background viewing indicate a slightly larger error band at low zenith angles, but without the extreme excursions at high zenith angles (Figures 67 and 69). However, this result may be due to the large number of points affected by the correction for the sensor noise floor and greybody optics.

4.2.2. Errors occur largely in the regions of the primary atmospheric absorbers.

Wavelength Region (microns)	Primary Atmospheric Absorber
2.0	H <sub>2</sub> O
2.75	H <sub>2</sub> O
3.3	CH <sub>4</sub>
4.3	CO <sub>2</sub>
4.8	CO <sub>2</sub> , O <sub>3</sub>
5.5	H <sub>2</sub> O

4.2.3. The large percent differences in the major blocking regions, 2.7 micron H<sub>2</sub>O and 4.3 micron CO<sub>2</sub>, are numerical artifacts. The low transmission of these regions (Figures 3 & 4) mean that relatively small changes in transmission (irradiance at the sensor) result in disproportionately large

Figure 66  
MODTRAN Odd Run Percent Difference  
Plotted Against Degrees

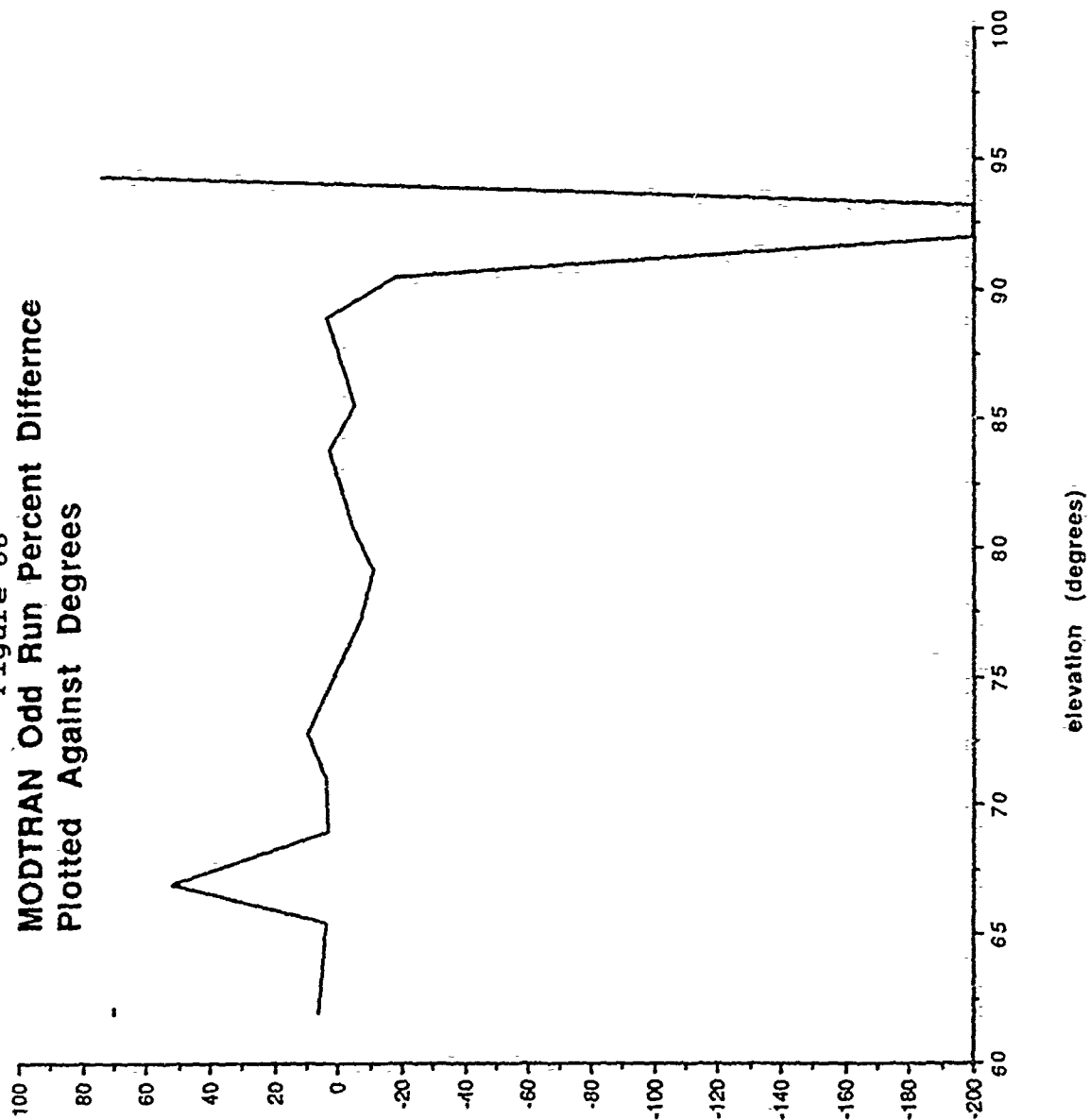


**Figure 67**  
**MODTRAN Even Run Percent Difference**  
**Plotted Against Degrees**

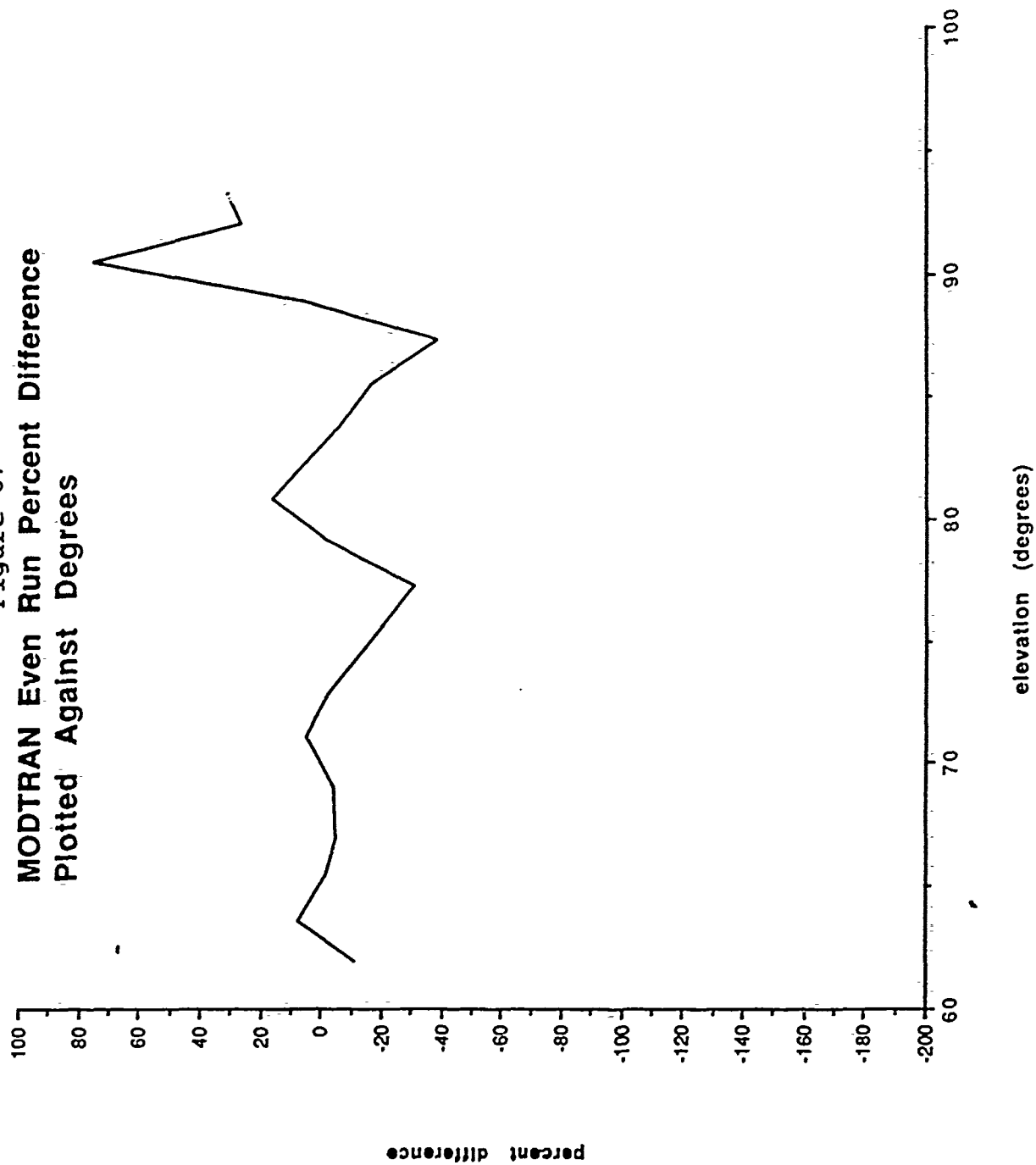


Figure 68  
LOWTRAN Odd Run Percent Difference  
Plotted Against Degrees

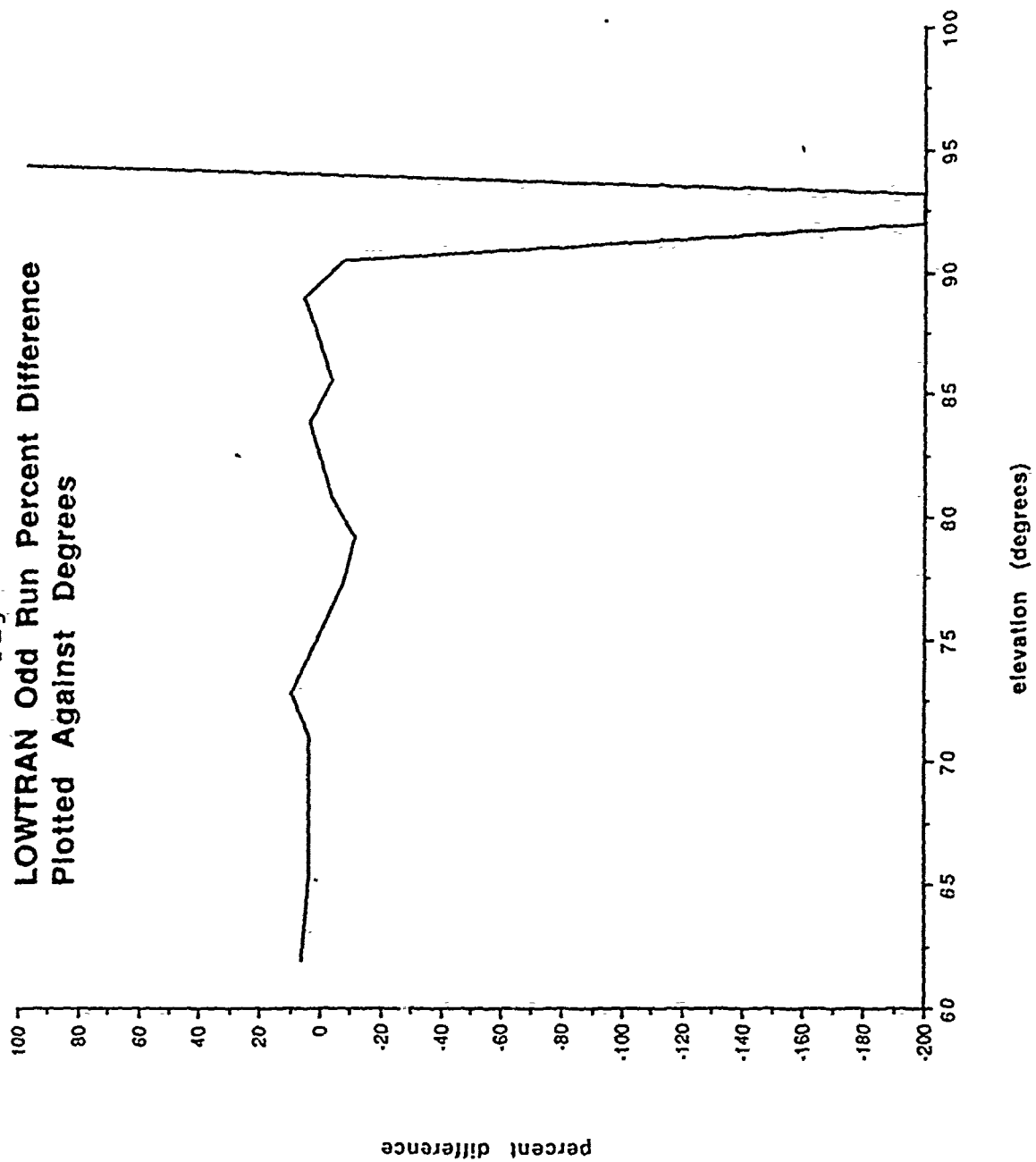
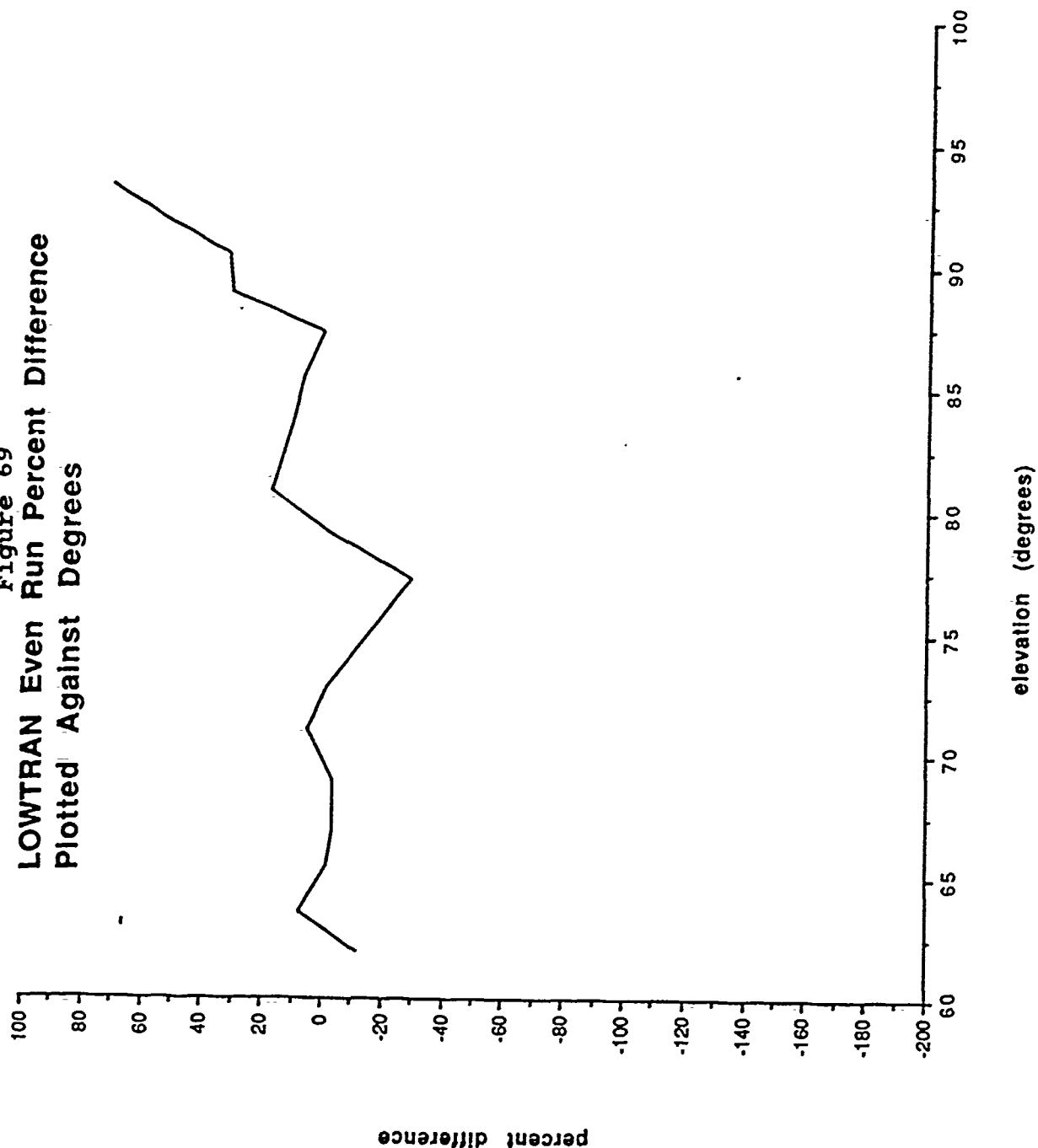


Figure 69  
LOWTRAN Even Run Percent Difference  
Plotted Against Degrees



percent difference measurements.

4.2.4. The increased viewing of higher density regions of the atmosphere results in broadened absorption lines. Curve of growth effects are clearly visible in the results of the 2.75, 3.3, and 4.3 micron regions for both MODTRAN and LOWTRAN. This causes the bands of large percent difference in these regions to "grow" in width as the zenith angle increases.

4.2.5. The error trend in the 2.0 - 2.4 micron region of the solar viewing observations appears to have a consistent shape. This shape appears independent of zenith angle and is the similar for both MODTRAN and LOWTRAN. The error indicates that the models are predicting more solar irradiance than is received by the sensor (Figures 18 and 19). Since this error does not change with angle it is not likely to be a result of error in transmission, which will change with view angle. The two other major sources of error are errors in the solar model or in the instrument calibration. Since the solar model was compiled based on multiple observations taken by many observers over time it is not as likely to contain the ~20% error indicated in the results. This suggests that the calibration curve for the AFGL instrument is in error in this wavelength region.

4.2.6. The error in the 5.2 - 5.5 micron region is angle

dependent. This indicates a possible failing in the transmission modeling. The primary constituent of this region is  $H_2O$ . As noted in the discussion (Section 2), the modeling of the continuum transmission of  $H_2O$  continues to be an area of research. Errors in the transmission could come from the water content provided by the standard model and from the transmission curve for water vapor continuum. Since errors exist in the primary water band at 2.7 microns as well as in this band it is suspected that the error in the 5.2 - 5.5 region is a result of both sources of error.

4.2.7. Standard deviation measurements (Figures 28 & 29) are a poor indicator of quality. Normally a smaller standard deviation is an indication of better data since it means there is less variance in the data. In the case of the percent difference measurements this is a false indication since the reduction of variation is a result of greater "limiting" of the results. The runs with lowest standard deviation are also the runs with the greatest number of "limited" points. These runs are at the highest zenith angles, already noted as the runs with the largest errors.

4.2.8. The difference in results in LOWTRAN and MODTRAN results in the low zenith angle runs where errors are essentially zero is an indication that the 2.68% upward bias



of the LOWTRAN PC generated values (shown in Table 4) is true bias and not just an artifact. This would indicate an upward bias of the PC based LOWTRAN results compared to field data. These results suggest that if accuracy is critical then a mainframe computer should be used to perform the calculations. (As part of the installation of MODTRAN a limited comparison was made between MODTRAN and LOWTRAN 7 results when both codes were run on the same mainframe. This limited comparison showed the two codes generating results that agreed much more closely than the results shown in Table 4. This suggests that the bias shown in Table 4 is due largely to the computer, not the model.)

4.2.9. Close examination of Table 7 shows the following discrepancies from the general trends noted above

4.2.9.a. There is a difference between the MODTRAN and LOWTRAN results for Runs 7, 26, 28, and 30. The difference for Run 7 lacks an explanation. The difference for runs 26, 28, and 30 (Figures 45 and 43 for Run 28) may be due to the increase in observed irradiance. For runs 26 and 28 LOWTRAN sees a lower value due to its coarser structure. It thus has a greater number of matches enforced by the fit to the sensor noise floor. By run 30, MODTRAN has sufficient

irradiance to achieve a match while LOWTRAN is now seeing just sufficient irradiance to be above the noise floor but not enough to achieve a match.

4.2.9.b. Increasing errors for both MODTRAN and LOWTRAN are observed in both Runs 18 and 22. This is due to an insufficient match to the data by the greybody and sensor noise corrections.

4.2.9.c. Runs 33 and 35 exhibit extreme error for both LOWTRAN and MODTRAN.

## 5. CONCLUSIONS AND RECOMMENDATIONS

The results of my thesis strongly parallel the results reported by Cundiff<sup>28</sup> in his analysis. As with Cundiff, errors increased as zenith angle increased. MODTRAN results closely mirror his results for LOWTRAN 5B, an expected result since the band models share a similar formulation. LOWTRAN 7 shows a significant improvement over LOWTRAN 6, as expected. Both models show improved performance in the 4.3  $\mu\text{m}$  region, compared to the results obtained by Cundiff.

Several overall conclusions can be drawn from the analysis and results.

5.1. LOWTRAN and MODTRAN give similar results. However, the

bias in the PC generated LOWTRAN data (most clearly indicated in the solar viewing cases at low zenith angles) indicates that the mainframe versions of the codes should be used whenever practical to obtain the most accurate results. In the region reviewed in this thesis no preference is indicated for either model. This conclusion may be due to the smoothing effect of the interpolation of the field data to  $5\text{ cm}^{-1}$  resolution, the similar smoothing effect obtained in the interpolation of LOWTRAN  $20\text{ cm}^{-1}$  resolution data to  $5\text{ cm}^{-1}$  data, and limiting output resolution of the MODTRAN model to the  $5\text{ cm}^{-1}$  resolution of LOWTRAN.

5.2. The computer models have error results within 10% for most viewing cases at zenith angles less than 90 degrees (Figures 67 and 68). This is especially true where transmission is the major factor.

5.3. Results for radiance with multiple scattering require further investigation. The adjustments for sensor noise floor and greybody radiation precluded full analysis of this part of the computer models. The large number of points affected by these corrections and the relative magnitude of the correction compared to the predicted values leaves doubt whether any observed differences are derived from the corrections imposed for analysis or a result of differences between the models and

real world conditions.

5.4. The inability to model the fine structure of the  $\text{CH}_4$  lines in the 3.3 micron region indicates a fundamental limitation of any band model code. If specific structural features are important in either data analysis or sensor design then a line-by-line code such as Fascode is required.

5.5. Improvements are required in the continuum modeling of  $\text{H}_2\text{O}$  in the 2.1 and 5.5 micron regions. These improvements should correct the errors in the transmission curves in these regions. Since the errors in these regions could also be a result of errors in the atmospheric input parameters to the codes it is recommended that research into this area utilize data from a set of measurements where the atmospheric viewing path is closely defined both in geometry (little or no refraction) and in atmospheric constituents.

Further conclusions require acquisition of additional data to verify the radiance with multiple scattering models. The sensor used to obtain this data must have sufficient sensitivity to confirm radiance modeling results in the region 2.7 - 4.5 microns. It was this region that was limited by the FISTA instrument noise floor. Calibration should include matching of the response in the  $\text{H}_2\text{O}$  regions and in the  $\text{CO}_2$  region at 4.3 microns to allow discrimination between sensor

calibration and computer model errors.

It is suggested that a separate set of measurements (similar to Cutten's<sup>10,11</sup>) be obtained at 90 degree zenith viewing. These measurements will require accurate site measurements of atmospheric data. The purpose of this experiment would be to separate errors due to the spherical refractive geometry and the transmission modeling at the high zenith angles, indicating which part of the computer model needs revision.

This experiment should be performed under controlled conditions where the atmosphere and path are well defined. Such a path could be achieved by setting up a path between two locations and fixing mirrors at each location. By arranging the viewing path such that it was bounced back and forth between the buildings a series of long paths could be obtained (by controlling the number of reflected paths). Atmospheric data could be collected for the path between the buildings, removing the other source of non-model error.

## 6. REFERENCES

1. Lillesand, T. M. and Kiefer, R. W. Remote Sensing and Image Interpretation, 2 ed, Wiley, 1987.
2. Schott, J. R., Lecture notes, Rochester Institute of Technology, Fall 1989.

3. Smith, H. J. P., Dube, D. J., et al, FASCODE - Fast Atmospheric Signature Code (Spectral transmission and radiance), AFGL-TR-78-0081, 1978.
4. Selby, J. E. A., and McClatchey, R. A. (1972) Atmospheric Transmittance from 0.25 to 28.5  $\mu$ m: Computer Code LOWTRAN 2, AFCRL-TR-72-0745, AD 763 721.
5. Kneizys, F. X., Shettle, E. P., et al, Atmospheric Transmittance/Radiance: Computer Code LOWTRAN 5, AFGL-TR-80-0067, AD A088215.
6. Kneizys, F. X., Shettle, E. P., et al, (1983) Atmospheric Transmittance/Radiance: Computer Code LOWTRAN 6, AFGL-TR-0187
7. Kneizys, F. X., Shettle, E. P., et al, (1988), Users Guide to LOWTRAN 7, AFGL-TR-0177.
8. Zachor, A. S., Whatever Happened to Band Models?, SPIE, Vol. 27, Atmospheric Transmission, 1981.
9. Pierluissi, J. H., and Tsai, C. H., New LOWTRAN models for the uniformly mixed gases, Applied Optics, Vol. 26, No. 4, 1987.
10. Cutten, D. R., Atmospheric transmission measurements and predictions in the 2100 - 2300  $\text{cm}^{-1}$  region: comparison of LOWTRAN 6 and FASCODE models, Applied Optics, Vol 25, No 5, 1986.
11. Cutten, D. R., Atmospheric transmission predictions in the 2000-2500  $\text{cm}^{-1}$  spectral region; using LOWTRAN, Applied Optics, Vol 27, No 8, 1988.
12. Pierluissi, J. H., Maragoudakis, C. E., and Thrani-Movahed, R., New LOWTRAN band model for water vapor, Applied Optics, Vol. 28, No. 18, 1989.
13. Clough, S. A., Kneizys, F. X., et al, (1981), Atmospheric spectral transmittance and radiance: FASCODE 1B, Proceedings of the SPIE, The International Society for Optical Engineering, 277, Atmospheric Transmission, R. W. Fenn, Ed., April 1981.
14. Ben-Shalom, A., Barzilai, D., et al, Sky radiance at wavelengths between 7 and 14  $\mu$ m: Measurement, calculation, and comparison with LOWTRAN 4 Predictions, Applied Optics, Vol 19, No. 838, 1980.

15. Clough, S. A., Kneizys, F. X., Atmospheric Radiance and Transmittance: Fascode2, Preprint Volume of Sixth Conference on Atmospheric Radiation, Williamsburg, VA, 13-16 May 1986 (American Meteorological Society, Boston, MA, 1986), pp 141-144.
16. Isaacs, R. G., Wang, W.-C., et al, Multiple Scattering LOWTRAN and FASCODE models, Applied Optics, Vol. 26, No. 7, 1987.
17. Robertson, D. C., Bernstein, L. S., Haimes, R., Addition of a 5 cm<sup>-1</sup> spectral resolution band model option to LOWTRAN 5, Aerodyne Research Report ARI-RR-232, 1980.
18. Bemporad, A., Search for a New Empirical Formula for the Representation of the Intensity of Solar Radiation With Zenith Angle, Meteorologishche Zeitschrift, Vol 24, July 1907.
19. Novoseller, D. E., Use of LOWTRAN in Transmission Calculations, Applied Optics, Vol. 26, No. 16, 1987.
20. Shettle, E. P., Comments on the use of LOWTRAN in transmission calculations with the ground elevated relative to sea level, Applied Optics, Vol. 28, No. 8, 1989.
21. Ibid 17.
22. Berk, A., Bernstein, L. S., et.al., MODTRAN: A Moderate Resolution Model for LOWTRAN 7, AFGL-TR-89-0122, 30 April 1989.
23. MODTRAN: Calculation of Atmospheric Transmittance and Background Radiance, Meeting Handout, GL/ASD-WRDC Users Modeling Workshop, LOWTRAN, MODTRAN, Fascode-HITRAN, Wright-Patterson AFB, OH, 14-16 November 1990.
24. Kneizys, F. X., Anderson, G. P., et.al., LOWTRAN 7: Status, Review, and Impact for Short to Long Wavelength Infrared Applications, Advisory Group for Aerospace Research and Development (AGARD), Paper Reprinted from Conference Proceedings No.454.
25. Huppi, R. J., Steed, A. J., and Huppi, E. R., Cryogenically cooled Fourier transform spectrometers, SPIE International FT-IR Conference, 1981.
26. Walker, R. P., and Rex, J. D., Interferometer design and data handling in an high vibration environment, SPIE, Vol. 191, 1979.

27. Advance draft of FISTA instrumentation report. Private correspondence with AFGL/OPF, June 1990.
28. Mills, F. P., FISTA: The Geophysics laboratory Flying Infrared Signatures Technology Aircraft: A Summary of its Capabilities, ESD # 89-531, SU Log # 234-89, Apr 1989.
29. Cundiff, S. T., Analysis of long range atmospheric transmission, Scitec report TR-86-003, February 1986.
30. Daniel, W. W., Applied Nonparametric Statistics, 2 ed, Ch. 8, 1990.
31. Royer, A., O'Neill, N. T., et al, Comparison of radiative transfer models used to determine atmospheric optical parameters from space, SPIE, Vol. 928, Modeling of the Atmosphere, 1988.
32. Richter, R., Some aspects of the atmospheric radiance model of LOWTRAN 6, Int. J. Remote Sensing, Vol. 6, No. 11, 1985.
33. Lisowski, J. K., Scitec internal memo, 1988.
34. Personal Conversation with Brian Sandford, AFGL/OPA, March 1991.
35. Ibid 26.
36. IMSL (International Math and Statistics Library). Users Manual. Math/Library FORTRAN Subroutines for Statistical Analysis, Ver 1.0, IMSL Inc, April 1987
37. Slater, P. N., Remote Sensing: Optics and Optical Systems, pp528-530, Addison-Wesley, 1980.
38. Personal Conversation with Brian Sandford, AFGL/OPA, March 1991.
39. Wolfe, W. L., Zissis, G. J., .ed, The Infrared Handbook, Chapter 7 (Optical Materials), Environmental Research Institute of Michigan for Office of Naval Research, 1978.



## Appendix 1

### Cundiff and Lisowski Report Extracts

## CUNDIFF EXTRACT

The derived atmospheric transmissions are presented in this chapter. The original solar spectral radiance data, collected by AFGL, is compiled in Appendix A.

The following table summarizes the major absorption regions and the absorbing molecule:

<u>Wavelength Region ( )</u>	<u>Primary Atmospheric Absorber</u>
2.0	H <sub>2</sub> O
2.75	H <sub>2</sub> O
3.3	CH <sub>4</sub>
4.3	CO <sub>2</sub>
4.8	CO <sub>2</sub> , O <sub>3</sub>
5.5	H <sub>2</sub> O

Figures 4 through 8 are the atmospheric transmission at the remaining zenith angles. The same general features described above are evident in these. The overall transmission decreases as the zenith angle increases. At the largest zenith angle there is no transmission above 0.8 and most bands usually considered atmospheric windows show average transmissions of 0.5 or less.

### 2.2 Comparison of LOWTRAN6 to Data

The models were compared to the data by calculating the percent difference between the data and model. The percent difference is defined as:

$$\Delta_{\%}(\lambda) = \frac{\tau_c(\lambda) - \tau_m(\lambda)}{\tau_m(\lambda)},$$

where  $\tau_c(\lambda)$  is the calculated transmission, and  $\tau_m(\lambda)$  is the measured transmission. A positive percent difference represents an overestimate of

the atmospheric transmission by the model and a negative value an underestimate. If  $\tau_m(\lambda)$  is less than 5%,  $\Delta\tau(\lambda)$  is undefined as it is felt that there is insufficient intensity to make an accurate measurement of the transmission.

LOWTRAN6 accurately models the atmospheric transmission at the smaller zenith angles. Figure 9 is the percent difference between LOWTRAN6 and the data. At 61.9° and 65.5° zenith, the percent difference is close to zero at most wavelengths. In the H<sub>2</sub>O and CO<sub>2</sub> absorption bands there is a significant deviation, but the transmission is very low in these regions, causing a small (5%) difference in transmission to be a large percent difference. As the zenith angle increases, so does the uncertainty.

There are a few noticeable features in the percent difference at the larger zenith angles. A large uncertainty, with a distinct structure, exists in the 2.1-2.4 micron region. This absorption is due to CH<sub>4</sub>. This absorption band is entirely missing from the LOWTRAN6 data base (note that it is not apparent at the smaller zenith angles). We made a modification to the LOWTRAN6 data base to include this band; it is discussed in Section 5. On the edge of the 2.8 micron H<sub>2</sub>O and 4.3 micron CO<sub>2</sub> absorption bands, there is a large difference. This is primarily due to low transmission as mentioned previously. A large difference also exists at 4.75 microns. Two molecules absorb in this region: O<sub>3</sub> - 4.75-4.8 microns and N<sub>2</sub>O - 4.8-4.9 microns. If the O<sub>3</sub> concentration is adjusted to obtain better agreement, the agreement in the 3.6 micron O<sub>3</sub> absorption band is lost, N<sub>2</sub>O is part of the uniformly mixed gases, so its concentration cannot be adjusted individually. This example indicates a basic modeling problem in LOWTRAN6.

### 2.3 Comparison of LOWTRAN5B Model to Data

LOWTRAN5B is a mid resolution atmospheric transmission model. It uses a band model parameter formulation to calculate the atmospheric transmission. This approach more accurately takes into account the changes in the transmission due to different line shapes at different temperatures

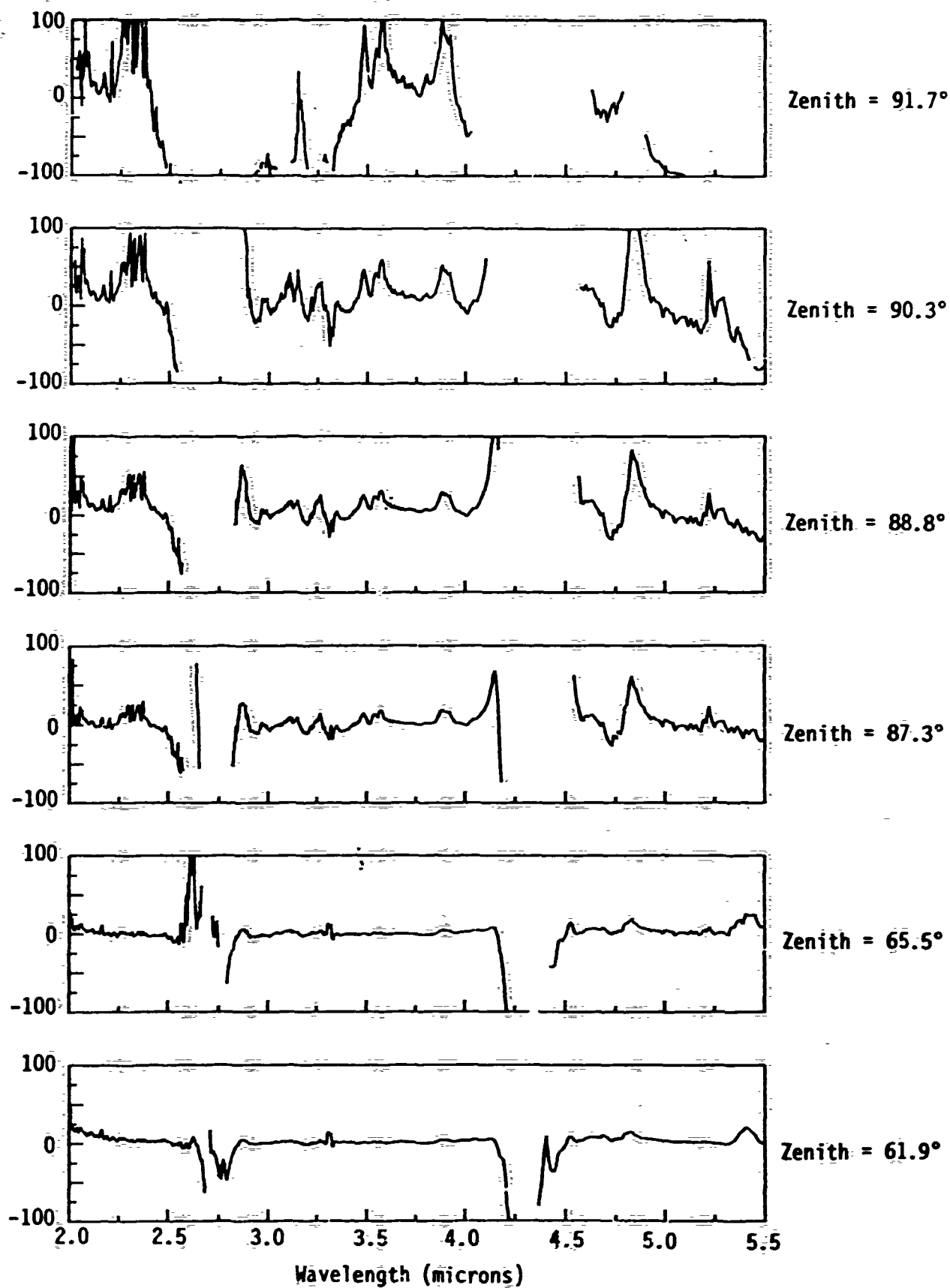


Figure 9. Percent Difference Between LOWTRAN Calculations and AFGL Data.

and pressures. Consequently, it is a more accurate model. It also has a data with a resolution of  $5\text{ cm}^{-1}$  as compared to the  $20\text{ cm}^{-1}$  resolution of LOWTRAN6. Due to this increased resolution, the calculations of LOWTRAN5B more accurately represent the structure of the atmospheric transmission, much of this structure is not present in the LOWTRAN6 calculation. The transmission data display much finer structure than the LOWTRAN5B calculation (on the order of  $0.01\text{ cm}^{-1}$ ) and FASCODE must be used if modeling of this fine structure is necessary. Note that there is more detail in the percent difference for LOWTRAN5B and FASCODE than for LOWTRAN6; this is because of the higher resolution of the calculations.

Figure 10 indicates the percent difference between LOWTRAN5B and the data. At the small zenith angles LOWTRAN5B does a fairly good job of modeling the atmosphere; essentially equal to LOWTRAN6. The percent difference at the  $61.7^\circ$  zenith angle is approximately 0 at most of the wavelengths, again, excepting the areas of the  $\text{CO}_2$  and the  $\text{H}_2\text{O}$  absorption bands where the atmospheric transmission drops quite low. It is quite good at the  $65.5^\circ$  zenith angle with small spikes being observed in the region of the  $\text{CH}_4$  absorption at 3.3 microns and the beginnings of an inaccuracy in modeling the ozone at 4.75-4.8 microns. This apparent modeling deficiency is of the same nature as that mentioned for LOWTRAN6. Attempting to correct the ozone content to make it more accurately model the 4.75 micron region decreases the ability to accurately model the ozone absorption at 3.6 microns. At a zenith angle of  $87.3^\circ$ , the methane absorption at 3.3 microns is more evident as being an area of uncertainty. There is significant structure to the  $\text{CH}_4$  absorption in this band. LOWTRAN5B does a significantly better job of modeling this structure than LOWTRAN6 which is inherent in the designed resolution of the respective models. At 2.3 microns, the sharp positive spike is due to methane absorption which is completely unmodeled in the LOWTRAN5B data base. This was mentioned in LOWTRAN6 as being a problem and the problem increases with increasing zenith. At a  $90.3^\circ$  zenith and at 4.8 microns the inaccuracy of modeling the  $\text{CO}_2$  absorption band is beginning to become evident as a positive percent difference.

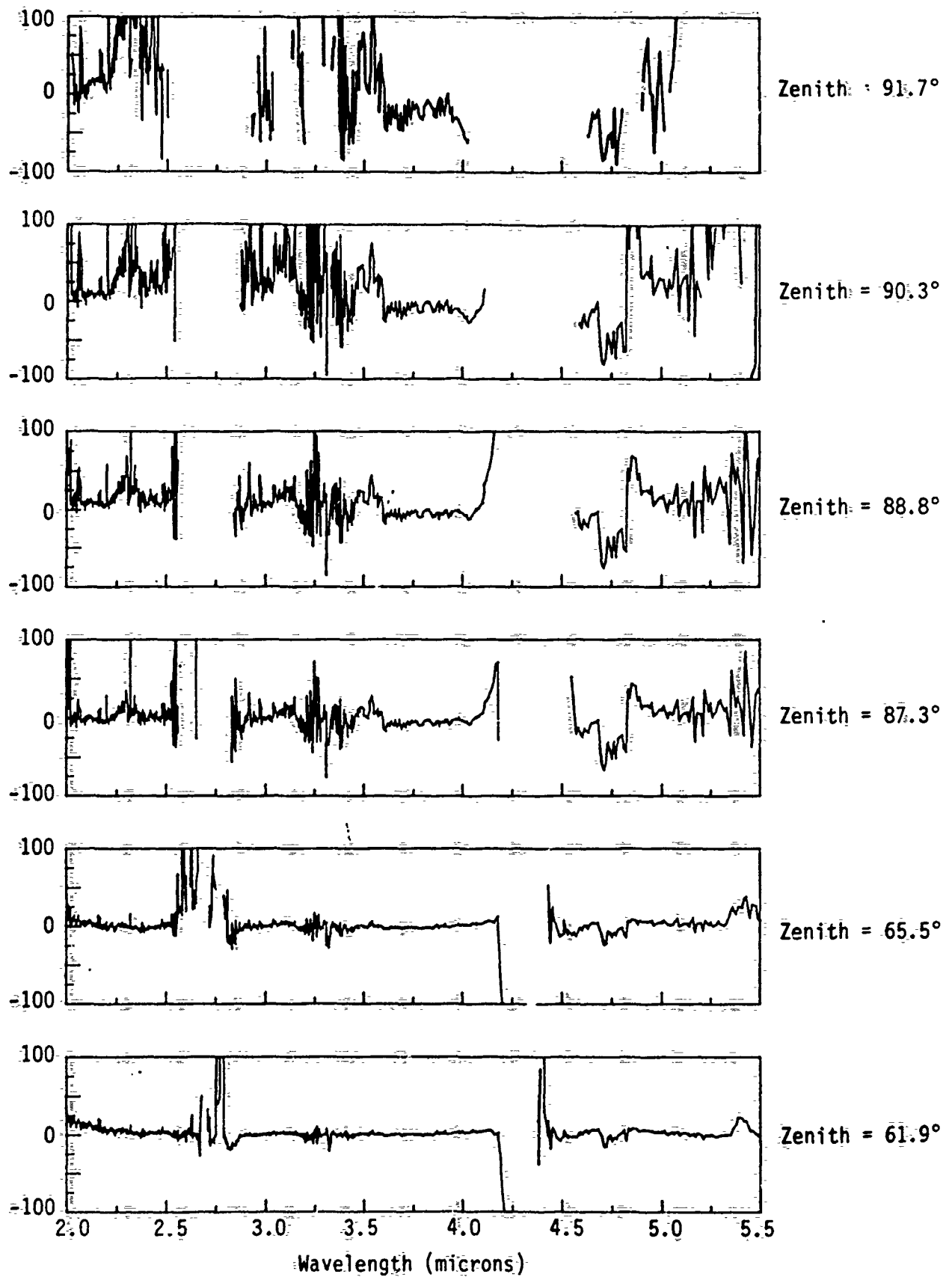


Figure 10. Percent Difference Between LOWTRAN5B Calculations and AFGL Data.

## LISOWSKI EXTRACT

The investigation was undertaken to determine the potential effects of uncertainties in actual CO<sub>2</sub> concentration (relatively minor), the difference between the band-model codes and the line-by-line codes (significant), and the effects of convolving the different code spectral transmissivity predictions with the spectral radiant intensity of the plume. The investigation has been performed for a number of scenarios and the complete results will be presented in a report which is currently being prepared. This effort has been exclusively devoted to the understanding of the atmospheric transmission effects in the 4.3-4.6 micron region.

Near the end of the computational phase of the effort we realized that the optical paths for each of the target altitudes were very similar to those encountered by AFGL during spectral radiant intensity measurements of the setting sun from an altitude of 29,000-39,000 ft. Therefore, we compared the code predictions with the AFGL measurements. The nomenclature and conditions are indicated in Table 1.

Table 1

<u>AFGL Run</u>	<u>Aircraft Altitude</u>	<u>Zenith Angle</u>
1	39,000 ft	61.9
5	29,000 ft	65.5
27	29,000 ft	87.3

Figure 2 indicates the comparison between the actual data and the predictions employing FASCOD2, LOWTRAN5B, and LOWTRAN6 for Run 1 (similar to a target at 30 km altitude in our computational scenario). Clearly, the LOWTRAN6 computations do not describe the spectral characteristics of the atmospheric transmission as well as either FASCOD2 or LOWTRAN5B. In fact, LOWTRAN5B gives slightly better agreement than FASCOD2.

Figures 3 and 4 indicate the results of the comparison between the predictions and data for Runs 5 and 27. For both cases LOWTRAN6 does not provide an adequate spectral description. In Run 5, both FASCOD2 and LOWTRAN5B provide very similar results, both quite good. For Run 27, FASCOD2 provides much better agreement with data.

A further test was conducted by convolving the actual transmission and the computed transmissions with a plume spectrum and a sample sensor spectral filter. The results are provided in Figures 5, 6, and 7 for Runs 1, 5, and 27, respectively. These results echo those stated in the previous paragraphs - namely, LOWTRAN6 is not to be used, LOWTRAN5B does better at higher target altitudes, FASCOD2 does better at low target altitudes.



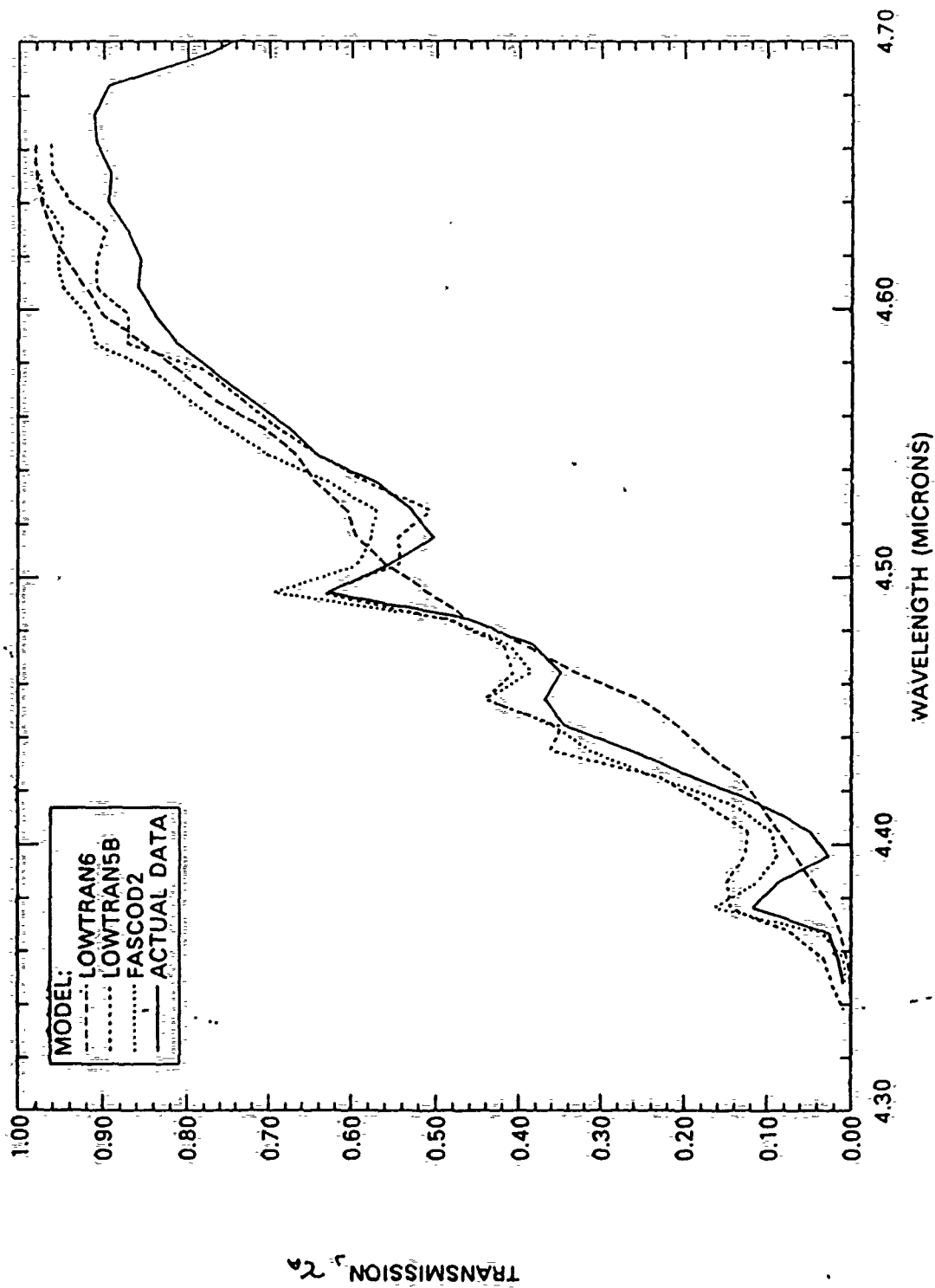


Figure 2. Comparison of Atmospheric Transmission Predictions with AFGL Data Run 1 Zenith Angle of 61.9 Degrees.

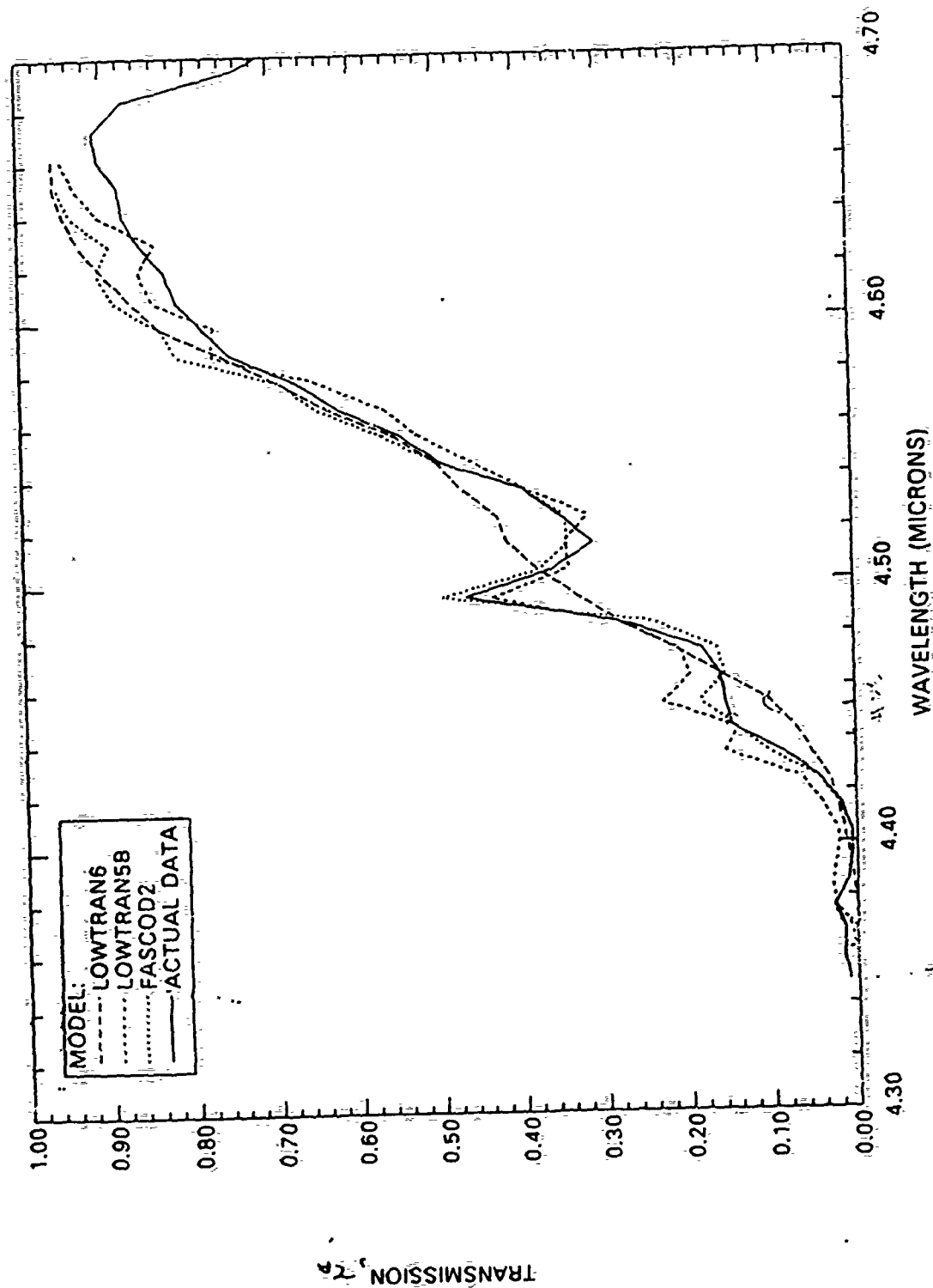


Figure 3. Comparison of Atmospheric Transmission Predictions with AFGL Data Run 5 Zenith Angle of 65.5 Degrees.

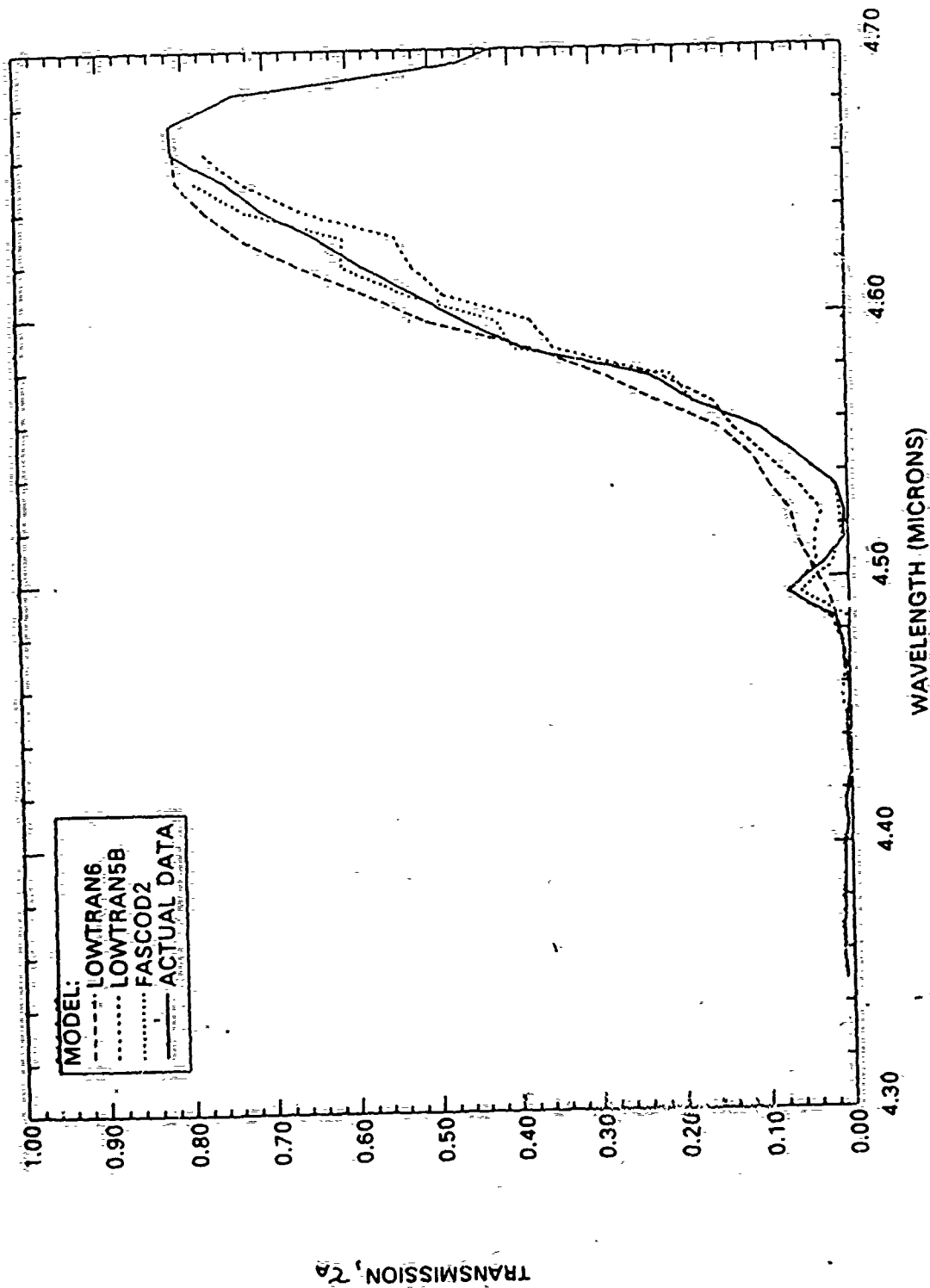


Figure 4. Comparison of Atmospheric Transmission Predictions with AFGL  
Data Run 27 Zenith Angle of 87.3 Degrees.

## Appendix 2

### AFGL File Format and VAX Backup Notes

Description of Magnetic Tape Format

Tape is 1/2 inch, <sup>1600</sup>800 bpi, 9 track and consists of files separated by EOF marks, with two EOF marks at the end of the data.

Each file consists of multiple records, the number depending on the type and amount of data in the file. Data will be of two types: spectral and spatial. Their respective formats will be discussed separately.

Spectral

The first physical record in a spectral data file will be a 180 byte ASCII header record. The ASCII header is broken down as follows:

- 1 to 11 bytes, 11 bytes - A multiplicative scale factor for the binary integer data array in E11.5 format
- 12 to 19 bytes, 8 bytes - The time or frequency spacing of the data array in F8.5 format
- 20 to 27 bytes, 8 bytes - For frequency data, the starting frequency of the data array in F8.2 format
- 28 to 32 bytes, 5 bytes - The number of data values in the data array in I5 format
- 33 to 47 bytes, 15 bytes - The AFGL mission designator in the ASCII format: "MISSION", 3A2
- 48 to 57 bytes, 10 bytes - The AFGL archival tape designator in the ASCII format: "TAPE", ~~FILE~~ <sup>FILE + file name</sup>
- ~~58 to 67 bytes, 11 bytes - The AFGL archival tape record number or Customer Service Number (CSN) in the ASCII format: "RECORD", or "CSN" I3. If this file is constructed from more than one archival record the record number will be zero and the source records description will be placed in the last 108 bytes.~~
- X 69 to 72 bytes, 4 bytes - ASCII blanks

73 to ~~180~~ <sup>113</sup> bytes, 108 bytes - The AFGL archival record descriptor in ASCII "A" format filled with blanks  
(truncate to char)

114 - 180 blanks

The remaining records in the file are binary records 2880 bytes long. They consist of 1440 16 bit words in two's-complement format. Each word represents one data point in the data array. If the record contains less than 1440 data points, it is zero filled. The number of data records in the file can be determined by dividing the number of data values as determined from bytes 28-32 in the header record, by 1440 and rounding

to the next larger integer. The value of each data point can be determined by multiplying the scale factor from header bytes 1-11, by the signed integer value in the data record. For frequency data, the frequency of the first data point and the frequency increment per data point are contained in bytes 12-27 of the header. For time domain data, the interferometer path increment is contained in bytes 12-19 of the header.

### Norelco SWIK Spatial

The first physical record is also a 180 byte ASCII header record. The header is broken down as follows:

<u>Bytes</u>	<u>Format</u>	<u>Description</u>
1-11	E11.5	A multiplicative scale factor for the data array
12-16	F5.2	The vertical angular spacing of the data points within a scan in milliradians
17-21	F5.2	The horizontal angular spacing of the data points between scans in milliradians
22-25	I4	# data points/scan (vertical)
26-29	I4	# scans/record
30-33	I4	# records/file
34-41	-	' FILE ' 8 ASCII characters
42-47	3A2	The AFGL file name in ASCII
48-53	-	' TAPE ' 6 ASCII characters
54-57	2A2	The AFGL Archival Tape ID (4 ASCII characters)
58-65	-	' RECORD ' 8 ASCII characters
66-68	I3	Record # on AFGL archival tape
69-72	-	4 ASCII Blanks (spaces)
73-144	36A2	Archival header info
73-73		'MM/RR' mission/run
79-90		2 ASCII Blanks (spaces)
81-92		'HH:MM:SS:CC ' Zulu Time and space
93-96		'FFF ' filter designator and space
97-98		'dB' dB setting in ASCII

.95387E-06 1.92847 1799.26 1765 MISSION 8202/01 FILE e:n00010  
105.MIS202. NKJ FROM R395-396/R491 SUN NO IN 21:58:42.8 (32)

Rcd 1// 2026 2506 2692 2841 2337 2047 2224 2130 1978 2043 2288 2370  
Rcd 2// 13824 14818 14521 14132 17502 13819 13410 13645 14543 14765 14214 13665  
EOF found for file # 1

.19073E-05 1.92847 1799.26 1765 MISSION 8202/07 FILE e:n00011  
105.MIS202. NKJ FROM R405-406/R491 SUN NO IN 22:11:28.0 (39)

Rcd 1// 1511 1359 1284 1462 1492 1355 1198 1055 1018 1095 1199 1267  
Rcd 2// 7240 7279 7225 6957 6613 6790 7024 7104 7225 7278 7074 6811  
EOF found for file # 2

.19073E-05 1.92847 1799.26 1765 MISSION 8202/05 FILE e:n00012  
105.MIS202. NKJ FROM R415-416/R491 SUN NO IN 22:25:22.0 (35)

Rcd 1// 1204 957 883 1120 1092 962 825 685 738 882 1007 1123  
Rcd 2// 7266 7319 7434 7253 7105 7186 7199 7300 7651 7871 7559 7185  
EOF found for file # 3

.95387E-06 1.92847 1799.26 1765 MISSION 8202/07 FILE e:n00013  
105.MIS202. NKJ FROM R407-410/R491 SUN NO IN 22:36:45.0 (22)

Rcd 1// 2542 2094 1918 2509 2934 2340 2207 1732 1691 2255 2344 2233  
Rcd 2// 15049 15118 14666 13874 13570 13717 13918 14104 14660 14996 14469 13543  
EOF found for file # 4

.95387E-06 1.92847 1799.26 1765 MISSION 8202/09 FILE e:n00014  
105.MIS202. NKJ FROM R413-415/R491 SUN NO IN 22:51:11.0 (39)

Rcd 1// 2433 2438 2151 2504 2638 2334 1919 1425 1558 2125 2214 2165  
Rcd 2// 14845 14943 14612 17773 13373 13870 14157 14168 14450 14605 14349 14101  
EOF found for file # 5

.95387E-06 1.92847 1799.26 1765 MISSION 8202/11 FILE e:n00015  
105.MIS202. NKJ FROM R417-420/R491 SUN NO IN 23:06:32.0 (35)

Rcd 1// 1874 1551 1418 2135 2351 2092 1720 1381 1557 2002 2278 2502  
Rcd 2// 14404 14507 14306 13750 13428 13593 13742 13957 14541 14865 14451 13953  
EOF found for file # 6

.95387E-06 1.92847 1799.26 1765 MISSION 8202/13 FILE e:n00016  
105.MIS202. NKJ FROM R421-424/R491 SUN NO IN 23:16:42.0 (24)

Rcd 1// 2118 1627 1455 2248 2283 1935 1580 1027 1335 2326 2657 2435  
Rcd 2// 13351 13570 13441 12761 12531 13007 13317 13367 13492 13514 13136 12789  
EOF found for file # 7

.19073E-05 1.92847 1799.26 1765 MISSION 8202/17 FILE e:n00017  
105.MIS202. NKJ FROM R427-430/R491 SUN NO IN 23:43:59.2 (32)

Rcd 1// 563 425 610 1018 1011 674 810 593 588 834 941 928  
Rcd 2// 8894 8906 8844 8450 8241 8435 8329 8713 8592 8993 8730 8534  
EOF found for file # 8

.19073E-05 1.92847 1799.26 1765 MISSION 8202/19 FILE e:n00018  
105.MIS202. NKJ FROM R431-434/R491 SUN NO IN 23:54:57.0 (34)

Rcd 1// 815 466 513 1052 1216 956 569 303 522 969 1027 1017  
Rcd 2// 9297 9731 9280 8773 8561 8755 8529 8530 8956 9173 9111 8806  
EOF found for file # 9

.19073E-05 1.92847 1799.26 1765 MISSION 8202/21 FILE e:n00019  
105.MIS202. NKJ FROM R435-438/R491 SUN NO IN

00:03:46.0 (39)

Rcd 1// 737 639 369 479 661 717 601 384 452 736 347 990  
 Rcd 2// 8495 8519 8383 8060 7917 8052 8147 8107 8062 8237 8240 8071  
 EOF found for file # 10

.95367E-06 1.92847 1799.26 1765 MISSION 8202/23 FILE #100000  
 105.MIS202. NML FROM R439-442/R491 SUN ND IN

00:19:52.2 (30)

Rcd 1// 716 689 670 1267 1759 1495 1154 663 1109 1210 1702 1734  
 Rcd 2// 14747 14458 13983 13524 13667 13581 14034 14008 14123 14531 14556 14094  
 EOF found for file # 11

.19073E-05 1.92847 1799.26 1765 MISSION 8202/25 FILE #101021  
 105.MIS202. NML FROM R447-448/R491 SUN ND IN

00:38:24.2 (34)

Rcd 1// 615 501 424 675 689 613 526 465 582 733 797 782  
 Rcd 2// 8741 8319 8052 7683 7627 7843 7924 7811 7779 7974 7992 7738  
 EOF found for file # 12

.95367E-06 1.92847 1799.26 1765 MISSION 8202/27 FILE #100022  
 105.MIS202. NML FROM R447-450/R491 SUN ND IN

00:40:57.0 (34)

Rcd 1// 793 672 724 1261 1216 501 527 664 8113 1427 1383 1763  
 Rcd 2// 14970 14748 14127 13520 13709 14766 14912 14115 13918 14379 14623 14277  
 EOF found for file # 13

.95367E-06 1.92847 1799.26 1765 MISSION 8202/29 FILE #100027  
 105.MIS202. NML FROM R451-454/R491 SUN ND IN

00:49:01.0 (36)

Rcd 1// 648 699 627 987 1046 714 473 445 774 1088 1107 1012  
 Rcd 2// 13623 13112 12437 12124 12408 13052 13116 12882 12761 12811 13115 12661  
 EOF found for file # 14

.95367E-06 1.92847 1799.26 1765 MISSION 8202/31 FILE #101124  
 105.MIS202. NML FROM R455-458/R491 SUN ND IN

00:58:10.2 (37)

Rcd 1// 515 531 496 478 495 545 546 410 581 408 418 371  
 Rcd 2// 13674 12771 11892 11053 12175 13215 13139 12254 11626 12898 12929 12427  
 EOF found for file # 15

.95367E-06 1.92847 1799.26 1765 MISSION 8202/33 FILE #100023  
 105.MIS202. NML FROM R459-462/R491 SUN ND IN

01:05:23.1 (44)

Rcd 1// 478 497 518 546 420 347 336 331 272 245 261 295  
 Rcd 2// 10871 8933 7511 7923 8767 11434 11160 9525 8247 10061 10329 9452  
 EOF found for file # 16

.47684E-06 1.92847 1799.26 1765 MISSION 8202/35 FILE #100026  
 105.MIS202. NML FROM R467-468/R491 SUN ND IN

01:11:54.0 (43)

Rcd 1// 1097 1091 1047 1124 1034 676 504 751 702 711 696 658  
 Rcd 2// 10725 6453 3677 4505 9427 13615 12858 9025 8124 11087 10921 8605  
 EOF found for file # 17

.11921E-06 1.92847 1799.26 1765 MISSION 8202/36 FILE #100488  
 105.MIS202. INFLT AVG/R4 155AD RESP

RESP. CURVE

Rcd 1// 4950 4929 4708 5101 4901 4252 4016 3708 3513 3646 3614 3547  
 Rcd 2// 0 0 0 0 0 0 0 0 0 0 0 0  
 EOF found for file # 18

.25502E-07 1.92847 1799.26 1765 MISSION 8202/37 FILE #100495  
 105.MIS202. CONSTRUCTED CURVE FROM R485

SMOOTHED CORRELATION CURVE

Rcd 1// 13295 17155 13244 13121 13365 13345 13721 13367 13312 13740 13371 13340  
 Rcd 2// 0 0 0 0 0 0 0 0 0 0 0 0



EDF found for file # 19

.100002-01 1.92847 1799.26 1765 MISSION 8202/cc FILE e:n00491  
105.MIS202. IRAD RESP (R4)\*R422+.9\* ND **CORRECTED RESP CURVE** C

Red 1//	3171	1207	1331	1273	1413	1490	1643	2157	2241	2254	2402	2573
Red 2//	2711	2665	2665	2773	2345	2220	2797	2721	2607	2593	2692	2797

EDF found for file # 20

.390638-02 1.92847 1799.26 1765 MISSION 8202/cc FILE e:n00491  
105.MIS202. IRAD RESP (R4)\*R422+.9\* ND **CORRECTED RESP w/ND** C NA

Red 1//	614	637	698	667	740	835	965	1051	1182	1195	1255	1334
Red 2//	698	685	685	713	731	724	713	698	668	666	691	715

EDF found for file # 21

.582085-10 1.92847 1799.26 1765 MISSION 8202/02 FILE e:n00493  
105.MIS202. NNL FROM R396-T28/R490 BKND **22:03: 23.0 (49)**

Red 1//	3719	7001	2127	2850	2779	2077	2335	2018	1987	1990	1944	1754
Red 2//	62	57	125	65	17	53	106	55	2	11	42	121

EDF found for file # 22

.391045-10 1.92847 1799.26 1765 MISSION 8202/04 FILE e:n00493  
105.MIS202. NNL FROM R410-403/R490 BKND **22:15: 29.0 (41)**

Red 1//	4756	4784	4071	4657	4753	3681	3487	3369	3096	3083	3231	3257
Red 2//	21	157	252	297	45	329	370	328	200	99	127	146

EDF found for file # 23

.582085-10 1.92847 1799.26 1765 MISSION 8202/06 FILE e:n00494  
105.MIS202. NNL FROM R404-401/R490 BKND **22: 30: 30.2 (40)**

Red 1//	3914	7815	3479	1092	3056	3743	1931	1725	2176	1767	1827	1997
Red 2//	14	36	22	2	9	37	114	157	56	6	52	15

EDF found for file # 24

.582085-10 1.92847 1799.26 1765 MISSION 8202/08 FILE e:n00495  
105.MIS202. NNL FROM R408-410/R490 BKND **22: 42: 23.0 (40)**

Red 1//	4482	4375	3771	3628	3594	3104	2941	2845	2462	2149	2032	2012
Red 2//	5	4	11	93	146	127	104	83	116	121	20	38

EDF found for file # 25

.582085-10 1.92847 1799.26 1765 MISSION 8202/10 FILE e:n00496  
105.MIS202. NNL FROM R414-416/R490 BKND **22: 59: 30.9 (44)**

Red 1//	4215	4106	3751	3748	3424	3155	3252	3058	2494	2207	2235	2342
Red 2//	31	74	65	37	83	130	83	4	45	54	25	6

EDF found for file # 26

.582085-10 1.92847 1799.26 1765 MISSION 8202/12 FILE e:n00497  
105.MIS202. NNL FROM R418-420/R490 BKND **23: 11: 03.0 (41)**

Red 1//	4409	4603	4133	3965	3466	3087	3262	3107	2452	2082	2066	2051
Red 2//	63	14	95	2	78	46	13	39	28	6	25	39

EDF found for file # 27

.582085-10 1.92847 1799.26 1765 MISSION 8202/14 FILE e:n00498  
105.MIS202. NNL FROM R422-424/R490 BKND **23: 22: 54.2 (47)**

Red 1//	4198	4314	4136	4124	3802	3350	3253	2977	2470	2335	2296	2181
Red 2//	36	10	119	64	42	92	123	96	12	57	25	7

EDF found for file # 28

.582085-10 1.92847 1799.26 1765 MISSION 8202/16 FILE e:n00499

105.MIS202. NNU FROM R432-433/R490 B/BND

23:49:14.0 (31)

Rec	1//	4177	3513	2764	3584	4101	3461	2955	2531	3005	2912	4245	4230
Rec	2//	329	35	95	5	75	51	12	122	77	111	124	145

EOF found for file # 29

.11642E-09 1.92647 1799.26 1765 MISSION 8202/20 FILE 8:n00511

105.MIS202. NNU FROM R432-434/R490 B/BND

23:58:53.8 (42)

Rec	1//	2452	2401	1213	2174	1970	1835	1920	1796	1485	1225	1164	1141
Rec	2//	121	107	103	55	24	40	32	15	20	26	26	20

EOF found for file # 30

.58208E-10 1.92647 1799.26 1765 MISSION 8202/22 FILE 8:n00501

105.MIS202. NNU FROM R436-439/R490 B/BND

00:11:05.0 (45)

Rec	1//	4153	4505	3876	3520	2952	2441	2448	2685	1095	1693	1512	1325
Rec	2//	54	161	44	78	74	75	30	132	227	141	3	39

EOF found for file # 31

.58208E-10 1.92647 1799.26 1765 MISSION 8202/24 FILE 8:n00502

105.MIS202. NNU FROM R440-443/R490 B/BND

00:26:20.1 (47)

Rec	1//	5764	5776	4710	4600	1931	2447	2759	1548	2454	2325	2482	2495
Rec	2//	14	75	34	54	62	2	25	37	55	210	230	59

EOF found for file # 32

.11642E-09 1.92647 1799.26 1765 MISSION 8202/26 FILE 8:n00503

105.MIS202. NNU FROM R444-445/R490 B/BND

00:36:08.0 (45)

Rec	1//	3125	3145	2737	2602	2352	2135	2157	2095	1575	1435	1403	1350
Rec	2//	25	71	21	47	47	5	14	23	7	15	44	55

EOF found for file # 33

.58208E-10 1.92647 1799.26 1765 MISSION 8202/28 FILE 8:n00504

105.MIS202. NNU FROM R448-450/R490 B/BND

00:44:37.0 (48)

Rec	1//	4655	4550	5514	6270	5887	5144	5105	4571	3972	3772	3645	3547
Rec	2//	162	72	67	105	57	63	59	55	208	250	173	121

EOF found for file # 34

.58208E-10 1.92647 1799.26 1765 MISSION 8202/30 FILE 8:n00505

105.MIS202. NNU FROM R452-454/R490 B/BND

00:52:49.0 (48)

Rec	1//	5001	6435	5974	5983	5458	4685	4413	4064	3531	3074	3730	3032
Rec	2//	24	13	15	59	75	92	76	7	5	74	26	65

EOF found for file # 35

.58208E-10 1.92647 1799.26 1765 MISSION 8202/32 FILE 8:n00506

105.MIS202. NNU FROM R456-457/R490 B/BND

01:01:47.2 (47)

Rec	1//	6159	5783	5321	5993	5784	4969	4353	4287	4070	4082	3940	3795
Rec	2//	234	191	179	100	165	341	353	217	178	268	345	345

EOF found for file # 36

.11642E-09 1.92647 1799.26 1765 MISSION 8202/34 FILE 8:n00507

105.MIS202. NNU FROM R460-462/R490 B/BND

01:08:28.0 (47)

Rec	1//	3437	3264	3083	3446	3272	2769	2544	2335	2334	2504	2414	2264
Rec	2//	35	41	42	35	37	52	59	73	102	94	47	49

EOF found for file # 37

.11642E-09 1.92647 1799.26 1765 MISSION 8202/36 FILE 8:n00508

105.MIS202. NNU FROM R464-467/R490 B/BND

01:14:52.0 (39)

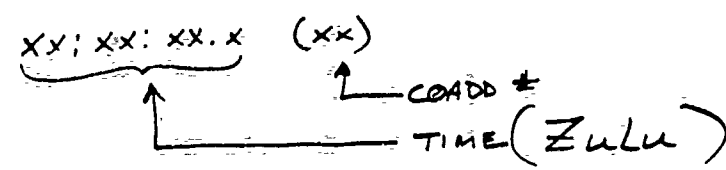
Rec	1//	3182	3114	2855	2742	2550	2272	2100	2150	2015	2702	2404	2477
-----	-----	------	------	------	------	------	------	------	------	------	------	------	------

120 177 180 183 186 189 192 195 198 201 204 207 210 213 216 219 222 225 228 231 234 237 240 243 246 249 252 255 258 261 264 267 270 273 276 279 282 285 288 291 294 297 300 303 306 309 312 315 318 321 324 327 330 333 336 339 342 345 348 351 354 357 360 363 366 369 372 375 378 381 384 387 390 393 396 399 402 405 408 411 414 417 420 423 426 429 432 435 438 441 444 447 450 453 456 459 462 465 468 471 474 477 480 483 486 489 492 495 498 501 504 507 510 513 516 519 522 525 528 531 534 537 540 543 546 549 552 555 558 561 564 567 570 573 576 579 582 585 588 591 594 597 600 603 606 609 612 615 618 621 624 627 630 633 636 639 642 645 648 651 654 657 660 663 666 669 672 675 678 681 684 687 690 693 696 699 702 705 708 711 714 717 720 723 726 729 732 735 738 741 744 747 750 753 756 759 762 765 768 771 774 777 780 783 786 789 792 795 798 801 804 807 810 813 816 819 822 825 828 831 834 837 840 843 846 849 852 855 858 861 864 867 870 873 876 879 882 885 888 891 894 897 900 903 906 909 912 915 918 921 924 927 930 933 936 939 942 945 948 951 954 957 960 963 966 969 972 975 978 981 984 987 990 993 996 999 1002 1005 1008 1011 1014 1017 1020 1023 1026 1029 1032 1035 1038 1041 1044 1047 1050 1053 1056 1059 1062 1065 1068 1071 1074 1077 1080 1083 1086 1089 1092 1095 1098 1101 1104 1107 1110 1113 1116 1119 1122 1125 1128 1131 1134 1137 1140 1143 1146 1149 1152 1155 1158 1161 1164 1167 1170 1173 1176 1179 1182 1185 1188 1191 1194 1197 1200 1203 1206 1209 1212 1215 1218 1221 1224 1227 1230 1233 1236 1239 1242 1245 1248 1251 1254 1257 1260 1263 1266 1269 1272 1275 1278 1281 1284 1287 1290 1293 1296 1299 1302 1305 1308 1311 1314 1317 1320 1323 1326 1329 1332 1335 1338 1341 1344 1347 1350 1353 1356 1359 1362 1365 1368 1371 1374 1377 1380 1383 1386 1389 1392 1395 1398 1401 1404 1407 1410 1413 1416 1419 1422 1425 1428 1431 1434 1437 1440 1443 1446 1449 1452 1455 1458 1461 1464 1467 1470 1473 1476 1479 1482 1485 1488 1491 1494 1497 1500 1503 1506 1509 1512 1515 1518 1521 1524 1527 1530 1533 1536 1539 1542 1545 1548 1551 1554 1557 1560 1563 1566 1569 1572 1575 1578 1581 1584 1587 1590 1593 1596 1599 1602 1605 1608 1611 1614 1617 1620 1623 1626 1629 1632 1635 1638 1641 1644 1647 1650 1653 1656 1659 1662 1665 1668 1671 1674 1677 1680 1683 1686 1689 1692 1695 1698 1701 1704 1707 1710 1713 1716 1719 1722 1725 1728 1731 1734 1737 1740 1743 1746 1749 1752 1755 1758 1761 1764 1767 1770 1773 1776 1779 1782 1785 1788 1791 1794 1797 1800 1803 1806 1809 1812 1815 1818 1821 1824 1827 1830 1833 1836 1839 1842 1845 1848 1851 1854 1857 1860 1863 1866 1869 1872 1875 1878 1881 1884 1887 1890 1893 1896 1899 1902 1905 1908 1911 1914 1917 1920 1923 1926 1929 1932 1935 1938 1941 1944 1947 1950 1953 1956 1959 1962 1965 1968 1971 1974 1977 1980 1983 1986 1989 1992 1995 1998 2001 2004 2007 2010 2013 2016 2019 2022 2025 2028 2031 2034 2037 2040 2043 2046 2049 2052 2055 2058 2061 2064 2067 2070 2073 2076 2079 2082 2085 2088 2091 2094 2097 2100 2103 2106 2109 2112 2115 2118 2121 2124 2127 2130 2133 2136 2139 2142 2145 2148 2151 2154 2157 2160 2163 2166 2169 2172 2175 2178 2181 2184 2187 2190 2193 2196 2199 2202 2205 2208 2211 2214 2217 2220 2223 2226 2229 2232 2235 2238 2241 2244 2247 2250 2253 2256 2259 2262 2265 2268 2271 2274 2277 2280 2283 2286 2289 2292 2295 2298 2301 2304 2307 2310 2313 2316 2319 2322 2325 2328 2331 2334 2337 2340 2343 2346 2349 2352 2355 2358 2361 2364 2367 2370 2373 2376 2379 2382 2385 2388 2391 2394 2397 2400 2403 2406 2409 2412 2415 2418 2421 2424 2427 2430 2433 2436 2439 2442 2445 2448 2451 2454 2457 2460 2463 2466 2469 2472 2475 2478 2481 2484 2487 2490 2493 2496 2499 2502 2505 2508 2511 2514 2517 2520 2523 2526 2529 2532 2535 2538 2541 2544 2547 2550 2553 2556 2559 2562 2565 2568 2571 2574 2577 2580 2583 2586 2589 2592 2595 2598 2601 2604 2607 2610 2613 2616 2619 2622 2625 2628 2631 2634 2637 2640 2643 2646 2649 2652 2655 2658 2661 2664 2667 2670 2673 2676 2679 2682 2685 2688 2691 2694 2697 2700 2703 2706 2709 2712 2715 2718 2721 2724 2727 2730 2733 2736 2739 2742 2745 2748 2751 2754 2757 2760 2763 2766 2769 2772 2775 2778 2781 2784 2787 2790 2793 2796 2799 2802 2805 2808 2811 2814 2817 2820 2823 2826 2829 2832 2835 2838 2841 2844 2847 2850 2853 2856 2859 2862 2865 2868 2871 2874 2877 2880 2883 2886 2889 2892 2895 2898 2901 2904 2907 2910 2913 2916 2919 2922 2925 2928 2931 2934 2937 2940 2943 2946 2949 2952 2955 2958 2961 2964 2967 2970 2973 2976 2979 2982 2985 2988 2991 2994 2997 3000 3003 3006 3009 3012 3015 3018 3021 3024 3027 3030 3033 3036 3039 3042 3045 3048 3051 3054 3057 3060 3063 3066 3069 3072 3075 3078 3081 3084 3087 3090 3093 3096 3099 3102 3105 3108 3111 3114 3117 3120 3123 3126 3129 3132 3135 3138 3141 3144 3147 3150 3153 3156 3159 3162 3165 3168 3171 3174 3177 3180 3183 3186 3189 3192 3195 3198 3201 3204 3207 3210 3213 3216 3219 3222 3225 3228 3231 3234 3237 3240 3243 3246 3249 3252 3255 3258 3261 3264 3267 3270 3273 3276 3279 3282 3285 3288 3291 3294 3297 3300 3303 3306 3309 3312 3315 3318 3321 3324 3327 3330 3333 3336 3339 3342 3345 3348 3351 3354 3357 3360 3363 3366 3369 3372 3375 3378 3381 3384 3387 3390 3393 3396 3399 3402 3405 3408 3411 3414 3417 3420 3423 3426 3429 3432 3435 3438 3441 3444 3447 3450 3453 3456 3459 3462 3465 3468 3471 3474 3477 3480 3483 3486 3489 3492 3495 3498 3501 3504 3507 3510 3513 3516 3519 3522 3525 3528 3531 3534 3537 3540 3543 3546 3549 3552 3555 3558 3561 3564 3567 3570 3573 3576 3579 3582 3585 3588 3591 3594 3597 3600 3603 3606 3609 3612 3615 3618 3621 3624 3627 3630 3633 3636 3639 3642 3645 3648 3651 3654 3657 3660 3663 3666 3669 3672 3675 3678 3681 3684 3687 3690 3693 3696 3699 3702 3705 3708 3711 3714 3717 3720 3723 3726 3729 3732 3735 3738 3741 3744 3747 3750 3753 3756 3759 3762 3765 3768 3771 3774 3777 3780 3783 3786 3789 3792 3795 3798 3801 3804 3807 3810 3813 3816 3819 3822 3825 3828 3831 3834 3837 3840 3843 3846 3849 3852 3855 3858 3861 3864 3867 3870 3873 3876 3879 3882 3885 3888 3891 3894 3897 3900 3903 3906 3909 3912 3915 3918 3921 3924 3927 3930 3933 3936 3939 3942 3945 3948 3951 3954 3957 3960 3963 3966 3969 3972 3975 3978 3981 3984 3987 3990 3993 3996 4000

.11642E-09 1.92647 1799.26 1745 MISSION B100177 FILE B1001509  
 105.MIS302. N.L FROM 8465-4677/8490 SUN ND OUT 01:17:23.8 (40)

Rec 1// 3151 01:11 2877 3346 3299 2859 2526 2255 2349 2543 2539 2591  
 Rec 2// 94 106 65 36 54 84 75 35 17 13 31 23  
 EOF found for file # 39

Second EOF Found



SUN AND BEG ARE IN PAIRS

SUN	FILE 10 / BEG	ND IN
"	" / " 492	
"	" / " 493	
"	" 12 / " 494	
"	" 13 / " 495	
"	" 14 / " 496	
"	" 15 / " 497	
"	" 16 / " 498	
"	" 17 / " 499	
"	" 18 / " 500	
"	" 19 / " 501	
"	" 20 / " 502	
"	" 21 / " 503	
"	" 22 / " 504	
"	" 23 / " 505	
"	" 24 / " 506	
"	" 25 / " 507	
"	" 26 / " 508	
"	" 509 / " 508	
37	36	

← ND OUT

BW  
 6/19/1990

## Appendix 3

Run 01 Numeric File

2130	2224	2047	2337	2141	2592	2533	2026
1982	1911	1994	2364	2373	2202	2042	1978
2192	2345	2356	2330	2246	1995	1725	1857
2181	2151	2119	2116	2116	2055	1929	1971
2591	2362	2166	2235	2736	2345	2266	2212
2672	2729	2704	2710	2676	2676	2657	2672
2776	2643	2655	2614	2764	2766	2745	2637
2691	2635	2624	2636	2743	2753	2792	2767
2747	2726	2911	2961	2943	2821	2761	2802
3034	2996	2973	2862	2896	2936	3033	2950
3060	3078	3064	3049	3025	3011	3093	3015
3162	3120	3131	3194	3177	3131	3042	3014
3159	3090	3052	3093	3133	3126	3171	3137
3291	3227	3223	3251	3241	3217	3169	3147
3251	3230	3276	3237	3192	3194	3277	3276
3215	3213	3219	3253	3290	3291	3269	3256
2991	3004	2997	3016	3092	3162	3204	3204
3051	2962	2942	2932	2965	2983	2975	2910
2809	2839	2904	2912	2769	2234	2247	2832
2894	2903	2863	2853	2872	2326	2821	2887
2621	2761	2972	3191	3139	2861	2773	2852
3525	3385	3131	2917	2806	2700	2620	2586
3545	3595	3643	3730	3717	3674	3641	3594
3550	3532	3532	3557	3563	3561	3595	3556
3364	3375	3414	3474	3509	3512	3509	3527
2812	2862	2954	3004	3037	3131	3233	3313
2204	2291	2370	2408	2459	2579	2684	2755
2447	2753	2856	2576	2273	2191	2186	2166
1523	1489	1467	1550	1664	1763	1897	2116
943	1051	1152	1317	1492	1634	1649	1564
87	144	219	309	446	593	698	801
114	228	600	699	436	179	92	71
92	17	14	27	44	53	76	90
48	31	89	70	56	74	117	136
16	5	12	22	34	20	2	9
19	14	22	42	43	65	44	0
342	261	152	81	59	4	56	38
504	235	251	306	339	389	458	432
4696	4614	4466	4234	3920	3213	2216	1213
4559	4550	4623	4709	4750	4716	4684	4688
4693	4666	4622	4574	4559	4568	4554	4543
4842	4774	4719	4719	4746	4730	4684	4681
4871	4860	4862	4874	4857	4808	4796	4842
4943	4929	4853	4729	4753	4867	4874	4860
5115	5103	5099	5119	5085	5043	5034	4985
5201	5153	5091	5139	5179	5139	5104	5107
5303	5297	5292	5276	5222	5163	5150	5163
5336	5353	5324	5317	5308	5311	5332	5320
5213	5226	5233	5209	5218	5243	5272	5297
5279	5351	5391	5316	5159	5030	5166	5229
5320	5292	5275	5274	5200	5220	5157	5207
5726	5764	5723	5640	5599	5444	5282	5305
5810	5777	5764	5703	5756	5757	5710	5711
5810	5777	5764	5703	5756	5757	5710	5711
5963	5974	5912	5871	5827	5980	5973	5867
6157	6082	6004	5932	5877	5901	5892	5866
6010	5912	5867	5926	6009	6045	6046	6113
6046	6096	6043	6013	6020	5994	5971	6009
6120	6049	6134	6186	6111	6045	6026	5999
6154	6090	6127	6203	6202	6132	6177	6205

6393	6379	6305	6243	6210	6095	6072	6160
6314	6308	6329	6304	6255	6202	6270	6308
6545	6522	6460	6403	6329	6283	6337	6364
6373	6505	6607	6610	6497	6275	6245	6417
6331	6354	6348	6356	6453	6478	6475	6395
6691	6610	6605	6601	6492	6397	6510	6500
6593	6507	6495	6542	6650	6644	6647	6719
6903	6893	6827	6748	6730	6731	6798	6736
6902	6854	6805	6742	6754	6772	6741	6793
6910	6757	6816	6905	6733	6748	6757	6814
6931	6950	6796	6699	6809	6917	6915	6950
6479	6639	6600	6730	6827	6709	6890	6886
6949	6448	6006	6320	7038	7126	6912	6848
6870	6743	7016	6952	6495	5973	6531	7117
7048	6726	5939	6247	6898	6970	6244	6207
6322	6941	7201	7114	6360	5804	6490	6981
7200	6844	6295	6590	7299	7306	7092	6410
6723	6845	7076	7146	6783	6257	6705	7264
3658	5316	6247	6561	6966	7426	7514	7104
6377	6933	7210	7059	6511	4730	2252	1976
7615	7696	7507	7253	7306	7409	7285	7129
7312	6437	6210	6698	7013	6917	6566	6963
6776	7432	7694	7357	6621	6640	7349	7640
7827	7609	6897	6626	7267	7579	7282	6714
7257	6757	7003	7606	7712	6965	6320	7147
7110	7566	7875	7532	6929	7036	7560	7660
7838	8034	7743	7338	7639	7929	7841	7356
8256	7987	7739	7836	8016	7377	7500	7482
8167	8038	8092	8034	8034	8016	8080	8206
8056	8231	8054	7829	7922	7930	7933	8139
7971	7959	7984	8122	8213	8153	8086	7963
8006	7903	7886	7927	8127	8228	8140	8031
8067	8169	8218	8177	8145	8077	8028	8074
8002	8066	8086	8077	8157	8136	8093	8065
8276	8345	8329	8220	8246	8408	8357	8133
8400	8274	8285	8335	8347	8295	8271	8218
8238	8280	8363	8479	8443	8333	8416	8518
8645	8639	8739	8853	8693	8446	8263	8175
8706	8664	8725	8681	8600	8597	8632	8640
8722	8827	8815	8789	8788	8763	8759	8791
8815	8802	8801	8772	8750	8777	8741	8663
8904	8801	8701	8762	8890	8910	8909	8866
9014	9034	9166	9206	9086	8991	8959	8944
9213	9138	9109	9016	8983	9016	8986	9030
9084	9091	9091	9128	9204	9177	9131	9220
9110	9122	9136	9108	9005	8985	9048	9082
8636	8856	8947	9121	9299	9349	9293	9170
8648	8844	8964	9000	9005	9074	9018	8711
8800	8697	8675	8596	8622	8745	8775	8641
8352	8344	8272	8378	8515	8448	8562	8839
8438	8339	8109	8207	8376	8346	8333	8336
7908	7959	8217	8320	8398	8424	8211	8277
7861	7849	8031	8112	8056	7979	8177	8170
8090	8011	8070	8070	8047	8051	8105	8034
4870	4057	4000	4014	3847	5735	6116	5550
2233	2028	3244	3599	3835	4322	4512	5061
20	145	298	426	609	1011	1307	1600
1268	2062	2160	1210	404	233	216	66
808	473	485	435	292	434	607	782
5207	5573	5316	4598	3755	3033	2210	1374

7906	7950	7914	7151	7075	7269	7250	4710
8516	3206	4421	5030	4867	5951	7307	7344
409	657	1044	1661	2514	3310	3715	7940
270	249	95	56	75	13	301	394
274	364	495	790	1406	1423	440	160
1632	771	477	293	727	342	270	274
1615	6351	5472	5340	4879	3527	7072	3723
9027	9371	9515	10125	10144	9279	9030	9374
9321	9630	9541	8861	9463	10540	10710	9893
6303	6142	6620	6307	10494	10679	10237	9731
7541	8601	10032	9538	6142	7610	6507	7503
4113	9467	9533	9139	3899	7081	6552	7773
10180	9503	6156	8247	7425	7432	6390	6064
9709	9716	9700	8505	6327	5714	7561	9540
10444	10456	9400	6792	3278	6651	3793	9287
9815	9177	10076	10121	9310	9540	8192	9145
10720	10047	8579	8311	6597	9097	10150	10739
10420	10667	10573	9978	9967	10566	10613	10771
11080	11135	10660	10092	9171	10005	10373	10461
11245	10904	10703	10423	10617	10825	10704	10723
10592	11227	11405	11334	11229	11460	11663	11510
11406	11143	10990	11064	11201	11213	10795	10593
11276	11319	11204	11166	11193	11406	11650	11609
11623	11319	11140	11069	11056	11237	11274	11133
10866	10974	10979	11122	11267	11117	11174	11576
11772	11234	11078	11369	11650	11712	11427	11003
11567	11634	11763	11729	11675	11742	11794	11963
12093	11926	11752	11711	11656	11459	11293	11411
12054	12125	12011	11746	11756	12119	12072	11942
11708	11723	11350	11844	11813	11894	11954	11967
11673	11506	11628	11730	11936	12051	11860	11735
11739	11737	11946	12054	12074	12251	12243	11961
12340	12168	11710	11780	12169	12240	12304	12074
12277	12398	12874	12833	12422	12091	12072	12182
12333	11916	11578	12441	12976	12608	11964	11927
12144	11901	11734	11540	11917	12075	11802	12155
10813	11949	12261	12753	12427	12210	12385	12473
12601	12424	12547	12638	12398	12412	12307	11237
12344	12424	12341	12239	12348	12869	13380	13060
12046	12125	12242	12186	12162	12157	12436	12455
13013	12745	12551	12772	12745	12606	12591	12362
12764	12752	12639	12712	13172	13249	12695	12666
12514	12734	13194	13057	12932	12953	12795	12749
12976	12842	12874	13061	12409	11350	12157	12545
12792	12083	12285	12800	13186	12953	12630	12788
12323	13039	13096	12366	12138	12635	13108	13399
12727	13147	12999	12613	12546	12523	12338	12053
12524	12244	12025	12699	13296	13073	12700	12555
12750	12006	12910	12763	12711	12650	12454	12418
12606	12399	12379	12557	12509	12692	13116	12069
12533	12299	12633	13034	12761	12297	12161	12430
12211	12754	13096	13725	14014	13692	13143	12917
12519	12464	12417	12496	12937	14207	12903	12933
12147	12177	12177	12177	12473	12644	12903	12701
12173	12140	12091	13108	13337	13432	13173	12000
13070	12304	13274	13347	13259	12912	12667	12877
13812	13575	13370	13655	13895	13963	13793	12151
14271	14725	14370	13623	13261	13118	13309	13619
13243	13523	13911	13777	13640	13561	13512	13099
12537	13173	12945	13059	12829	12712	12704	13013

13645	13418	13519	13532	14078	14531	14716	13234
13766	13972	14117	13727	13665	14214	14765	14546
12297	11359	12251	12940	12751	12410	12973	13733
13703	13891	13494	12792	12599	12443	12391	12624
13096	13226	13444	13117	14504	14454	13907	13614
1301	12633	12571	12909	13373	13667	13673	13251
14313	14641	14501	13756	13333	13901	14263	14111
14719	14616	14125	13469	13276	13343	13266	13619
12973	13362	14093	14573	14151	13329	13370	14398
13306	13605	13114	13064	13421	13677	13746	13336
14207	14410	13927	13694	13907	13556	13673	13612
13440	14017	13705	12991	12954	12746	12101	13413
13715	14292	14142	13347	13664	14036	14397	13624
13474	13193	13915	14376	13691	13301	13764	12737
13436	13212	13056	13697	13591	13291	13999	14161
13664	13476	13021	13706	14017	13413	13222	13321
13215	12193	12213	12333	12571	12416	12455	13099
11533	12361	12399	12232	12331	12656	12099	13401
11025	11331	12111	11506	12019	12475	12531	11634
13540	13126	12573	12693	12351	11729	11625	11037
14210	14192	13559	13738	13976	14356	14499	13739
15069	14345	13230	12835	12919	13757	13630	13377
14497	14541	14303	13943	13193	13690	13244	13573
12907	13401	13194	11974	12691	13331	13473	13673
10547	11054	11171	10720	11332	12142	12596	13034
10844	10377	9688	9942	9742	9614	10492	10805
8919	8943	9293	10039	10847	11223	11122	10758
12602	12147	11516	10061	9263	9532	9492	9096
12901	12941	13597	13217	12735	13114	13323	12909
12649	12706	12655	13791	13050	12322	13367	14074
13664	13930	13152	13285	13439	13634	13379	12419
11745	12027	12994	12720	12477	13367	13413	12217
12307	13012	13084	12932	13247	13014	13171	12770
12525	11893	11054	10947	10914	10647	11332	12161
12562	12466	12191	11552	11963	13455	13759	13066
13390	12143	13199	13599	12790	11952	11450	12223
12733	13113	12537	14115	14553	13340	13422	14651
14834	13757	14386	14421	13260	14366	13359	11849
14325	14368	14246	15468	14347	12703	13512	15526
14630	14181	13754	13775	13656	13509	13753	14157
0	0	0	0	12402	14569	14906	14376



**Appendix 4**  
**Run 01 Data File**

0	2020	0.0019321	1726.26	0.00051574
1	2021	0.0019411	1731.19	0.00051711
2	2022	0.0019502	1736.12	0.00051848
3	2023	0.0019594	1741.05	0.00051985
4	2024	0.0019686	1745.97	0.00052121
5	2025	0.0019778	1750.90	0.00052258
6	2026	0.0019870	1755.83	0.00052395
7	2027	0.0019962	1760.76	0.00052532
8	2028	0.0020054	1765.69	0.00052669
9	2029	0.0020146	1770.62	0.00052806
10	2030	0.0020238	1775.54	0.00052943
11	2031	0.0020330	1780.47	0.00053080
12	2032	0.0020422	1785.40	0.00053217
13	2033	0.0020514	1790.33	0.00053354
14	2034	0.0020606	1795.26	0.00053491
15	2035	0.0020698	1800.19	0.00053628
16	2036	0.0020790	1805.12	0.00053765
17	2037	0.0020882	1810.05	0.00053902
18	2038	0.0020974	1814.97	0.00054039
19	2039	0.0021066	1819.90	0.00054176
20	2040	0.0021158	1824.83	0.00054313
21	2041	0.0021250	1829.76	0.00054450
22	2042	0.0021342	1834.69	0.00054587
23	2043	0.0021434	1839.62	0.00054724
24	2044	0.0021526	1844.54	0.00054861
25	2045	0.0021618	1849.47	0.00055000
26	2046	0.0021710	1854.40	0.00055137
27	2047	0.0021802	1859.33	0.00055274
28	2048	0.0021894	1864.26	0.00055411
29	2049	0.0021986	1869.19	0.00055548
30	2050	0.0022078	1874.12	0.00055685
31	2051	0.0022170	1879.05	0.00055822
32	2052	0.0022262	1883.97	0.00055959
33	2053	0.0022354	1888.90	0.00056096
34	2054	0.0022446	1893.83	0.00056233
35	2055	0.0022538	1898.76	0.00056370
36	2056	0.0022630	1903.69	0.00056507
37	2057	0.0022722	1908.62	0.00056644
38	2058	0.0022814	1913.54	0.00056781
39	2059	0.0022906	1918.47	0.00056918
40	2060	0.0023000	1923.40	0.00057055
41	2061	0.0023092	1928.33	0.00057192
42	2062	0.0023184	1933.26	0.00057329
43	2063	0.0023276	1938.19	0.00057466
44	2064	0.0023368	1943.12	0.00057603
45	2065	0.0023460	1948.05	0.00057740
46	2066	0.0023552	1952.97	0.00057877
47	2067	0.0023644	1957.90	0.00058014
48	2068	0.0023736	1962.83	0.00058151
49	2069	0.0023828	1967.76	0.00058288
50	2070	0.0023920	1972.69	0.00058425
51	2071	0.0024012	1977.62	0.00058562
52	2072	0.0024104	1982.54	0.00058699
53	2073	0.0024196	1987.47	0.00058836
54	2074	0.0024288	1992.40	0.00058973
55	2075	0.0024380	1997.33	0.00059110
56	2076	0.0024472	2002.26	0.00059247
57	2077	0.0024564	2007.19	0.00059384
58	2078	0.0024656	2012.12	0.00059521
59	2079	0.0024748	2017.05	0.00059658

1740	14424	0.0137529	5154.50	0.000193924
1741	14386	0.0137195	5156.73	0.000193921
1742	13757	0.0131194	5158.65	0.000193849
1743	14334	0.0141457	5160.58	0.000193777
1744	15524	0.0148067	5162.51	0.000193754
1745	13512	0.0128760	5164.44	0.000193632
1746	12703	0.0121143	5166.37	0.000193560
1747	14347	0.0136823	5168.30	0.000193477
1748	15462	0.0147514	5170.23	0.000193415
1749	14346	0.0141532	5172.15	0.000193343
1750	14303	0.0137023	5174.08	0.000193271
1751	14323	0.0136613	5176.01	0.000193199
1752	14157	0.0135011	5177.94	0.000193127
1753	13753	0.0131158	5179.87	0.000193055
1754	13509	0.0128831	5181.80	0.000192973
1755	13656	0.0130233	5183.73	0.000192911
1756	13775	0.0131368	5185.65	0.000192840
1757	13754	0.0131168	5187.58	0.000192768
1758	14181	0.0135240	5189.51	0.000192696
1759	14630	0.0139522	5191.44	0.000192625
1760	14376	0.0137100	5193.37	0.000192553
1761	14806	0.0141200	5195.30	0.000192482
1762	14569	0.0138940	5197.22	0.000192410
1763	12402	0.0118274	5199.15	0.000192339
1764	0	0.0000000	5201.08	0.000192268
1765	0	0.0000000	5203.01	0.000192196
1766	0	0.0000000	5204.94	0.000192125
1767	0	0.0000000	5206.87	0.000192054

## Appendix 5

Run 01 Calibrated Data File

1799.24	7.65532797799597E-0007	5.5571	1.47747829975196E-0004
1801.19	9.37960247000224E-0007	5.5519	3.04252416265993E-0004
1803.12	1.01330017529949E-0006	5.5450	3.29239961500685E-0004
1805.05	1.05746210079977E-0006	5.5400	3.45398962430910E-0004
1806.97	5.87291479099911E-0007	5.5341	2.87967074133761E-0004
1808.97	7.76503749299736E-0007	5.5272	2.54052726891947E-0004
1810.88	5.42020001949527E-0007	5.5223	2.76377320195513E-0004
1812.76	8.00953037199217E-0007	5.5164	2.65523700751835E-0004
1814.69	7.48320153598772E-0007	5.5106	2.46430153350603E-0004
1816.62	7.74564199700241E-0007	5.5047	2.55539983414967E-0004
1818.54	3.76577551999922E-0007	5.4989	2.75037956064470E-0004
1820.47	3.97715772999670E-0007	5.4931	2.98359754158902E-0004
1822.40	6.99657970499722E-0007	5.4873	2.98339522593709E-0004
1824.33	7.56167436793995E-0007	5.4815	2.51621232966180E-0004
1826.26	6.89454865800306E-0007	5.4757	2.30215893369579E-0004
1828.19	7.52592580999592E-0007	5.4699	2.51296214744399E-0004
1830.12	7.36715775999063E-0007	5.4641	2.36798963411991E-0004
1832.04	6.49513446899355E-0007	5.4584	2.16504481950652E-0004
1833.97	7.14472105000490E-0007	5.4526	2.40904384215737E-0004
1835.90	7.75442766500231E-0007	5.4469	2.61644150147511E-0004
1837.83	7.63451066199966E-0007	5.4412	2.59285062459647E-0004
1839.76	7.39363463200110E-0007	5.4355	2.50345874275743E-0004
1841.69	7.03350036400374E-0007	5.4298	2.39570398725546E-0004
1843.61	6.57556223999415E-0007	5.4241	2.22272526613772E-0004
1845.54	5.90998356700227E-0007	5.4185	2.01168752826719E-0004
1847.47	5.78061107199615E-0007	5.4128	1.97112737302607E-0004
1849.40	6.15716245400480E-0007	5.4072	2.10697225401457E-0004
1851.33	6.34658639699429E-0007	5.4015	2.17565040157464E-0004
1853.26	6.34061653998971E-0007	5.3959	2.17360389080046E-0004
1855.19	6.24698926399620E-0007	5.3903	2.18744451511321E-0004
1857.11	6.44157431200136E-0007	5.3847	2.20853976530044E-0004
1859.04	6.52982719992550E-0007	5.3791	2.25448416681706E-0004
1860.97	6.62119312499349E-0007	5.3735	2.29423747856172E-0004
1862.90	6.78999361499420E-0007	5.3680	2.35695820967941E-0004
1864.83	7.01616326399507E-0007	5.3624	2.43546645071707E-0004
1866.76	7.13678717999613E-0007	5.3569	2.49077744447490E-0004
1868.68	6.33315640699796E-0007	5.3514	2.37245213304593E-0004
1870.61	6.56222337099173E-0007	5.3458	2.29440056282781E-0004
1872.54	7.06027912799299E-0007	5.3403	2.47301972926550E-0004
1874.47	7.74184067999818E-0007	5.3348	2.72163069864995E-0004
1876.40	7.95221101798967E-0007	5.3294	2.81125314642416E-0004
1878.33	7.93513590099937E-0007	5.3239	2.79978286957583E-0004
1880.26	7.86951255999334E-0007	5.3184	2.73171414607176E-0004
1882.18	7.99322175898919E-0007	5.3130	2.81596069454881E-0004
1884.11	8.08635500399411E-0007	5.3075	2.86887226692123E-0004
1886.04	8.06622517399505E-0007	5.3021	2.86700084928260E-0004
1887.97	8.13364251198934E-0007	5.2967	2.90343438922753E-0004
1889.90	7.96778820599982E-0007	5.2913	2.84248266932519E-0004
1891.83	7.83139242399199E-0007	5.2859	2.80419061038373E-0004
1893.76	8.18464039199079E-0007	5.2805	2.93067828150750E-0004
1895.68	5.30646343199723E-0007	5.2751	2.96990871357927E-0004
1897.61	3.23257467500067E-0007	5.2698	2.96434125623524E-0004
1899.54	3.37994353999373E-0007	5.2644	3.02304505278369E-0004
1901.47	3.49951845149111E-0007	5.2591	3.07195057497167E-0004
1903.40	3.46161413100336E-0007	5.2537	3.06896104266166E-0004
1905.33	3.25980857799800E-0007	5.2484	3.00215264626313E-0004
1907.25	8.23141994399368E-0007	5.2431	2.97633263473429E-0004
1909.18	8.30326484799540E-0007	5.2378	3.02364172886094E-0004
1911.11	8.18602019499876E-0007	5.2326	2.99223844339558E-0004
1913.04	3.15294937098546E-0007	5.2273	2.98015005096186E-0004

5154.33	3.71737646859979E-0006	1.9399	9.82945422705939E-0003
5156.73	3.72356833649654E-0006	1.9392	9.84450256559910E-0007
5158.65	3.55761569279314E-0006	1.9385	9.48597521354902E-0007
5160.58	3.61547918359629E-0006	1.9378	1.02276011269122E-0002
5162.51	3.99261174229552E-0006	1.9370	1.03558093828364E-0002
5164.44	3.49735053199698E-0006	1.9363	9.37484260811061E-0007
5166.37	3.23867485659727E-0006	1.9356	8.81547585694512E-0003
5168.30	3.70368915159763E-0006	1.9349	9.79194526865967E-0007
5170.23	3.97328950999521E-0006	1.9342	1.06506235095194E-0002
5172.15	3.33677061799676E-0006	1.9334	1.02312816574965E-0002
5174.08	3.69481149269796E-0006	1.9327	9.90414747191437E-0003
5176.01	3.69555924639333E-0006	1.9320	9.90615118435519E-0002
5177.94	3.65463676119765E-0006	1.9313	9.79646491339019E-0003
5179.87	2.55034213359723E-0006	1.9305	9.51623932893599E-0007
5181.80	3.48465953729762E-0006	1.9298	9.34662350406708E-0003
5183.73	3.51909100949699E-0006	1.9291	9.43311189545329E-0003
5185.65	3.53291903439773E-0006	1.9284	9.55370920076720E-0003
5187.58	3.54474961599890E-0006	1.9277	9.50129829272272E-0003
5189.51	3.63947068799525E-0006	1.9270	9.75580337045304E-0003
5191.44	3.74638893520240E-0006	1.9262	1.01833459474654E-0002
5193.37	3.69443370000153E-0006	1.9255	9.90313480262728E-0003
5195.30	3.61964355999215E-0006	1.9248	1.03829747422566E-0002
5197.22	3.72620407199792E-0006	1.9241	9.93654417611367E-0003
5199.15	3.20051809479804E-0006	1.9234	3.69999990931092E-0003

## Appendix 6

Run 01 Interpolated Data File (cm<sup>-1</sup> units)

1301.000000000000	3.4215065 E-07
1305.000000000000	1.0607084 E-06
1310.000000000000	3.1087319 E-07
1315.000000000000	7.4667764 E-07
1320.000000000000	2.0413941 E-07
1325.000000000000	7.1440773 E-07
1330.000000000000	7.1234223 E-07
1335.000000000000	7.3590742 E-07
1340.000000000000	7.3516572 E-07
1345.000000000000	6.0735971 E-07
1350.000000000000	6.2494736 E-07
1355.000000000000	4.7418952 E-07
1360.000000000000	6.5693133 E-07
1365.000000000000	7.0762802 E-07
1370.000000000000	6.3532961 E-07
1375.000000000000	7.0552517 E-07
1380.000000000000	7.6670102 E-07
1385.000000000000	3.0737565 E-07
1390.000000000000	7.9541678 E-07
1395.000000000000	8.3060365 E-07
1400.000000000000	8.4197188 E-07
1405.000000000000	8.2396526 E-07
1410.000000000000	8.2697302 E-07
1415.000000000000	8.3487413 E-07
1420.000000000000	7.8891162 E-07
1425.000000000000	8.1900464 E-07
1430.000000000000	8.7857336 E-07
1435.000000000000	7.9999239 E-07
1440.000000000000	8.9674813 E-07
1445.000000000000	8.4756374 E-07
1450.000000000000	8.8933291 E-07
1455.000000000000	8.2629764 E-07
1460.000000000000	8.9569294 E-07
1465.000000000000	9.0849676 E-07
1470.000000000000	8.9001099 E-07
1475.000000000000	9.3763316 E-07
1480.000000000000	9.1948527 E-07
1485.000000000000	9.3797314 E-07
1490.000000000000	9.1300069 E-07
1495.000000000000	8.9944803 E-07
2000.000000000000	9.2425393 E-07
2005.000000000000	9.4966612 E-07
2010.000000000000	9.4391953 E-07
2015.000000000000	9.6141787 E-07
2020.000000000000	9.3310496 E-07
2025.000000000000	9.4712982 E-07
2030.000000000000	9.5233221 E-07
2035.000000000000	9.6291501 E-07
2040.000000000000	9.4135395 E-07
2045.000000000000	9.3693785 E-07
2050.000000000000	9.2207915 E-07
2055.000000000000	8.7429430 E-07
2060.000000000000	8.7050410 E-07
2065.000000000000	8.680478 E-07
2070.000000000000	8.5365190 E-07
2075.000000000000	8.8906513 E-07
2080.000000000000	6.3176407 E-07
2085.000000000000	8.4590829 E-07
2090.000000000000	8.3752925 E-07
2095.000000000000	8.1523271 E-07



5100.000000000000  
5105.000000000000  
5110.000000000000  
5115.000000000000  
5120.000000000000  
5125.000000000000  
5130.000000000000  
5135.000000000000  
5140.000000000000  
5145.000000000000  
5150.000000000000  
5155.000000000000  
5160.000000000000  
5165.000000000000  
5170.000000000000  
5175.000000000000  
5180.000000000000  
5185.000000000000  
5190.000000000000  
5195.000000000000

3.3103112 F-06  
3.4126096 E-06  
3.0933673 F-06  
3.2765940 E-06  
3.0324306 E-06  
3.5004971 E-06  
3.5251135 E-06  
3.3928901 E-06  
3.4026214 E-06  
3.3190083 E-06  
3.6073352 E-06  
3.7323121 E-06  
3.7057537 E-06  
3.3697556 E-06  
3.9653969 E-06  
3.6073712 E-06  
3.5433761 E-06  
3.5723537 E-06  
3.6765462 E-06  
3.8011495 E-06

## Appendix 7

Run 01 Interpolated Data File (micron units)

5.5556	2.73614746168160E-0004
5.5402	3.44623184438841E-0004
5.5249	2.64916325576792E-0004
5.5096	2.45294805028884E-0004
5.4945	2.92718332189246E-0004
5.4795	2.37297160558203E-0004
5.4645	2.37804637632566E-0004
5.4496	2.53837491130948E-0004
5.4346	2.48221218797973E-0004
5.4201	2.06186338552961E-0004
5.4054	2.13310328229577E-0004
5.3908	2.17641420239945E-0004
5.3763	2.26670505224735E-0004
5.3619	2.44081523913753E-0004
5.3476	2.29580397804297E-0004
5.3333	2.75424762871346E-0004
5.3191	2.77343834369503E-0004
5.3050	2.86103607588295E-0004
5.2910	2.83379016730922E-0004
5.2770	2.97484850249496E-0004
5.2632	3.03151975418636E-0004
5.2493	3.00043975834718E-0004
5.2356	3.00861904585226E-0004
5.2219	3.05367736157969E-0004
5.2083	2.90067046442299E-0004
5.1948	3.02704114900187E-0004
5.1813	3.26411967609186E-0004
5.1680	2.98761158019190E-0004
5.1546	3.36630280605821E-0004
5.1414	3.19811225904854E-0004
5.1282	3.37301739544493E-0004
5.1151	3.37878817687987E-0004
5.1020	3.43211582344960E-0004
5.0891	3.49898442390195E-0004
5.0761	3.44527704222219E-0004
5.0633	3.64809621550943E-0004
5.0505	3.59564714996985E-0004
5.0378	3.68651583329882E-0004
5.0251	3.60648967337784E-0004
5.0125	3.57085365347842E-0004
5.0000	3.68777338024984E-0004
4.9875	3.80816113840776E-0004
4.9751	3.80404290377889E-0004
4.9628	3.89388658407430E-0004
4.9505	3.79801712101280E-0004
4.9383	3.87423452886004E-0004
4.9261	3.91482429484835E-0004
4.9140	3.97785005426421E-0004
4.9020	3.90793637108366E-0004
4.8900	3.90871732355969E-0004
4.8780	3.86558631625178E-0004
4.8662	3.68318331278594E-0004
4.8544	3.68510500651453E-0004
4.8426	3.69333947896067E-0004
4.8309	3.64897601826453E-0004
4.8193	3.81874840789997E-0004
4.8077	2.72669372626044E-0004
4.7962	3.66853507295151E-0004
4.7847	3.64966195048666E-0004
4.7733	3.56956345423765E-0004

4.7619	3.63832675388309E-0004
4.7506	3.71590832725754E-0004
4.7393	3.56688142099326E-0004
4.7281	4.14258633242959E-0004
4.7170	3.50730099727414E-0004
4.7059	3.40159165542004E-0004
4.6946	3.73480422829697E-0004
4.6838	4.46410314082879E-0004
4.6729	4.77697684249989E-0004
4.6620	4.91548832754596E-0004
4.6512	4.77864923284610E-0004
4.6404	4.76513082822816E-0004
4.6296	4.76484878179306E-0004
4.6189	4.73659883116095E-0004
4.6083	4.74536077258225E-0004
4.5977	4.75119391791345E-0004
4.5872	4.60853292963304E-0004
4.5767	4.51580107350580E-0004
4.5662	4.19850472815675E-0004
4.5558	4.03634201825209E-0004
4.5455	3.81772197367347E-0004
4.5351	3.50159053903010E-0004
4.5249	3.29570843089488E-0004
4.5147	3.03273511154778E-0004
4.5045	3.07358216494968E-0004
4.4944	3.95815170368241E-0004
4.4843	3.27296886787121E-0004
4.4743	2.50499693712491E-0004
4.4643	2.12343106723800E-0004
4.4543	2.18073896881554E-0004
4.4444	2.36823638584793E-0004
4.4346	1.81194135368212E-0004
4.4248	1.38409662550742E-0004
4.4150	9.32264203673538E-0005
4.4053	4.33904186120659E-0005
4.3956	1.47167661776054E-0005
4.3860	1.53723804625083E-0005
4.3764	1.00357174496191E-0004
4.3668	2.67344146779869E-0005
4.3573	1.07219689513133E-0005
4.3478	4.70322125262213E-0006
4.3384	4.35103637085738E-0006
4.3290	1.65560689860400E-0005
4.3197	7.52567030280066E-0006
4.3103	9.56959207591701E-0006
4.3011	5.08753563016324E-0008
4.2918	3.51333858080935E-0006
4.2827	4.88583620231013E-0007
4.2735	1.22313433934852E-0006
4.2644	4.94436474970938E-0006
4.2553	1.93371374406642E-0006
4.2463	4.87607675549173E-0006
4.2373	4.21883355385816E-0006
4.2283	1.83646567946949E-0005
4.2194	4.41825173344568E-0005
4.2105	4.29338428041270E-0005
4.2017	3.58992208229214E-0005
4.1929	1.56728949333829E-0004
4.1841	5.55281668577656E-0004
4.1754	7.12293226338367E-0004

4.1667	7.53896068758309E-0004
4.1580	7.60075199529808E-0004
4.1494	7.50687935606287E-0004
4.1408	7.37796610533081E-0004
4.1322	7.42594525260820E-0004
4.1237	7.49476580351072E-0004
4.1152	7.67927269716751E-0004
4.1068	7.73746061244474E-0004
4.0984	7.76324118550775E-0004
4.0900	7.98686151196826E-0004
4.0816	7.94329194158117E-0004
4.0733	8.10422241801945E-0004
4.0650	8.12128707833537E-0004
4.0566	8.16402564537633E-0004
4.0486	7.92166262735705E-0004
4.0404	8.31285970459561E-0004
4.0323	8.50238460751385E-0004
4.0241	8.66002264505283E-0004
4.0161	8.67871992105584E-0004
4.0080	8.69921010813179E-0004
4.0000	8.84705855590973E-0004
3.9920	8.83496966828545E-0004
3.9841	8.86320273039587E-0004
3.9761	9.02914931622867E-0004
3.9683	9.16929644708020E-0004
3.9604	9.25048421510866E-0004
3.9526	9.24525938814647E-0004
3.9448	9.32927168388886E-0004
3.9370	9.27611049839072E-0004
3.9293	9.18760874436764E-0004
3.9216	9.23007419489252E-0004
3.9139	9.24722658599997E-0004
3.9062	9.04200845930347E-0004
3.8986	9.59154507832238E-0004
3.8911	9.33382268978100E-0004
3.8835	9.38486686135498E-0004
3.8760	9.46559436380667E-0004
3.8685	9.57900687953206E-0004
3.8610	9.84241481440051E-0004
3.8536	1.03023292304982E-0003
3.8462	1.04021123595466E-0003
3.8388	1.04911839729205E-0003
3.8314	1.06047862767866E-0003
3.8241	1.06446704767826E-0003
3.8168	1.07717132035923E-0003
3.8095	1.08966071492667E-0003
3.8023	1.09435310932149E-0003
3.7951	1.09870467944795E-0003
3.7879	1.10302187952804E-0003
3.7807	1.11509771667428E-0003
3.7736	1.10209059215371E-0003
3.7665	1.10842683035806E-0003
3.7594	1.14908684660620E-0003
3.7523	1.14017796689581E-0003
3.7453	1.12828579568891E-0003
3.7383	1.12291018671407E-0003
3.7313	1.13639554091449E-0003
3.7244	1.14760582897944E-0003
3.7175	1.16515450316612E-0003
3.7106	1.15167924397852E-0003

3.7037	1.17610476998387E-0003
3.6969	1.16922133195629E-0003
3.6900	1.20334709512981E-0003
3.6832	1.20030561022411E-0003
3.6765	1.18522635561469E-0003
3.6697	1.20023850199580E-0003
3.6630	1.20607181739096E-0003
3.6563	1.23925615571707E-0003
3.6496	1.25656313836409E-0003
3.6430	1.22444906245356E-0003
3.6364	1.25228704809643E-0003
3.6298	1.26019902873331E-0003
3.6232	1.24804241387544E-0003
3.6166	1.28377929123857E-0003
3.6101	1.30024030790743E-0003
3.6036	1.25569003167492E-0003
3.5971	1.32986408217306E-0003
3.5907	1.28211822242363E-0003
3.5842	1.30823529040747E-0003
3.5778	1.28365447787360E-0003
3.5714	1.29321378778258E-0003
3.5651	1.31136470804449E-0003
3.5587	1.34953725056519E-0003
3.5524	1.36647445748572E-0003
3.5461	1.36505927128283E-0003
3.5398	1.35283223351124E-0003
3.5336	1.35441114375112E-0003
3.5273	1.41346653065888E-0003
3.5211	1.40467630895458E-0003
3.5149	1.44548575532610E-0003
3.5088	1.41651727490810E-0003
3.5026	1.41841127816633E-0003
3.4965	1.45294556623377E-0003
3.4904	1.43729388464919E-0003
3.4843	1.43691347021857E-0003
3.4783	1.44586761090082E-0003
3.4722	1.48006680787738E-0003
3.4662	1.46576230487305E-0003
3.4602	1.49012823719197E-0003
3.4542	1.48064450048224E-0003
3.4483	1.48215634633253E-0003
3.4423	1.48066888938381E-0003
3.4364	1.45452161775594E-0003
3.4305	1.57230515354101E-0003
3.4247	1.33131633774397E-0003
3.4188	1.58076460739132E-0003
3.4130	1.34548288535008E-0003
3.4072	1.56433906605180E-0003
3.4014	1.34643992272387E-0003
3.3956	1.56428068794412E-0003
3.3898	1.32967360295311E-0003
3.3841	1.59819917176485E-0003
3.3784	1.32080957160419E-0003
3.3727	1.64237582552396E-0003
3.3670	1.43597060875145E-0003
3.3613	1.67921873659616E-0003
3.3557	1.47530014160502E-0003
3.3501	1.67314926699369E-0003
3.3445	1.48221153095562E-0003
3.3389	1.65882450743915E-0003

3.3333	1.56501682394605E-0003
3.3278	1.76175529331601E-0003
3.3223	1.55023193306647E-0003
3.3167	1.10817645829719E-0003
3.3113	5.35507250057243E-0004
3.3058	1.63936163812828E-0003
3.3003	1.63610388188040E-0003
3.2949	1.72842785147509E-0003
3.2895	1.73439758623495E-0003
3.2841	1.84502825638866E-0003
3.2787	1.59861197558498E-0003
3.2733	1.68721148846984E-0003
3.2680	1.52336550090126E-0003
3.2626	1.84865312471061E-0003
3.2573	1.60721569033129E-0003
3.2520	1.87431859005649E-0003
3.2468	1.66026232291472E-0003
3.2415	1.82756272004525E-0003
3.2362	1.75762676445324E-0003
3.2310	1.79478540358957E-0003
3.2258	1.84012598877281E-0003
3.2206	1.73607327621639E-0003
3.2154	1.89581493747859E-0003
3.2103	1.74040201525294E-0003
3.2051	1.98129011794990E-0003
3.2000	1.80363280502505E-0003
3.1949	2.00718693654522E-0003
3.1898	1.92579428365569E-0003
3.1847	1.96958355534704E-0003
3.1797	1.99935304157606E-0003
3.1746	1.99162874840297E-0003
3.1696	2.12649639637874E-0003
3.1646	2.07476233785542E-0003
3.1596	2.09650687005336E-0003
3.1546	2.11835891407830E-0003
3.1496	2.06222852407834E-0003
3.1447	2.04774668686625E-0003
3.1397	2.13958625957389E-0003
3.1348	2.13434911248811E-0003
3.1299	2.15461852889476E-0003
3.1250	2.10852005748308E-0003
3.1201	2.16085038414349E-0003
3.1153	2.13510967336461E-0003
3.1104	2.11561331065724E-0003
3.1056	2.15640086040736E-0003
3.1008	2.19425803861739E-0003
3.0960	2.20688713261907E-0003
3.0912	2.18707038662203E-0003
3.0864	2.21411944322014E-0003
3.0817	2.20118819752457E-0003
3.0769	2.23926438086863E-0003
3.0722	2.26503055103677E-0003
3.0675	2.29627290580225E-0003
3.0628	2.26617199232138E-0003
3.0581	2.30276666926343E-0003
3.0534	2.29177649982049E-0003
3.0488	2.36996964928693E-0003
3.0441	2.33602857331405E-0003
3.0395	2.34095201203743E-0003
3.0349	2.29966918185553E-0003

3.0303	2.39282306219479E-0003
3.0257	2.47834747009534E-0003
3.0211	2.45004448305153E-0003
3.0166	2.44475261598964E-0003
3.0120	2.48678747312781E-0003
3.0075	2.49445479162347E-0003
3.0030	2.51199534731583E-0003
2.9985	2.52985495341917E-0003
2.9940	2.51961383264643E-0003
2.9895	2.53912191556438E-0003
2.9851	2.54871937662671E-0003
2.9806	2.56432502565218E-0003
2.9762	2.60271050766292E-0003
2.9718	2.57042241826255E-0003
2.9674	2.60247683427650E-0003
2.9630	2.64053503155637E-0003
2.9586	2.71241831340419E-0003
2.9542	2.67291307452311E-0003
2.9499	2.67219729436619E-0003
2.9455	2.67817423566186E-0003
2.9412	2.73337004863095E-0003
2.9369	2.74580368550659E-0003
2.9326	2.76439570642850E-0003
2.9283	2.74333846932961E-0003
2.9240	2.74527435676930E-0003
2.9197	2.73369557674030E-0003
2.9155	2.77815138606385E-0003
2.9112	2.80590086316224E-0003
2.9070	2.85304366496320E-0003
2.9028	2.73595058554577E-0003
2.8986	2.68163698644130E-0003
2.8944	2.78893399665137E-0003
2.8902	2.77219427719544E-0003
2.8860	2.67833201007761E-0003
2.8818	2.70987503380127E-0003
2.8777	2.70899945251912E-0003
2.8736	2.77496160195412E-0003
2.8694	2.65648592446510E-0003
2.8653	2.60989379091114E-0003
2.8612	2.63719581377231E-0003
2.8571	2.64337964143735E-0003
2.8531	2.58034177763378E-0003
2.8490	2.67668991804371E-0003
2.8450	2.68462045177387E-0003
2.8409	2.66391271281208E-0003
2.8369	2.53705060768539E-0003
2.8329	2.60335561057090E-0003
2.8289	2.62407572072476E-0003
2.8249	2.50466133728366E-0003
2.8209	2.28444270048556E-0003
2.8169	2.24641738773457E-0003
2.8129	2.15096222074607E-0003
2.8090	1.96932588286458E-0003
2.8050	1.72990584522559E-0003
2.8011	1.38376213015690E-0003
2.7972	1.53447704595955E-0003
2.7933	1.24667493004083E-0003
2.7894	9.41843296824452E-0004
2.7855	4.69776098972918E-0004
2.7816	2.19314727552877E-0004



2.7778	6.03134213842393E-0005
2.7739	4.13225775814374E-0005
2.7701	1.29241615515197E-0004
2.7663	7.59638739877389E-0004
2.7624	2.56260794540886E-0004
2.7586	1.06097976647179E-0004
2.7548	1.58780662322666E-0004
2.7510	4.49680666896324E-0004
2.7473	1.16406057126639E-0003
2.7435	1.84480851307889E-0003
2.7397	1.65767362931923E-0003
2.7360	2.44734657892920E-0003
2.7322	2.61574975107592E-0003
2.7285	2.74006808277960E-0003
2.7248	2.05234598482562E-0003
2.7211	1.66919837964485E-0003
2.7174	1.28686794484700E-0003
2.7137	1.19258003825884E-0003
2.7100	4.79136286458015E-0004
2.7064	1.64828265738493E-0004
2.7027	2.06837340218369E-0005
2.6991	1.86588696530210E-0005
2.6954	1.01552586589948E-0004
2.6918	2.98056959638249E-0004
2.6882	2.84689400269489E-0004
2.6846	1.14687339876185E-0004
2.6810	1.03324804205163E-0004
2.6774	1.02865119223194E-0004
2.6738	3.54206086789155E-0004
2.6702	1.11264943407541E-0003
2.6667	1.91767898142814E-0003
2.6631	2.58797505014030E-0003
2.6596	3.35614832292563E-0003
2.6560	3.75406734150019E-0003
2.6525	3.46272550475391E-0003
2.6490	3.83613833053786E-0003
2.6455	3.45577295354005E-0003
2.6420	3.59639781451904E-0003
2.6385	3.68914351729899E-0003
2.6350	3.94097324705456E-0003
2.6316	3.18862644547124E-0003
2.6281	2.84713311157248E-0003
2.6247	2.90569229724724E-0003
2.6212	3.69336969686884E-0003
2.6178	2.92586322503041E-0003
2.6144	2.98219458500861E-0003
2.6110	3.54432667297289E-0003
2.6076	3.40847788800502E-0003
2.6042	2.80969300582967E-0003
2.6008	3.34567843261269E-0003
2.5974	3.86862288054601E-0003
2.5940	2.19763113382854E-0003
2.5907	3.64013966240151E-0003
2.5873	3.31172606729169E-0003
2.5840	3.39616901415241E-0003
2.5806	3.50312789908358E-0003
2.5773	4.08230696074696E-0003
2.5740	3.71739518972447E-0003
2.5707	3.99253165979019E-0003
2.5674	3.73433040957494E-0003

2.5641	3.84837813129835E-0003
2.5608	3.27988573191007E-0003
2.5575	4.15849601321128E-0003
2.5543	4.28602076863882E-0003
2.5510	3.93016123788215E-0003
2.5478	4.23077073516254E-0003
2.5445	4.15652504558039E-0003
2.5413	3.97448754467433E-0003
2.5381	4.48495796372583E-0003
2.5349	4.30504007812260E-0003
2.5316	4.25279504229081E-0003
2.5284	4.43425021939703E-0003
2.5253	4.70891046135336E-0003
2.5221	4.56537439274030E-0003
2.5189	4.61352372602164E-0003
2.5157	4.32835989066405E-0003
2.5126	4.59739837599216E-0003
2.5094	4.52801541172221E-0003
2.5063	4.77924531033835E-0003
2.5031	4.64780519938301E-0003
2.5000	4.64539494814886E-0003
2.4969	4.62434488854058E-0003
2.4938	4.64321083045860E-0003
2.4907	4.64399295371720E-0003
2.4876	4.87608067061984E-0003
2.4845	4.66787328760887E-0003
2.4814	4.62118607349993E-0003
2.4783	4.57788007280158E-0003
2.4752	4.93991545270944E-0003
2.4722	4.73431129807267E-0003
2.4691	5.01576085792266E-0003
2.4661	4.99761739471438E-0003
2.4631	5.01299714245818E-0003
2.4600	4.94517281669005E-0003
2.4570	4.86516052347241E-0003
2.4540	5.03024777651007E-0003
2.4510	5.20893194946126E-0003
2.4480	5.22888599623883E-0003
2.4450	5.06990932966289E-0003
2.4420	5.24998625121498E-0003
2.4390	5.19430024669987E-0003
2.4361	5.15273701584817E-0003
2.4331	5.11707632864500E-0003
2.4301	5.17868285513856E-0003
2.4272	5.21085724179926E-0003
2.4242	5.06297755960361E-0003
2.4213	5.36194725135175E-0003
2.4184	5.33546175051214E-0003
2.4155	5.21832655670096E-0003
2.4125	5.42059779700566E-0003
2.4096	5.42101780325055E-0003
2.4067	5.33759596413574E-0003
2.4038	5.44242245467785E-0003
2.4010	5.51769725120721E-0003
2.3981	5.75023327535007E-0003
2.3952	5.38668668082920E-0003
2.3923	5.82530703270834E-0003
2.3895	5.36460733747646E-0003
2.3866	5.57448012145301E-0003
2.3838	5.49956171867905E-0003

2.3810	5.33751377479064E-0003
2.3781	5.63521977742454E-0003
2.3753	5.59368405049554E-0003
2.3725	5.93616205887315E-0003
2.3697	4.95870062290038E-0003
2.3669	5.73951966613606E-0003
2.3641	5.84269881160537E-0003
2.3613	5.84763318571646E-0003
2.3585	6.08904881375594E-0003
2.3557	5.70519950965576E-0003
2.3529	5.77011440358888E-0003
2.3502	5.76081166411058E-0003
2.3474	5.71545422437225E-0003
2.3447	5.66143923312268E-0003
2.3419	5.94032369487962E-0003
2.3392	6.04800906000236E-0003
2.3364	6.10597914593569E-0003
2.3337	6.02662975851587E-0003
2.3310	6.13527671610115E-0003
2.3283	6.08049912302988E-0003
2.3256	6.10457762025618E-0003
2.3229	6.19941138374713E-0003
2.3202	6.13114323748931E-0003
2.3175	5.96375046057318E-0003
2.3148	6.03010530456061E-0003
2.3121	6.19496774236694E-0003
2.3095	6.16123585675865E-0003
2.3068	6.41146463741649E-0003
2.3041	5.88821357127500E-0003
2.3015	6.54838806725166E-0003
2.2989	5.99945319839179E-0003
2.2962	6.46533796303572E-0003
2.2936	5.92692936694306E-0003
2.2910	6.17660147499777E-0003
2.2883	6.42024389001961E-0003
2.2857	6.21716571178865E-0003
2.2831	6.52258904595726E-0003
2.2805	6.01287485275748E-0003
2.2779	6.24609328399117E-0003
2.2753	6.32088590295865E-0003
2.2727	6.44187687733222E-0003
2.2701	6.41703520321357E-0003
2.2676	6.42952660170693E-0003
2.2650	6.29344114313568E-0003
2.2624	6.36192914885214E-0003
2.2599	6.16557811955687E-0003
2.2573	6.59404714178180E-0003
2.2548	6.33535296503851E-0003
2.2523	6.77716098312686E-0003
2.2497	7.02270911425273E-0003
2.2472	6.52412579373163E-0003
2.2447	6.99302553012160E-0003
2.2422	6.97749432899997E-0003
2.2396	6.95498055150523E-0003
2.2371	6.93803865559772E-0003
2.2346	6.52404198792311E-0003
2.2321	6.81653009988281E-0003
2.2297	6.79319926855015E-0003
2.2272	7.04107091778639E-0003
2.2247	6.66286745497047E-0003

2.2222	6.66686162745833E-0003
2.2198	6.94570859712229E-0003
2.2173	7.00238854908974E-0003
2.2148	6.99992076922484E-0003
2.2124	7.34801001561181E-0003
2.2099	7.08559210305992E-0003
2.2075	7.22377127353013E-0003
2.2051	6.99229696634518E-0003
2.2026	7.71430032035880E-0003
2.2002	7.36023603638358E-0003
2.1978	7.27350130978976E-0003
2.1954	7.44833568451497E-0003
2.1930	7.04185163384352E-0003
2.1906	6.84834662217781E-0003
2.1882	6.99779854329563E-0003
2.1858	7.40546817762322E-0003
2.1834	7.90655953923647E-0003
2.1810	7.32746591674527E-0003
2.1786	7.46673777203455E-0003
2.1763	7.86195253476762E-0003
2.1739	7.56697370366055E-0003
2.1716	7.54870525062046E-0003
2.1692	6.92096771538075E-0003
2.1668	7.09351903186217E-0003
2.1645	6.67820065802971E-0003
2.1622	6.83115982979388E-0003
2.1598	7.06429698284694E-0003
2.1575	7.68037592349913E-0003
2.1552	7.75363184315836E-0003
2.1529	7.87011140167238E-0003
2.1505	7.36036172898480E-0003
2.1482	7.60327272567451E-0003
2.1459	7.46298569968218E-0003
2.1436	7.09577174687581E-0003
2.1413	8.06844923874905E-0003
2.1390	7.56001017900587E-0003
2.1368	8.29679073810041E-0003
2.1345	7.63352866097478E-0003
2.1322	7.55352557573730E-0003
2.1299	8.23197375015638E-0003
2.1277	8.15357882184742E-0003
2.1254	7.95987019891697E-0003
2.1231	7.93043580688391E-0003
2.1209	7.66953628933464E-0003
2.1186	7.79256028284436E-0003
2.1164	7.60021093051932E-0003
2.1142	7.90565608048155E-0003
2.1119	8.05862470835450E-0003
2.1097	8.06947038392991E-0003
2.1075	8.07373997074023E-0003
2.1053	7.44014505334434E-0003
2.1030	7.84597042243718E-0003
2.1008	7.82007182908728E-0003
2.0986	8.32160356522138E-0003
2.0964	8.22793610126382E-0003
2.0942	8.05614968317059E-0003
2.0921	7.82771660489345E-0003
2.0899	8.48049372430637E-0003
2.0877	7.90820766304989E-0003
2.0855	8.09186863826028E-0003

2.0833	8.14194106982313E-0003
2.0812	7.99070777033251E-0003
2.0790	7.91057360602565E-0003
2.0768	8.28299627953299E-0003
2.0747	8.16367177797872E-0003
2.0725	7.46392086815462E-0003
2.0704	7.50458207573246E-0003
2.0683	7.85308472306667E-0003
2.0661	7.30175070410866E-0003
2.0640	7.65381328524484E-0003
2.0619	7.63308481060676E-0003
2.0597	7.39154051373703E-0003
2.0576	7.29512619385275E-0003
2.0555	7.33081247810219E-0003
2.0534	6.90257638346026E-0003
2.0513	7.53137785510916E-0003
2.0492	7.86663525289555E-0003
2.0471	8.49417495174976E-0003
2.0450	8.63734354500423E-0003
2.0429	8.46869010193529E-0003
2.0408	8.32423998249965E-0003
2.0387	8.30314343161831E-0003
2.0367	8.26642300459923E-0003
2.0346	8.81698771539163E-0003
2.0325	8.48706677133748E-0003
2.0305	9.20822923420417E-0003
2.0284	8.97163590437344E-0003
2.0263	8.67931977730052E-0003
2.0243	7.99850450458450E-0003
2.0222	8.16961816332196E-0003
2.0202	7.74314212848282E-0003
2.0182	6.86167551414485E-0003
2.0161	6.68562420630536E-0003
2.0141	6.31084572711416E-0003
2.0121	6.30905156200612E-0003
2.0101	6.88906990927762E-0003
2.0080	7.19839195352989E-0003
2.0060	6.50060137762409E-0003
2.0040	5.73388425233645E-0003
2.0020	6.14175466127875E-0003
2.0000	6.27875146358292E-0003
1.9980	7.95262542033015E-0003
1.9960	8.60370075525907E-0003
1.9940	8.37798855471306E-0003
1.9920	8.39449205881238E-0003
1.9900	9.24912381908882E-0003
1.9881	8.75290374968074E-0003
1.9861	8.28182095445129E-0003
1.9841	8.40984859802063E-0003
1.9822	8.85518998863688E-0003
1.9802	8.93692503963450E-0003
1.9782	8.47596505848003E-0003
1.9763	8.31310506330851E-0003
1.9743	8.37897493104833E-0003
1.9724	8.47482749369988E-0003
1.9704	8.75126636317702E-0003
1.9685	8.74666109376676E-0003
1.9666	8.14208675387817E-0003
1.9646	7.14843876483684E-0003
1.9627	7.41898544578845E-0003

1.9608	8.60221601162436E-0003
1.9589	8.88750327108312E-0003
1.9569	8.08256091956139E-0003
1.9550	8.45969611380326E-0003
1.9531	8.07251584954827E-0003
1.9512	9.18530439059850E-0003
1.9493	9.26816121842933E-0003
1.9474	8.93776141629132E-0003
1.9455	9.21891788239293E-0003
1.9436	8.77721833882106E-0003
1.9417	9.61099442051250E-0003
1.9399	9.90863547512788E-0003
1.9380	9.85723073468137E-0003
1.9361	8.97820529618798E-0003
1.9342	1.05888191713319E-0002
1.9324	9.86547132727367E-0003
1.9305	9.49855114660636E-0003
1.9286	9.48731497180688E-0003
1.9268	9.89364096572842E-0003

**Appendix 8**  
**Figures 30-65**

Figure 30  
MODTRAN Percent Difference  
Run 01

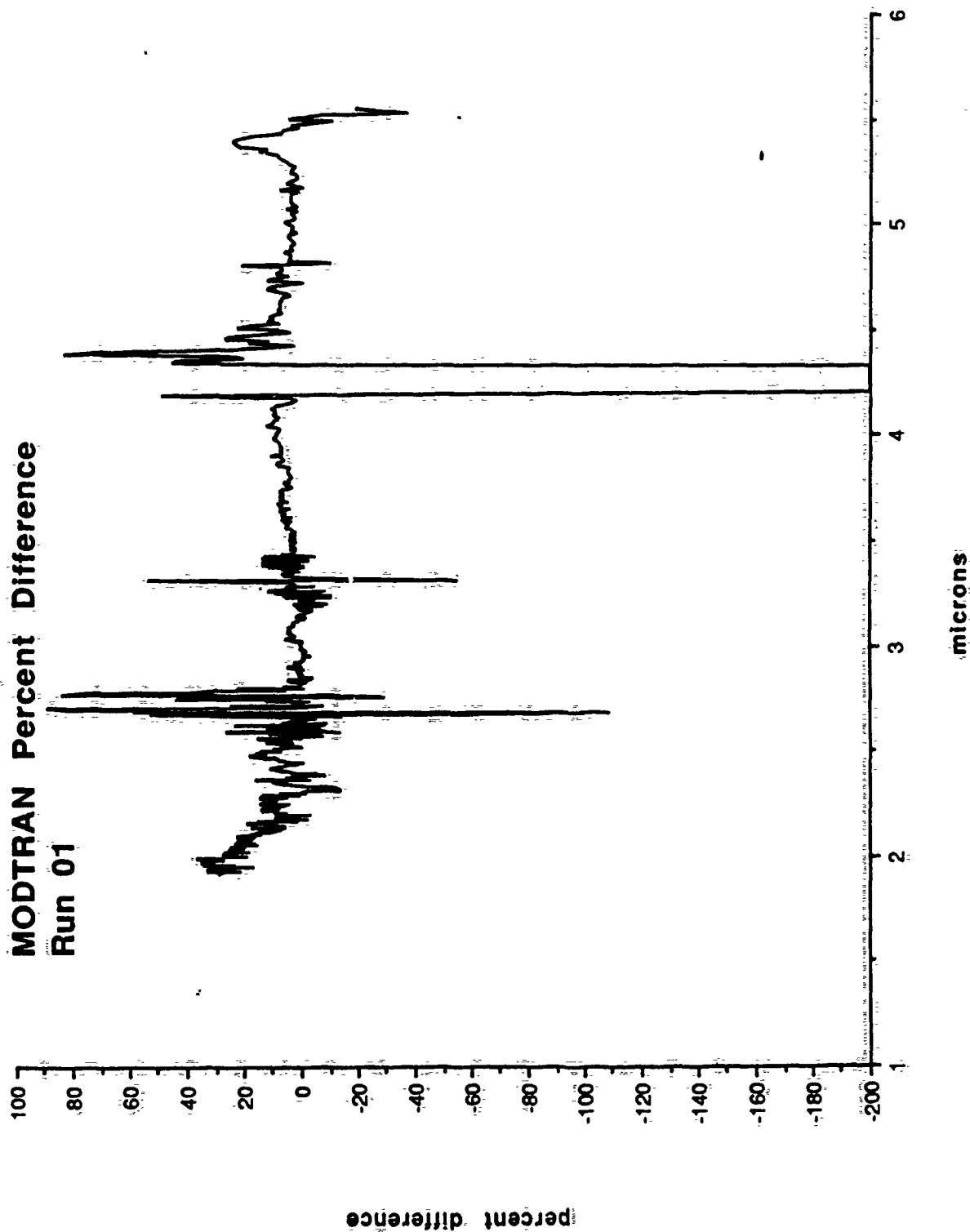




Figure 31

MODTRAN Percent Difference

Run 05

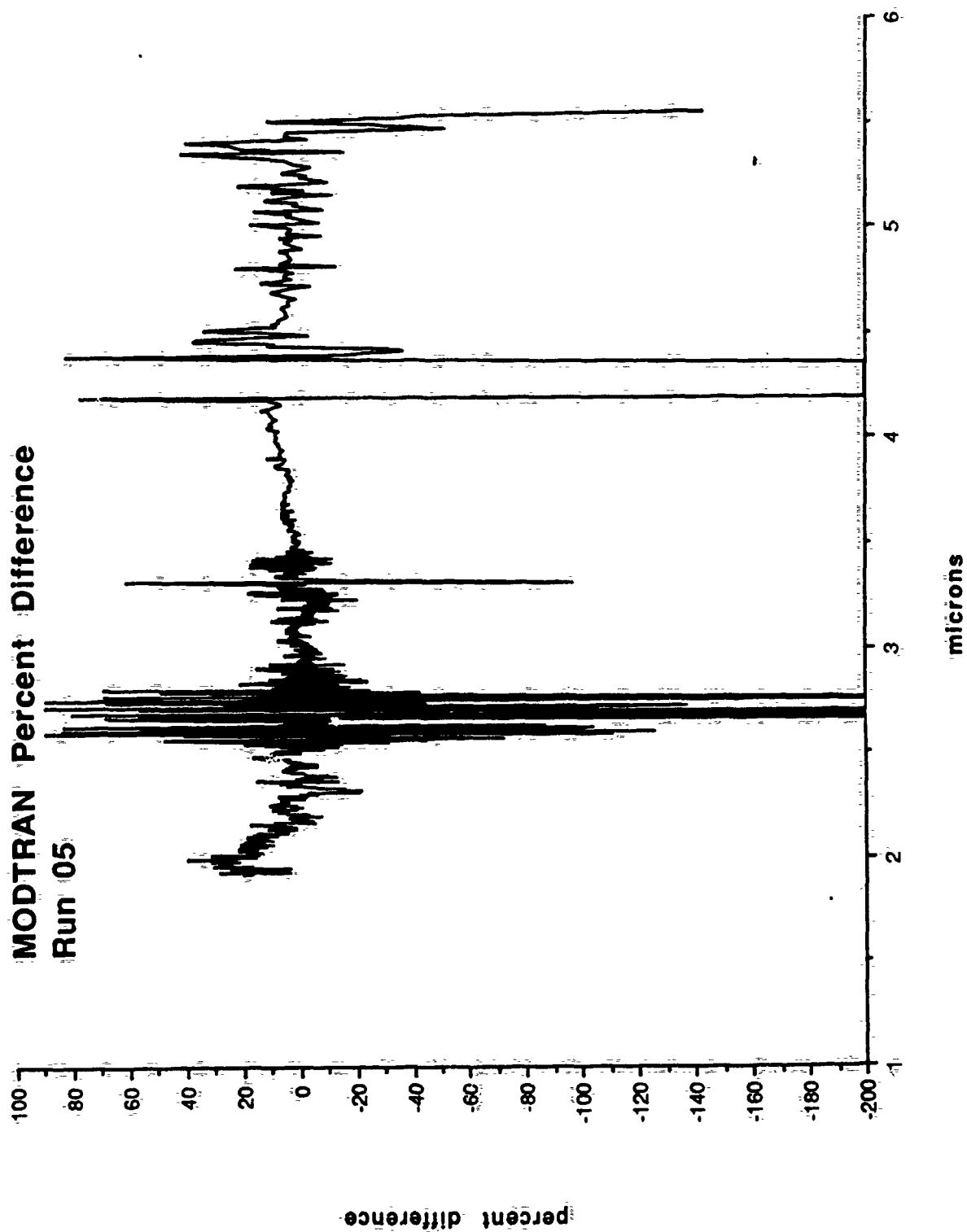


Figure 32  
MODTRAN Percent Difference  
Run 09

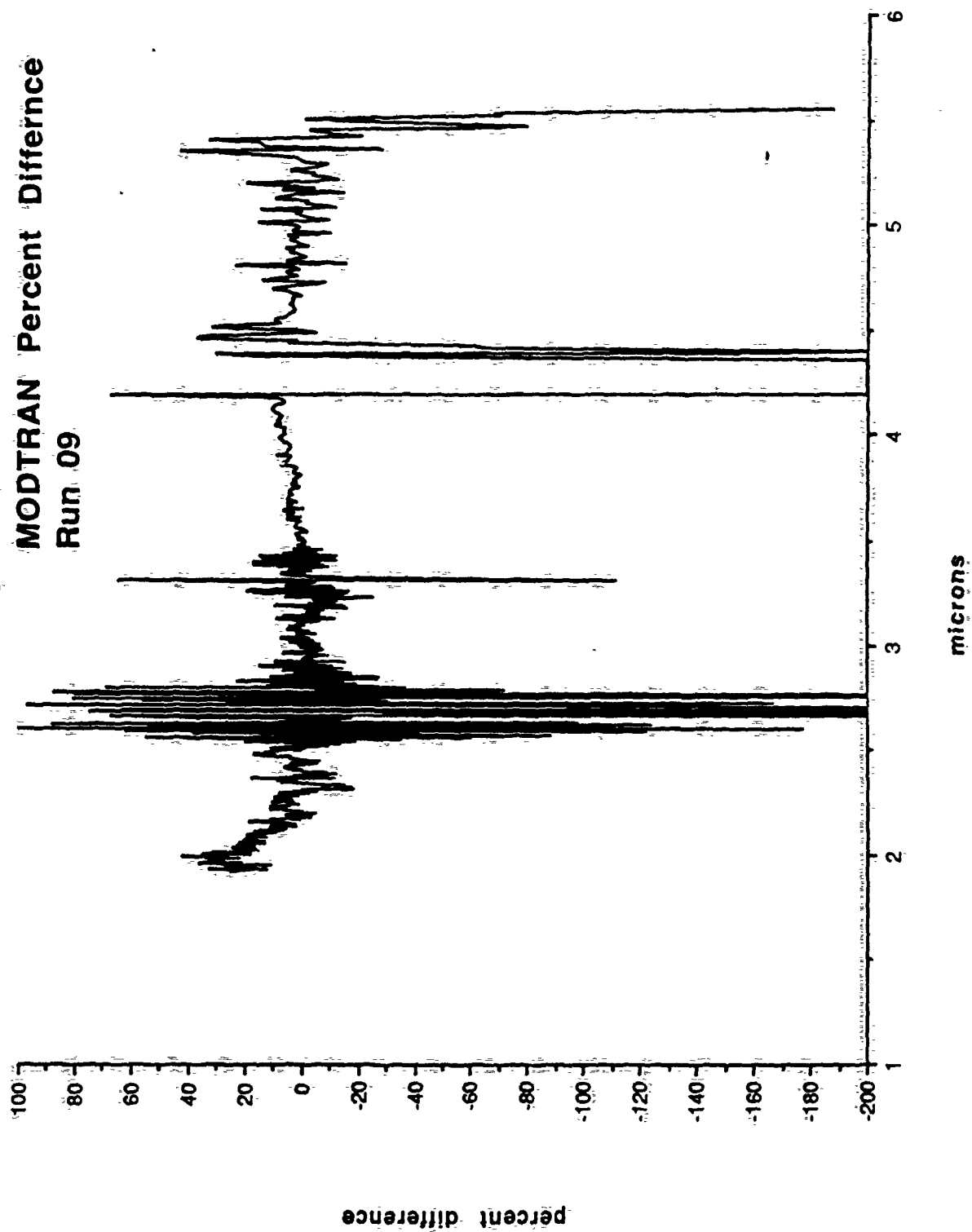


Figure 33

MODTRAN Percent Difference  
Run 13

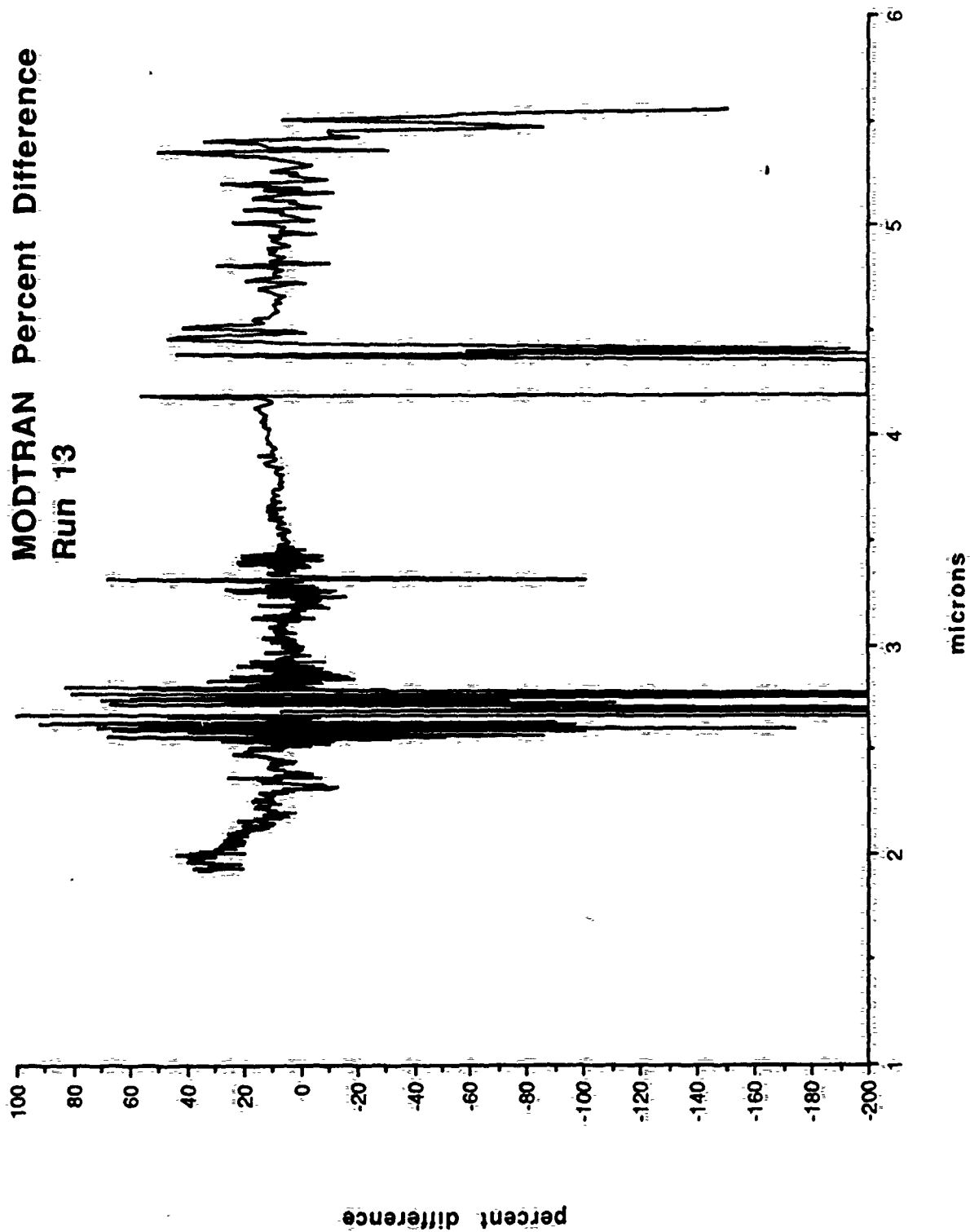


Figure 34

MODTRAN Percent Difference  
Run 19

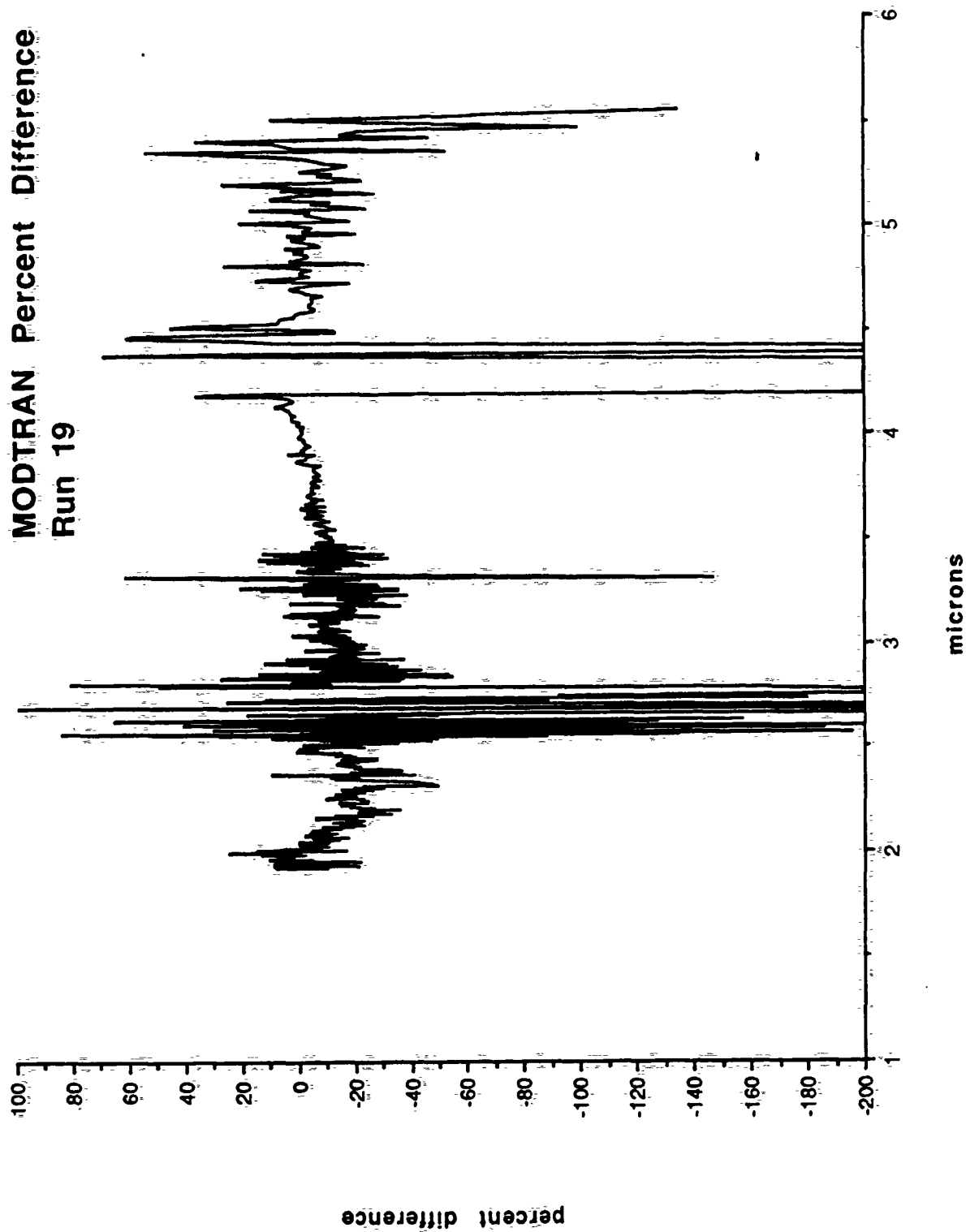
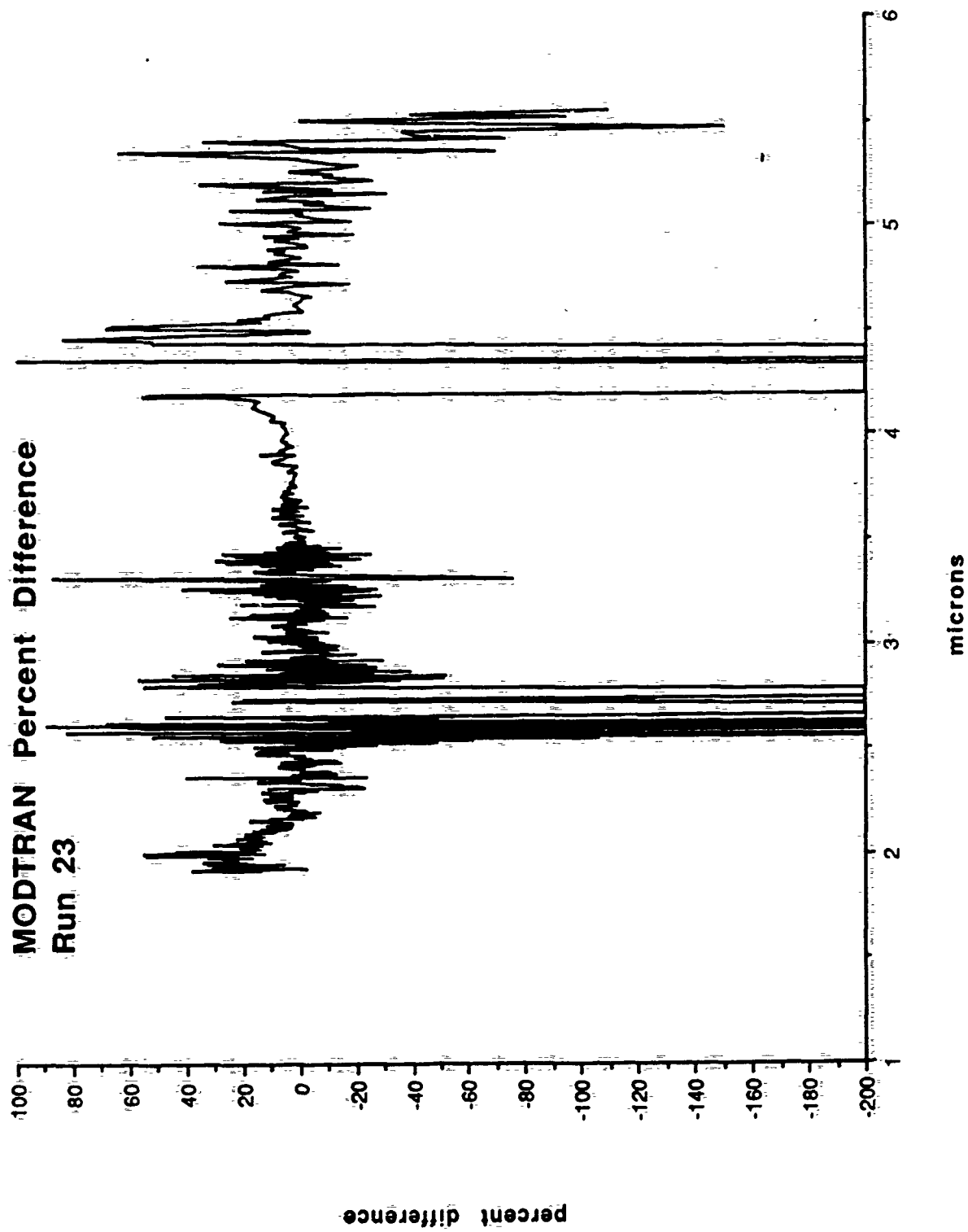


Figure 35.  
MODTRAN Percent Difference  
Run 23



**Figure 36**  
**MODTRAN Percent Difference**  
**Run 27**

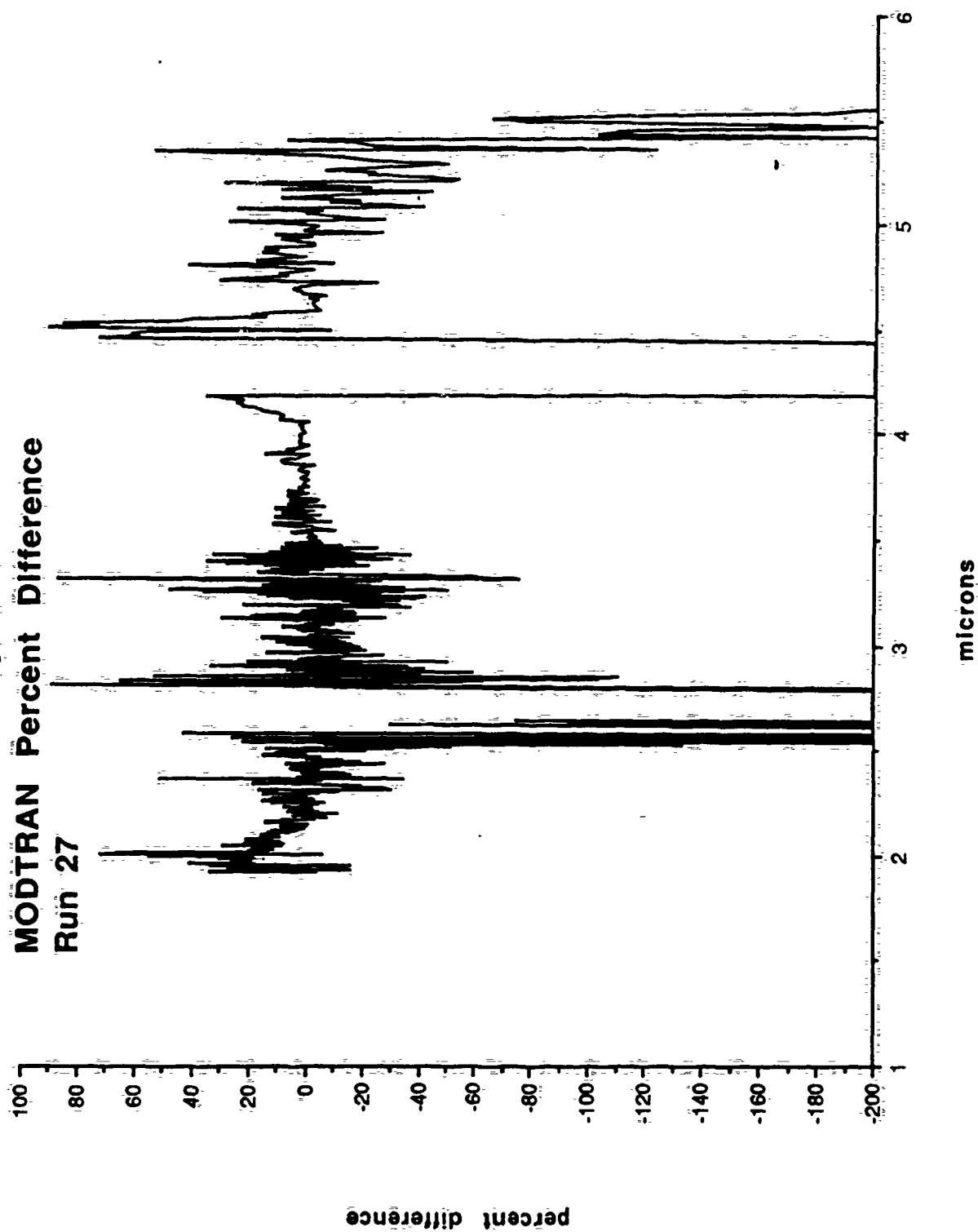


Figure 37  
MODTRAN Percent Difference  
Run 31

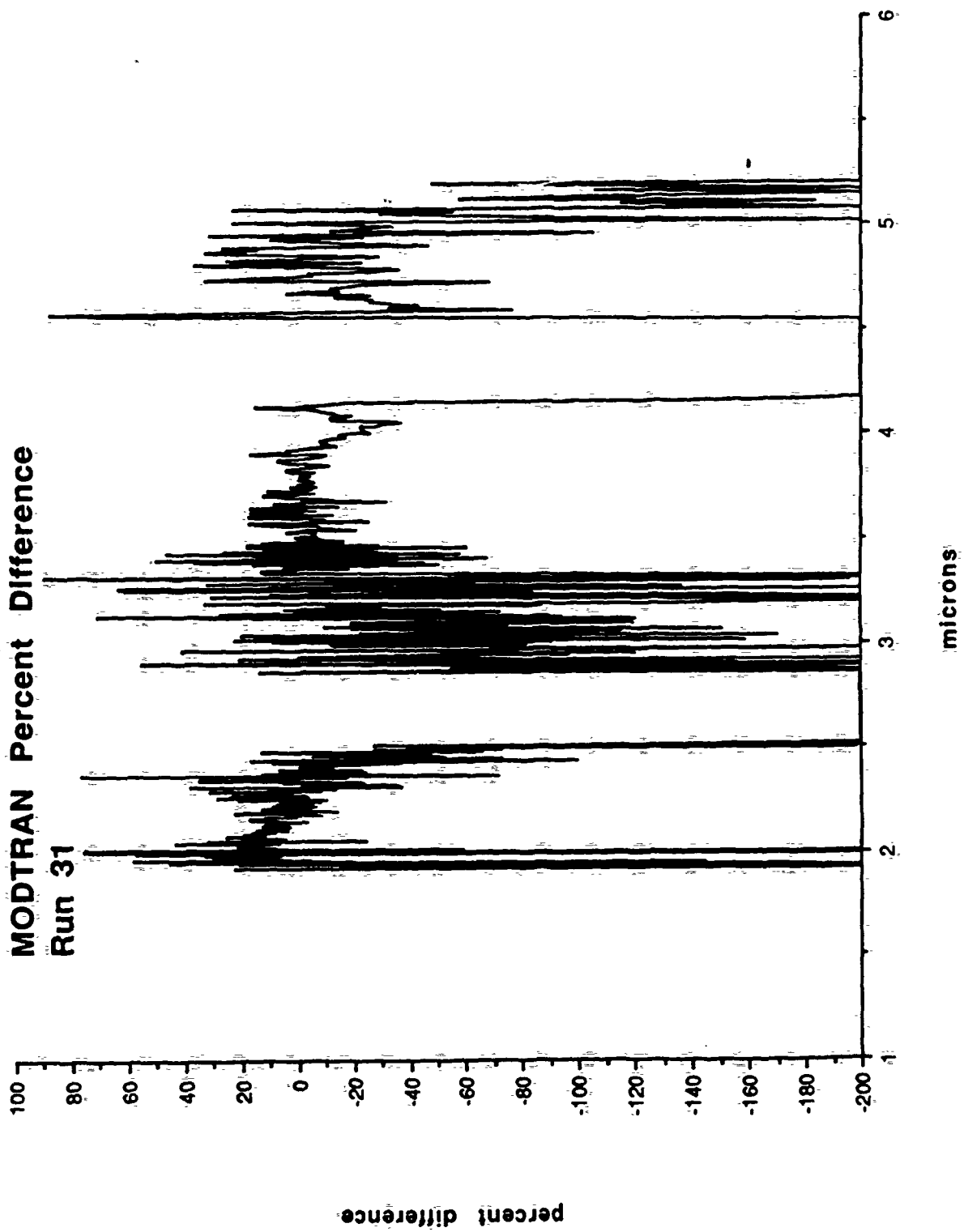


Figure 38

MODTRAN Percent Difference  
Run 37

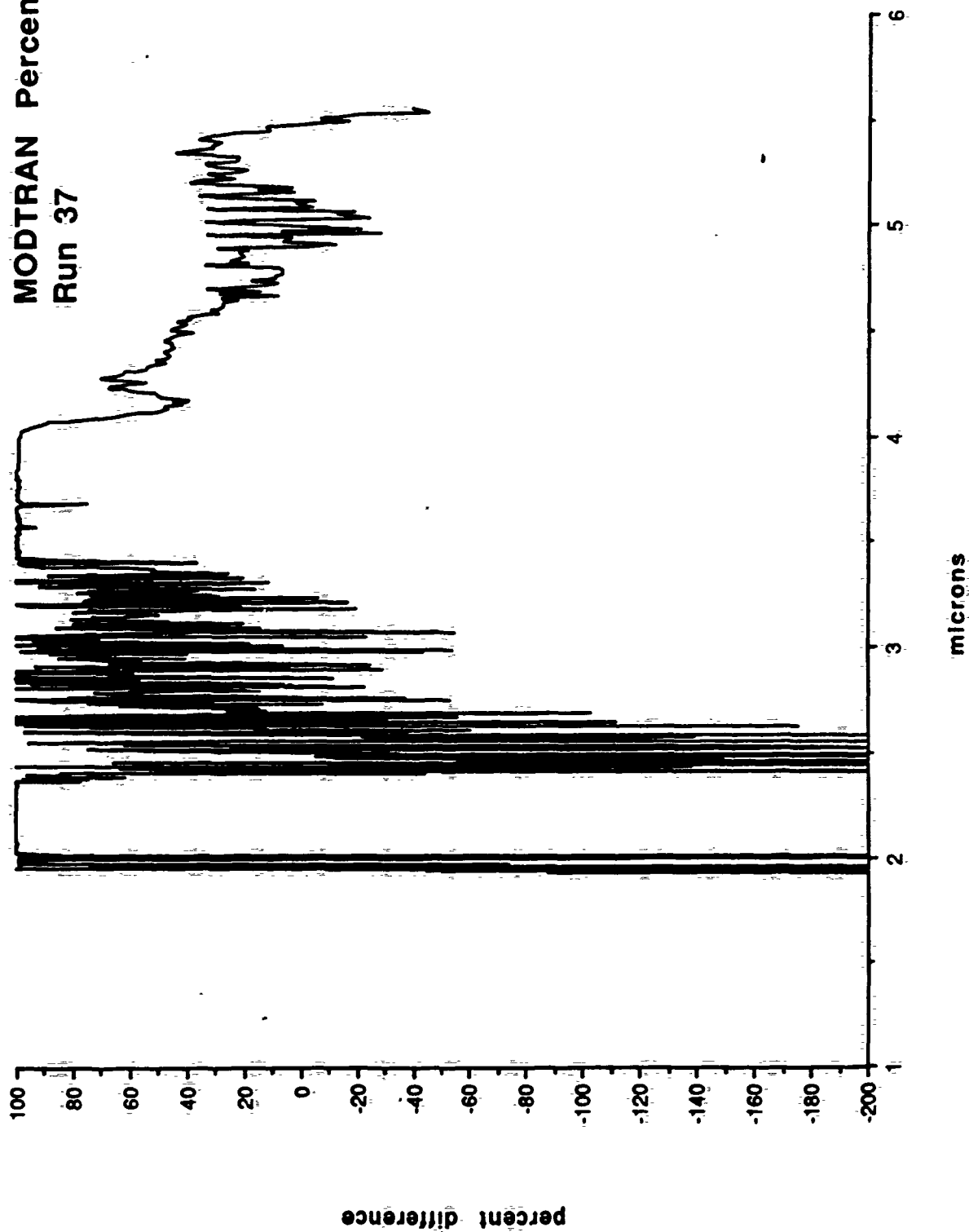




Figure 39

MODTRAN Percent Difference  
Run 02

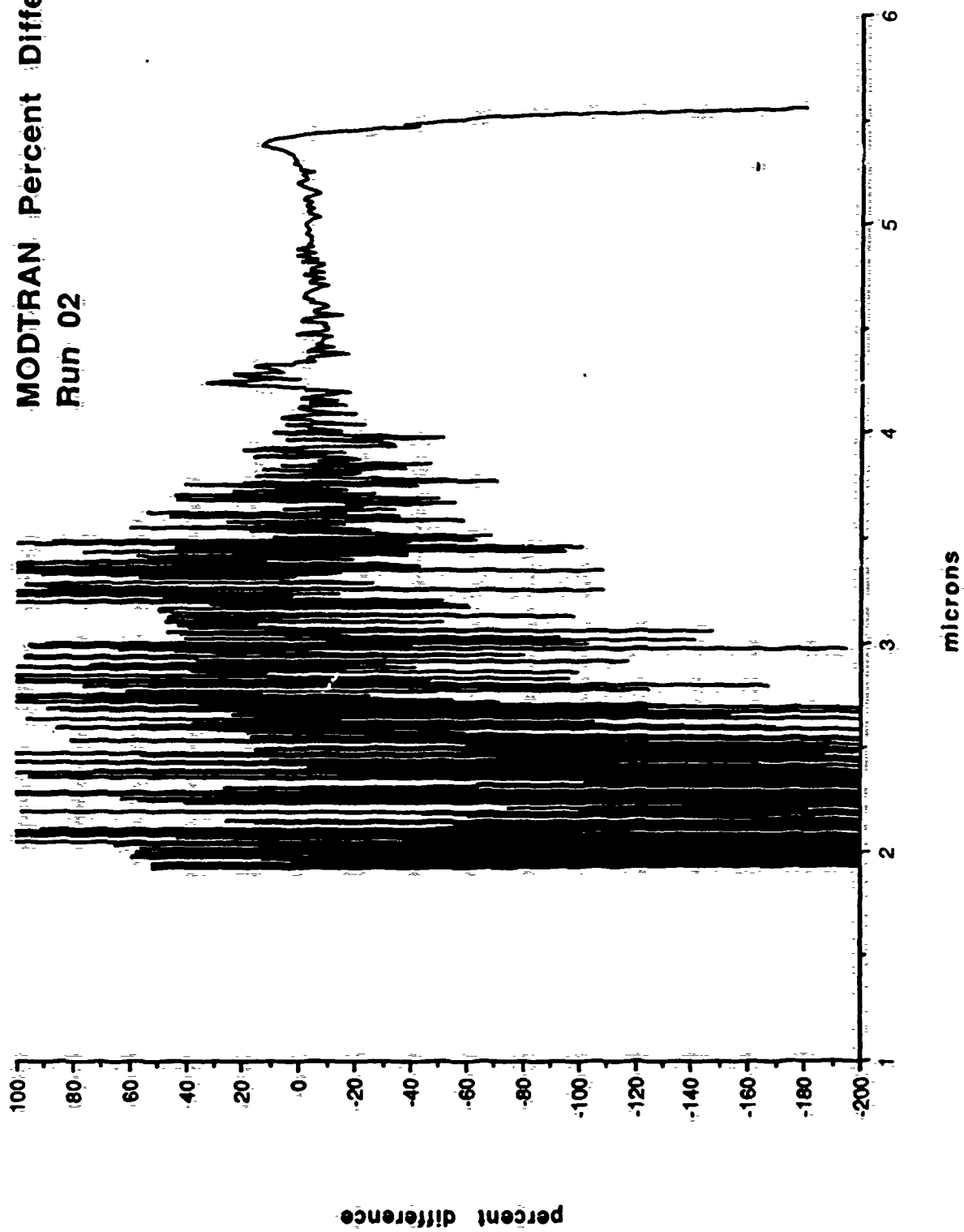
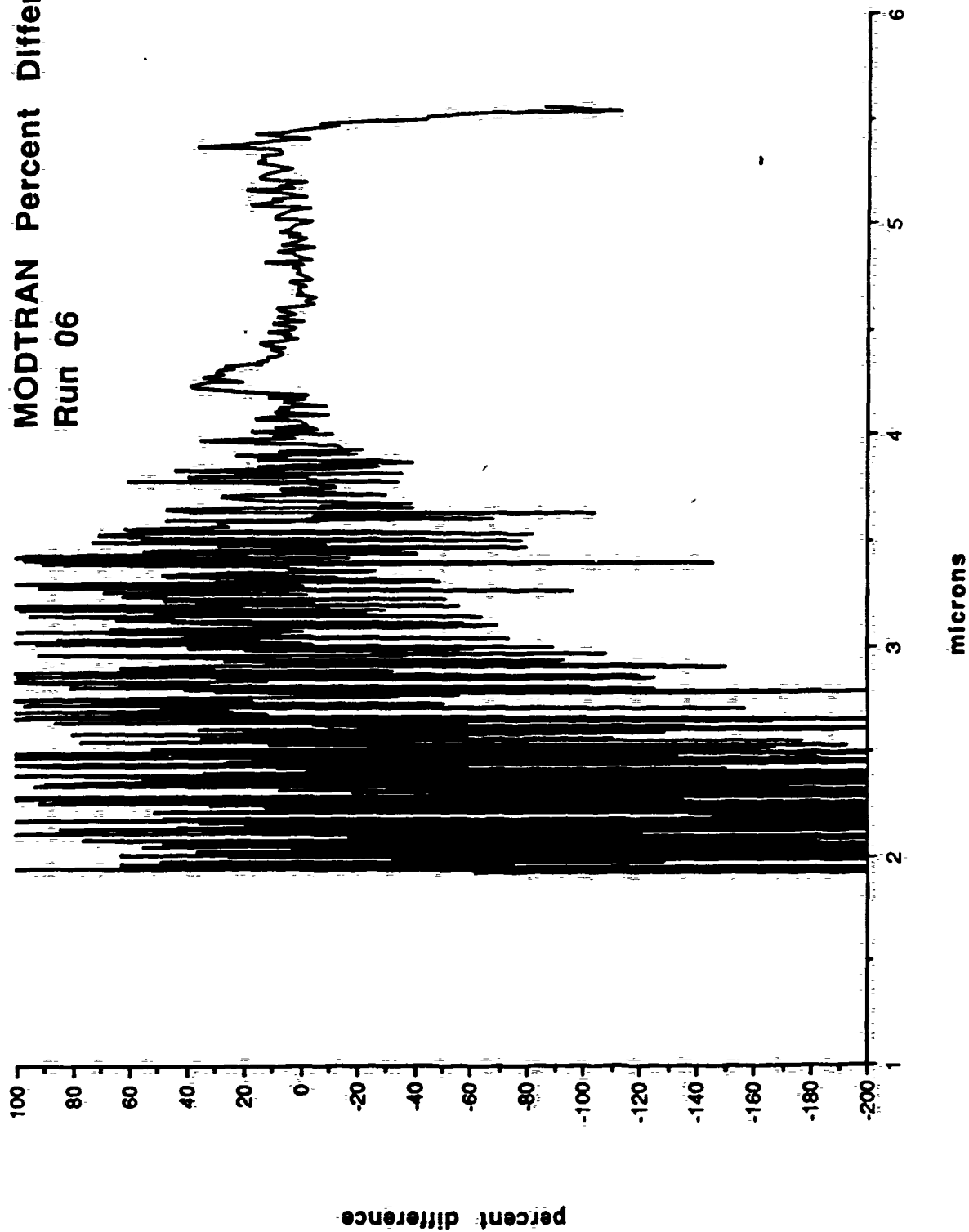


Figure 40

MODTRAN Percent Difference  
Run 06



MODTRAN Percent Difference  
Run 10

Figure 41

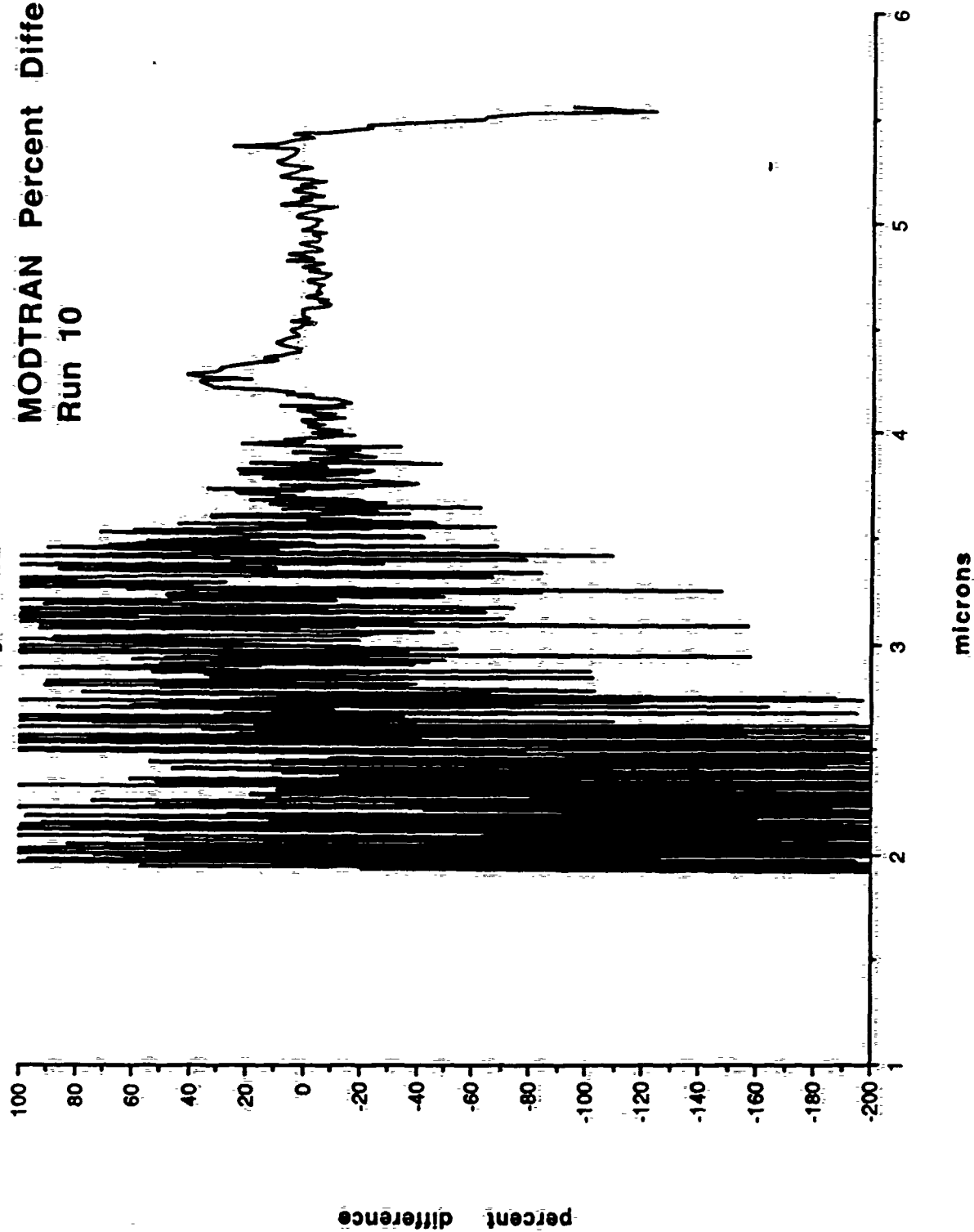


Figure 42

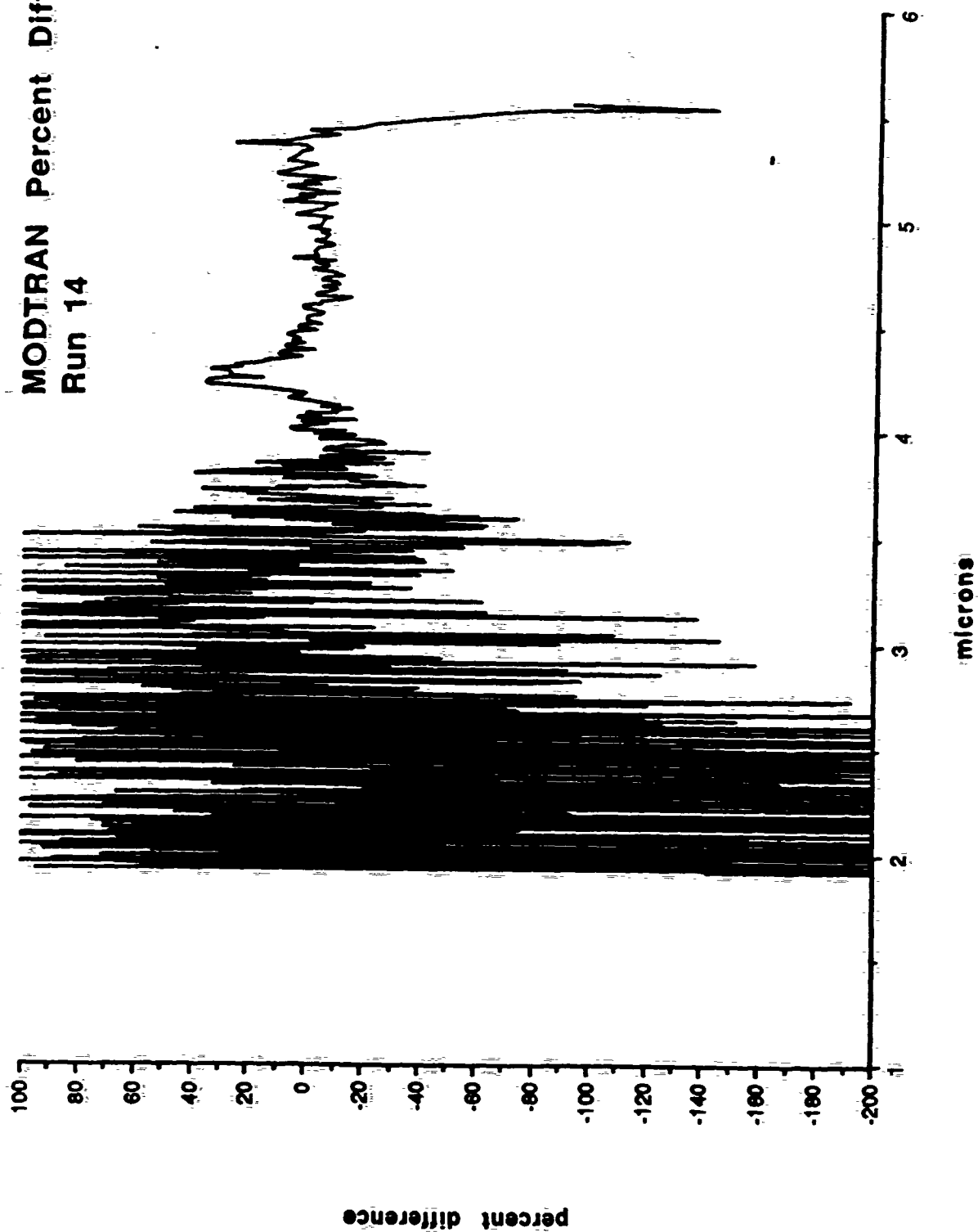


Figure 43

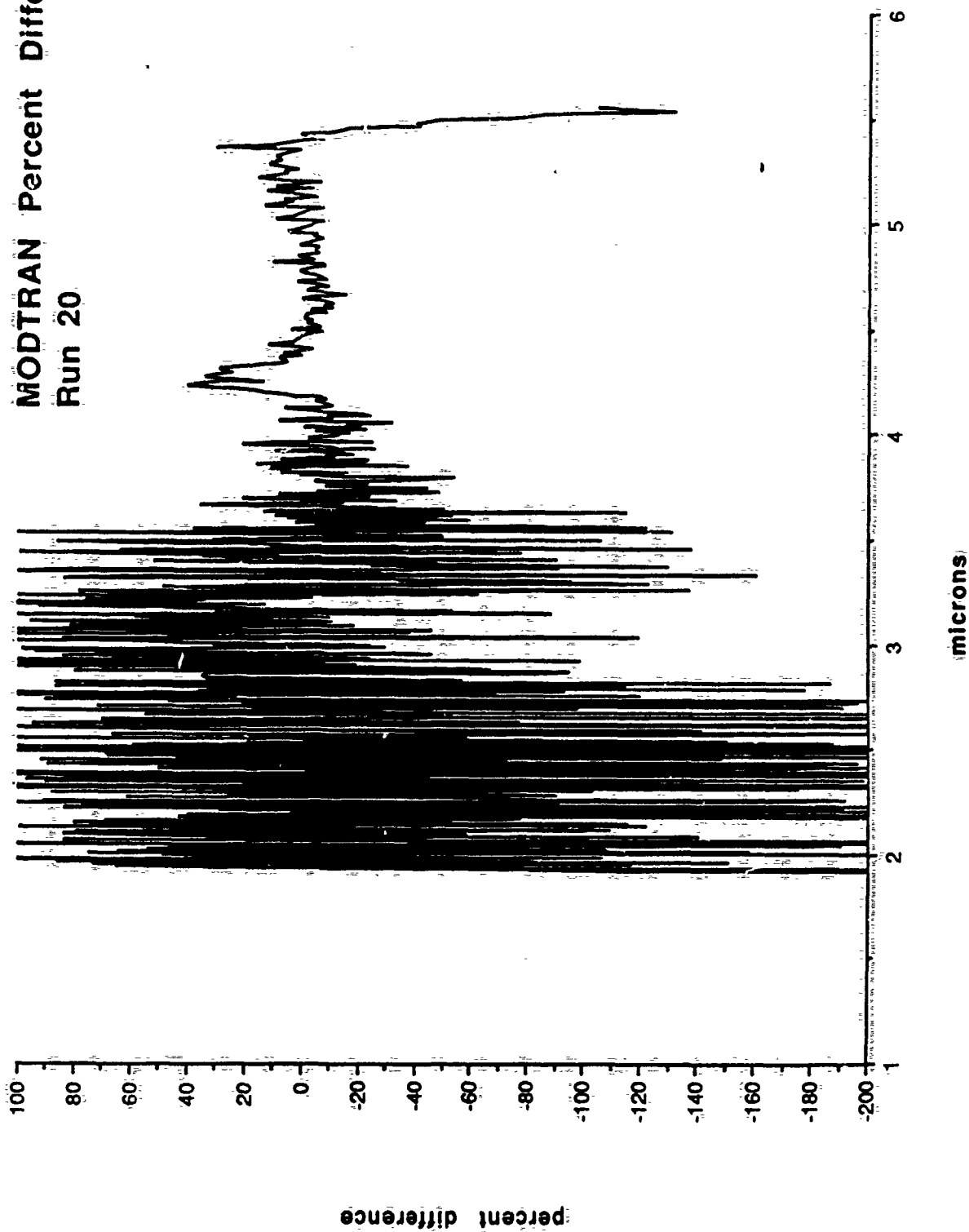


Figure 44

MODTRAN Percent Difference  
Run 24

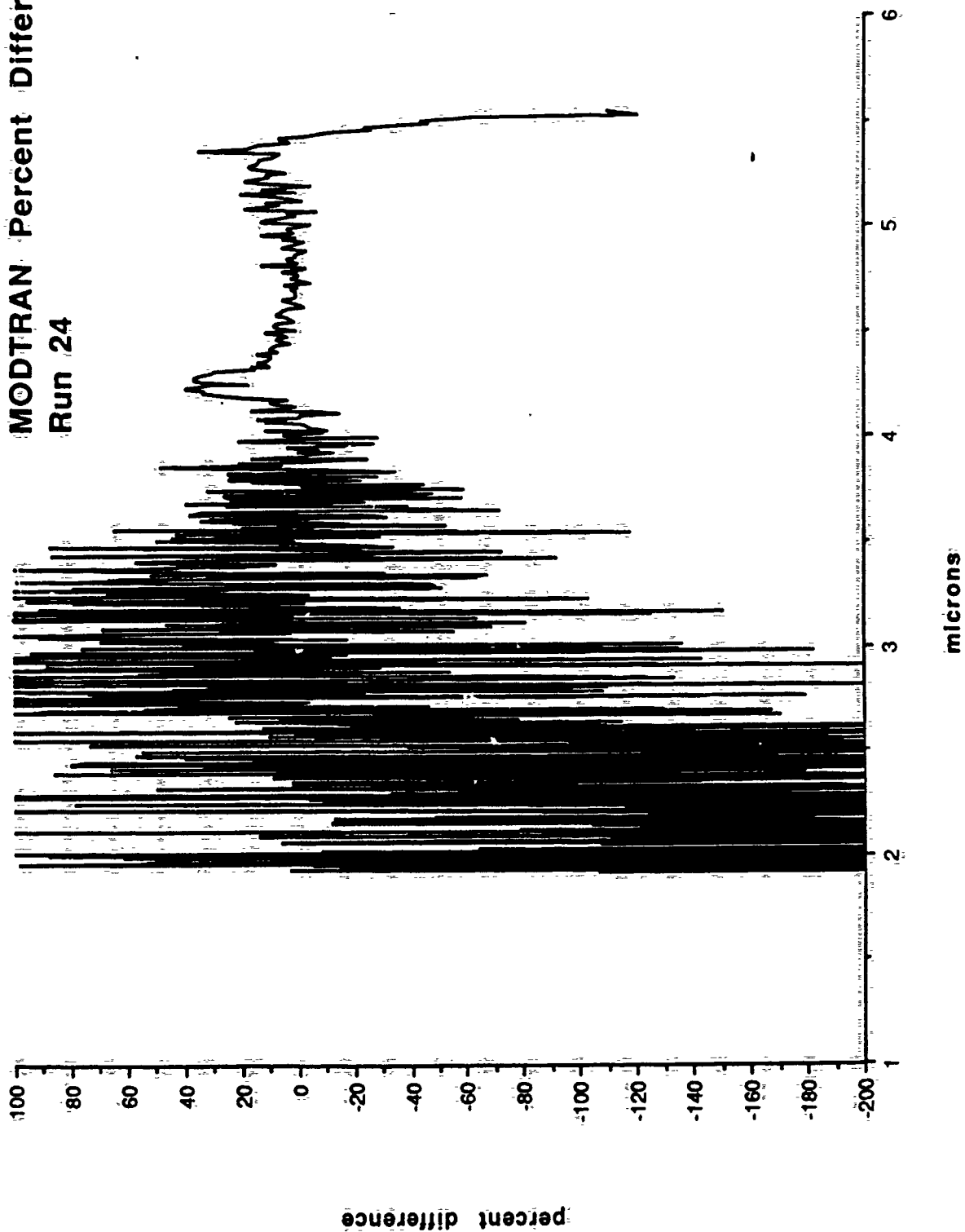


Figure 45

MODTRAN Percent Difference  
Run 28

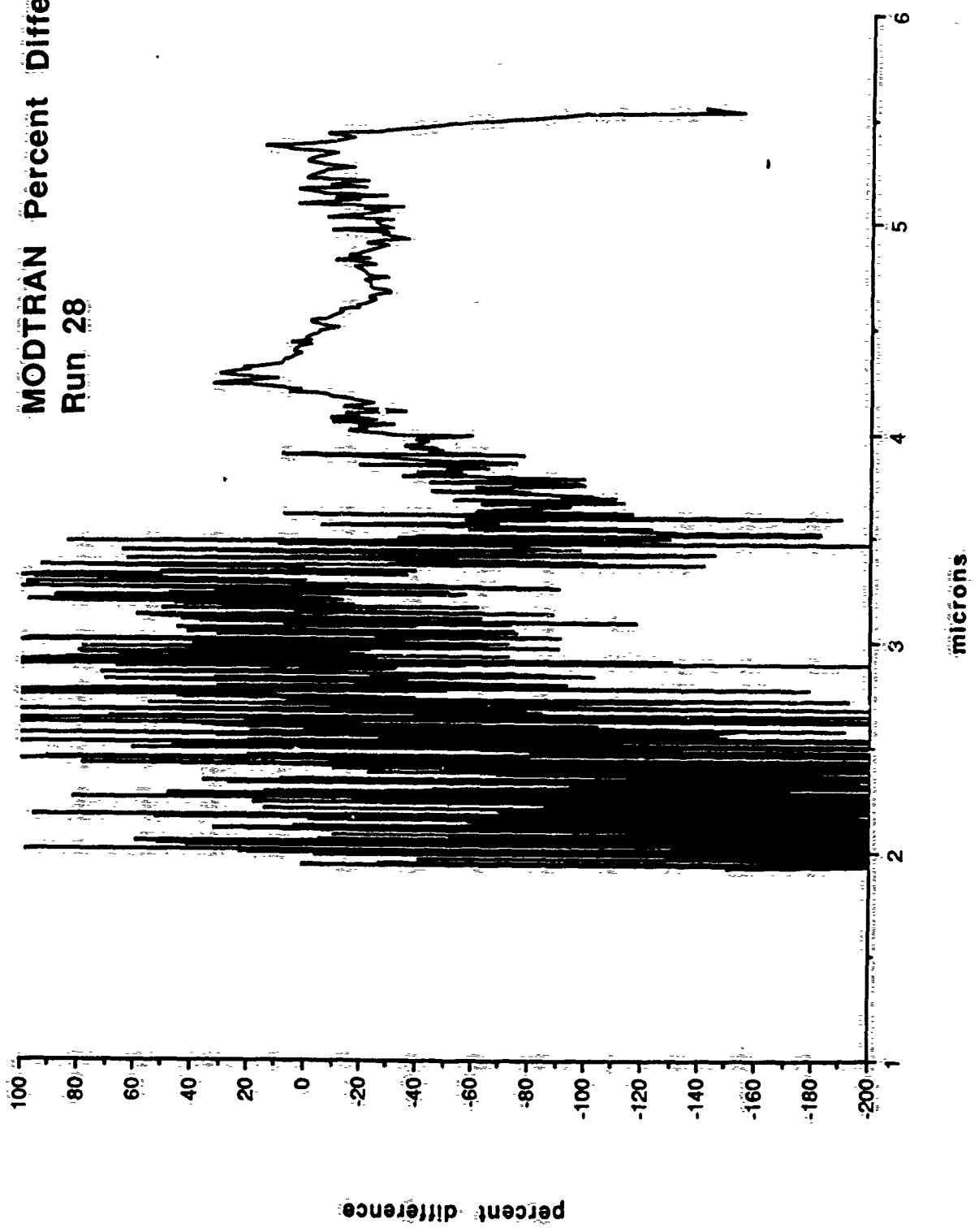


Figure 46

MODTRAN Percent Difference  
Run 32

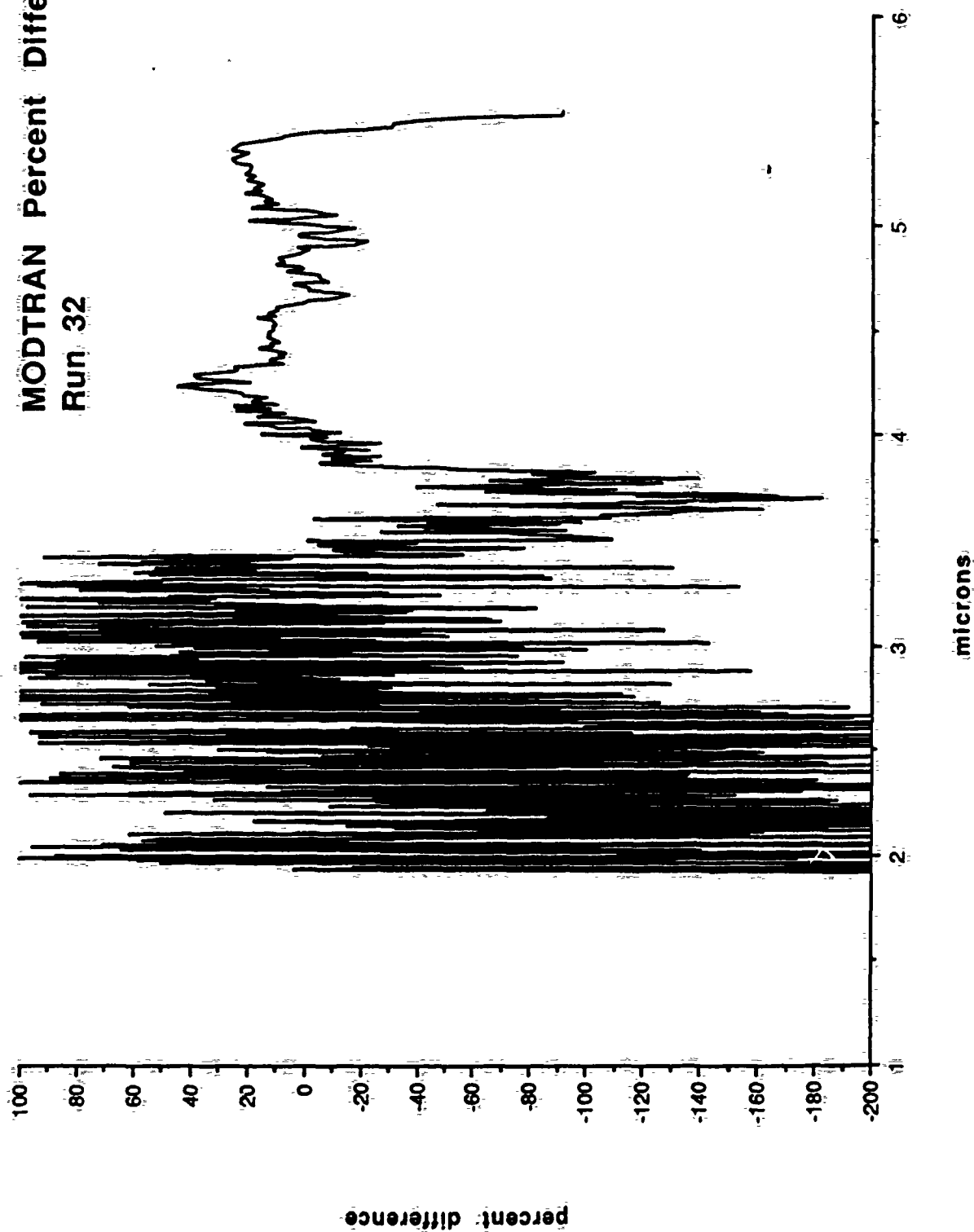




Figure 47

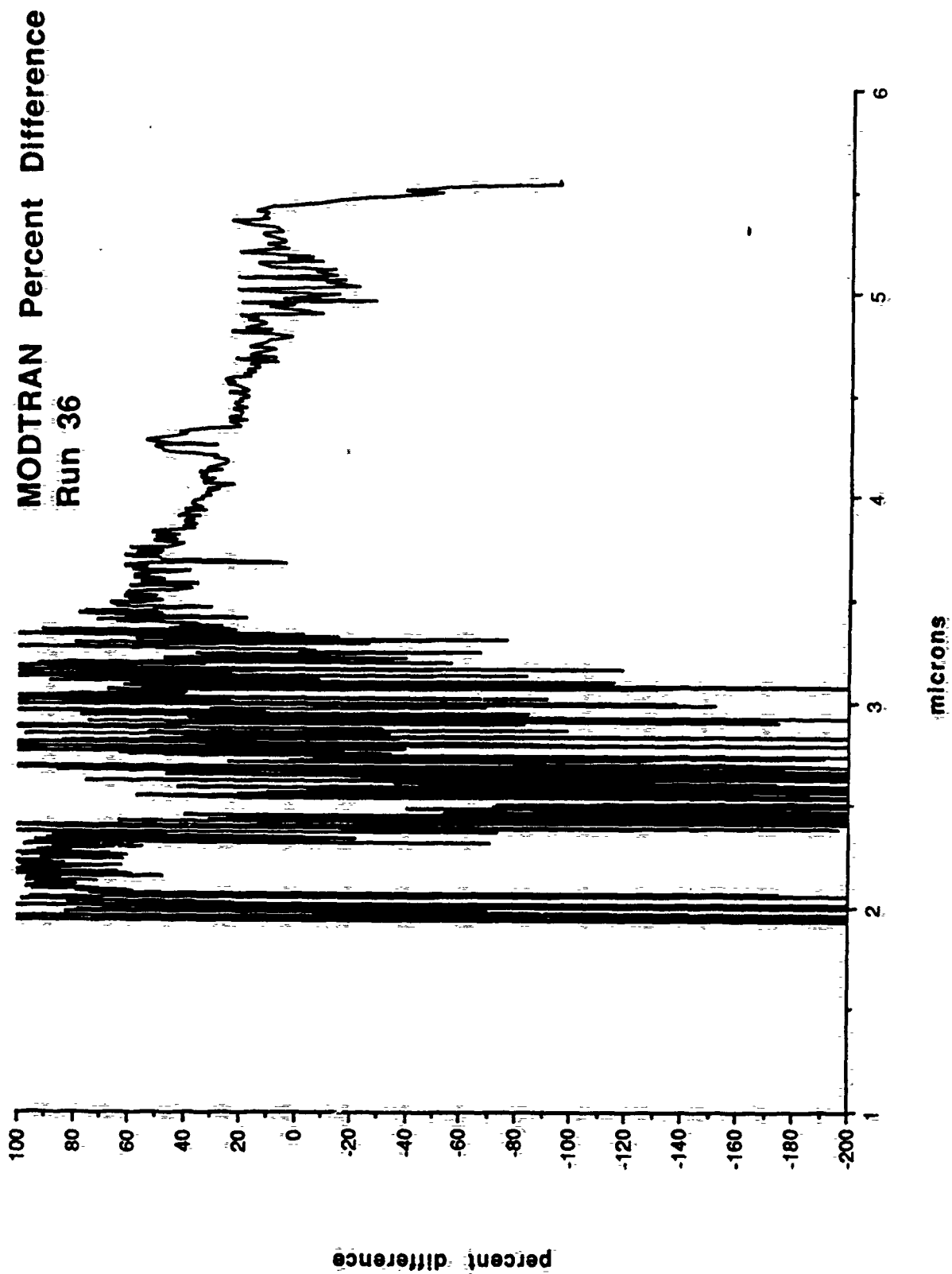


Figure 48

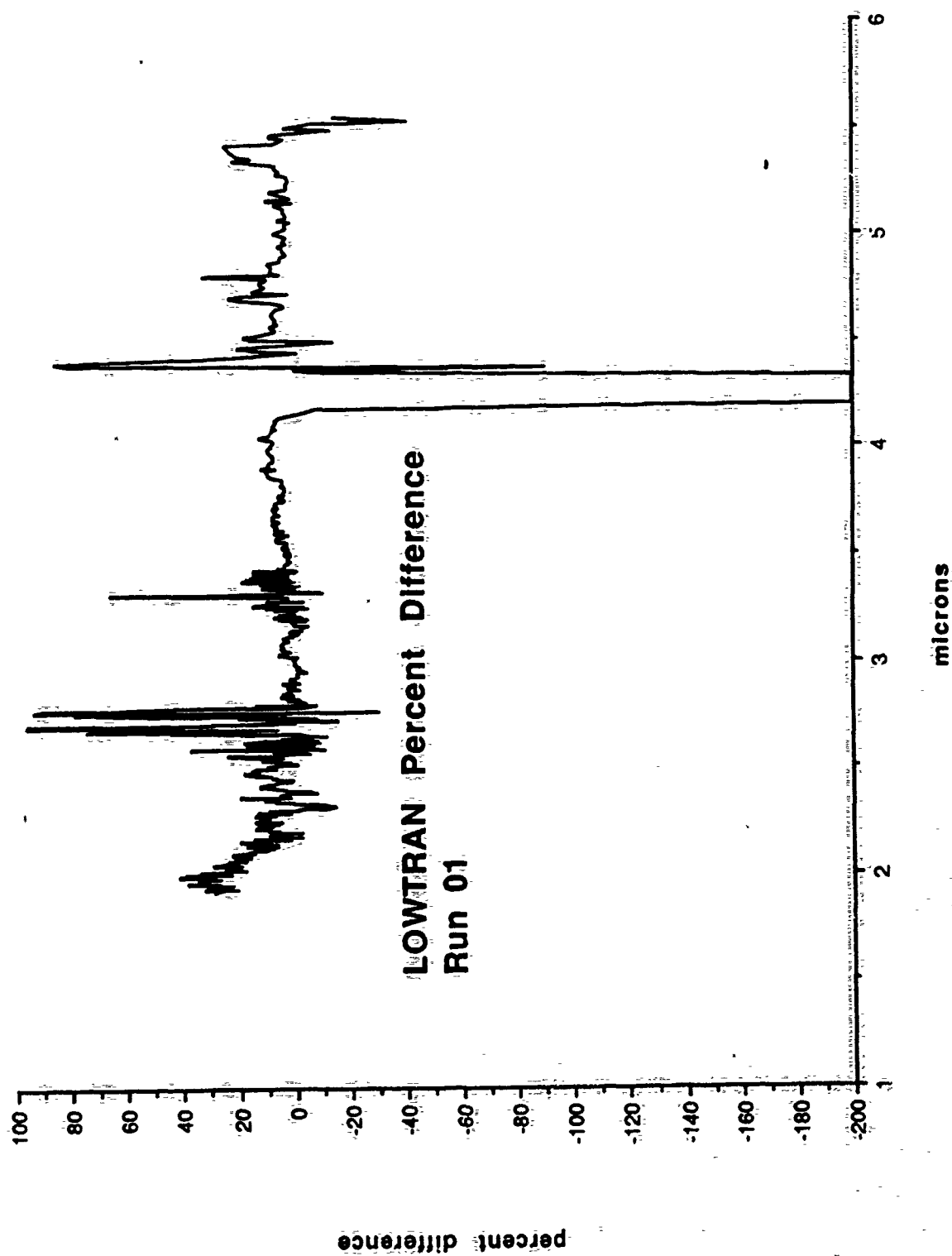


Figure 49

LOWTRAN Percent Difference  
Run 05

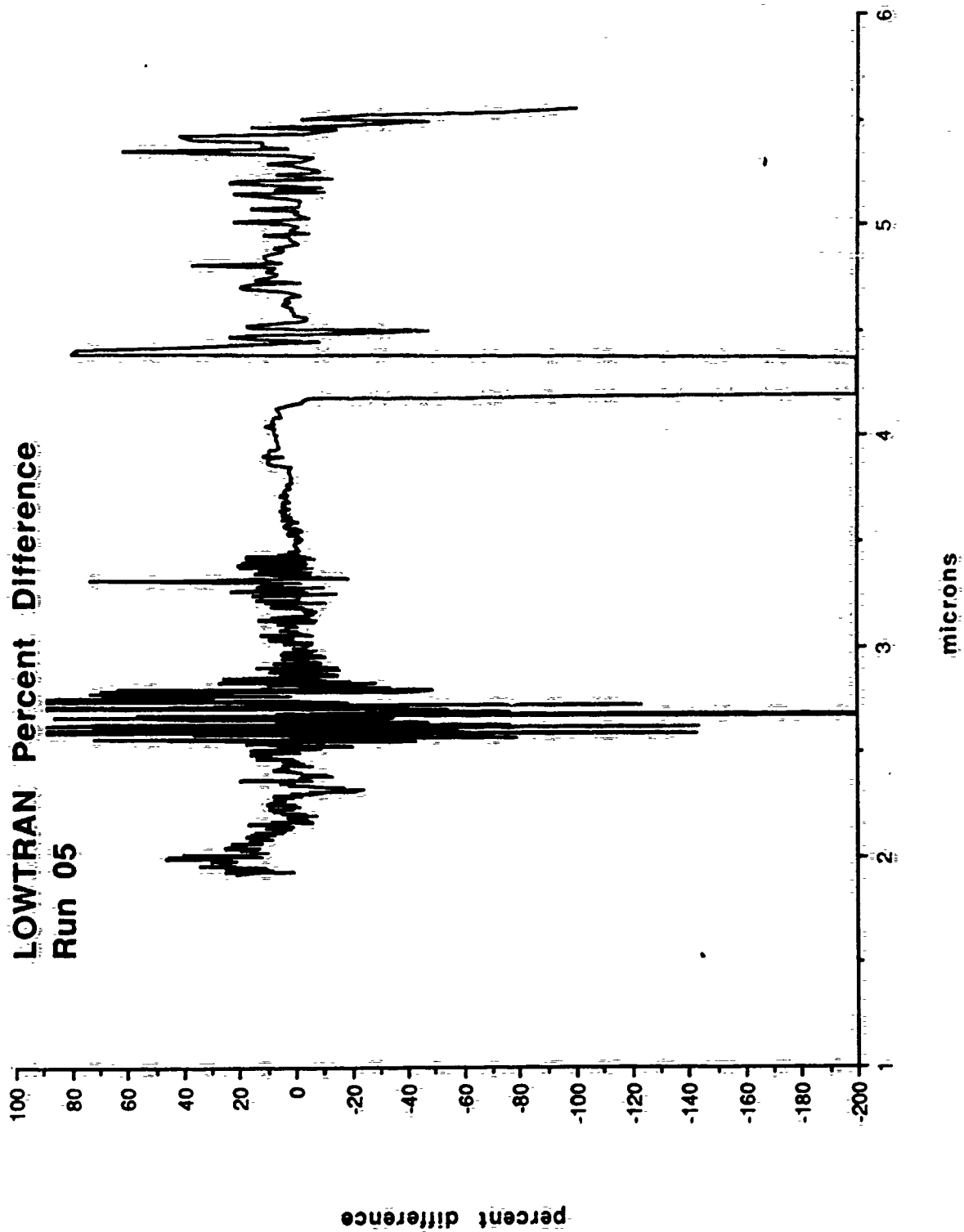


Figure 50

LOWTRAN Percent Difference

Run 09

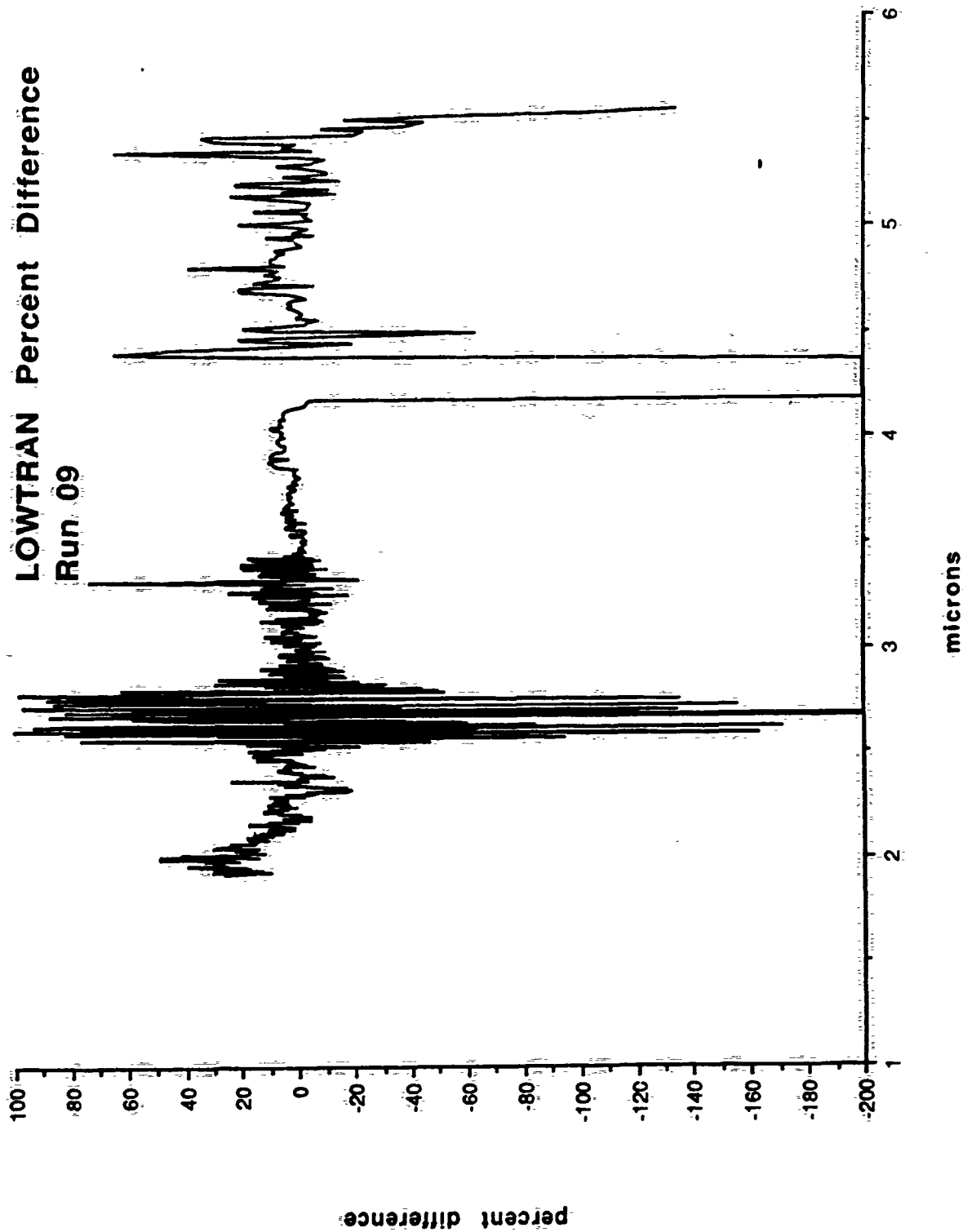
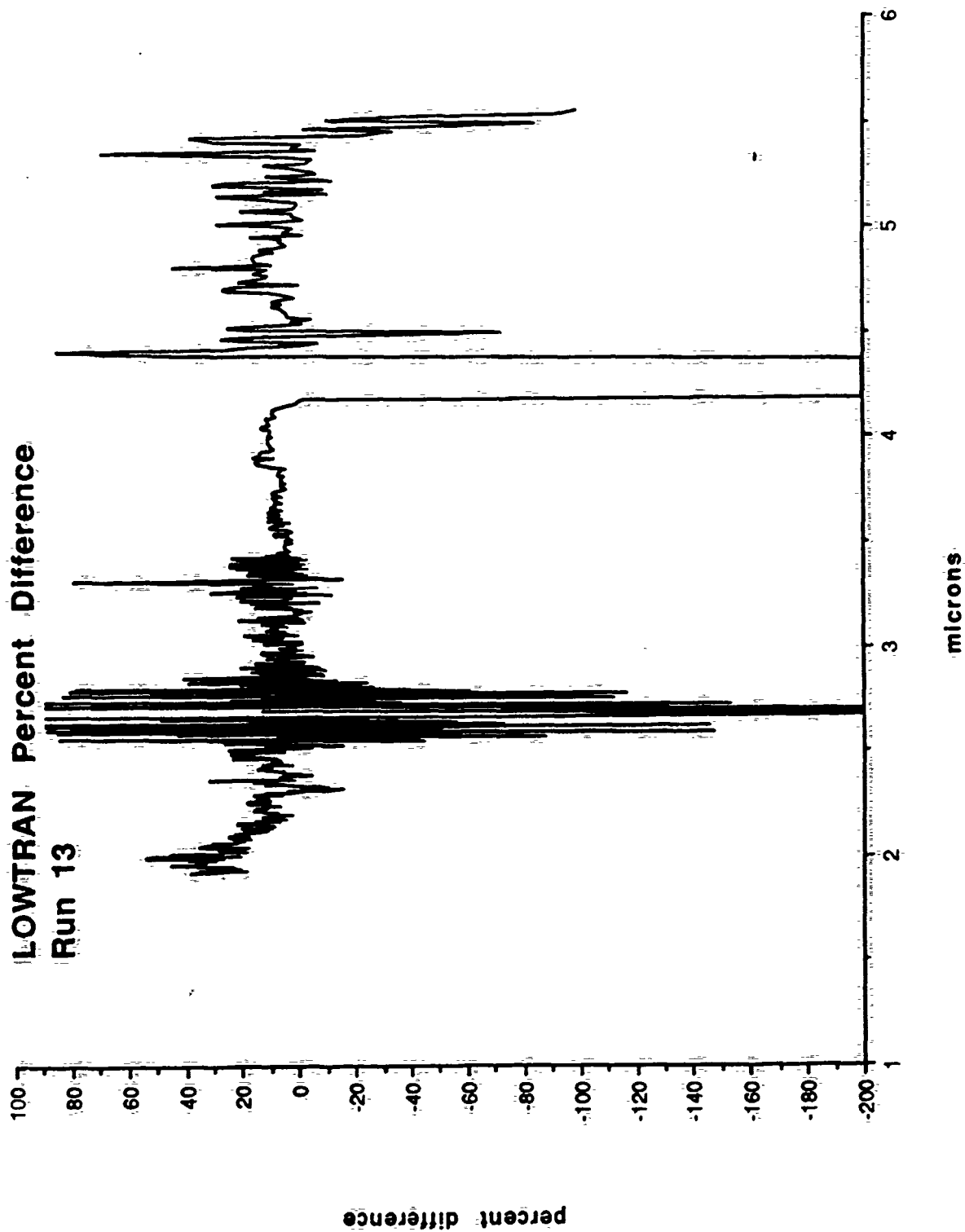


Figure 51

LOWTRAN Percent Difference

Run 13



**Figure 52**  
**LOWTRAN Percent Difference**  
**Run 19**

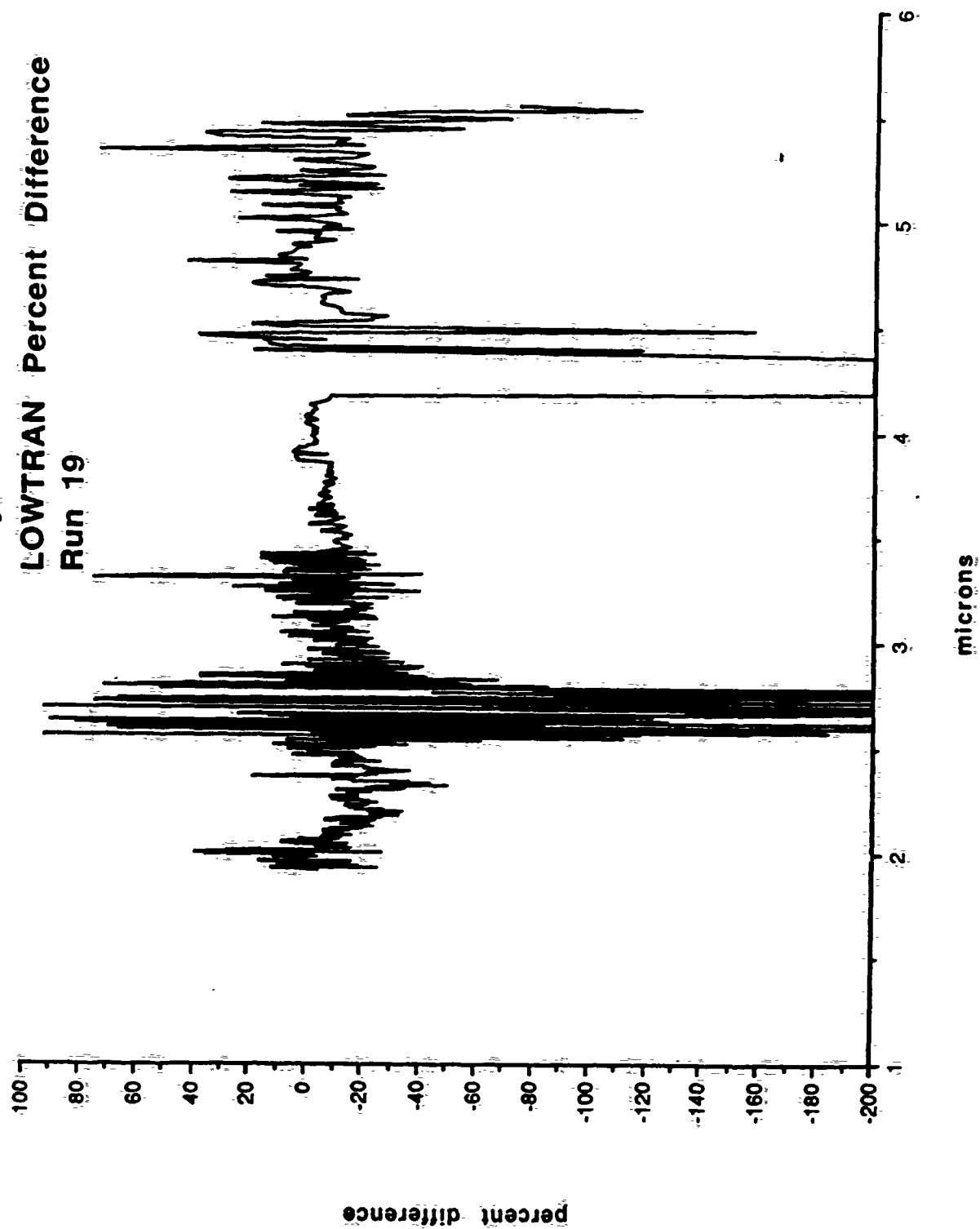


Figure 53

LOWTRAN Percent Difference  
Run 23

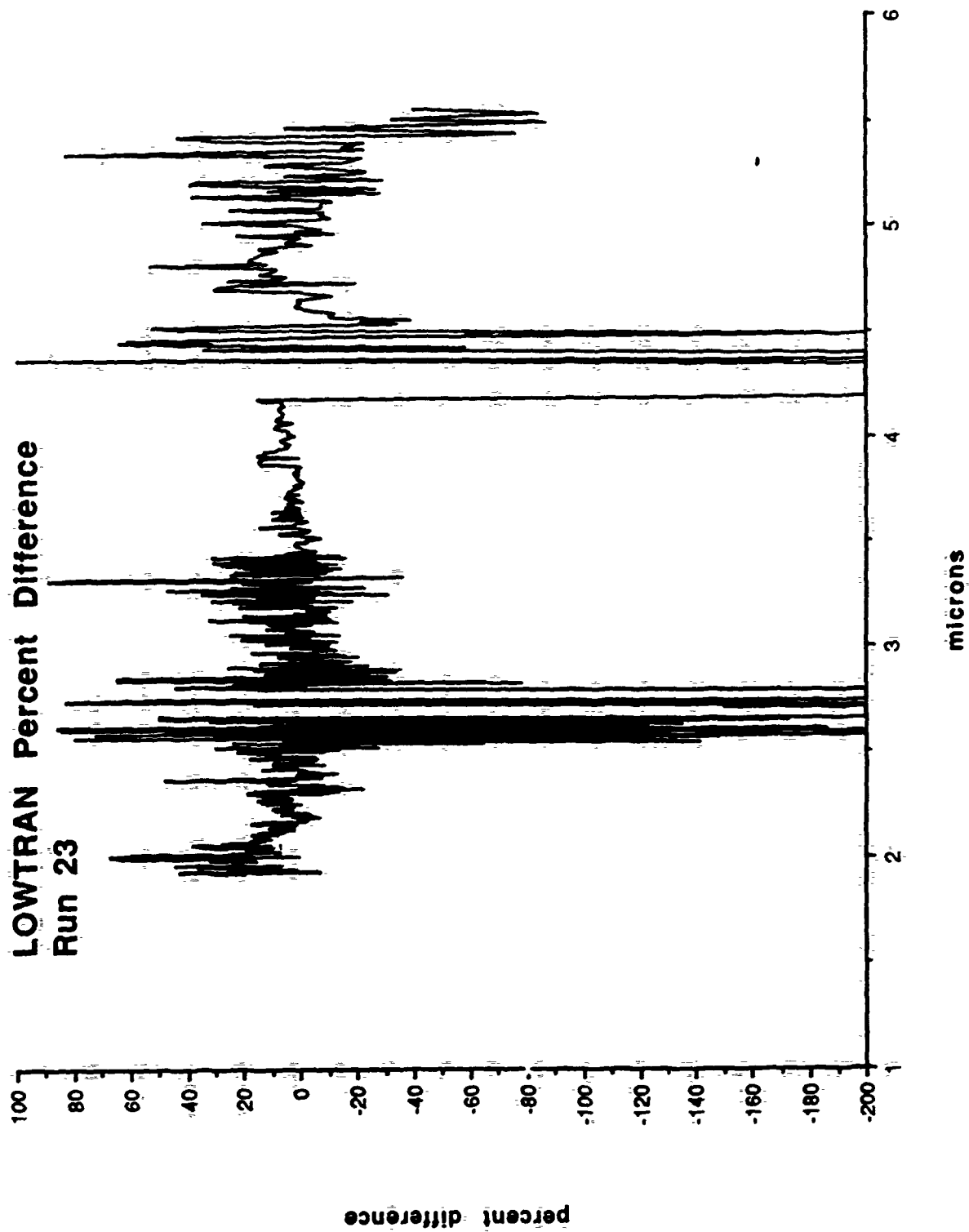


Figure 54

LOWTRAN Percent Difference  
Run 27

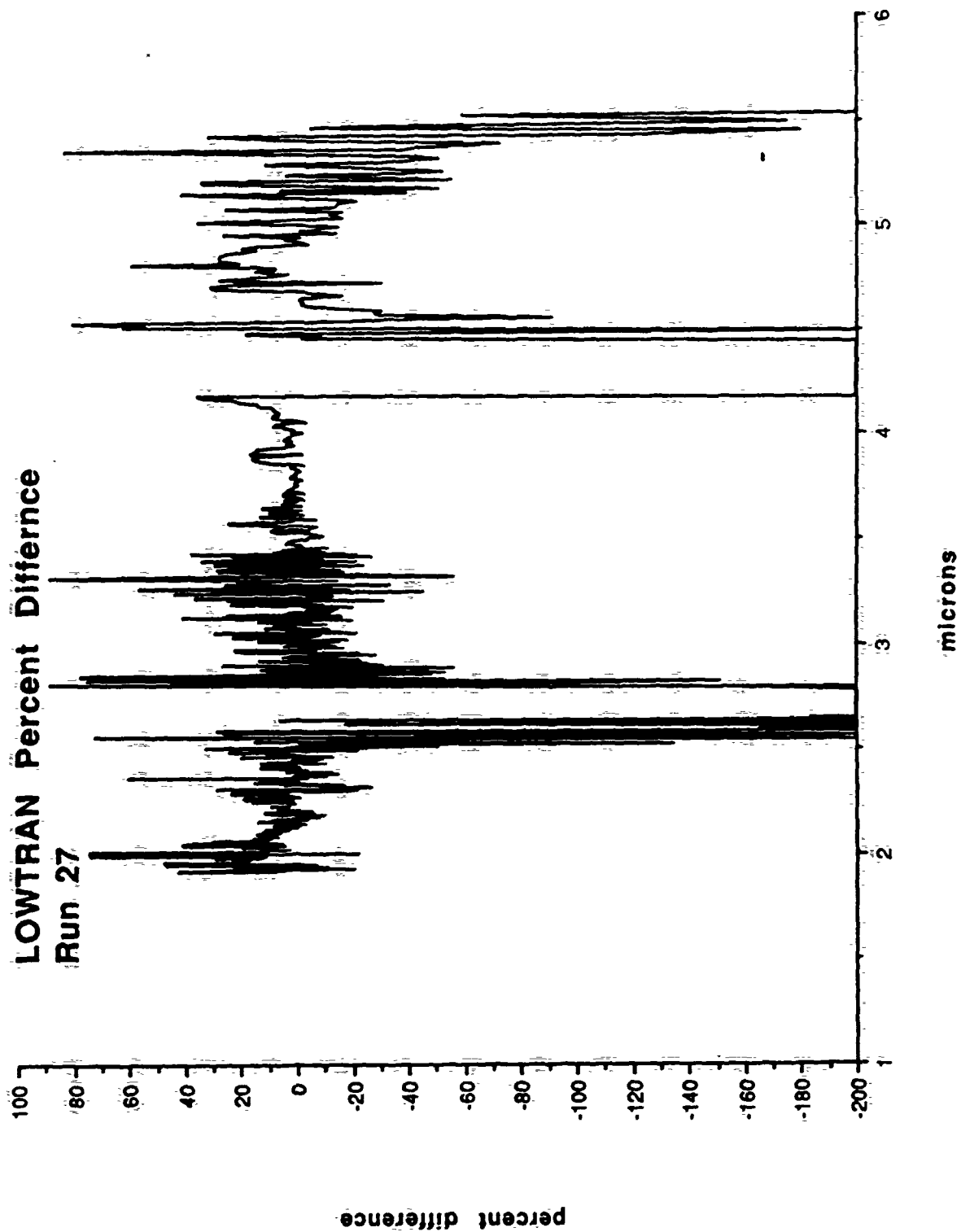
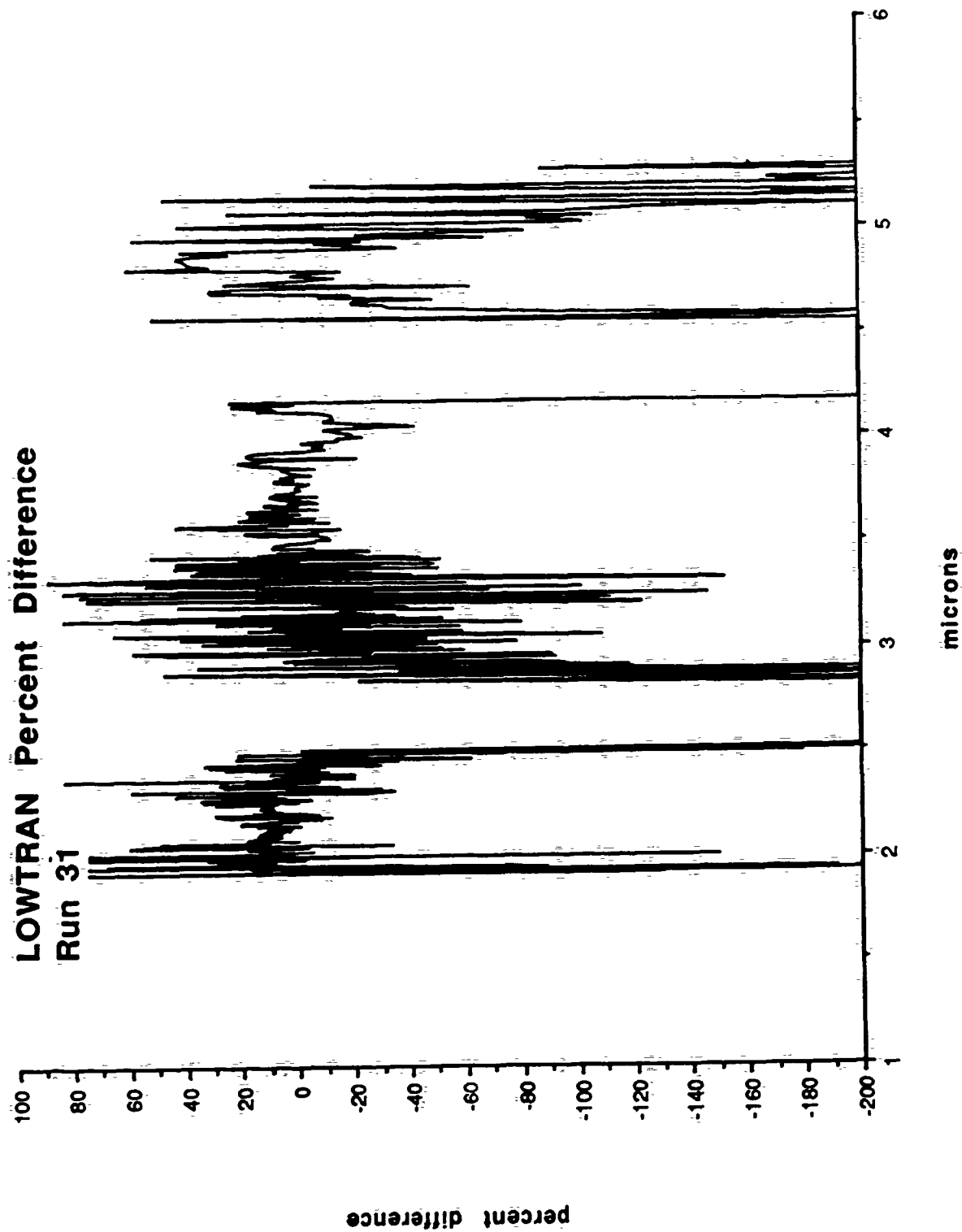




Figure 55



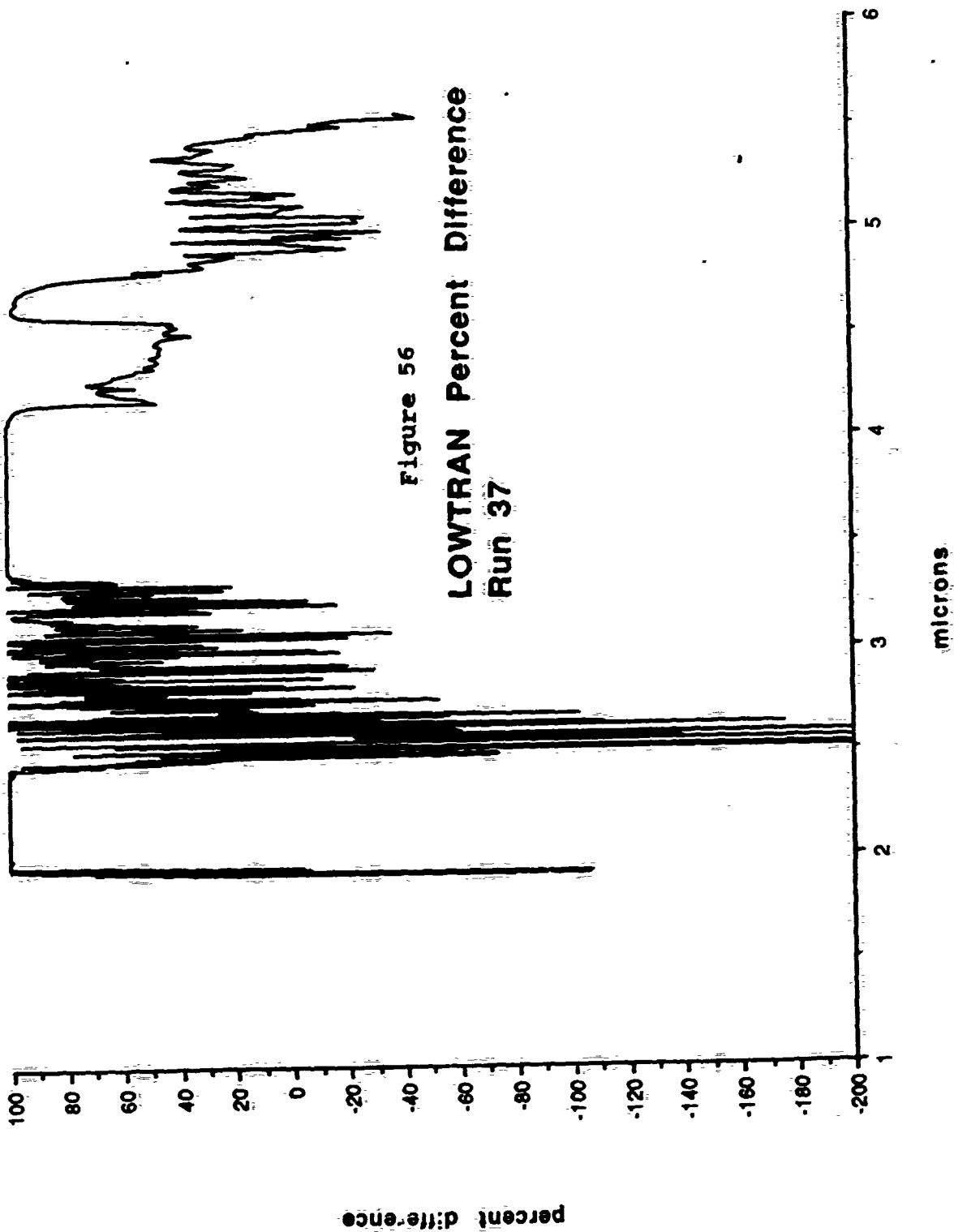


Figure 57

LOWTRAN Percent Difference  
Run 02

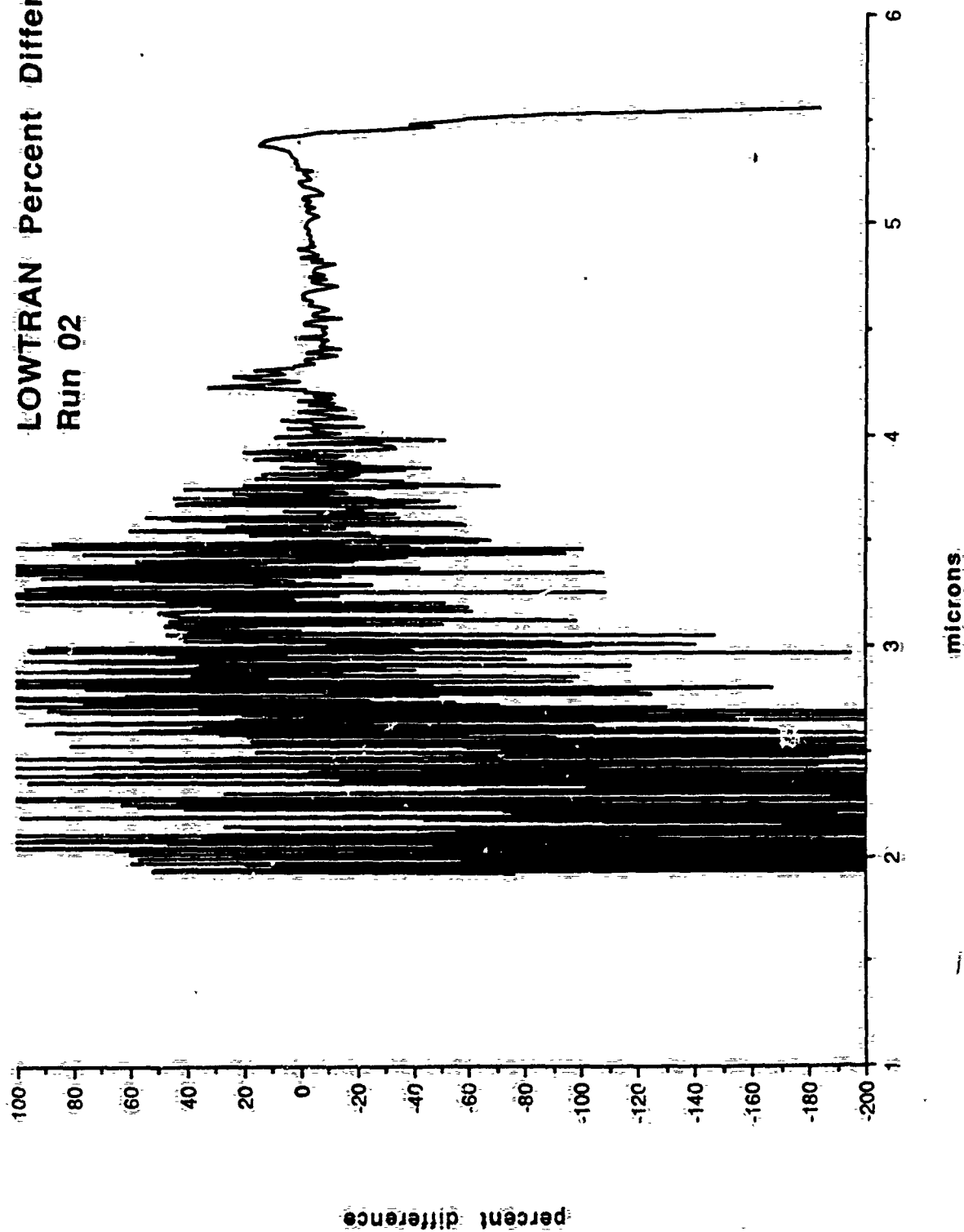


Figure 58

LOWTRAN Percent Difference  
Run 06

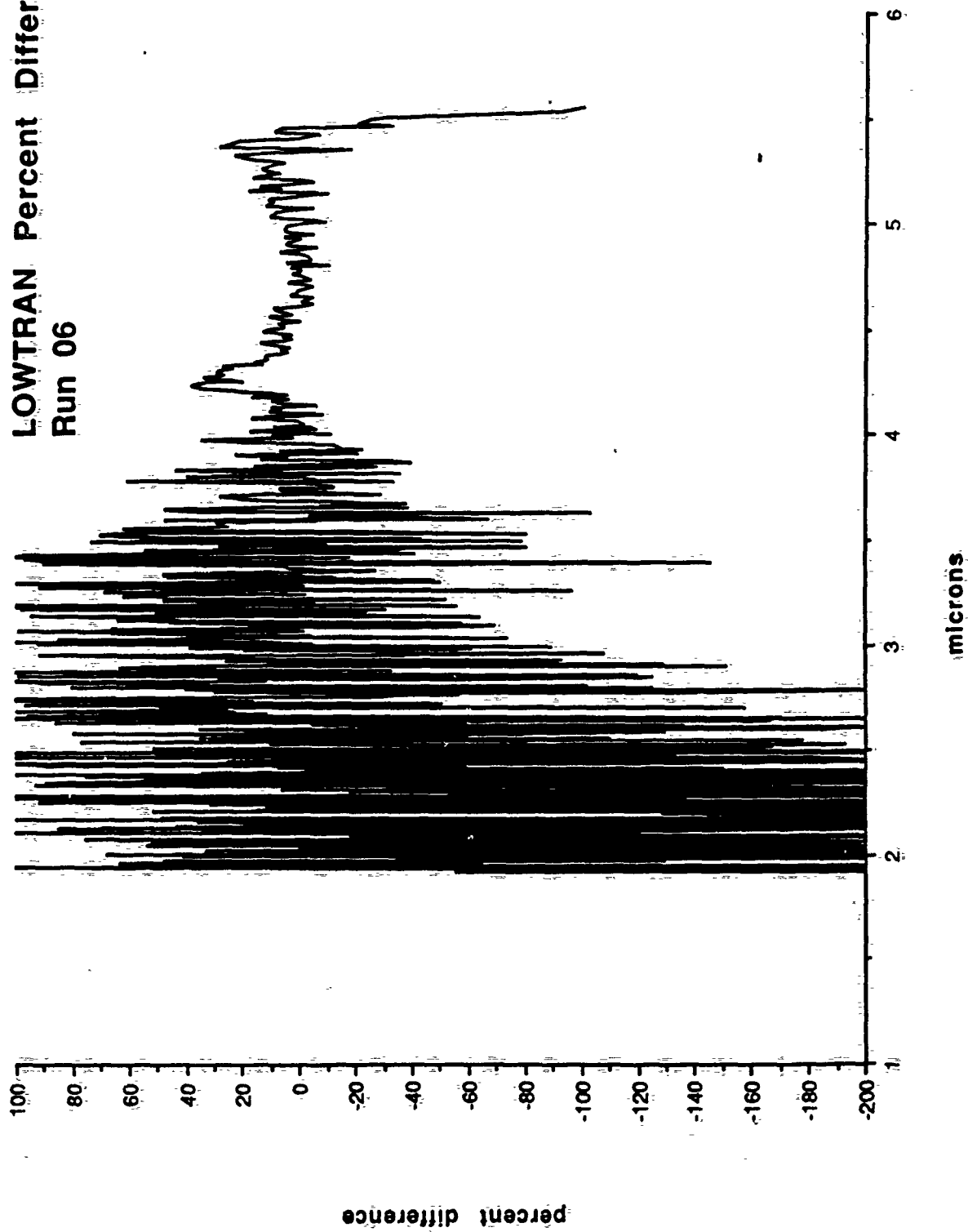


Figure 59  
LOWTRAN Percent Difference  
Run 10

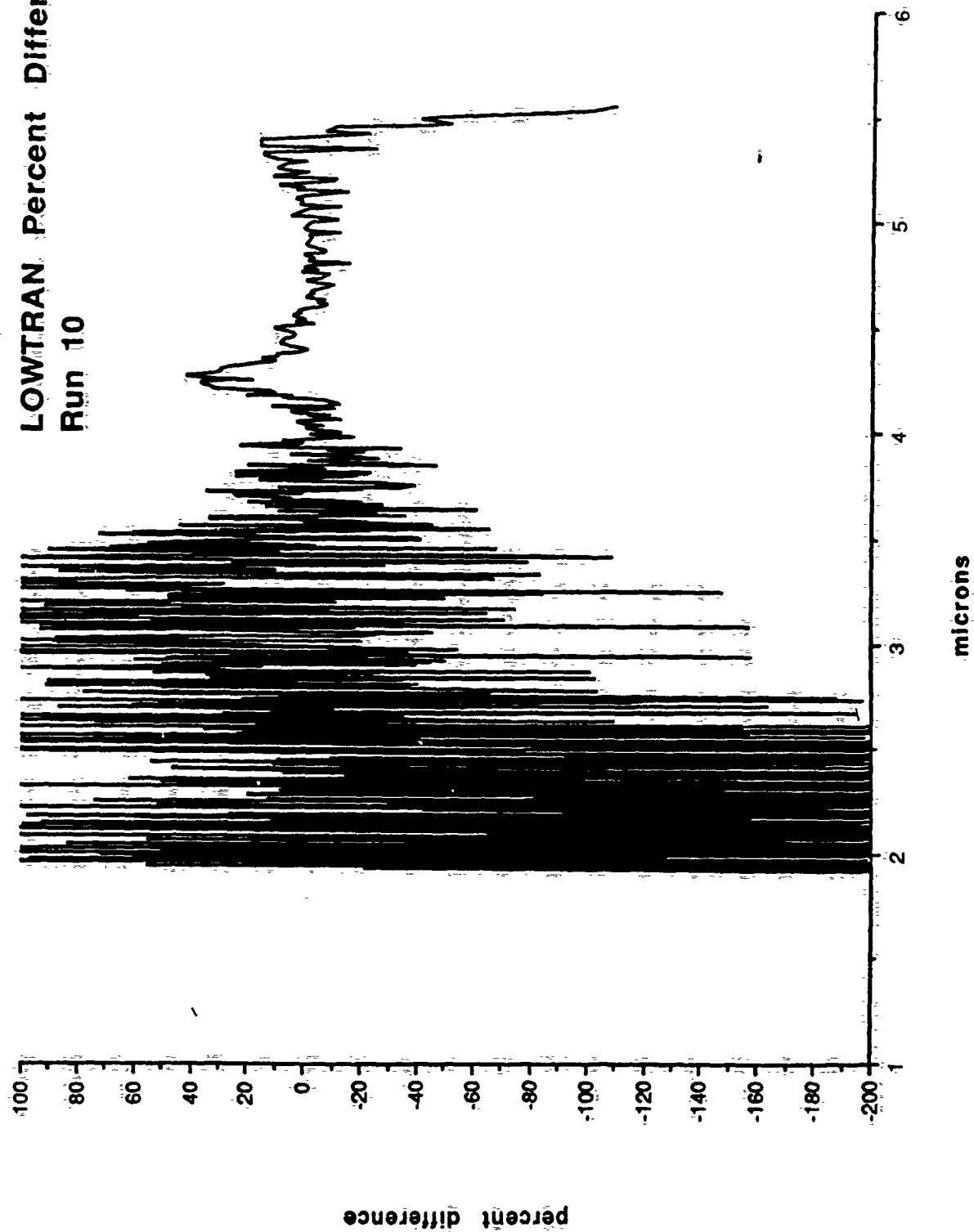


Figure 60  
LOWTRAN Percent Difference  
Run 14

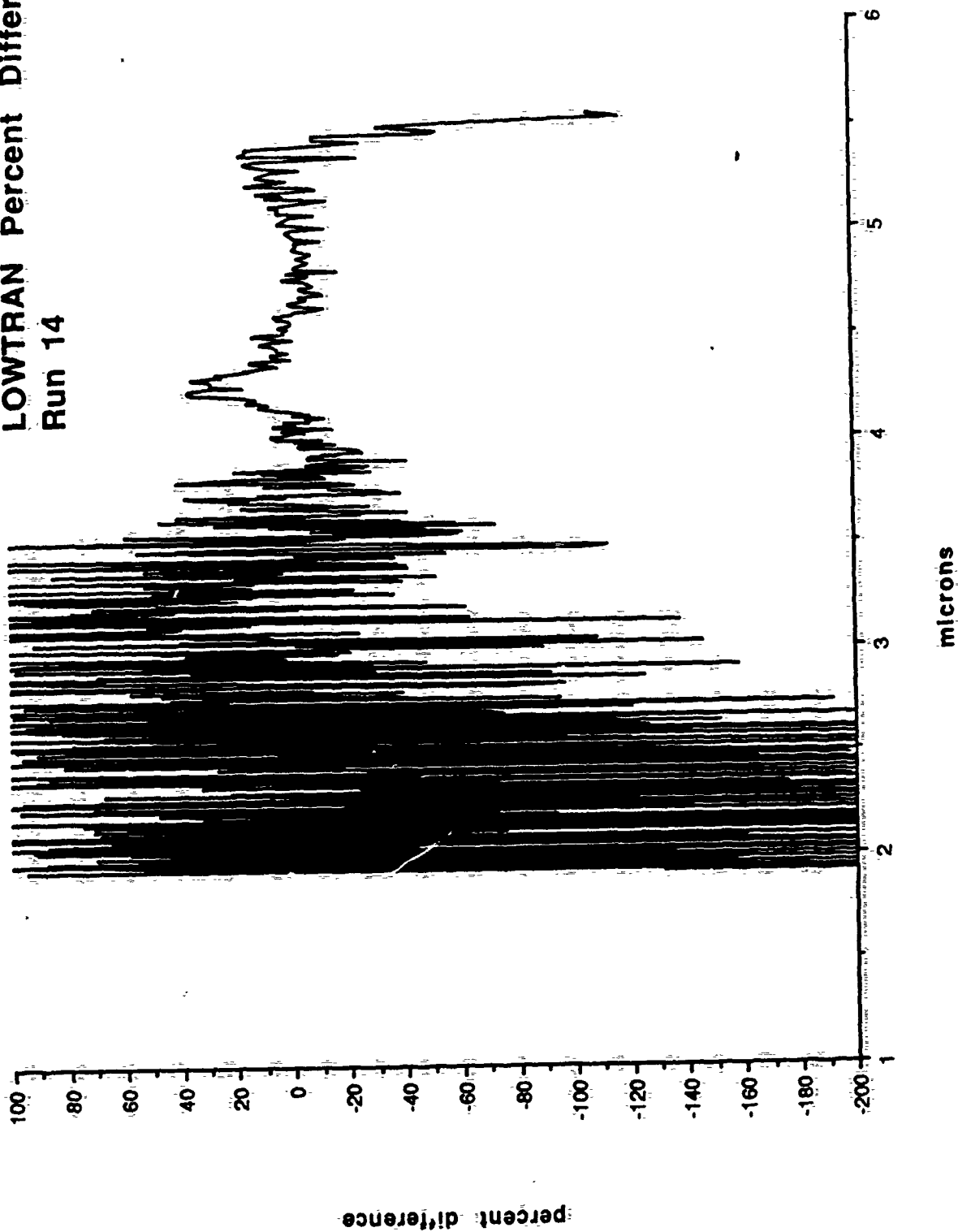


Figure 61

LOWTRAN Percent Difference  
Run 20

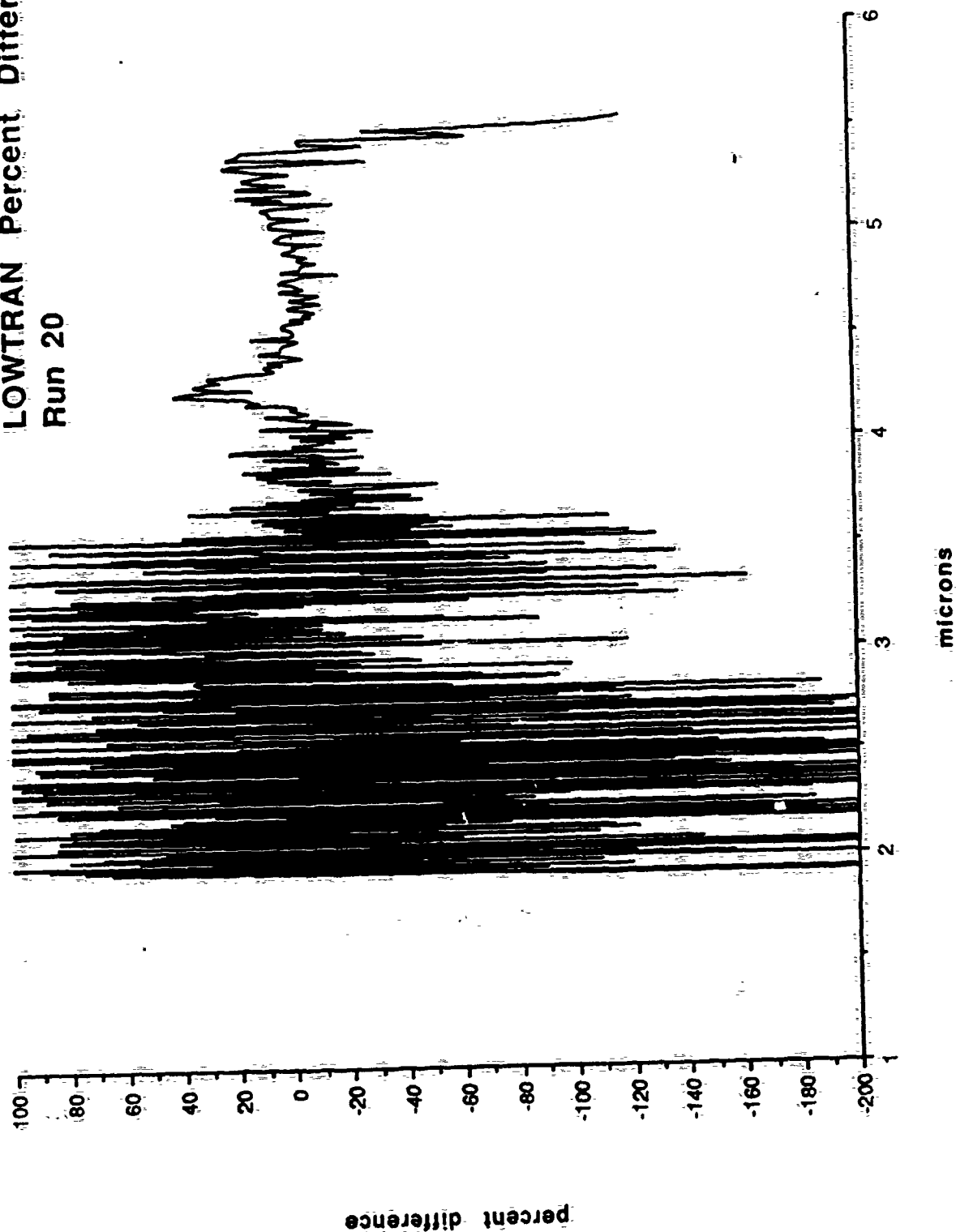


Figure 62  
LOWTRAN Percent Difference  
Run 24

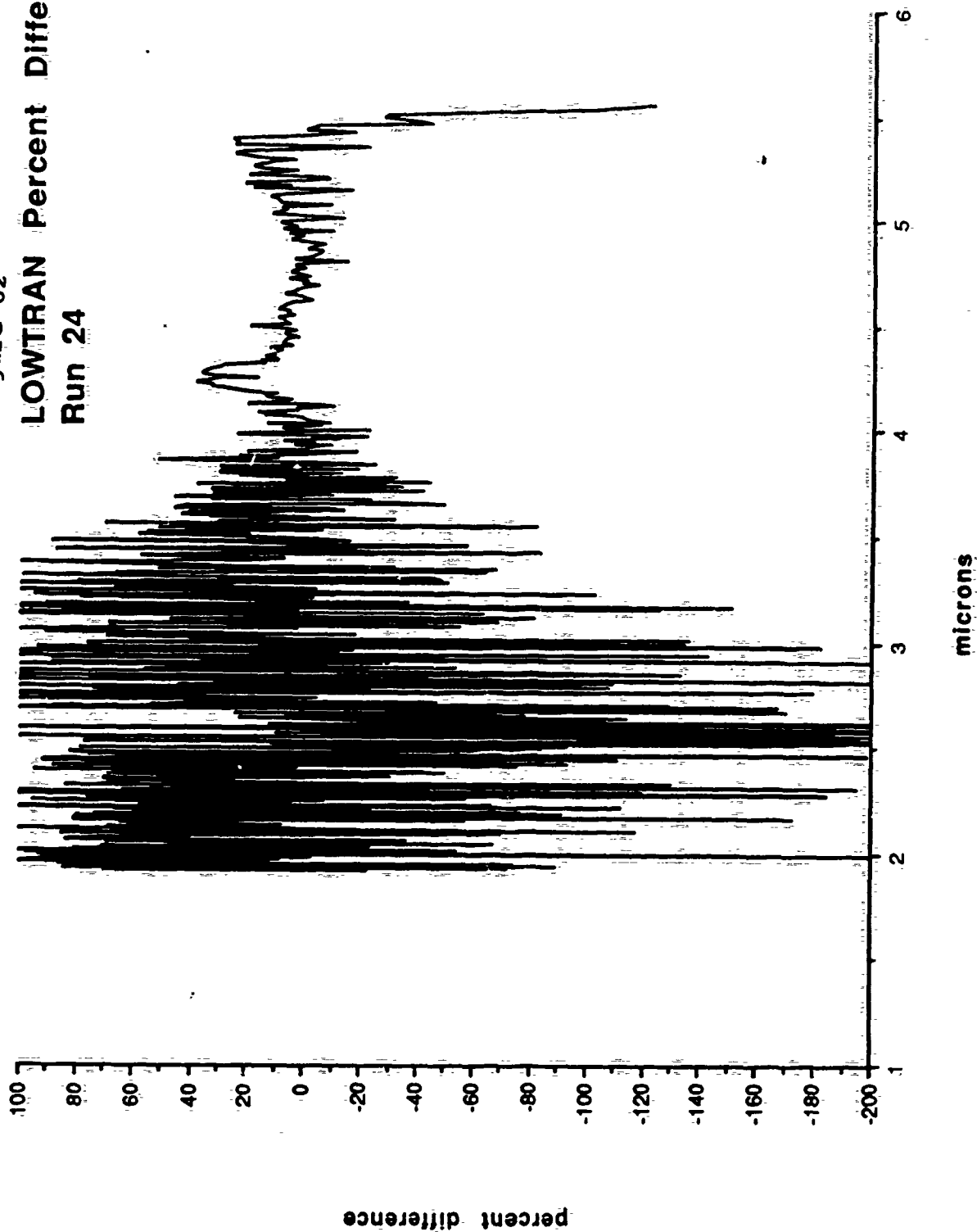




Figure 63  
LOWTRAN Percent Difference  
Run 28

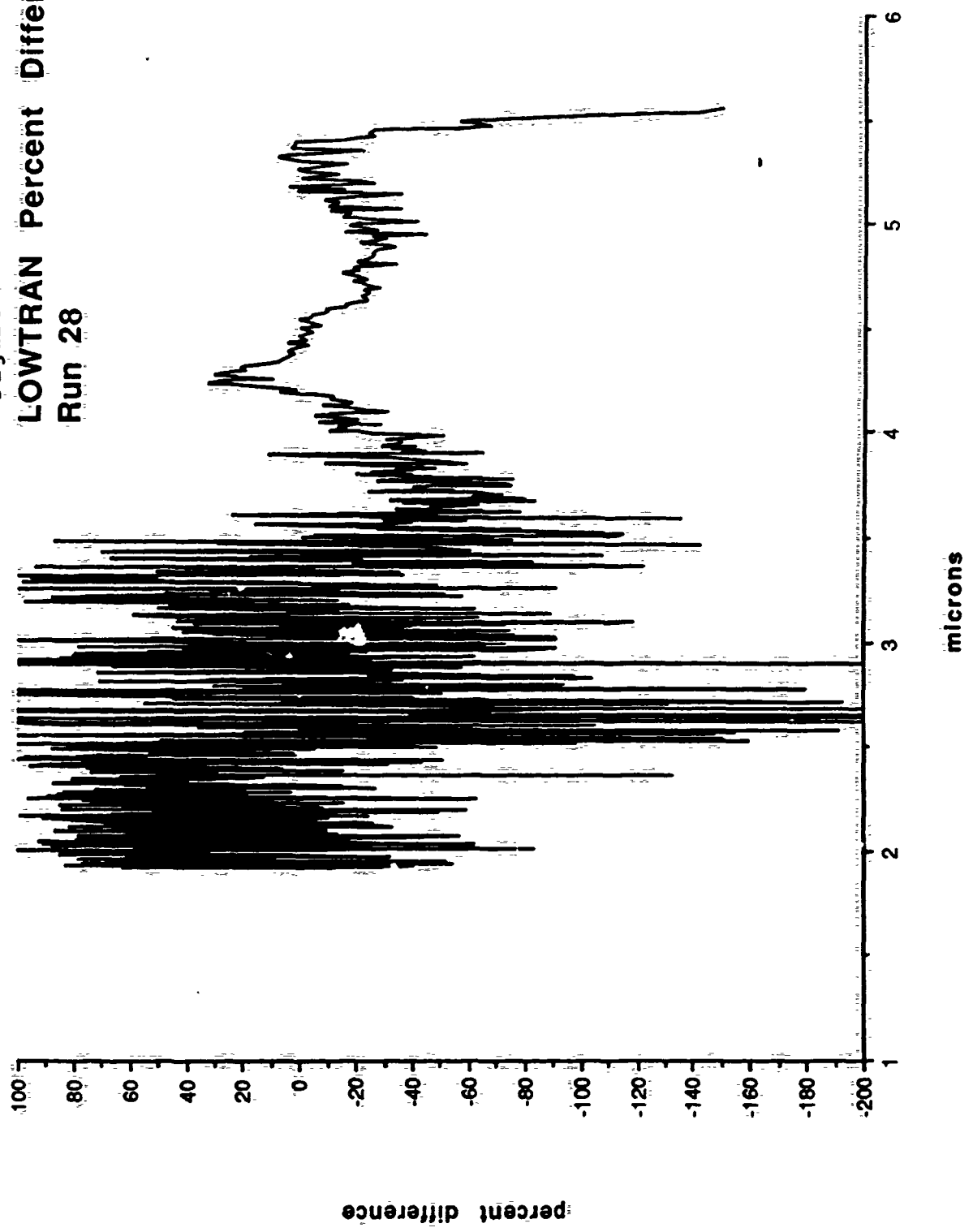


Figure 64

LOWTRAN Percent Difference  
Run 32

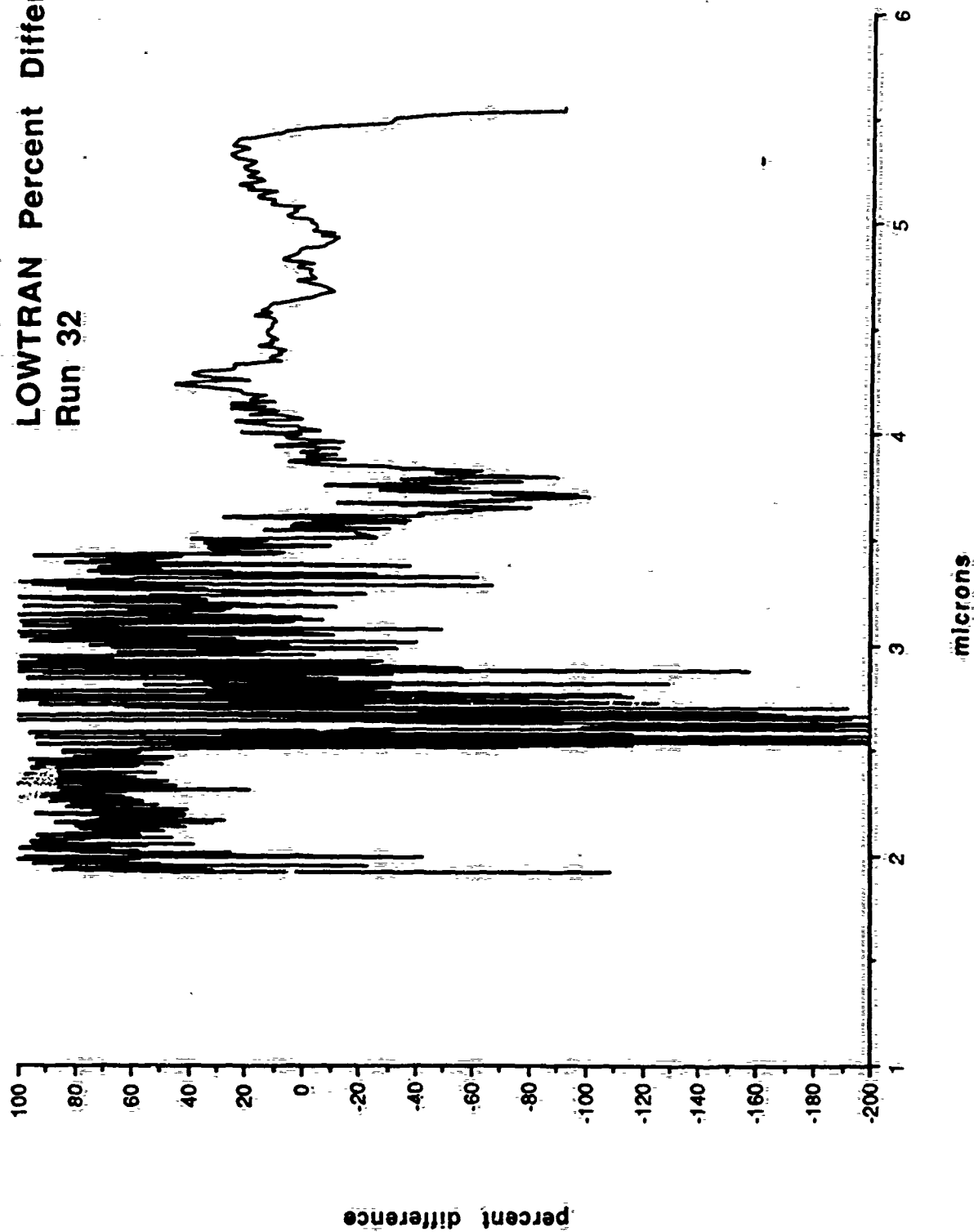


Figure 65

LOWTRAN Percent Difference  
Run 36

